

Regioselective Rhodium Catalyzed Isomerizing Hydroformylation and Iron Catalyzed Hydroformylation of Alkenes and Plant Oils

Thesis Submitted to AcSIR for the Award of
the Degree of

DOCTOR OF PHILOSOPHY

In

Chemical Sciences

By

SWECHCHHA PANDEY

(Registration Number: 10CC13J26012)

Under the Guidance of

Dr. SAMIR H. CHIKKALI



Polymer Science and Engineering Division

CSIR-NATIONAL CHEMICAL LABORATORY

PUNE – 411008, INDIA

May 2018

Dedicated to

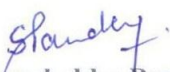
My Beloved Parents and Teachers.....

Declaration by the Candidate

I hereby declare that the original research work embodied in this thesis entitled, “**Regioselective Rhodium Catalyzed Isomerizing Hydroformylation and Iron Catalyzed Hydroformylation of Alkenes and Plant Oils**” submitted to the Academy of Scientific and Innovative Research for the award of the degree of the Doctor of Philosophy (Ph.D.) is the outcome of experimental investigations carried out by me under the supervision of **Dr. Samir H. Chikkali**, Senior Scientist, CSIR-National Chemical Laboratory, Pune. I affirm that the work incorporated is original, and has not been submitted to any other academy, university or institute for the award of any degree or diploma.

May 2018

Polymer Science & Engineering Division
CSIR-National Chemical Laboratory
Pune-411008


Swechha Pandey
(Research Student)



सीएसआईआर - राष्ट्रीय रासायनिक प्रयोगशाला

(वैज्ञानिक तथा औद्योगिक अनुसंधान परिषद)

डॉ. होमी भाभा मार्ग, पुणे - 411 008. भारत

CSIR - NATIONAL CHEMICAL LABORATORY

(Council of Scientific & Industrial Research)

Dr. Homi Bhabha Road, Pune - 411 008, India



Dr. Samir H. Chikkali

Senior Scientist and Assistant Professor (AcSIR)

Polymer Science and Engineering Division

CSIR-National Chemical Laboratory

Dr. Homi Bhabha Road, Pashan, Pune-411008,

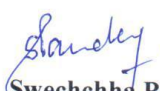
Maharashtra, India. Tel.: 020-2590-3145


E-mail: s.chikkali@ncl.res.in

29th May 2018

Ph.D. Thesis Certificate

This is to certify that the work incorporated in this Ph.D. thesis entitled “**Regioselective Rhodium Catalyzed Isomerizing Hydroformylation and Iron Catalyzed Hydroformylation of Alkenes and Plant Oils**” submitted by **Ms. Swechcha Pandey (Registration Number: 10CC13J26012)** to the Academy of Scientific and Innovative Research (AcSIR) in fulfillment of the requirements for the award of the Degree of the Doctor of Philosophy, embodies original research work under my supervision. I further certify that this work has not been submitted to any other University or Institution in part or full for the award of any degree or diploma. Research material obtained from other sources has been duly acknowledged in the thesis. Any text, illustration, table, etc., used in the thesis from other sources, have been duly cited and acknowledged.


Ms. Swechchha Pandey
(Research Student)


Dr. Samir H. Chikkali
(Research Supervisor)

Communication Channels	+91 - 20 - 2590 2380 +91 - 20 - 2590 2663 +91 - 20 - 2590 2690 (Stores)	FAX +91 - 20 - 2590 2664	E-MAIL sspo@ncl.res.in	WEBSITE www.ncl-india.org
-------------------------------	---	------------------------------------	---	--

ACKNOWLEDGEMENT

The process of earning a doctorate and writing a dissertation is long and arduous and it is certainly not done singlehandedly. So, I am using this opportunity to express my gratitude to everyone who helped and supported me throughout the course of my research.

*Firstly, I would like to express my special appreciation and thanks to my research supervisor **Dr. Samir Chikkali** for his valuable guidance and scholarly inputs. I have enjoyed the opportunity to watch and learn from his knowledge and experience. His enthusiasm, encouragement and faith in me throughout have been extremely helpful. He is the one who moulded me into a good researcher. I am thankful to the god almighty for giving me such a wonderful and humble personality as my mentor. He has given me full freedom in my research and I could not imagine to have a better mentor than him.*

I wish to express my sincere thanks to the Doctoral Advisory Committee members, Dr. Benudhar Punji, Dr. Darbha Srinivas, Dr. Amitava Das and Dr. Subhash P. Chavan whose contribution in stimulating suggestions and encouragement helped me to coordinate my work.

I am grateful to Prof. A. K. Nangia, Director, NCL, Dr. V. K. Pillai and Prof. S. Pal (Former Director, NCL), Dr. Ulhas Kharul, Head, PSE Division, and Dr. Ashish Lele (Former HoD, PSE Division) for giving me this opportunity and providing all necessary infrastructure and facilities. I also acknowledge the financial support of UGC, New Delhi in terms of junior and senior research fellowships.

I extend my thanks to our collaborators Dr. K. Sreekumar and Varchaswal Kashyap for electrochemical analysis, Dr. Kumar Vanka and K. Vipin Raj for DFT calculations, Dinesh Shinde for the timely help with NMR measurements and Dr. C.P. Vinod for XPS analysis. I would also like to thank Mrs. B. Santhakumari, for HRMS analysis, Dr. Rajamohanan and Dr. Sapna Ravindranathan for NMR facilities.

I also want to thank my Master's project mentor Prof. R. M. Singh from BHU for getting me interested in research and making me realize that I can take it further too. I would like to thank all seniors from BHU and Dr. Bhawana Singh who have offered unconditional support and help during my initial Ph.D. days.

I want to convey my thanks to Dr. Asha's lab members Sandeep, Moumita, Shrikant and Sarabjot for their timely help with IR measurements and help of any sort during my Ph.D.

A special thanks goes to My lab seniors Shahaji Gaikwad and Vijay Koshti for their valuable advice and help in lab practices which I greatly acknowledge and other lab colleagues and seniors Dr. Ketan Patel, Dr. Shilpi Kushwaha, Dr. Dipa Mandal, Dr. Sandip Pawal, Satej, Nilesh, Anirban, Dynaneshwar, Ravi, Bhausahab, Rohit, Amol and Kishore for the lively lab atmosphere and endless discussions. Also, I am thankful to Dr. Punji's lab members Dr. Shrikant, Hanuman, Dr. Vineeta, Ulhas, Dilip, Rahul, and Dipesh for their help.

A special thanks goes to all my friends from CSIR-NCL, Praveen, Veer, Nivedita, Nidhi, Smrati, Pragati, Amit, Manoj, Dharmesh, Ragini, Vijay, Sandip Singh, Pravin, Bhawana, Garima, Nilesh, Sandip, Rajasekar from IISER Pune for their help .

I owe a lot to my beloved parents who encouraged and helped me at every stage of my personal and academic life, and longed to see this achievement come true. My sincere thanks to my beloved brothers Alok and Abhigyan for their endless support. I am very much indebted to my whole family..... Who supported me in every possible way to see the completion of this research work.

Above all, I owe it all to Almighty God for granting me the wisdom, health and strength to undertake this research task and enabling me to its completion.

Swechchha Pandey

TABLE OF CONTENTS

Abbreviations

Preface

Chapter 1	<i>Introduction</i>	<i>1-17</i>
1.1	Introduction to Hydroformylation	2
1.1.1	Overview	2
1.1.2	Cobalt Catalyzed Hydroformylation	2
1.1.3	Rhodium Catalyzed Hydroformylation	4
1.2	Challenges and Opportunities	5
1.3	Setting the Goals	14
1.4	References	16
Chapter 2	<i>Regioselective Isomerizing Hydroformylation of Long Chain Internal Olefins</i>	<i>18-47</i>
2.1	Abstract	19
2.2	Introduction	19
2.3	Result and Discussion	21
2.4	Experimental Section	26
2.4.1	General methods and materials	26
2.4.2	Synthesis of L1	27
2.4.2.1	Synthesis of phosphorochloridite (2)	27
2.4.2.2	Synthesis of ligand L1	28
2.4.3	Synthesis of Pd complex of L1 (M1)	31
2.4.4	Mechanistic investigation: <i>In-situ</i> high pressure NMR	33
2.4.5	Isomerizing hydroformylation : General procedure	35
2.4.5.1	Isomerizing hydroformylation of methyl oleate	35
2.4.5.2	Separation and characterization of aldehydes	38
2.4.5.3	Isomerizing hydroformylation of cis-2-octene	39
2.4.6	Functionalization of linear aldehyde	41
2.4.6.1	Reduction of linear aldehyde to hydroxy-fatty acid (3)	42
2.5	Conclusion	45
2.6	References	46

Chapter 3	<i>Isomerizing Hydroformylation of Non-Edible Plant Oils</i>	48-84
3.1	Abstract	49
3.2	Introduction	49
3.3	Result and Discussion	51
	3.2.1 Isomerizing hydroformylation of CNSL-monoene	52
	3.2.2 Isomerizing hydroformylation of CNSL-cardanol	55
	3.2.3 Unsymmetrical α,ω -difunctional building blocks and monomers	57
	3.2.4 Coordination behavior of L4 and detection of catalyst resting state by high-pressure NMR	59
3.4	Experimental Section	60
	3.4.1 General methods and materials	60
	3.4.2 Cashew nut shell liquid and conversion to monoene	60
	3.4.3 Isomerizing hydroformylation of CNSL-monoene	63
	3.4.4 Determination of conversion and selectivity in case of I-HF of CNSL-monoene	64
	3.4.5 Synthesis of Me-protected monoene (S2)	64
	3.4.6 Isomerizing hydroformylation of Me-protected monoene (S2)	65
	3.4.7 Isomerizing hydroformylation of CNSL-cardanol	66
	3.4.8 Determination of conversion & selectivity for I-HF of CNSL-cardanol	67
	3.4.9 Reduction of diolefinic monoaldehyde (P6)	70
	3.4.10 Preparation, separation and characterization of linear aldehyde	73
	3.4.11 Control experiments	77
	3.4.11.1 In presence of conjugated diene	77
	3.4.11.2 One pot isomerization-hydroformylation-hydrogenation	78
	3.4.12 Mechanistic investigation: <i>In-situ</i> high pressure NMR	79
	3.4.12.1 Reaction of [Rh(acac)(CO) ₂] and ligand L4	79
	3.4.12.1 Reaction of [Rh(acac)(CO) ₂], ligand L4 in presence of substrate	80
3.5	Conclusion	82
3.6	References	83

Chapter 4 ***Iron Catalyzed Hydroformylation of Alkenes under Mild Conditions : Evidence of an Fe (II) Catalyzed Process*** : 85-150

4.1	Abstract	86
4.2	Introduction	86
4.3	Result and discussion	91
	4.3.1 Hydroformylation of 1-Octene	91

4.3.2	Scope of Fe Catalyzed Hydroformylation	93
4.3.3	Acetic Acid Promoted Iron Catalyzed Hydroformylation	96
4.3.4	Mechanistic investigations	97
4.3.4.1	NMR Spectroscopy	97
4.3.4.2	Cyclic Voltammetry	99
4.3.4.3	Computational and Additional Experimental Evidence	100
4.3.4.4	Is it Iron or Rhodium?	102
4.4	Experimental Section	103
4.4.1	General Methods and Materials	103
4.4.2	Synthesis of iron complexes $[\text{Fe}(\text{CO})_5]$ and $[\text{HFe}(\text{CO})_4][\text{PPN}]$	105
4.4.3	General Procedure for Hydroformylation	108
4.4.3.1	Iron Catalyzed Hydroformylation of 1-Octene	108
4.4.3.2	Iron Catalyzed Hydroformylation of 1-Hexene	109
4.4.3.3	Iron Catalyzed Hydroformylation of Long Chain Olefins	111
4.4.3.4	Iron Catalyzed Hydroformylation of Functional Olefins	113
4.4.3.5	Iron catalyzed hydroformylation of styrene and styrene derivatives	117
4.4.3.6	Mechanistic Investigations	124
4.4.3.6.1	Coordination of Ligand followed by Generation of Dihydride Species	124
4.4.3.6.2	Formation of Dihydride Complex followed by Ligand Coordination	132
4.4.3.6.3	From $[\text{Fe}(\text{CO})_3(\text{PPh}_3)_2]$ to Iron Dihydride Complex	133
4.4.3.6.4	Trapping Iron-Acyl Intermediate D	134
4.4.3.6.5	Cyclic Voltammetry	137
4.4.3.6.6	Control Experiments	139
4.4.3.6.7	Computational Investigations	140
4.4.3.6.8	Who Catalyses the HF: Is It Iron or Rhodium?	140
4.4.3.6.8.1	Hydroformylation Using the Precursors	140
4.4.3.6.8.2	Bulk and Surface Analyses	142
4.5	Conclusion	146
4.6	References	147

Chapter 5 Iron Catalyzed Asymmetric Hydroformylation of Olefins

151-169

5.1	Abstract	152
-----	----------	-----

152

5.2	Introduction	152
5.2.1	Co Catalyzed Asymmetric Hydroformylation	153
5.2.2	Rh Catalyzed Asymmetric Hydroformylation	154
5.2.3	Pt Catalyzed Asymmetric Hydroformylation	157
5.3	Result and discussion	158
5.3.1	Fe Catalyzed A-HF of 2,3-DHF	159
5.3.2	Fe Catalyzed A-HF of 2,5-DHF	160
5.3.3	Coordination studies	160
5.3.3.1	Reaction of (R,R)-DIOP with Fe Precursor (1)	161
5.3.3.2	Reaction of (S)-tButyl-Josphos with Fe Precursor (1)	163
5.4	Experimental Section	165
5.4.1	General Procedure for Hydroformylation	165
5.4.2	Fe Catalyzed A-HF of 2,3-DHF	166
5.4.3	Fe Catalyzed A-HF of 2,5-DHF	166
5.5	Conclusion	167
5.6	References	168
 Chapter 6 Summary and Outlook		170-179
6.1	Summary	171
6.2	Outlook	177

ABBREVIATIONS

acac	Acetylacetonate
AAS	Atomic Absorption Spectroscopy
Ac ₂ O	Acetic Anhydride
A-HF	Asymmetric Hydroformylation
BASF	Baden Aniline and Soda Factory
BIPHEPHOS	6,6' -[(3,3' -Di- <i>tert</i> -butyl-5,5' -dimethoxy-1,1'-biphenyl-2,2' diyl)bis(oxy)]bis(dibenzo[d,f][1,3,2]dioxaphosphepin)
BDTBPMB	1,2-bis((di- <i>tert</i> butylphosphanyl)methyl)benzene
BINOL	1,1'-Bi-2-naphthol
Cp	Cyclopentadienyl
CNSL	Cashew Nut Shell Liquid
Co ₂ (CO) ₈	Dicobalt octacarbonyl
[(COD)PdCl ₂]	Dichloro(1,5-cyclooctadiene)palladium(II)
(R,R)- DIOP	2,3- <i>O</i> -isopropylidene-2,3-dihydroxy-1,4 bis(diphenylphosphino)butane
DCE	1,2-dichloroethane
DCM	Dichloromethane
DFT	Density functional theory
DME	Dimethoxy ethane
ESI-MS	Electrospray Ionization - Mass Spectrometry
Fe(CO) ₅	Iron Pentacarbonyl
[Fe ₂ (CO) ₉]	Diiron nonacarbonyl
[Fe ₃ (CO) ₁₂]	Triiron dodecacarbonyl
Galvinoxyl	2,6-Di- <i>tert</i> -butyl- α -(3,5-di- <i>tert</i> -butyl-4-oxo-2,5-cyclohexadien-1-ylidene)- <i>p</i> -tolylloxy
GC	Gas Chromatography
HPLC	High performance liquid chromatography
HRMS	High resolution mass spectrometry
HCo(CO) ₄	Cobalt tetracarbonyl hydride
[H ₂ Fe(CO) ₄]	Iron tetracarbonyl hydride
I-HF	Isomerizing Hydroformylation
ICI	Imperial Chemical Industries
ICP	Inductively coupled plasma
LiClO ₄	Lithium perchlorate
MeOH	Methanol
MP-AES	Microwave Plasma Atomic Emission Spectroscopy
NMP	1-Methyl-2-pyrrolidone

NSAID	Non-Steroidal Anti-Inflammatory Drug
Pd/C	Palladium on Charcoal
Pd(COD)Cl ₂	Dichloro(1,5 cyclooctadiene)palladium(II)
PCl ₃	Phosphorus Trichloride
[Rh(acac)(CO) ₂]	Dicarbonyl(acetylacetonato)rhodium(I)
[Ru ₃ (CO) ₁₂]	Triruthenium dodecacarbonyl
RuCl ₃	Ruthenium(III) chloride
Shvo's Catalyst	1-Hydroxytetraphenylcyclopentadienyl-(tetraphenyl-2,4-cyclopentadien-1-one)-μ-hydrotetracarbonyl diruthenium(II)
<i>t</i> -Bu Josiphos	(S)-1-[(R _P)-2-(Diphenylphosphino)ferrocenyl]ethyl-di-tertbutylphosphine
TEMPO	(2,2,6,6-Tetramethylpiperidin-1-yl)oxyl
TOF	Turnover frequency
TON	Turnover number
UCC	Union Carbide Corporation
XPS	X-ray photoelectron spectroscopy

PREFACE



Synopsis of the Thesis to be submitted to the Academy of Scientific and Innovative Research for Award of the Degree of Doctor of Philosophy in Chemistry

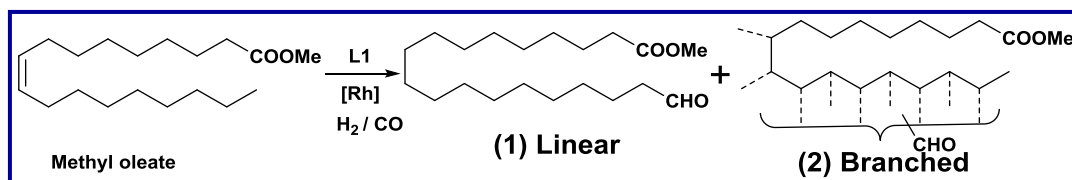
Name of the Candidate	Swechchha Pandey
Degree Enrolment No. & Date	Ph.D. in Chemical Sciences (10CC13J26012); January 2013
Title of the Thesis	Regioselective Rhodium Catalyzed Isomerizing Hydroformylation and Iron Catalyzed Hydroformylation of Alkenes and Plant Oils
Research Supervisor	Dr. Samir Chikkali

The thesis titled “Regioselective Rhodium Catalyzed Isomerizing Hydroformylation and Iron Catalyzed Hydroformylation of alkenes and Plant Oil” is divided into six different chapters. **Chapter-1** deals with detailed literature survey on the hydroformylation of olefins. Initial cobalt (Co) based catalysts to recent rhodium (Rh) based catalysts and its impact on hydroformylation process is discussed in great details.¹ Role of alternative transition metals (apart from Co and Rh) and earth abundant first row transition metal such as iron (Fe) in catalyzing hydroformylation is highlighted.² In addition to this, isomerizing hydroformylation of olefins, challenges associated with it and suitable ligand design to catalyze this process efficiently is presented. **Chapter-2** deals with the synthesis and characterization of a bulky bisphosphite ligand L1 and its application in isomerizing hydroformylation of long chain internal olefins such as methyl oleate. **Chapter-3** describes the methodology developed for the isomerizing hydroformylation of non edible plant oils such as cashew nut shell liquid (CNSL) and Methyl ricinoleate (derived from castor seeds). The iron catalyzed hydroformylation of olefins and the underlying mechanism is illustrated in **Chapter-4**. **Chapter-5** deals with the development of methodology for Fe catalyzed asymmetric hydroformylation of olefins. Chapter-6 concludes the work and provides future direction.

Chapter 2. Regioselective Isomerizing Hydroformylation of Long Chain Internal Olefins

Today’s chemical world rely mainly on fossils fuel resources. However due to depleting fossils fuel resources and consequently ever increasing prices of crude oil in global market, a sustainable alternative is highly desirable. The prime source of olefins today is crude oil, which needs a sustainable replacement. Plant oil derived fatty acids and cashew nut shell liquid can serve as an alternative as they are highly abundant and have characteristic long methylene sequence with an internal double bond. This internal double bond provides an excellent opportunity to further functionalize the plant oil to useful chemicals and materials. Therefore it has been a long cherished dream of organometallic chemists to isomerize the double bond to terminal position and

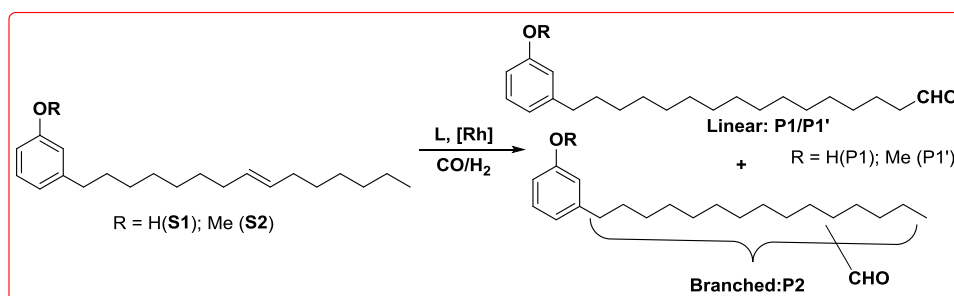
functionalize it selectively. However isomerization of internal double bond to terminal olefins is thermodynamically unfavorable which makes the terminal functionalization of plant oil a challenging transformation. In this chapter, synthesis of a bulky bisphosphite ligand L1 and its implication in isomerizing hydroformylation of plant oil derived methyl oleate with an unprecedented terminal selectivity of 75% is reported (Scheme 1).³ The formed linear aldehyde was isolated and further converted to hydroxy-acid (AB type) bifunctional molecule.



Scheme 1: Isomerizing hydroformylation of methyl oleate

Chapter 3. Isomerizing hydroformylation of non-edible plant oils

In this chapter, development of a methodology for isomerizing hydroformylation of cashew nut shell liquid is discussed. Under optimized reaction conditions, monoene derived from CNSL led to 28% terminal selective aldehyde (Scheme 2). When free –OH group of monoene was protected in the form of –OMe, the terminal selectivity improved to 50%. The isomerizing hydroformylation of crude cardanol was found to be highly selective and terminal selectivity as high as 74% was obtained under mild conditions.⁴ Thus various AB and AA type of difunctional molecules were synthesized starting from CNSL (Scheme 3).



Scheme 2. Isomerizing hydroformylation of monoene

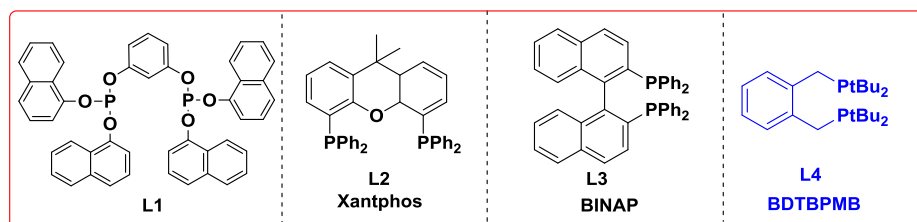
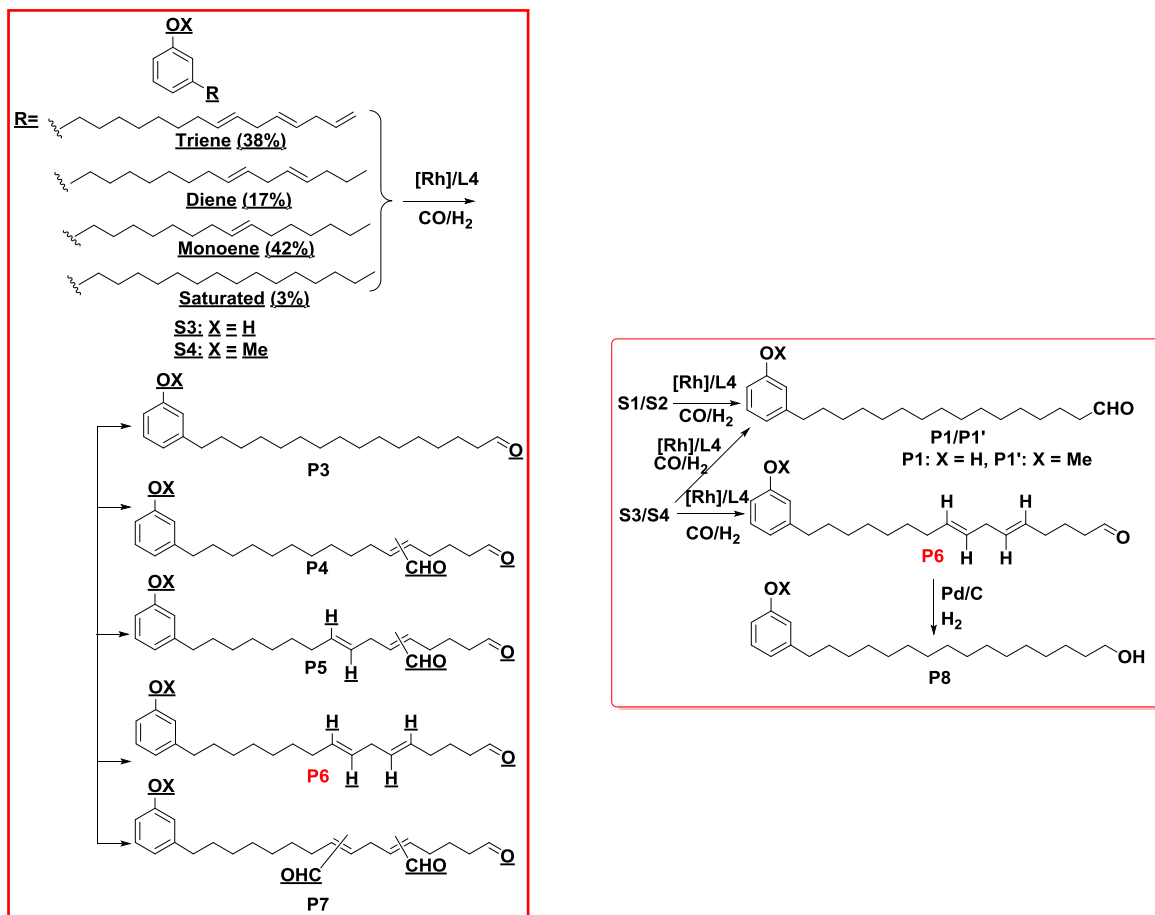


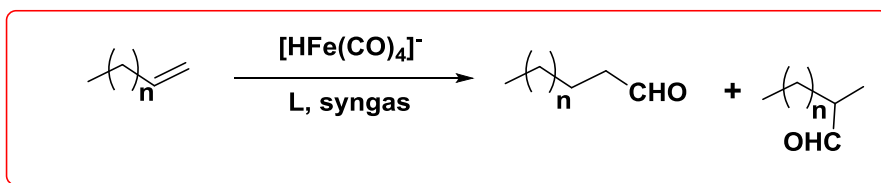
Figure 1: Ligands used for I-HF of CNSL



Scheme 3. Feedstock chemicals synthesized from isomerizing hydroformylation of CNSL

Chapter 4. Fe catalyzed hydroformylation of olefins under mild conditions: Evidence of an Fe (II) catalyzed process

Earth abundant, first row transition metals offer a cheap and sustainable alternative to the rare and precious metals. However, utilization of first row metals in catalysis requires harsh reaction conditions, suffers from limited activity, and fails to tolerate functional groups. In this chapter we report a highly efficient iron catalyzed hydroformylation of alkenes under mild conditions. This protocol operates at 10-30 bars syngas pressure below 100 °C, utilizes readily available ligands and applies to an array of olefins (Scheme 4).⁵ Thus, the iron precursor [HFe(CO)₄(Ph₃PNPPh₃)] (**1**) in the presence of triphenyl phosphine catalyzes the hydroformylation of linear alpha olefins as well as styrene and its derivatives. Remarkably, the addition of 1 mol% acetic acid promotes the reaction to completion within 16-24 hours. Detailed mechanistic investigations revealed *in-situ* formation of an iron-dihydride complex [H₂Fe(CO)₂(PPh₃)₂] (**A**) as an active catalytic species. This finding was further supported by cyclic voltammetry investigations and intermediacy of an Fe(0)-Fe(II) species was established. A mechanism based on an Fe(II) catalyzed hydroformylation of olefins is proposed (Figure 1). Identification of methyl heptanoate, derived from an iron-acyl intermediate (figure 1 D) further authenticates the mechanistic proposal. Thus, combined experimental and computational investigations support the existence of an iron-dihydride as the catalyst resting state, which then follows a Fe(II) based catalytic cycle to produce aldehyde and regenerates the di-hydride species A.



Scheme 4: Fe catalyzed hydroformylation of olefins

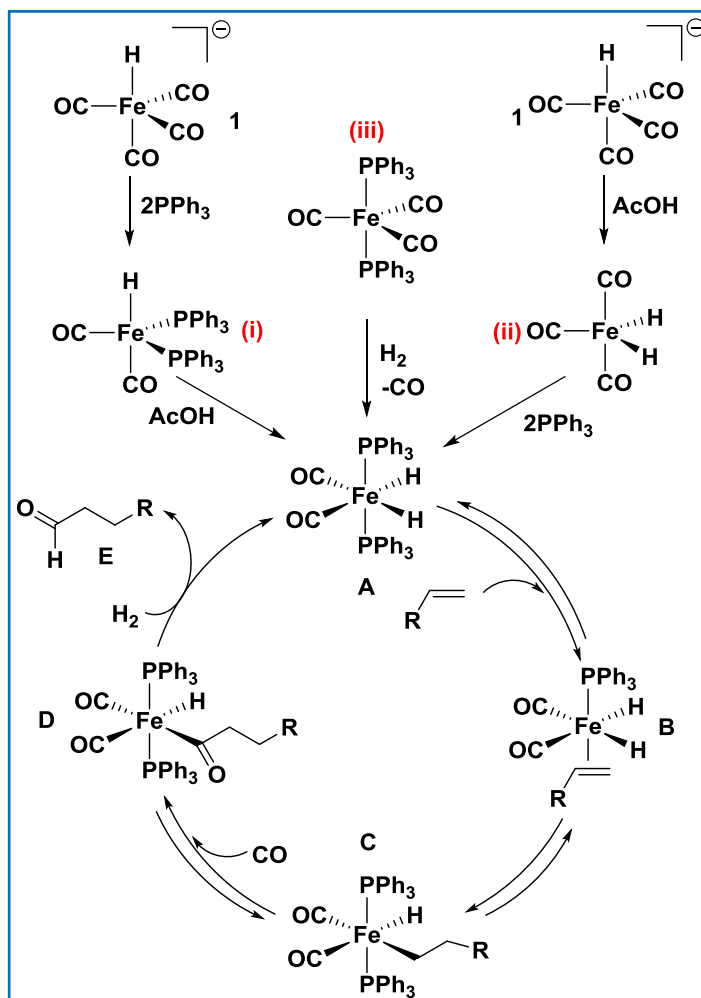
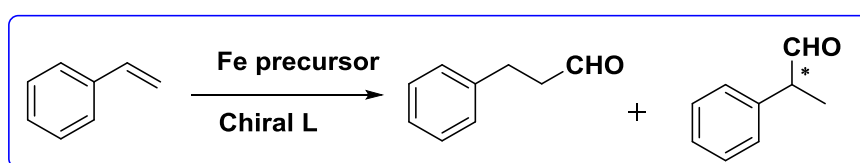


Figure 2: Proposed mechanistic cycle for Fe catalyzed hydroformylation of olefins

Chapter 5. Fe catalyzed asymmetric hydroformylation of olefins

An efficient methodology for Fe catalyzed asymmetric hydroformylation of prochiral olefins is discussed in this chapter. Synthesized Fe precursor (1) is treated with chiral bidentate ligands to induce chirality in formed aldehyde product (Scheme 5).



Scheme 5. Asymmetric hydroformylation of styrene using Fe complex

Chapter 6. Conclusions and outlook

This work summarizes the synthesis of a bulky bisphosphite ligand L1 which can be used for isomerizing hydroformylation of long chain internal olefins such as plant oils. Thus, isomerizing hydroformylation of plant oil derived methyl oleate using L1 led to 75% linear product. Isomerizing hydroformylation of non-edible plant oil derived cardanol using a bulky bisphosphine ligand yielded the formylated product with 74% selectivity to linear aldehyde. With the help of developed methodology various bifunctional molecules were synthesized and structurally characterized. Apart from use of renewable starting materials, use of earth abundant metals in catalysis is highly desirable. Hence, a methodology based on Fe catalyzed hydroformylation is discussed in great details. It has been found that a Fe (0) precursor $[\text{HFe}(\text{CO})_4]^-$ in presence of triphenyl phosphine catalyzes hydroformylation of an array of alkenes under mild conditions (10-30 bar, 100°C) to corresponding aldehydes. Further advancements in this area such as asymmetric hydroformylation has also been included.

References

- (1) For recent reviews on hydroformylation see: (a) Torres, G. M.; Frauenlob, R.; Franke, R.; Boerner, A. *Catal. Sci. Technol.* **2015**, *5*, 34-54. (b) Deng, Y.; Wang, H.; Sun, Y.; Wang, X. *ACS Catal.* **2015**, *5*, 6828-6837. (c) Chikkali, S. H.; van der Vlugt, J. I.; Reek, J. N. H. *Coord. Chem. Rev.* **2014**, *262*, 1-15. (d) Vilches-Herrera, M.; Domke, L.; Boerner, A. *ACS Catal.* **2014**, *4*, 1706-1724. (e) Franke, R.; Selent, D.; Boerner, A. *Chem. Rev.* **2012**, *112*, 5675-5732 and the references therein. (f) van Leeuwen, P. W. N. M.; Kamer, P. C. J.; Claver, C.; Pàmies, O.; Diéguez, M. *Chem. Rev.* **2011**, *111*, 2077-2118.
- (2) Pospech, J.; Fleischer, I.; Franke, R.; Buchholz, S.; Beller, M. *Angew. Chem. Int. Ed.* **2013**, *52*, 2852-2872.
- (3) Pandey, S.; Chikkali, S. H. *ChemCatChem* **2015**, *7*, 3468-3471.
- (4) Pandey, S.; Shinde D.; Chikkali, S. H. *ChemCatChem* **2017**, *9*, 3397-4004.
- (5) Pandey, S.; Vipinraj, K.; Shinde, D. R.; Vanka, K.; Kashyap, V.; Kurungot, S.; Vinod, C. P.; Chikkali, S. H. *J. Am. Chem. Soc.* **2018**, *140*, 4430-4439.

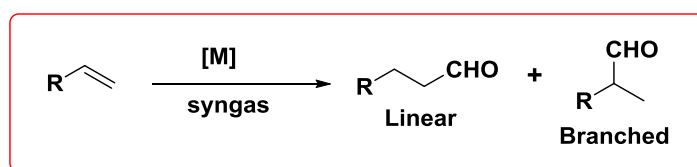
Chapter 1

Introduction

1.1: Introduction to Hydroformylation

1.1.1: Overview

Crude oil is rich in hydrocarbons. It would be quite interesting to functionalize the hydrocarbons obtained from petrochemical resources to increase their applicability. The functionalization is mainly concerned with introduction of oxygen into hydrocarbon chain. For this three methods are widely known: oxidation, carbonylation and hydroformylation. Out of these three, hydroformylation has gained significant attention due to its wider applicability in industrial settings. Hydroformylation, also known as oxo process, is a powerful synthetic tool to convert alkenes into aldehydes with perfect atom economy and valuable homologous aldehydes are generated using cheap syngas as one carbon source (**scheme 1.1**). It is considered as World's largest homogenous reaction catalyzed on an industrial scale and produces more than 12 million tons of oxo products per annum.^{1,2}



Scheme 1.1: General representation of a hydroformylation reaction

This process was accidentally discovered by German industrial chemist Professor Otto Roelen at Ruhrchemie in late 1930s when he was studying the Fischer-Tropsch reaction (syn-gas conversion to liquid fuels) using a heterogeneous cobalt catalyst.³ In a mechanistic experiment Roelen studied whether alkenes were intermediates in this process of syngas to fuel. He found that alkenes were converted to aldehydes or alcohols containing one more carbon atom. It took more than a decade before the reaction was taken further, but now it was considered as desired conversion of petrochemical hydrocarbons into oxygenates. Later on, it was concluded that the reaction was not catalysed by the heterogenous cobalt oxide supported over silica but in fact by homogenous $[\text{HCo}(\text{CO})_4]$ which was formed in the liquid state.⁴ The term hydroformylation was coined by Adkins.⁵

Hydroformylation is catalyzed by most of the late transition metals however most active catalysts involve Co, Rh, Ru, Pd and Pt as active metal center.^{1e,6}

1.1.2: Cobalt Catalyzed Hydroformylation

The original Ruhrchemie process involved cobalt tetracarbonyl hydride as catalyst to synthesize propanal starting with ethane. These reactions were performed at high temperature (150-180 °C) and high pressure (200-350 bar).⁷ Catalyst separation was a major difficulty in this case.

To overcome the limitations of original Ruhrchemie process and also to increase the substrate scope BASF developed an oxo process that relies on cobalt carbonyl based catalyst and uses mostly higher olefins. The reaction conditions used in this case were similar to Ruhrchemie process, however the recovery of cobalt from the reaction mixture was facilitated by its oxidation to water soluble Co^{2+} followed by the addition of aqueous formic or acetic acid.

Further modifications related to catalyst recovery was suggested in Exxon process, also known as, Kuhlmann oxo process.⁸ In order to recover the catalyst, an aqueous sodium hydroxide solution or sodium carbonate was added to the organic phase. The cobalt carbonyl hydride was recovered by extraction with olefin and neutralization of excess base by addition of sulfuric acid solution under carbon monoxide pressure.

In 1950s Shell introduced the use cobalt complexes modified with monodentate phosphine ligands for hydroformylation of C7-C14 olefins to get aldehydes which are directly hydrogenated in the reaction mixture to get detergent alcohols.⁹ C7-C14 olefins are mainly obtained either from wax cracker (mixture of internal and terminal olefins) or from the ethylene oligomerization process (internal olefins). Due to high isomerization activity offered by cobalt catalyst $[\text{HCo}(\text{CO})_4]$, this process is still preferred by industries to form long chain linear alcohols. Formed alcohols can easily be separated from catalyst by distillation. Due to use of phosphine ligands, the olefins could be hydroformylated at relatively milder conditions such as 40-80 bar syngas pressure and at temperature 150-180 °C.

The first and generally accepted mechanism for Co catalyzed hydroformylation was proposed by Heck and Breslow¹⁰ in 1961 starting with $[\text{HCo}(\text{CO})_4]$ as an active catalyst (**figure 1.1**). The $\text{Co}_2(\text{CO})_8$ first reacts with H_2 via a binuclear oxidative addition to give $[\text{HCo}(\text{CO})_4]$. Next, CO dissociation from metal generates the vacant sites (**A**) required for the alkene and H_2 . The first steps resemble hydrogenation in that an alkyl is formed by alkene insertion (**B & C**). Since at this stage there is no hydride on the metal, so instead of being trapped by reductive elimination with a hydride, as happens in hydrogenation, the alkyl undergoes a migratory insertion of CO to give the corresponding acyl complex (**D**). In the last step dihydrogen reacts with the acyl complex to form the aldehyde product (**E**) and to regenerate the starting complex hydrido cobalt carbonyl. In cobalt-catalysed hydroformylation the last step is often rate determining. In an alternative pathway, $[\text{HCo}(\text{CO})_4]$ can also cleave the acyl to give the aldehyde by a binuclear reductive elimination, but this is probably a minor pathway in the catalytic cycle.

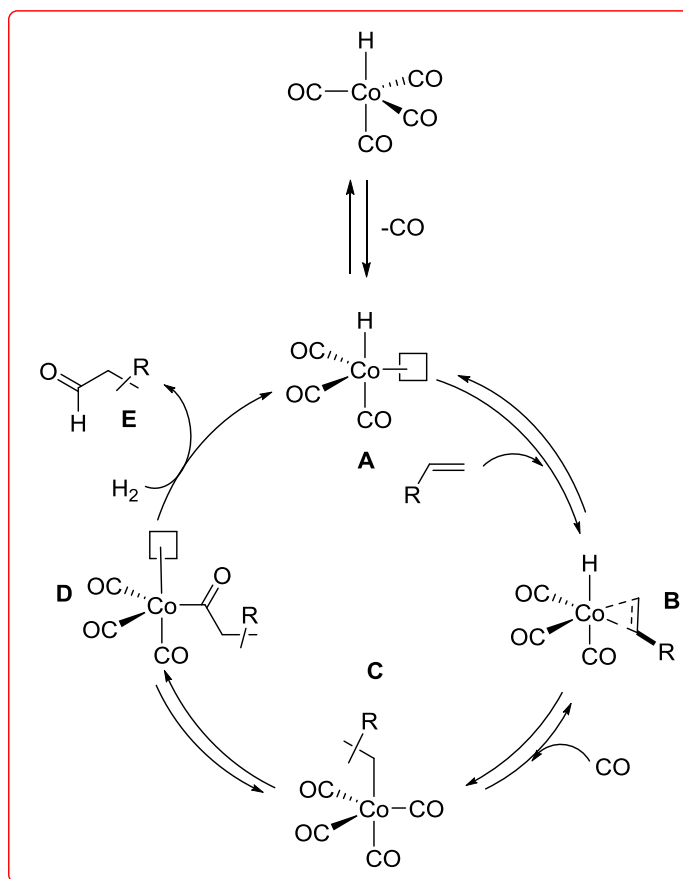


Figure 1.1: Heck and Breslow mechanism for Co catalyzed hydroformylation

The cobalt based processes suffer from low chemo and regioselectivity and significant amount of alkane formation was observed. The reaction conditions employed are very harsh in the presence of cobalt catalyst.

1.1.3: Rhodium Catalyzed Hydroformylation

The second generation of hydroformylation catalyst used rhodium as metal along with phosphine ligands. The first Rh catalyzed hydroformylation process was reported in 1974 by Celanese, followed by other companies such as UCC in 1976 and Mitsubishi Chemical Corporation in 1978. All of these processes used triphenylphosphine as ligand.¹¹ Rh based catalysts are not only more active than cobalt resulting in milder reaction conditions (10-60 bar, 80-135 °C) but also their atom economy is much better than cobalt based systems. Since the reaction could be performed at milder conditions, Rh based processes are often termed as low pressure oxo (LPO) process.¹² In the mid seventies Rh based catalyst started replacing Co based systems in case of hydroformylation of propene and butenes. For detergent alcohol production though, even today, the cobalt systems are preferred, because there is no good alternative yet for the hydroformylation of internal higher alkenes to mainly linear product.

The third generation of hydroformylation catalysts concerned mainly with the catalyst recovery and a biphasic system was developed in 1986 for hydroformylation of propene. This process is popularly known as Ruhrchemie or Rhone–Poulenc process in which Rh was in aqueous phase and substrate and product in the organic phase. A highly water soluble sulphonated triphenyl phosphine is used in this case.¹³ The two-phase process is not suitable for higher alkenes because of the low solubility of higher alkenes in water and the first-order dependency of the rate on alkene concentration.

Along with phosphines, phosphite ligands emerged as an alternative candidates for hydroformylation of higher olefins. Many bulky monoposphite (**figure 1.2**) and bisphosphites ligands were designed to get selective terminal product.¹⁴

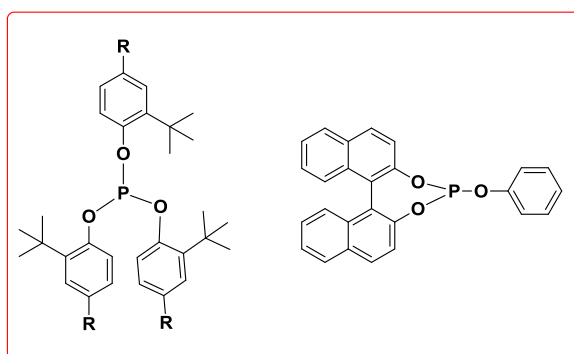


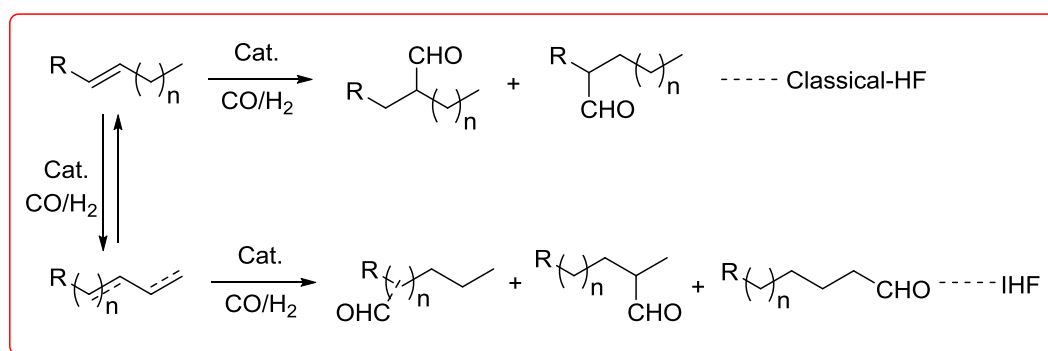
Figure 1.2: Typical examples of phosphite ligands

Apart from Co and Rh other late transition metals such as Ru is well explored in case of hydroformylation of olefins. Platinum and palladium based catalysts have been studied and the results of the Pd catalyzed hydroformylation seem very promising in the presence of basic bidentate phosphine ligand and acid co-catalyst.¹⁵ Platinum has been known for many years to have a high preference for the formation of linear products, but ligand decomposition hampers applications.¹⁶ First row transition metal such as Fe has also been used to carry out this important transformation, however the reports dealing with iron are very primitive (detailed discussion is given in chapter 4).

1.2: Challenges and Opportunities

One of the key issue in hydroformylation process is the regioselectivity for the formed aldehydes. As it is evident from previous section that hydroformylation process generates two types of aldehyde : linear and branched. Both of these products have different commercial applications. In general, the linear aldehydes are the desired species due to their potential consecutive chemistry. For example, the aldehydes can be oxidized to corresponding acids or hydrogenated to the alcohols which are valuable starting materials for synthesis of polymer plasticizers.¹⁷ When

terminal olefin is used as substrate, linear aldehyde is obtained in a highly selective manner. But it would be extremely advantageous to utilize mixtures of linear monounsaturated olefins (for example, raffinate I–III, mixture of positional and geometrical isomers) to directly produce the same terminal aliphatic aldehyde. If an internal olefin is used as a substrate, the process is termed as isomerizing hydroformylation (**scheme 1.2**), since it involves two different transformations, isomerization and hydroformylation.



Scheme 1.2: Hydroformylation vs isomerizing hydroformylation

In tandem isomerization and hydroformylation reactions,¹⁸ migration generally proceeds through an alkyl mechanism (hydride mechanism) and terminal selectivity can be obtained if the catalyst meets the following criteria (**figure 1.3**):

- 1) The isomerization of an internal olefin to a terminal olefin should be faster than the hydroformylation event.
- 2) The rate of terminal formylation should be faster than the rate of internal formylation.
- 3) The catalyst should be selective towards terminal formylation.

In case of isomerizing hydroformylation mainly two types of phosphorus ligands are used: phosphines & phosphites, apart from few random attempts. Out of these two, phosphites are preferred over phosphines because of two reasons:

- 1) It is more economical to synthesize a P-O bond than a P-C bond as phosphites can easily be synthesized from PCl_3 and alcohol. They are not as sensitive as phosphines to air although they can hydrolyze in presence of moisture.
- 2) They generate an electronic asymmetry around the metal center as they are σ -donor as well as π - acceptor, unlike phosphines that are mainly σ -donor. Electronic asymmetry around metal center may result in a better discrimination between the various internal olefins and the terminal olefin and might led to increased rate of isomerizing hydroformylation.

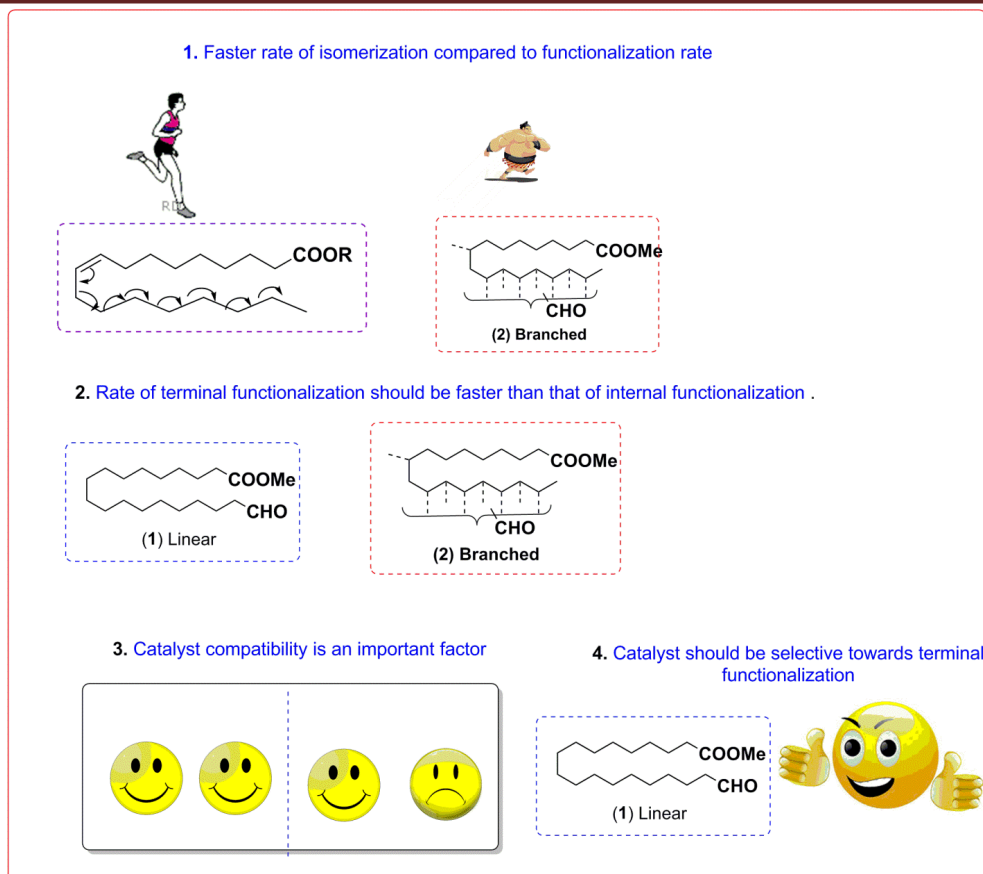
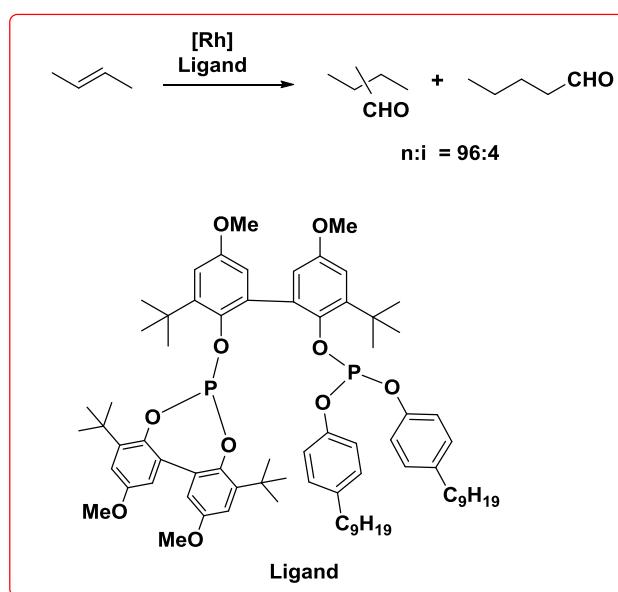


Figure 1.3: Challenges in isomerizing hydroformylation

The first example of Rh catalyzed isomerizing hydroformylation of internal olefin to terminal aldehyde was reported as early as 1987 by Billig and co workers¹⁹ with excellent selectivities (n:i = 96:4) in case of isomerizing hydroformylation of 2-butene by using a chelating but sterically demanding bisphosphite ligand (**scheme 1.3**).



Scheme 1.3: First report of isomerizing hydroformylation

However, due to the complex structure of ligand, it was very difficult to synthesize. These ligands are thermally unstable and get decomposed over the time.

Subsequent investigation indicate that sterically demanding bisphosphite ligands or in some case phosphine ligands provide better terminal selectivity. Later on Beller et.al.²⁰ used a dual catalytic approach to systematically investigate the olefin isomerization under hydroformylation conditions. They first tested the activity of rhodium (III) acetate (0.01 mol%) in the presence of 100 equiv. triphenylphosphane, a well-known and common hydroformylation catalyst and observed the formation of pentanal with n:i = 73:27 starting with 1-butene (Entry 1, **table 1.1**). However the catalytic activity dropped drastically (by a factor of 10) when 2-butene was used as a substrate (n:i = 7:93, entry 2).

Table 1.1: Isomerizing hydroformylation of 2- butene^a

Entry	Substrate	Ligand	L/Rh	[Ru ₃ (CO) ₁₂ (mol %)]	Conversion (%)	n/i	TOF (h ⁻¹)
01.	1-butene	PPh ₃	100:1	-----	96	73:27	48000
02.	2-butene	PPh ₃	100:1	-----	10	7:93	5000
03.	2-butene	PPh ₃	100:1	0.03	77	4:96	1500
04.	2-butene	L2	5:1	-----	10	1:99	400
05.	2-butene	L2	5:1	0.5	10	56:44	2000
06.	2-butene	L2	----	0.5	<5	66:43	0.6

^aConditions: Temp.: 120 °C, Syngas: 48 bar (CO/H₂, 1:1); catalyst : 0.01 mol% Rh (III) acetate (3 h activation under same conditions).

Use of [Ru₃(CO)₁₂] as an isomerizing agent improved the total conversion with little improvement in n/i ratio (entry 3). This can be explained by the fact that use of a large excess of ligand (100 eq.) suppresses the activity of co-catalyst. In the absence of ligand, the rhodium catalyst afforded a nearly 1:1 mixture of linear and branched aldehyde, regardless of the starting olefin. This observation suggested the use of chelating phosphine phosphite ligand L2 (**figure 1.5**) which reacts with 1-butene with much higher reaction rate (tof 15800 h⁻¹) making it a better hydroformylation catalyst for terminal olefins compared to Rh/PPh₃ system. However, the use of a ruthenium (0) carbonyl species leads to a fast equilibration of 2-butene to give a mixture of E/Z-2-butene (95%) and 1-butene (5%). This olefinic mixture gives significantly higher n:i ratios (56:44, entry 5) in the hydroformylation reaction than does the reaction of the internal olefin with unmodified rhodium. Control experiment suggests the role of ruthenium (0) carbonyl as an isomerizing agent (entry 6) as no significant oxo products could be detected in the absence of Rh precursor. Although phosphite based ligands were active enough to give the linear oxo products in case of isomerizing hydroformylation of internal olefins, their long term stability was very low.

Studies by Casey and co-workers revealed high selectivities towards linear aldehydes can be obtained with rigid diphosphanes with chelate bite angles close to 120° .²¹

In view of this Piet Van Leeuwen and co-workers described the synthesis of new dibenzophospholyl and phenoxaphosphanyl-substituted xanthene ligands L3 and L4, and their high activity and selectivity in the rhodium catalyzed isomerizing hydroformylation of internal olefins (**table 1.2**) such as trans-2-octene and trans-4-octene.²²

Table 1.2: Isomerizing hydroformylation of internal octenes^a

Entry	Substrate	Ligand	L/Rh	Conversion (%)	n/i	1-nonanal (%)	TOF (h ⁻¹)
01.	2-octene	PPh ₃	10:1	8.5	0.9	46	39
02.	2-octene	L3	10:1	10	9.5	90	65
03.	2-octene	L4	10:1	22	9.2	90	112
04.	4-octene	PPh ₃	10:1	9	0.3	23	2.4
05.	4-octene	L3	10:1	54	6.1	86	15
06.	4-octene	L4	10:1	67	4.4	81	20

^aConditions: Solvent = toluene, Temp. = 80 °C under an atmosphere of CO/H₂ (1:1) with an initial pressure of 20 bar, catalyst precursor: [Rh(CO)₂(dipivaloylmethanoate)], [Rh].1.0 mm, Rh:P:1-octene.1:10:673.

In general, the regioselectivity of the hydroformylation is influenced by π - acceptor and σ -donor properties of the respective ligand. Higher regioselectivity is obtained with ligands that possess strong π -acceptor and weak σ -donor properties.²³ Investigations based on the CO stretching frequencies and ³¹P NMR chemical shifts in RhCl(CO)L complexes show the high π -acceptor character of 1-pyrrolylphosphanes²⁴ compared to phosphanes and even phosphites (**figure 1.4**) and can significantly yield n-selective product when employed in hydroformylation of terminal olefins such as 1-hexene.²⁵

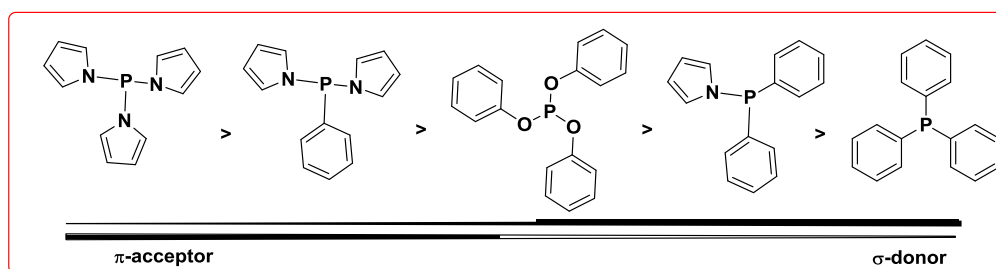


Figure 1.4: π -acceptor and σ -donor properties of different P ligands

In view of this Beller and co-workers synthesized several novel substituted pyrrole phosphine ligands and investigated their catalytic activities in isomerizing hydroformylation of internal olefins for the first time.²⁶ A ligand with increased π -acidity was proved to be the best ligand for isomerizing hydroformylation of 2-pentene. The best n/iso ratios of about 60:40 were obtained at

low synthesis gas pressure (10 bar) in the presence of the simple P(pyrrolyl)₃ ligand (L5 and L6, **figure 1.5**).

Later on good yield and excellent regioselectivities were obtained using binaphthyl substituted Naphos ligand and its derivatives (IPHOS L7 and L8, **figure 1.5**) for isomerizing hydroformylation of various internal olefins.²⁷ They developed a simple and general strategy for the synthesis of NAPHOS derivatives (mainly fluorinated substituents). In general, such electron deficient substituents in aryl diphosphanes (with large bite angles) have a positive effect on the activity and the linear : branched selectivity of hydroformylation catalysts.²⁸ This can be explained by a preference for the diequatorial over the equatorial– apical binding mode of the ligand²⁹ and hence excellent regioselectivities were obtained in case of 2-pentene, 2-butene, 2-octene and further challenging trans-4-octene.

Because of the high reactivity several novel phosphites have been synthesized. Boerner and co-workers³⁰ synthesized an acylphosphite ligand (L9 and L10) and impressively demonstrated, for the first time, the possibility of mainly n-selective isomerizing hydroformylation of long-chain internal octenes through rhodium compounds.

In 2003, Behr et.al reported synthesis of n-nonanal by a consecutive isomerization–hydroformylation reaction of trans-4-octene using a homogeneous catalyst system consisting of [Rh(acac)(CO)₂] and BIPHEPHOS (L11, **figure 1.5**). In the presence of syngas these two precursor molecules form the catalytically active species *in-situ*. At a reaction temperature of 125 °C and a syngas pressure of 20 bar the linear C9-aldehyde is formed in 88% yield and only little amount of the saturated hydrocarbon and the branched C9-aldehydes was detected.³¹ Later on in 2005 same group revisited this important transformation³² using trans-4-octene as a substrate and an improved terminal selectivity of upto 90 % was reported using thermomorphic multicomponent solvent (TMS) system comprised of propylene carbonate/dodecane/p-xylene. Catalyst recovery was one of the important features of this report in which product separation was achieved with application of a thermomorphic multi-solvent catalytic reaction system which changes from a two-phase to a single-phase system by simply raising the temperature. Here propylene carbonate was used as a polar phase or catalyst phase and n-dodecane was used as non-polar or substrate-product phase. A solvent of medium polarity for eg. p-xylene was used as solvent mediator. At a reaction temperature of 80 °C these systems led to the formation of single phase system for catalysis and again after lowering the temperature to 25 °C, two distinct phases were observed. Selectivity to n-nonanal was found to be dependent on concentration of propylene carbonate. This can be attributed to strong electronic impact of three electron withdrawing oxygen atoms to the β-hydride atoms of σ-Rh complex. This interaction can possibly weaken the C-H bond and hydride can be easily transferred to metal and thereby increasing the rate of isomerization.

Although this system was designed to recover the catalyst and also was successful to some extent but these systems are far from being applicable to an industrial scale as a strong Rh leaching (47%) was observed from ICP analysis. Higher the concentration of solvent mediator (p-xylene), higher Rh leaching was observed. Hence a careful selection of solvent mediator is required to make these systems an industrially relevant one in terms of catalyst recycling.

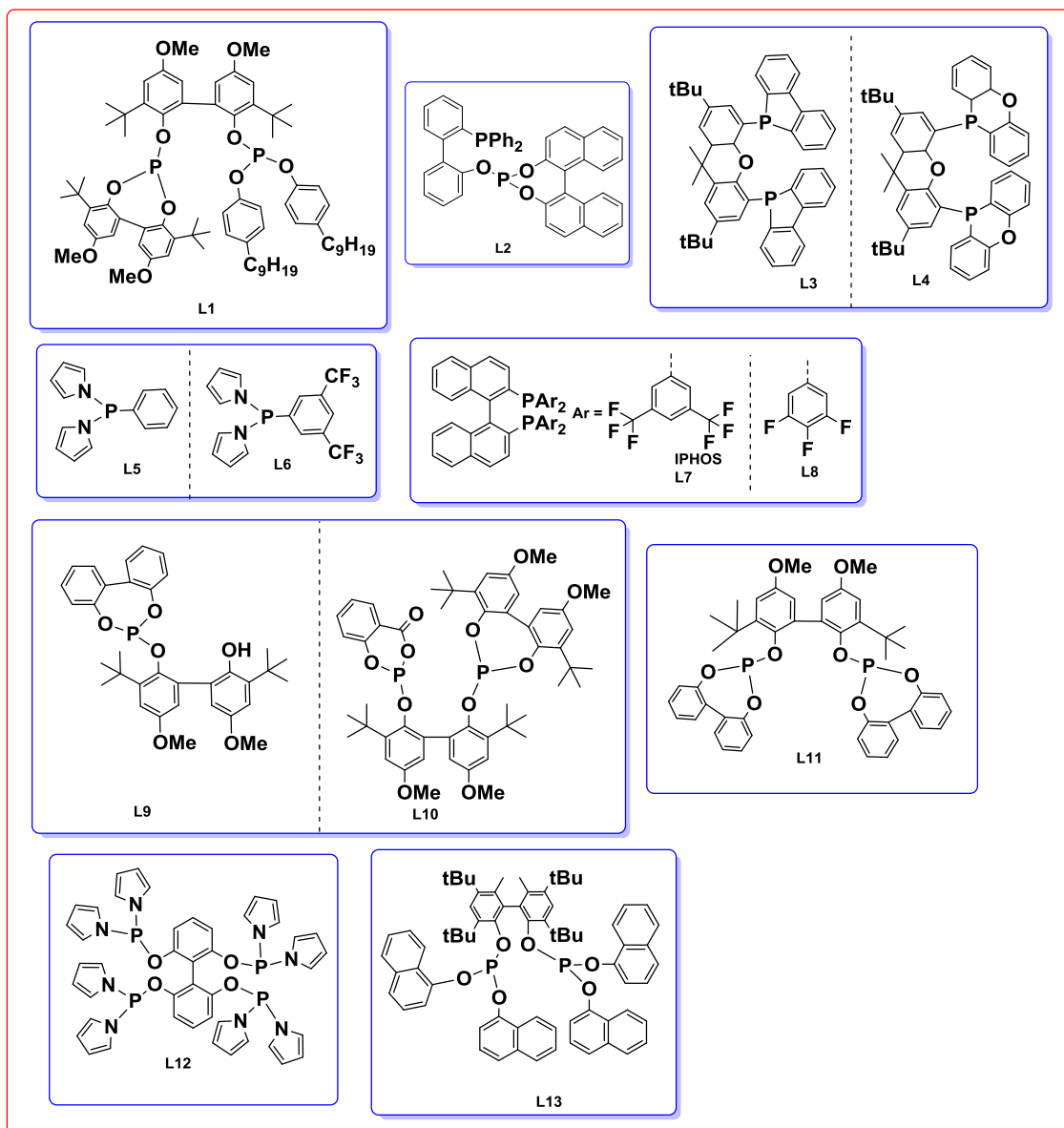


Figure 1.5: Typical ligands used in isomerizing hydroformylation

Zhang and co-workers reported the design and synthesis of a conceptually new pyrrole based tetraphosphorus ligand (L12) with enhanced chelating ability for the regioselective homogeneous isomerizing-hydroformylation of internal olefins (**table 1.3**).³³ Zhang's catalyst was proved to be the most active catalyst for 2-olefins.

Table 1.3: Isomerizing HF of various internal olefins catalyzed by tetraphosphorus ligand L12.^a

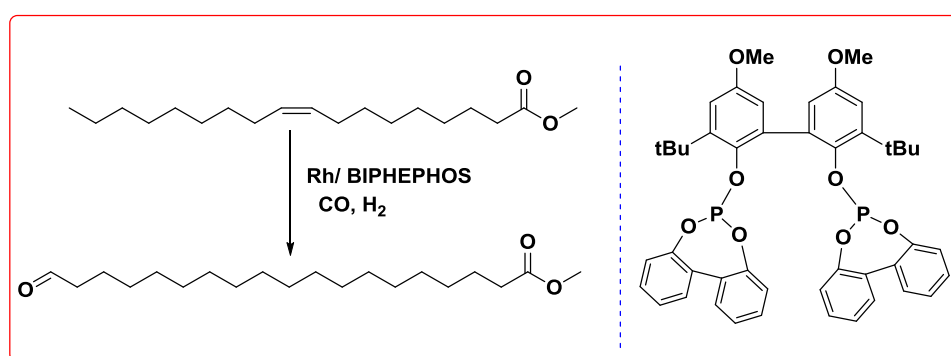
Entry	Substrate	Temperature (°C)	Pressure (Bar)	Time (h)	n/i	Linear (%)	TOF (h ⁻¹)
01.	2-octene	100	5	1	51.7	98.1	1500
02.	2-octene	100	5	12	38	97.4	642
03.	2-hexene	100	5	1	80.6	98.8	2300
04.	2-hexene	100	5	12	56	98.2	500

^aConditions: Solvent = Toluene, S/C = 10000, [Rh] = 0.69 mM (for 2-hexene) and 0.57 mM (for 2-octene), ligand/Rh = 3:1, linear to branched ratio was determined by GC.

Hydroformylated product was not observed within one hour when trans-4-octene was used as a substrate possibly due to slow rate of isomerization and large steric bulk associated with the ligand. Among 2-olefins also n/i ratio was better in 2-hexene compared to that of 2-octene. The possible explanation could be presence of more amount of 1-hexene in statistical mixture at equilibrium as compared to 2-octene since number of internal isomers will be less in 2-hexene.

The protocol of isomerizing hydroformylation is well documented for terminal as well as short-chain internal olefins such as 2-octene, 3-octene, 4-octene³⁴ etc but in case of long chain fatty acid esters catalyst suffers from poor reactivity as well as selectivity. There are only two reports in the public literature where long chain fatty acid esters are successfully converted to linear α - ω difunctional compounds following isomerizing hydroformylation.

In 2005 Behr *et.al.*³⁵ demonstrated that the isomerizing hydroformylation of methyl oleate can be performed at relatively low temperature and syngas pressure (**scheme 1.4**). The best yield obtained in case of oleic acid ester was 26%. Chelating bisphosphite ligand BIPHEPHOS with rhodium precursor ($[\text{Rh}(\text{acac})(\text{CO})_2]$) in-situ generated the active species which was responsible for above selectivity. Hydrogenation is believed to be the major side reaction in that case.

**Scheme 1.4:** Isomerizing hydroformylation of methyl oleate using chelating bisphosphite ligand

The same trend was observed by Nozaki and co-workers in 2013.³⁶ They developed a tandem isomerization-hydroformylation-hydrogenation sequence using ternary catalyst system for methyl oleate (**figure 1.6**).

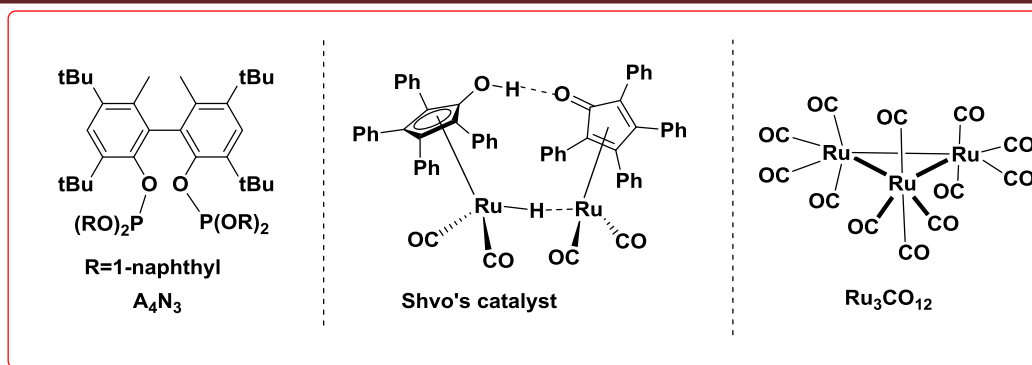


Figure 1.6: Catalyst components used by Nozaki *et.al*

The best yield in favor of linear alcohol from methyl oleate was 53%. Conversion of internal olefins to terminal alcohols was obtained in a tandem isomerization-hydroformylation-hydrogenation sequence by applying a rhodium/bisphosphite and Ru based Shvo's catalyst. From control experiments the co-existence of Shvo's catalyst and Rh(I) was found to be essential. Rh/bisphosphite system was required for isomerizing hydroformylation and Ru based Shvo's catalyst was necessary to convert the generated aldehyde into alcohols. Along with hydrogenation of aldehydes Shvo's catalyst was also involved in increasing the rate of isomerization. In case of methyl oleate (double bond 9 carbon away from terminal position) another isomerizing component $[\text{Ru}_3(\text{CO})_{12}]$ was added to facilitate the isomerization.

In general, there could be two possible ways to promote renewable science. Utilization of plant oils to feedstock chemicals would be one of the sustainable approaches (as discussed in previous section). The second approach would be replacement of rare and precious transition metals with earth abundant first row transition metals. For e.g. Hydroformylation of olefins is mainly catalyzed by noble Rh metal and its extensive utilization in catalytic converter of automobile exhaust limits its usage elsewhere. This is directly reflected in its cost (**table 1.4**). Fe is an earth abundant first row transition metal and much cheaper than Co and Rh. Hence utilization of Fe as an active metal in hydroformylation of olefins would be really advantageous and would certainly provide new dimensions towards a sustainable future. However use of Fe in hydroformylation is largely missing and this second approach is rarely reported.

Table 1.4: Comparison of cost of Fe with Co and Rh

S. No.	Metals	Cost (USD/Kg)
01.	Co	38.074
02.	Rh	27,218.37
03.	Fe	0.0643

1.3: Setting the Goals

The past decade has witnessed significant advancements in the field of isomerizing hydroformylation of olefins and several ligands have been designed and implemented to achieve great success in case of I-HF of short chain olefins. However in case of isomerizing hydroformylation of long chain internal olefins such as methyl oleate, there are very few reports, and highest selectivity for terminal aldehyde is reported to be 26% only. Therefore, there is an immense need of design and development of new ligands to catalyze the isomerizing hydroformylation of methyl oleate in highly selective manner and to deliver the highest terminal selectivity.

Thus, the aim of this work is to rationally design a bisphosphorus ligand and to develop an efficient methodology for isomerizing hydroformylation of long chain internal olefins (**figure 1.7**). For this type of transformations bisphosphite and in some case bisphosphines are the most suitable candidates, hence new bisphosphite ligands will be designed with a rigid backbone in order to obtain fixed bite angle which is needed to achieve high linear selectivity. An attempt will be made to understand the coordination behavior of these ligands around Rh.

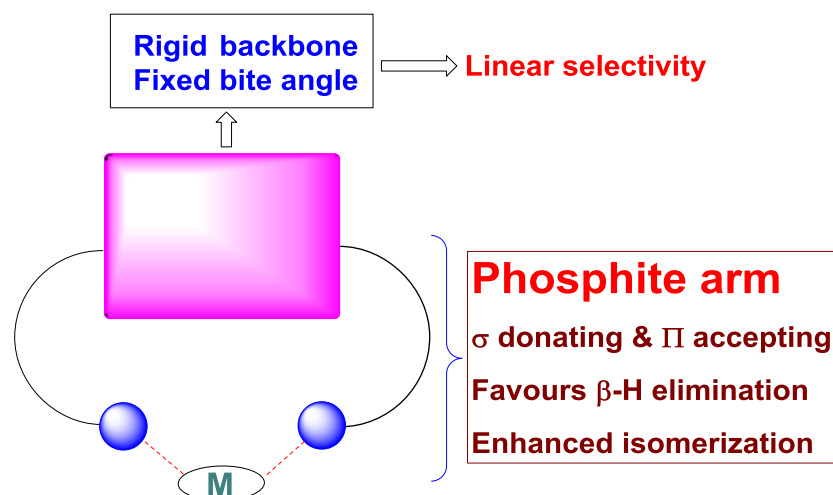


Figure 1.7: Rational designing of ligand

Three new bisphosphorus ligands are proposed with varying steric parameters (**figure 1.8**). Out of which L2 and L3 were found to be highly unstable.

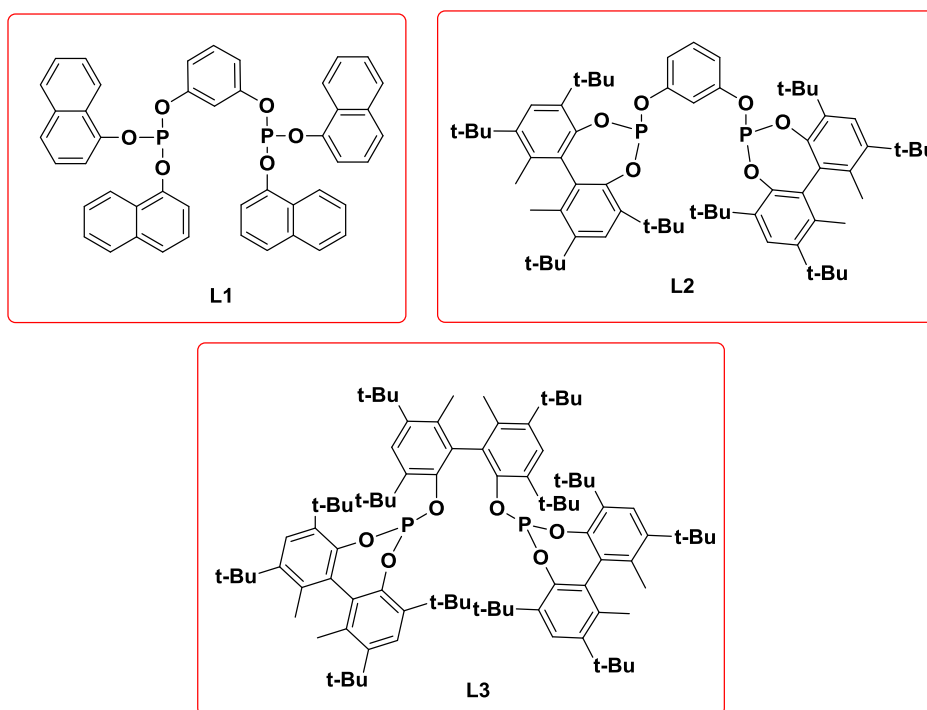


Figure 1.8: Bisphosphite ligands

Although the renewable resources such as plant oils are highly abundant but methyl oleate falls under the category of edible plant oils. Hence the next objective of this work will be to develop an efficient methodology for non-edible plant oils such as cashew nut shell liquid to avoid direct competition with food chain.

Since renewability is the main theme of present work, various renewable substrates will be utilized for I-HF. Another approach of looking at renewability is replacement of noble metals with earth abundant transition metals. Less natural abundance of Rh imposes economical constraints to the existing methodology of hydroformylation of olefins. Hence an efficient hydroformylation methodology using abundant and cheap alternate metal is highly desirable. An iron catalyzed hydroformylation will be attempted. Efforts will be made to understand the mechanism and various other aspects of this industrially relevant transformation.

In short, the goal of the present study is, 1) to synthesize novel bidentate phosphorus ligand and utilize them for isomerizing hydroformylation of long chain internal olefins, 2) to develop an efficient methodology for isomerizing hydroformylation of non-edible plant oils to synthesize various feedstock chemicals, 3) to replace the noble metal Rh used in hydroformylation with earth abundant Fe, 4) to understand modus operandi of Fe catalyzed hydroformylation.

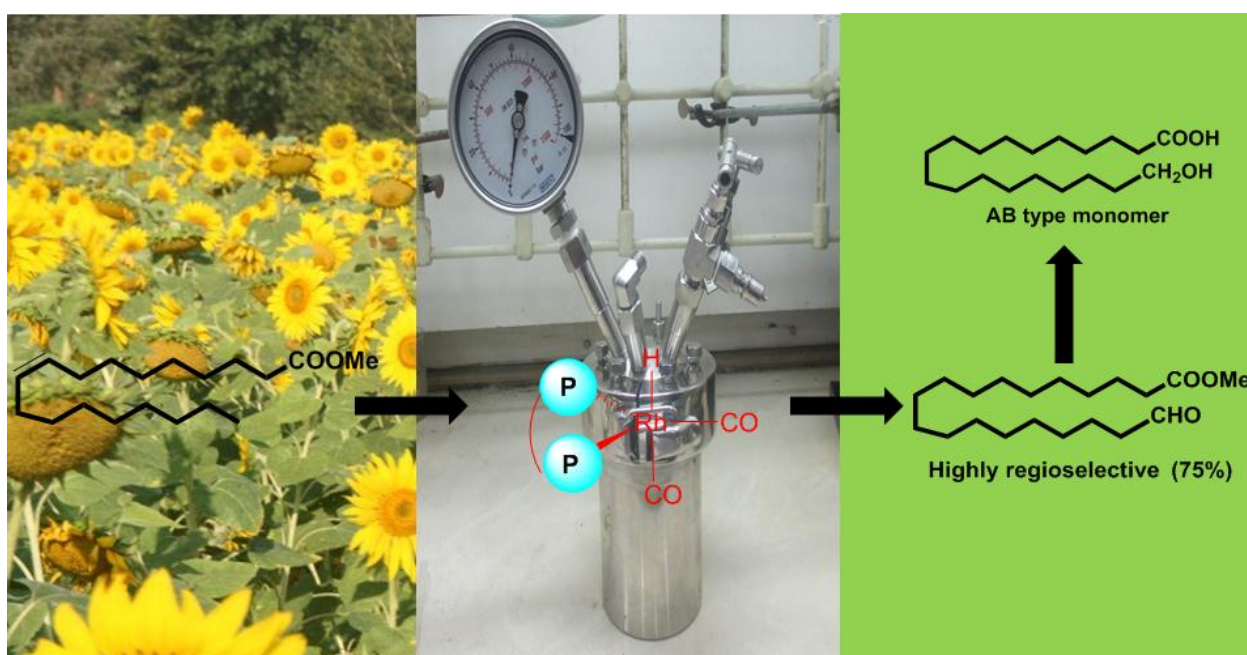
1.4: References

1. For recent reviews on hydroformylation see: (a) Torres, G. M.; Frauenlob, R.; Franke, R.; Boerner, A. *Catal. Sci. Technol.* **2015**, *5*, 34-54. (b) Deng, Y.; Wang, H.; Sun, Y.; Wang, X. *ACS Catal.* **2015**, *5*, 6828-6837. (c) Chikkali, S. H.; van der Vlugt, J. I.; Reek, J. N. H. *Coord. Chem. Rev.* **2014**, *262*, 1-15. (d) Franke, R.; Selent, D.; Boerner, A. *Chem. Rev.* **2012**, *112*, 5675-5732 and the references therein. (e) van Leeuwen, P. W. N. M.; Kamer, P. C. J.; Claver, C.; Pàmies, O.; Diéguez, M. *Chem. Rev.* **2011**, *111*, 2077-2118.
2. Kaemper, A.; Kucmierczyk, P.; Seidensticker, T.; Vorholt, A. J.; Franke, R.; Behr, A. *Catal. Sci. Technol.* **2016**, *6*, 8072-8079.
3. a) Roelen, O. . DRP 849548, 1938. (b) Henrici-Olive, G.; Olive, S. *J. Mol. Catal.* **1978**, *3*, 443-446.
4. Wender, I.; Orchin, M.; Storch, H. H. *J. Am. Chem. Soc.* **1950**, *72*, 4842-4843.
5. Adkins, H.; Krsek, G. *J. Am. Chem. Soc.* **1948**, *70*, 383-386.
6. Pospesch, J.; Fleischer, I.; Franke, R.; Buchholz, S.; Beller, M. *Angew. Chem. Int. Ed.* **2013**, *52*, 2852-2872. (b) Evans, D.; Osborn, J. A.; Wilkinson, G. *J. Chem. Soc. A*, **1968**, 3133-3142.
7. (a) Duembgen, G.; Neubauer, D. *Chem. Ing. Tech.* **1969**, *41*, 974-980. (b) Bohnen, H. W.; Cornils, B. *Advances in Catalysis*, Vol. 47, Academic Press, New York, 2002, pp. 1-64.
8. van Leeuwen, P. W. N. M. *Homogeneous Catalysis: Understanding the Art*; Kluwer Academic Publishers: Dordrecht, The Netherlands, 2004, pp 125–174.
9. Lutz, E. F. *J. Chem. Educ.* **1986**, *63*, 202-203.
10. Heck, R. F.; Breslow, D. S. *J. Am. Chem. Soc.* **1961**, *83*, 4023–4027.
11. Bohnen, H. W.; Cornils, B. *Adv. Synth. Catal.* **2002**, *47*, 1-64.
12. Claver, C.; van Leeuwen P. W. N. M. *Rhodium Catalyzed Hydroformylation*, Springer, Berlin, 2008 and the references therein.
13. Hermann, A. W.; Kohlpaintner, C. W. *Angew. Chem. Int. Ed.* **1993**, *32*, 1524-1544.
14. (a) van Leeuwen, P. W. N. M.; Roobeek, C. F. *J. Organometal. Chem.* **1983**, *258*, 343-350; Brit. Pat. 2,068, 377, US Pat. 4, 467,116 (to Shell Oil); *Chem. Abstr.* **1984**, *101*, 191142. (b) Jongasma, T.; Challa, G.; van Leeuwen, P. W. N. M. *J. Organometal. Chem.* **1991**, *421*, 121-128. (c) van Rooy, A.; Orij, E. N.; Kamer, P. C. J.; van Leeuwen, P. W. N. M. *Organometallics*, **1995**, *14*, 34-43.
15. (a) Klein, H.; Jackstell, R.; Wiese, K.-D.; Borgmann, C.; Beller, M. *Angew. Chem.* **2001**, *113*, 3505 – 3508; *Angew. Chem. Int. Ed.* **2001**, *40*, 3408 – 3411. (b) Bronger, R. P. J.; Kamer, P. C. J.; van Leeuwen, P.W. N. M. *Organometallics*, **2003**, *22*, 5358 –5369. (c) Jennerjahn, R.; Piras, I.; Jackstell, R.; Franke, R.; Wiese, K.-D.; Beller, M. *Chem. Eur. J.* **2009**, *15*, 6383 – 6388.

16. (a) Meessen, P.; Vogt, D.; Keim, W.; *J. Organomet. Chem.* **1998**, *551*, 165 – 170. (b) Kawabata, Y.; Hayashi, T.; Ogata, I.; *J. Chem. Soc. Chem. Commun.* **1979**, 462 – 463.
17. (a) Commereuc, D.; Chauvin, Y.; Gaillard, J.; Leonard, J.; Andrews, J. *Hydrocarbon processing* **1984**, *63*, 118-120. (b) Beller, M.; Cornils, B.; Frohning, C. D.; Kohlpaintner, C. W. *J. Mol. Catal. A: Chem.* **1995**, *104*, 17-85. (c) Bauer, K.; Garbe, D.; Surburg, H. *Common fragrance and flavor materials : preparation, properties and uses*; John Wiley & Sons, 2006.
18. Vilches-Herrera, M.; Domke, L.; Borner, A. *ACS Catal.* **2014**, *4*, 1706-1724.
19. Billig, E.; Abatjoglou, A. G.; Bryant, D. R. *Chem. Abstr.* **1987**, *107*, 7392.
20. Beller, M.; Zimmermann, B.; Geissler, H. *Chem. Eur. J.* **1999**, *5*, 1301-1305.
21. (a) Casey, C. P.; Whiteker, G. T.; Melville, M. G.; Petrovich, L. M.; Gavney, J. A.; Powell, D. R. *J. Am. Chem. Soc.* **1992**, *114*, 5535-5543. (b) Casey, C. P.; Petrovich, L. M. *J. Am. Chem. Soc.* **1995**, *117*, 6007-6014.
22. van der Veen, L. A.; Kamer, P. C. J.; van Leeuwen, P. W. N. M. *Angew. Chem. Int. Ed.* **1999**, *38*, 336-338.
23. Grimblot, J.; Bonnelle, J. P.; Vaccher, C.; Mortreux, A.; Petit, F.; Peiffer, G. *J. Mol. Catal.* **1980**, *9*, 357-368.
24. Moloy, K. G.; Petersen, J. L. *J. Am. Chem. Soc.* **1995**, *117*, 7696-7710.
25. M. Trzeciak, A.; Glowiak, T.; Grzybek, R.; J. Ziolkowski, J. *J. Chem. Soc., Dalton Trans.* **1997**, 1831-1838.
26. Jackstell, R.; Klein, H.; Beller, M.; Wiese, K.-D.; Röttger, D. *Eur. J. Org.* **2001**, *2001*, 3871-3877.
27. Klein, H.; Jackstell, R.; Wiese, K.-D.; Borgmann, C.; Beller, M. *Angew. Chem. Int. Ed.* **2001**, *40*, 3408-3411.
28. Casey, C. P.; Paulsen, E. L.; Beuttenmueller, E. W.; Proft, B. R.; Petrovich, L. M.; Matter, B. A.; Powell, D. R. *J. Am. Chem. Soc.* **1997**, *119*, 11817-11825.
29. van der Veen, L. A.; Boele, M. D. K.; Bregman, F. R.; Kamer, P. C. J.; van Leeuwen, P. W. N. M.; Goubitz, K.; Fraanje, J.; Schenk, H.; Bo, C. *J. Am. Chem. Soc.* **1998**, *120*, 11616-11626.
30. Selent, D.; Hess, D.; Wiese, K.-D.; Röttger, D.; Kunze, C.; Borner, A. *Angew. Chem. Int. Ed.* **2001**, *40*, 1696-1698.
31. Behr, A.; Obst, D.; Schulte, C.; Schosser, T. *J. Mol. Catal. A: Chem.* **2003**, *206*, 179-184.
32. Behr, A.; Obst, D.; Turkowski, B. *J. Mol. Catal. A: Chem.* **2005**, *226*, 215-219.
33. Yan, Y.; Zhang, X.; Zhang, X. *J. Am. Chem. Soc.* **2006**, *128*, 16058-16061.
34. Goldbach, V.; Roesle, P.; Mecking, S. *ACS Catal.* **2015**, *5*, 5951-5972.
35. Behr, A.; Obst, D.; Westfechtel, A. *Eur. J. Lipid Sci. Technol.* **2005**, *107*, 213-219.
36. Yuki, Y.; Takahashi, K.; Tanaka, Y.; Nozaki, K. *J. Am. Chem. Soc.* **2013**, *135*, 17393-17400.

Chapter 2

Regioselective Isomerizing Hydroformylation of Long Chain Internal Olefins



This chapter has been adapted from following publication

Pandey, S; Chikkali, S. H. *ChemCatChem*. **2015**, 7, 3468-3471

2.1: Abstract

Isomerizing hydroformylation of internal olefins is mainly catalyzed by bulky bisphosphite ligands, however most of the ligands are highly unstable and difficult to synthesize. The single-step synthesis, coordination behavior, and application of a bis(phosphite) ligand [1,3-phenylene tetra(naphthalen-1-yl) bis(phosphite)] in the isomerizing hydroformylation of internal olefins is presented here. The desired complex was synthesized by treating ligand and metal precursor [Rh(acac)(CO)₂] under syngas pressure. Interestingly, high pressure NMR spectroscopy investigations revealed unexpected inequivalency of the two phosphorus nuclei, which display bisequatorial coordination of the bis(phosphite) ligand in a trigonal bipyramidal rhodium complex. Upon employment in the isomerizing hydroformylation of the exceedingly challenging plant oil derived substrate methyl oleate, the bis(phosphite) rhodium complex revealed an unprecedented linear selectivity of 75 %.

2.2: Introduction

Today's chemical world rely on fossils fuel resources as most of the platform chemicals we get from them. But due to their extensive use these fossils fuel resources are depleting day by day and also it is promoting the emission of green -house gases.³⁷ Currently there exists an intense focus on production of transportation fuels and other chemicals from renewable resources because of consistent rise in in crude oil prices.³⁸ In this quest, there is significant contributions from scientific community over the last decade, and various renewable resources have been identified.³⁹ The resurgence in the renewable chemical industry has led to the successful launch of several renewable products such as sugarcane-based polyethylene, polylactic acid, and polyhydroxyalkanoates, to name a few.⁴⁰ Among the various renewable resources, plant oils are considered as an attractive alternative, as they provide direct entry to chemical modification. Their easy access and high H/C ratios (almost equivalent to crude oil) make them substrates of choice.⁴¹ These attractive features are directly reflected in their 35% share in the renewable chemical industry, although they contribute only 2% to the total biomass produced. Today plant oils are the most important renewable raw material for the chemical industry (e.g., in Germany 30% of the 2.7 million tons of renewable raw materials in 2005 were plant oils; in total approximately 10% of all resources were renewable) and are heavily used as raw materials for surfactants, cosmetic products, and lubricants.⁴² In addition, plant oils have been used for decades in paint formulations, as flooring materials and for coating and resin applications. The probably best known application example is Linoleum, which was already industrially produced in 1864

and developed by F. Walton in London, UK.⁴³ Its main component is linseed oil and it provides a durable and environment friendly alternative to PVC floorings. From a chemists point of view, plant oils offer a large variety of fatty acids with different chain lengths and functional groups as well as different numbers and positions of C=C double bonds (**figure 2.1**). As plant oils mainly consist of internal double bonds, these internal double bonds provide an excellent opportunity to further functionalize plant oils to useful chemicals and materials. Therefore, it has been a long cherished dream of organometallic chemists to isomerize the internal double bond to terminal position and functionalize it selectively. However, isomerization of internal double bond to terminal olefins is thermodynamically unfavourable which makes the terminal functionalization of plant oils a challenging transformation. A very few attempts have been made to address this bottle-neck in the past.⁴⁴

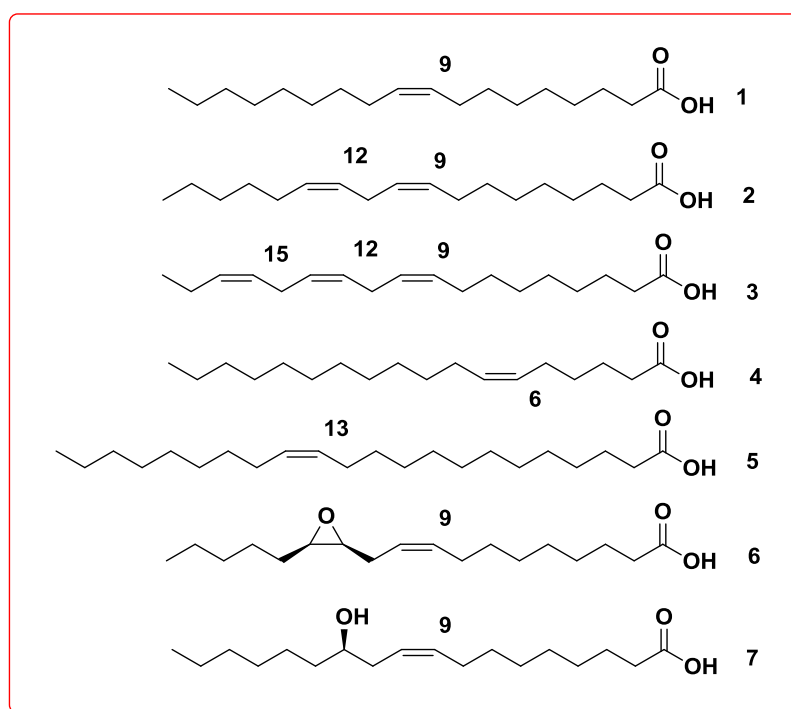


Figure 2.1 : Fatty acids as starting materials for the synthesis of renewable platform chemicals: oleic acid (1), linoleic acid (2), linolenic acid (3), petroselinic acid (4), erucic acid (5), vernolic acid (6), ricinoleic acid (7).

Isomerizing hydroformylation of fatty acid methyl esters (FAMES) was first reported by Behr et al.³⁵ and very limited success was achieved (26% terminal aldehyde). The conversion is slightly improved in case of isomerizing hydroboration (45%).⁴⁵ Isomerizing metathesis is of significant importance⁴⁶ and is successfully up scaled and various products such as candle waxes, cosmetics etc. are claimed to be produced by this transformation.⁴⁷ The most successful example is

isomerizing alkoxy-carbonylation (>95% terminal selectivity) which was first introduced by Cole-Hamilton⁴⁸ and later developed by Mecking et al.⁴⁹ (**figure 2.2**). This particular process has been investigated mechanistically by Mecking et al.⁵⁰ and provides an easy access to symmetrically functionalized molecules having long chain segments. Attaining similar terminal selectivity in a one-pot isomerizing hydroformylation reaction will be of paramount significance, as it would provide a powerful tool for the hetero-functionalization of plant oils along with complete feedstock utilization.

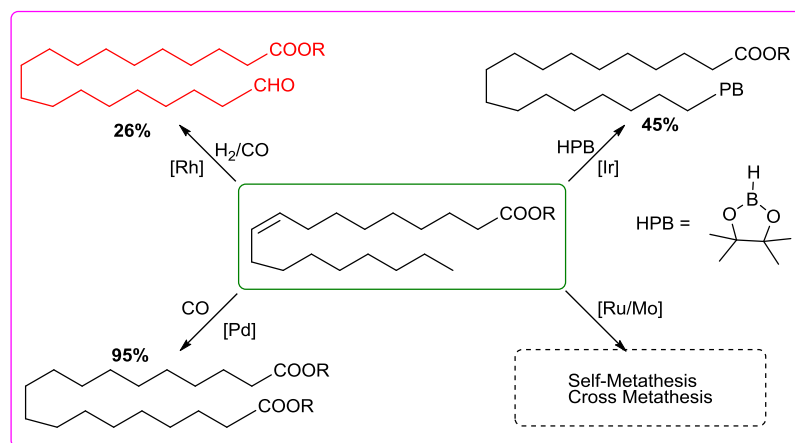


Figure 2.2: Representative examples of metal catalysed isomerizing functionalization of plant oils

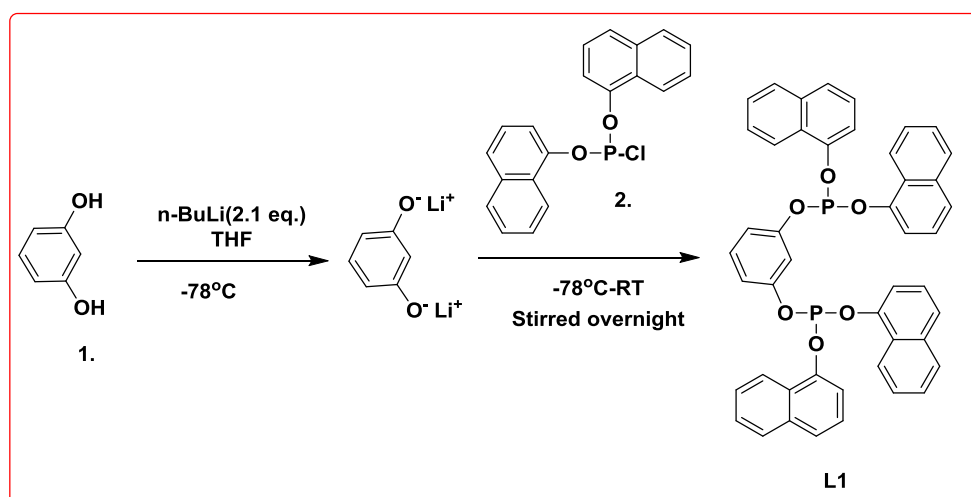
This chapter aims to address the challenges associated with isomerizing hydroformylation of plant oils and presents our attempts in the isomerizing hydroformylation of internal olefins and plant oils by using a bis(phosphite)–Rh complex and further functionalization of the resultant linear aldehydes to hydroxy–acid bifunctional molecules.

2.3: Results and discussion

Transition-metal-catalyzed hydroformylation is arguably one of the largest homogeneously catalyzed reactions. Since its discovery in 1938, numerous aldehydes have been prepared by using this transformation.⁸ A more recent addition to the fold of hydroformylation is tandem or isomerizing hydroformylation of internal alkenes to linear aldehydes.^{19,20} Isomerizing hydroformylation has attracted increasing attention in recent years, as it offers a single-window isomerizing-functionalization protocol for long-chain internal alkenes such as methyl oleate.³⁶ We anticipated that a catalyst should meet the following criteria to ensure successful isomerizing hydroformylation of internal olefins to linear aldehydes:

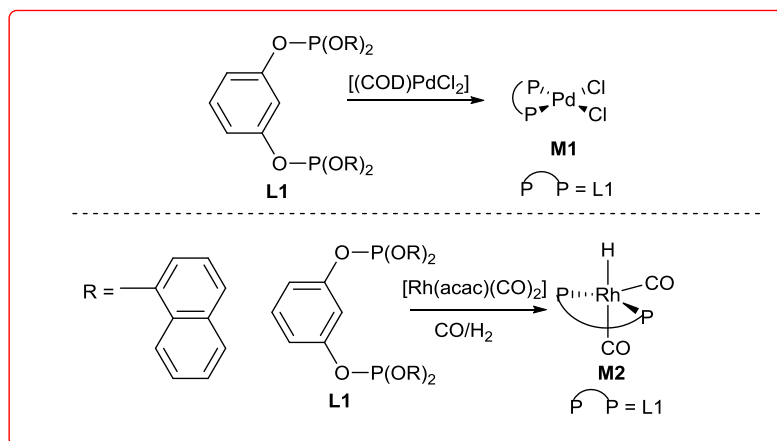
- 1) The isomerization of an internal olefin to a terminal olefin should be faster than the hydroformylation event
- 2) The rate of terminal formylation should be faster than the rate of internal formylation
- 3) The catalyst should be selective towards terminal formylation

The combined effect of the above factors will ensure higher selectivity to a linear aldehyde than an internal aldehyde. The first challenge is to identify or design a catalytic system that would meet the above criteria. A quick literature review indicated that the majority of the isomerizing functionalization reactions employ bidentate phosphite ligands and in a few cases phosphine ligands.¹⁸ Given the above stringent requirements and literature precedent, we envisioned that bis-phosphites will most likely produce higher linear aldehyde. Thus, we set out to investigate isomerizing hydroformylation of internal olefins using bis-phosphite ligand L1. In our pursuit to realize this goal, we attempted synthesis of bis-phosphite ligand L1. Deprotonation of resorcinol by *n*-BuLi, followed by addition of di(naphthalen-1-yl) phosphorochloridite 2 yielded the anticipated bis-phosphite ligand L1 (**scheme 2.1**).



Scheme 2.1: Synthesis of L1

The ³¹P NMR of the reaction mixture displayed characteristic resonance at 130 ppm suggesting presence of L1. The identity of L1 was unambiguously ascertained using a combination of spectroscopic and analytical tools and L1 was isolated in 40% yield. The coordinating ability of L1 towards neutral palladium complexes was evaluated.



Scheme 2.2: Coordination behaviour of L1

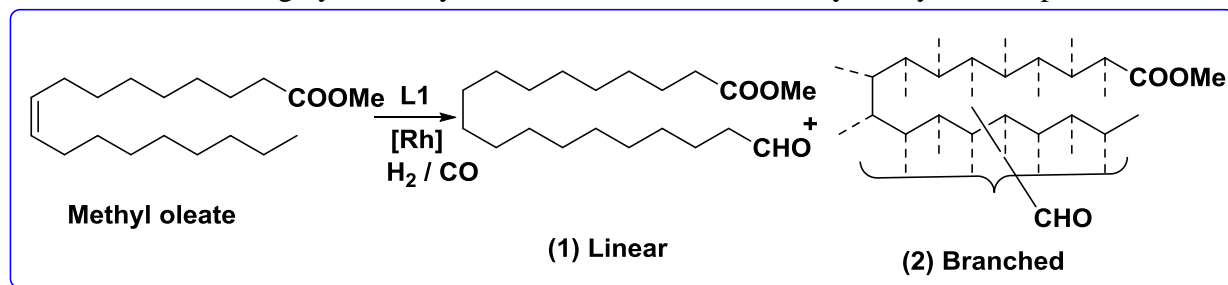
THF was added to the mixture of L1 and $[(\text{COD})\text{PdCl}_2]$ (1:1) and the reaction mixture was stirred at room temperature for 3 hours (**scheme 2.2**). The volatiles were evaporated and the residue was dissolved in DCM. Appearance of a ^{31}P NMR resonance at 84.5 ppm suggested formation of desired metal complex and the existence of M1 was established using a combination of spectroscopic and analytical tools.

It is well known that ligand coordination influences the regio-selectivity in a hydroformylation reaction.^{1c} In our pursuit to identify the catalyst resting state, we treated L1 with $[\text{Rh}(\text{acac})(\text{CO})_2]$ in presence of syngas (10 bars) in an NMR tube experiment. *In-situ* high pressure ^{31}P NMR analysis revealed a characteristic doublet of doublet at 144.1 ($^1J_{\text{Rh-P}} = 240$ Hz) and 135.9 ppm ($^1J_{\text{Rh-P}} = 243$ Hz). The observed chemical shifts and coupling constants are in good agreement with previously reported data.⁵¹ The above splitting pattern indicates that the two phosphorus nuclei are not identical. This observation (in-equivalent P-nuclei) support the equatorial-axial coordination of the two phosphorus atoms in a trigonal bipyramidal rhodium $[(\text{bis-phosphite})\text{Rh}(\text{CO})_2\text{H}]$ complex. However, the *in-situ* high-pressure proton NMR displayed a broad hydride resonance at -9.86 ppm without a large (> 30 Hz) $^2J_{\text{P-H}}$ trans-coupling.⁵² Thus, the large $^1J_{\text{Rh-P}}$ coupling constant and a small $^1J_{\text{Rh-H}}$, $^2J_{\text{P-H}}$ coupling constants (3.5 Hz) supports the accidental in-equivalency of the two phosphorus nuclei and formation of an equatorial-equatorial complex of type M2 (**scheme 2.2**) as a catalyst resting state.^{8,53}

After establishing the coordination behaviour, we evaluated performance of L1 in isomerizing hydroformylation of internal olefins to linear aldehydes and **table 1** summarizes the significant findings. The anticipated catalytically active species was generated *in-situ* by mixing ligand L1 and rhodium precursor $[\text{Rh}(\text{acac})(\text{CO})_2]$ in presence of syngas. To test our ligand, we started with isomerizing hydroformylation of short-chain olefin, 1-Octene (S1). Our preliminary screening

without much optimization displayed a linear to branched ratio of 68:32 at a L/M ratio of 2. Similarly, slightly more challenging *cis*-2-Octene displayed linear to branched selectivity of 64:56 at L/M = 2. These results indicated preferred formation of linear aldehyde. Without further experimentation with S1 & S2, we set out to evaluate L1 in the isomerizing hydroformylation of exceedingly challenging substrate methyl oleate (S3). Note that the double bond has to isomerize over 9-carbon atoms to reach to terminal position, which gives a statistical regio-selectivity of 11%.

Table 2 1: Isomerizing hydroformylation of internal olefins catalyzed by Rh complexes of L1.^a



Run	Sub.	L:M	Solvent	Temp (°C)	Syngas (bars)	Time (h)	Conv. % ^b	L:B ^c
1	S1	1	Tol.	100	5	16	>99	66:34
2	S1	2	Tol.	100	5	16	>99	68:32
3	S1	3	Tol.	100	5	16	>99	63:37
4	S1	4	Tol.	100	5	16	>99	62:38
5	S2 ^d	2	Tol.	100	5	18	>99	64:36
6	S1	2	Diox.	120	1	16	>99	54:46
7	S2	2	Diox.	120	1	16	>99	82:18
8	S3	2	Tol.	120	2.5	16	47	15:85
9	S3	2	Diox.	120	2.5	16	40	18:82
10	S3	2	DME	120	2.5	16	53	16:84
11	S3	2	NMP	120	2.5	16	11	5:95
12	S3	3	Diox.	120	2.5	16	50	10:90
13	S3	4	Diox.	120	2.5	16	50	6:94
14	S3	5	Diox.	120	2.5	16	49	5:95
15	S3	2	Diox.	100	2.5	16	47	8:92
16	S3	2	Diox.	80	2.5	16	93	5:95
17	S3	2	Diox.	60	2.5	16	>99	0:99
18	S3	2	Diox.	120	1	16	20	43:57
19	S3	2	Diox.	120	5	16	77	18:82
20	S3	2	Diox.	120	10	16	95	1:99
21	S3	2	Diox.	120	1	48	32	75:25
22	S3 ^e	2	Diox.	120	2.5	16	16	0:99
23	S3 ^f	4	Diox.	120	2.5	16	NP	NP ---
24	S3	---	Tol	100	5	16	10	0:99

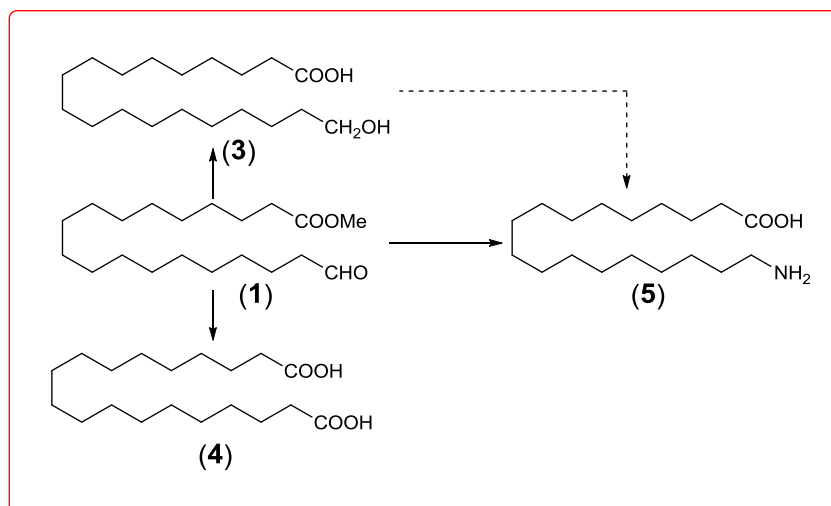
^aConditions: Sub. = Substrate, S/M = 100, S1 = 1-Octene, S2 = *cis*-2-octene, S3 = Methyl-oleate; ^b: Determined by ¹H NMR; ^c: Determined by GC; ^dS/M = 200, ^eXantphos as ligand, ^fIn absence of [Rh(acac)(CO)₂], NP = No product was found.

Our initial screening of ligand to metal ratio in toluene displayed very poor selectivity of 15:85 (**table 1**, run 8). Screening of various solvents pointed at a slightly better selectivity (18:82) in dioxane (run 8-11). Therefore, dioxane was used as a solvent of choice for rest of the isomerizing hydroformylation experiments. Optimization of ligand to metal ratio suggested L/M = 2 as the most suited combination, although at slightly lower conversion (run 9 versus run 12-14). Decreasing the temperature from 120 °C to 60 °C resulted into better conversions, but at the expense of diminishing selectivity (run 9 versus run 15-17). Thus, the best linear selectivity was obtained at 120 °C, whereas fully branched aldehyde was obtained at 60 °C. This observation suggests that high temperature is necessary to facilitate the consecutive β -hydride elimination and internal to terminal double bond isomerization process.

Next, the effect of syngas pressure on the regio-selectivity was investigated. A surprisingly higher linear to branched ratio of 43:57 was observed at a low syngas pressure of 1 bar (run 18). The higher linear selectivity at low syngas pressure indicates decreased rate of internal hydroformylation at lower pressure. Further to our delight, prolonged reaction time at 1 bar syngas pressure provided the highest linear selectivity of 75%, importantly with enhanced total conversion (run 21).

We attribute the dramatically enhanced selectivity to the reduced rate of internal hydroformylation, as syngas pressure further lowers (lower than 1 bar, as it is consumed for the hydroformylation process) down over a period of time. Control experiments such as use of bisphosphine ligand (xantphos) and in the absence of either ligand or metal precursor resulted in very poor conversions (run 22-24). Under optimized reaction conditions for methyl oleate (run 9), smaller internal olefin such cis-2-octene resulted in 82% terminal selectivity (run 7), that further supplements our hypothesis. To our knowledge, the linear/internal selectivity of 75:25 is the highest linear selectivity ever reported in the isomerizing hydroformylation of methyl oleate.

In our pursuit to confirm the existence of linear aldehyde, **1** was isolated as a colourless liquid after column chromatography. A proton resonance at 9.77 ppm can be ascribed to the terminal aldehyde proton (proton of the internal aldehyde appears at 9.40 ppm). Due to the versatile reactivity of the aldehyde, **1** can be easily transformed into AA or AB type monomers and platform chemicals (**scheme 2.3**).



Scheme 2.3: Plant oil derived α , ω -functionalized monomers/platform chemicals

In our pursuit to demonstrate the utility of the linear aldehyde, the isolated linear aldehyde was treated with KOH followed by acidic workup⁵⁴ to yield the anticipated 19-hydroxynonadecanoic acid (3), which is unprecedented to the best of our knowledge.⁵⁵ A characteristic broad proton resonance at 11.95 and a broad triplet at 5.33 ppm indicated presence of acidic and hydroxyl protons respectively. The existence of 3 was unambiguously ascertained using a combination of 1-2D NMR spectroscopy (details are given in section 2.4: experimental section). These linear α,ω -acid-hydroxy functionalized molecules can act as AB type monomers to produce polyesters. Such linear long-chain polyesters have been reported by Mecking and co-workers.^{49b} However a diol and diacid was required to prepare these polyesters and maintaining the exact stoichiometry is usually a limiting step to achieve high molecular weight polymers in these reactions. The reported compound 3 can circumvent this limitation as it can act as a single monomer to produce same polyesters.

2.4: Experimental Section

2.4.1: General methods and materials

Unless noted otherwise, all manipulations were carried out under an inert atmosphere using standard Schlenk techniques or m-Braun glove box. All solvents were distilled from sodium, sodium/benzophenone under argon atmosphere. $[\text{Rh}(\text{acac})(\text{CO})_2]$ was procured from Acros organics and used without further purification. Pyridine was supplied by Spectrochem Pvt. Ltd. and distilled and dried before use. Syngas (1:1 mixture of $\text{CO}:\text{H}_2$) was supplied by Ms. Vadilal Chemicals Ltd., Pune, India. 1-naphthol, resorcinol and PCl_3 were purchased from Alfa Aesar and Spectrochem Pvt. Ltd. respectively and used without further purification. n-BuLi (1.6 M in

hexane) was purchased from Acros Organics/Alfa Aesar. All other reagents/chemicals, solvents were purchased from local suppliers (Spectrochem Pvt. Ltd.; Avra Synthesis Pvt. Ltd.; Thomas Baker Pvt. Ltd. etc). The isomerizing hydroformylation was run in a Amar Equipment Pvt. Ltd. high pressure reactor equipped with pressure regulators and safety rupture valve.

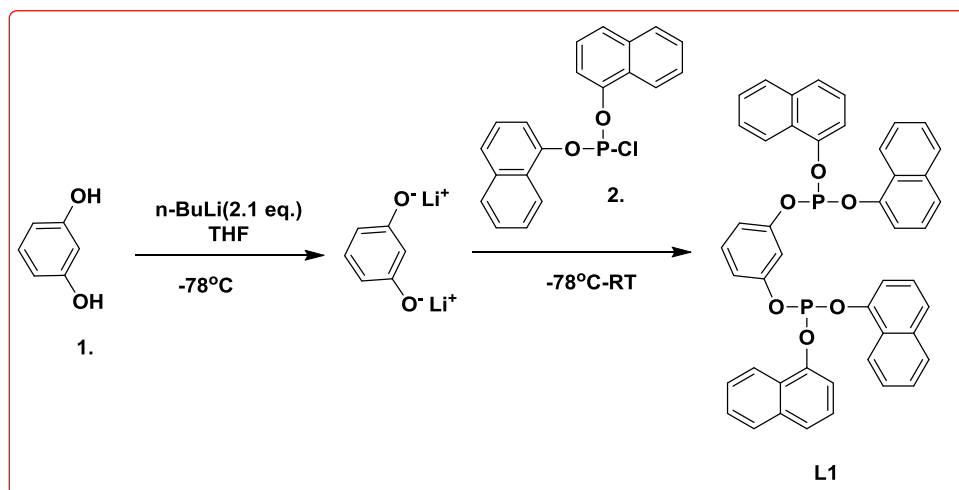
Solution NMR spectra were recorded on a Bruker Avance 200, 400, 500 and 700 MHz instruments. Chemical shifts are referenced to external reference TMS (^1H and ^{13}C) or 85% H_3PO_4 ($\Xi = 40.480747$ MHz, ^{31}P). Coupling constants are given as absolute values. Multiplicities are given as follows s: singlet, d: doublet, t: triplet, m: multiplet. *In-situ* High pressure NMR was recorded in Wilmad quick pressure valve NMR tube. Mass spectra were recorded on Thermo scientific Q-Exactive mass spectrometer; with Hypersil gold C18 column (150 x 4.6 mm diameter 8 μm particle size mobile phase used is 90% methanol + 10 % water + 0.1 % formic acid). GC analysis was carried out on an Agilent 7890B GC system using HP-05 column (30 m \times 320 μm \times 0.25 μm , split ratio 50:1, column flow 1.5 mL/min., injector temperature of 260 $^\circ\text{C}$, detector temperature of 330 $^\circ\text{C}$, argon carrier gas; temperature program, starting from 50 $^\circ\text{C}$, hold for 3 min; heating to 300 $^\circ\text{C}$ at a rate of 8 $^\circ$ /min, hold for 10 min.).

2.4.2: Synthesis of ligand L1

2.4.2.1: Synthesis of phosphorochloridite (2)

In a 250 ml Schlenk flask dry toluene (50 ml) was taken and PCl_3 (1 ml, 11.4 mmol) was added. The temperature of the solution was maintained at -10 $^\circ\text{C}$. Next, 1-naphthol was dissolved in toluene in another Schlenk flask and pyridine (1.875 ml) was added to it. The thus obtained solution was transferred to an addition funnel with the help of cannula. The 1-naphthol solution was added dropwise to PCl_3 solution at -10 $^\circ\text{C}$. Once the addition is completed, the resultant reaction mixture was stirred further for 2.5 hours. Side product (Py.HCl) was filtered with the help of cannula-filtration & filtrate was concentrated to 50 ml. Toluene solution contains the phosphorochloridite as major product.

^{31}P (500 MHz, Toluene, 298 K): $\delta = 161$.



Scheme 2.1: Synthesis of L1

2.4.2.2: Synthesis of ligand L1

Resorcinol (0.68 g, 5.7 mmol) was dissolved in dry THF & the temperature of the solution was maintained at -78°C . 7.5 ml of $n\text{-BuLi}$ (1.6 M in ether, 2.1 eq.) solution was dropwise added to the above reaction mixture. The resulting solution was stirred for 2 hrs. Next, toluene solution of phosphorochloridite was added to the above reaction mixture at -78°C and the reaction mixture was allowed to warm to RT & stirred overnight. Reaction mixture was passed through a column of celite to remove the precipitated LiCl. Volatiles were evaporated in vacuo to get the crude compound. Crude was purified by silica gel column chromatography using toluene: hexane (1:5) as eluents to get the pure compound in 40% yield.

$^1\text{H NMR}$ (500 MHz, CDCl_3 , 298 K): $\delta = 7.36$ (s, 1H), 7.38-7.44 (m, 14H), 7.49-7.52 (m, 5H), 7.65 (d, $J_{\text{H-H}} = 7.71$ Hz, 4H), 7.84 (d, $J_{\text{H-H}} = 8.25$ Hz, 4H), 8.13 (d, $J_{\text{H-H}} = 8.57$ Hz, 4H). $^{31}\text{P NMR}$ (500 MHz, CDCl_3 , 298K) $\delta = 129.9$ (s). $^{13}\text{C NMR}$ (125 MHz, CDCl_3 , 298K) $\delta = 147.7$ (d, $^2J_{\text{P-C}} = 2.20$ Hz), 134.9, 127.7, 127.4, 126.6, 126.1, 125.6, 124.2, 122.3, 115.1, 115.0. **Elemental analysis** (%) calculated for $\text{C}_{46}\text{H}_{32}\text{O}_6\text{P}_2$ (742.70): C-74.39, H-4.34; Found : C-74.46, H-3.26.

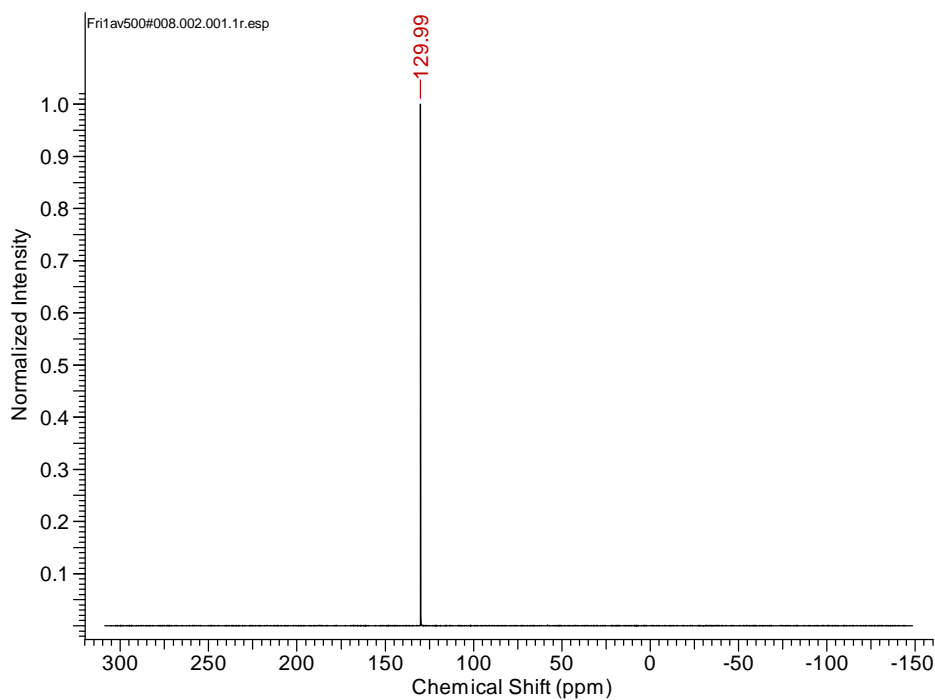


Figure 2.3: ^{31}P NMR spectrum of ligand L1 in CDCl_3

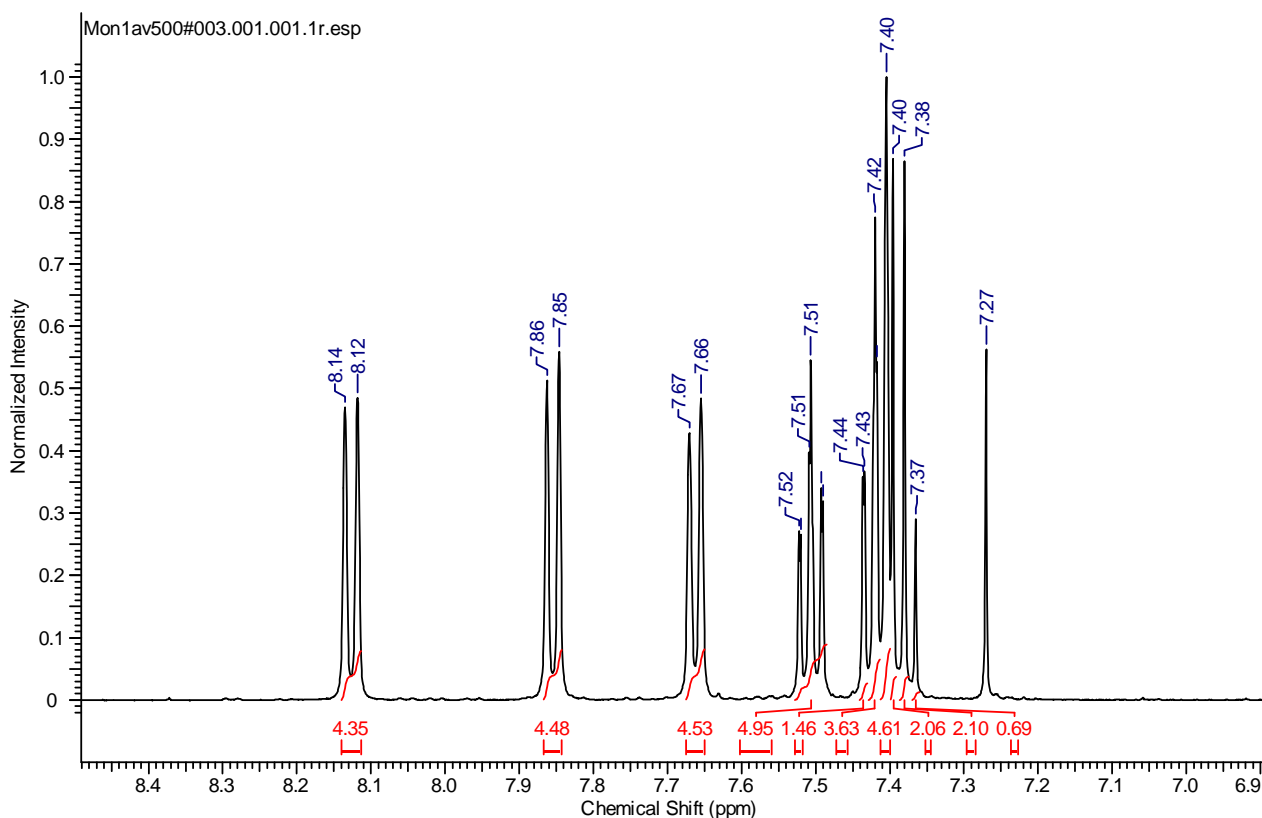


Figure 2.4: ^1H NMR spectrum of ligand L1 in CDCl_3

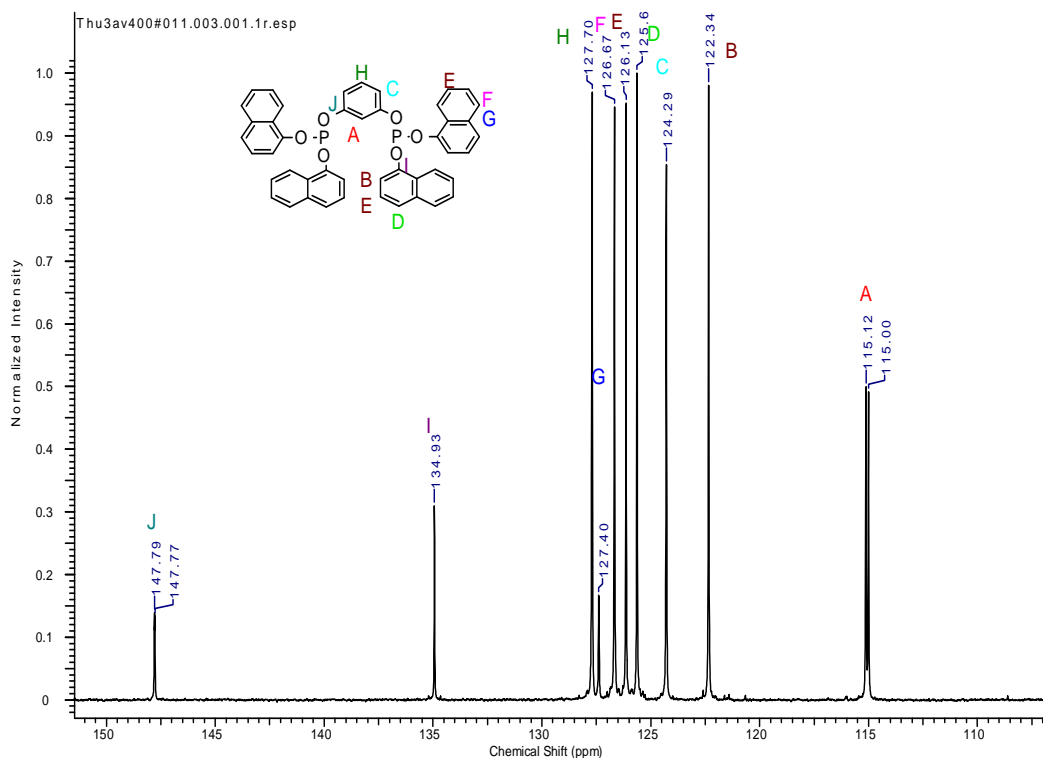


Figure 2.5: ^{13}C NMR spectrum of ligand L1 in CDCl_3

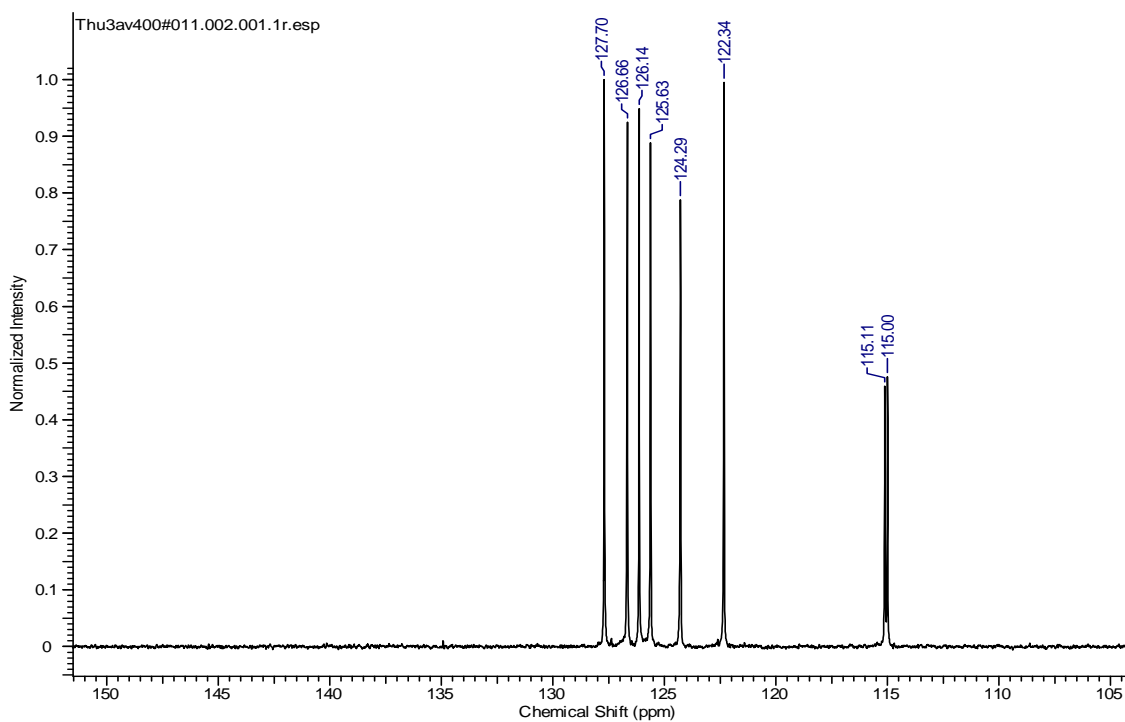


Figure 2.6: $^{135}\text{-DEPT}$ spectrum of ligand L1 in CDCl_3

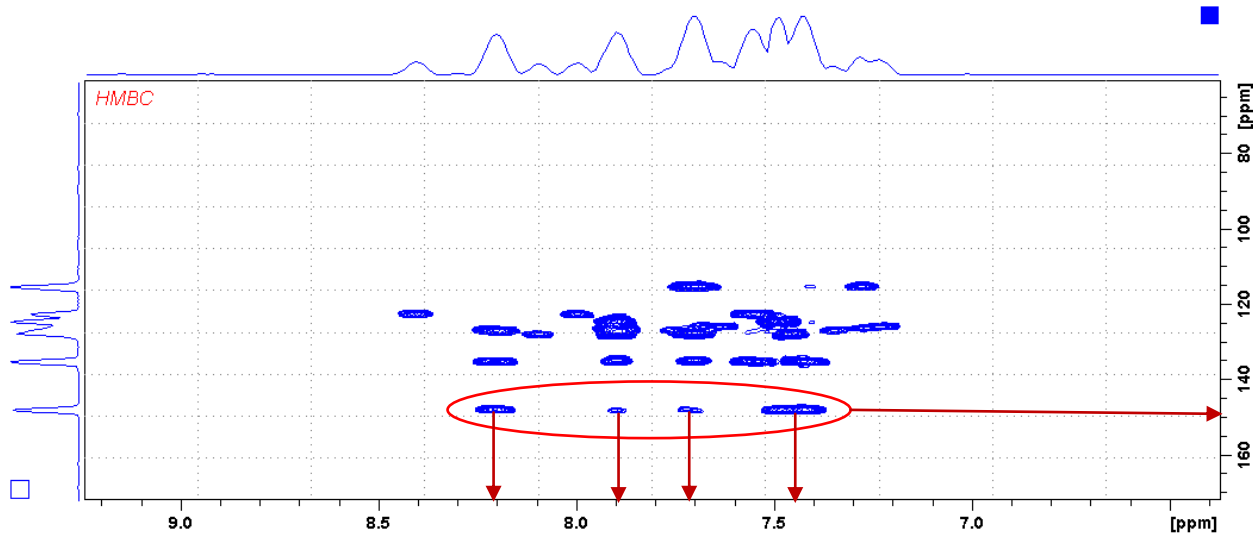
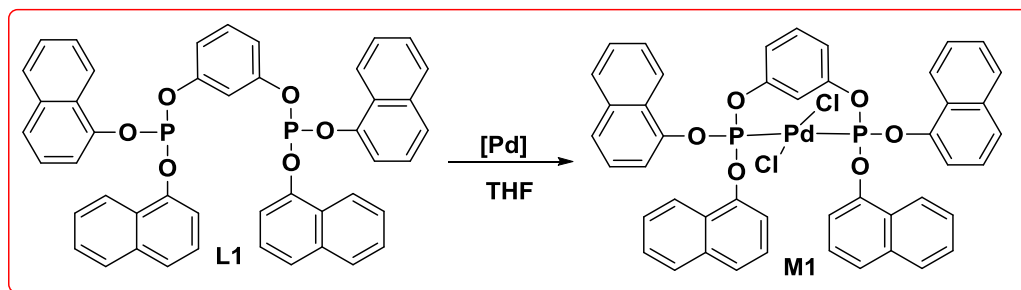


Figure 2.7: HMBC NMR spectrum of ligand L1 in CDCl_3

2.4.3: Synthesis of Pd complex of L1 (M1)

$[\text{Pd}(\text{COD})\text{Cl}_2]$ (0.026 g, 1 eq.) and ligand L1 (0.068 g, 1 eq.) were taken in a Schlenk flask under inert conditions. THF (10 ml) was added to it and reaction mixture was stirred at room temperature. After 3 hours, solvent was evaporated in vacuum to get yellowish residue. Next, residue was washed two times with dry pentane. Obtained residue was fully dried to get desired Pd complex as yellow coloured powder.



Scheme 2.4: Synthesis of Pd complex of L1 (M1)

^1H NMR (500 MHz, CDCl_3 , 298 K): $\delta = 6.91$ (t, $J_{\text{H-H}} = 7.70$ Hz, 4H), 7.17 (t, $J_{\text{H-H}} = 7.92$ Hz, 4H), 7.32 (t, $J_{\text{H-H}} = 7.48$ Hz, 7H), 7.58 (dd, $J_{\text{H-H}} = 8.15$ Hz, 9H), 7.69 (d, $J_{\text{H-H}} = 8.20$ Hz, 4H), 7.87 (d, $J_{\text{H-H}} = 8.48$ Hz, 4H). ^{31}P NMR (400 MHz, CDCl_3 , 298K): $\delta = 84.5$.

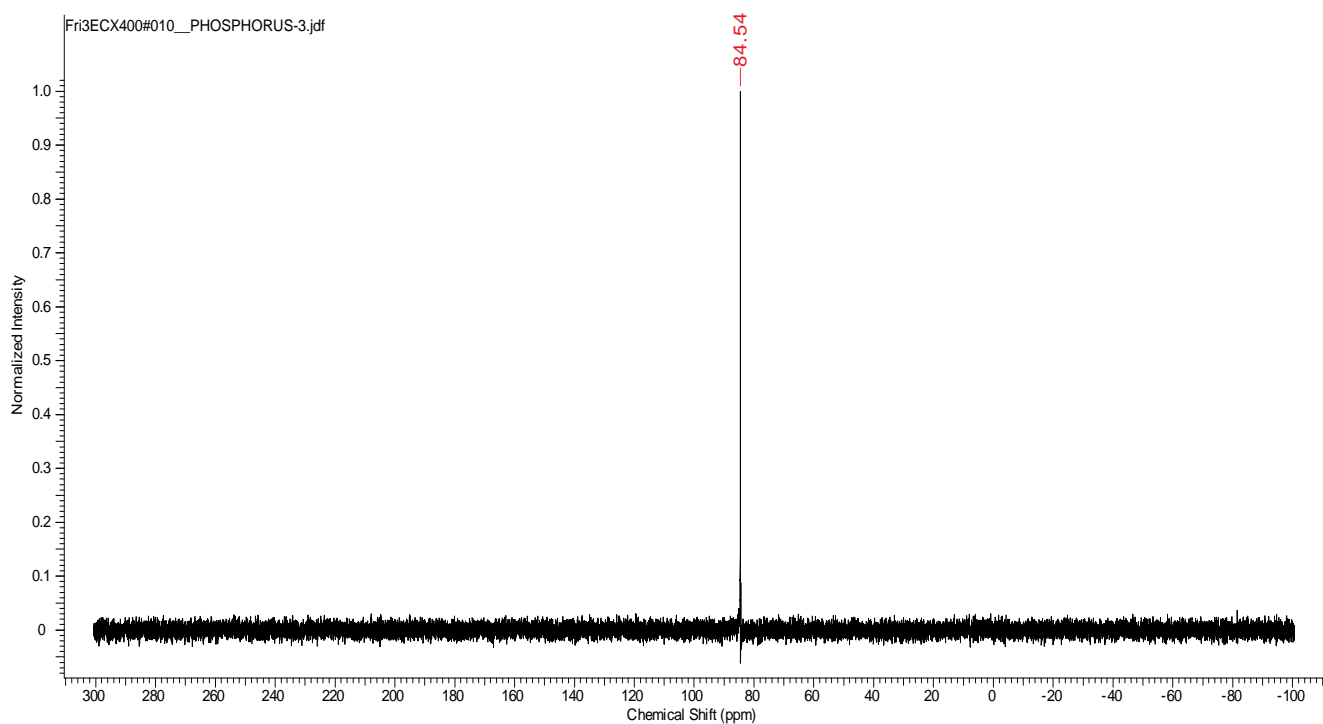


Figure 2.8: ^{31}P NMR spectrum of palladium complex M1 in CDCl_3

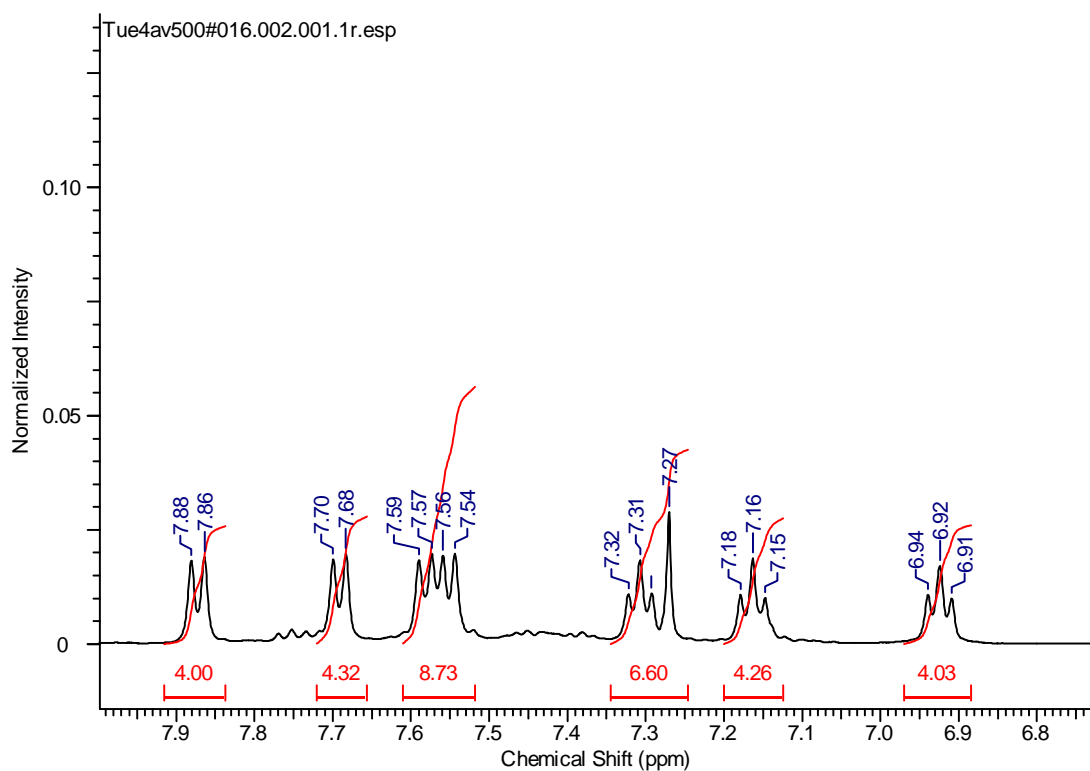
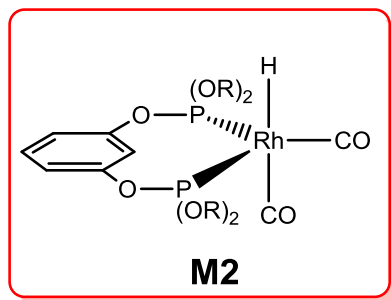


Figure 2.9: ^1H NMR of palladium complex M1 in CDCl_3

2.4.4: Mechanistic investigation: *In-situ* high pressure NMR

It is well known that the coordination mode of the ligand influences the selectivity in an asymmetric hydroformylation reaction. In our pursuit to investigate the coordination mode of our ligand L1, we attempted the following experiment.

[Rh(acac)(CO)₂] (0.008 g, 0.000031 mol) and ligand L1 (0.023 g, 0.000031 mol) were dissolved in dry toluene-d₈ (0.3 ml) under inert conditions. This mixture was mixed properly to get a clear solution. Next, the reaction mixture was transferred to a high pressure NMR tube. The tube was degassed using freeze-pump-thaw cycles. Next, the NMR tube was purged 2-3 times with syngas and then pressurized to 10 bars. After this the tube was heated at 50 °C for 16 hours. An orange red solution was obtained which was



analyzed using ³¹P and ¹H NMR spectroscopy.

In-situ high pressure ³¹P NMR analysis revealed a characteristic double doublet at 144.1 (¹J_{Rh-P} = 240 Hz) and 135.9 ppm (¹J_{Rh-P} = 243 Hz). The observed chemical shifts and coupling constants are in good agreement with previously reported data.⁵¹ The above splitting pattern indicates that the two phosphorus nuclei are not identical. This observation (in-equivalent P-nuclei) supports the equatorial-axial coordination of the two phosphorus atoms in a trigonal bipyramidal rhodium [(bis-phosphite)Rh(CO)₂H] complex. However, the *in-situ* high-pressure proton NMR displayed a broad hydride resonance at -9.86 ppm without a large (> 30 Hz) ²J_{P-H} trans-coupling. Thus, the small ²J_{P-P} and ²J_{P-H} coupling constant and a small coupling constant (3.5 Hz) supports the accidental in-equivalency of the two phosphorus nuclei and formation of an equatorial-equatorial complex of type M2 as a catalyst resting state.

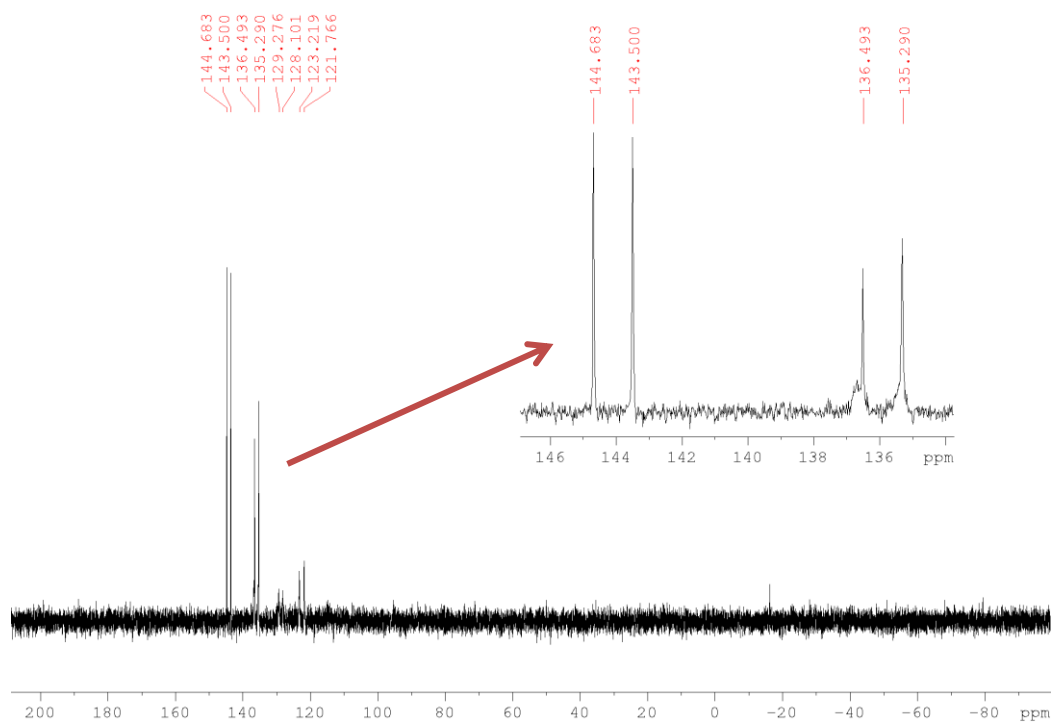


Figure 2.10: High pressure ^{31}P NMR spectrum of the *in-situ* generated $[\text{L1RhH}(\text{CO})_2]$ complex in Tol-d_8

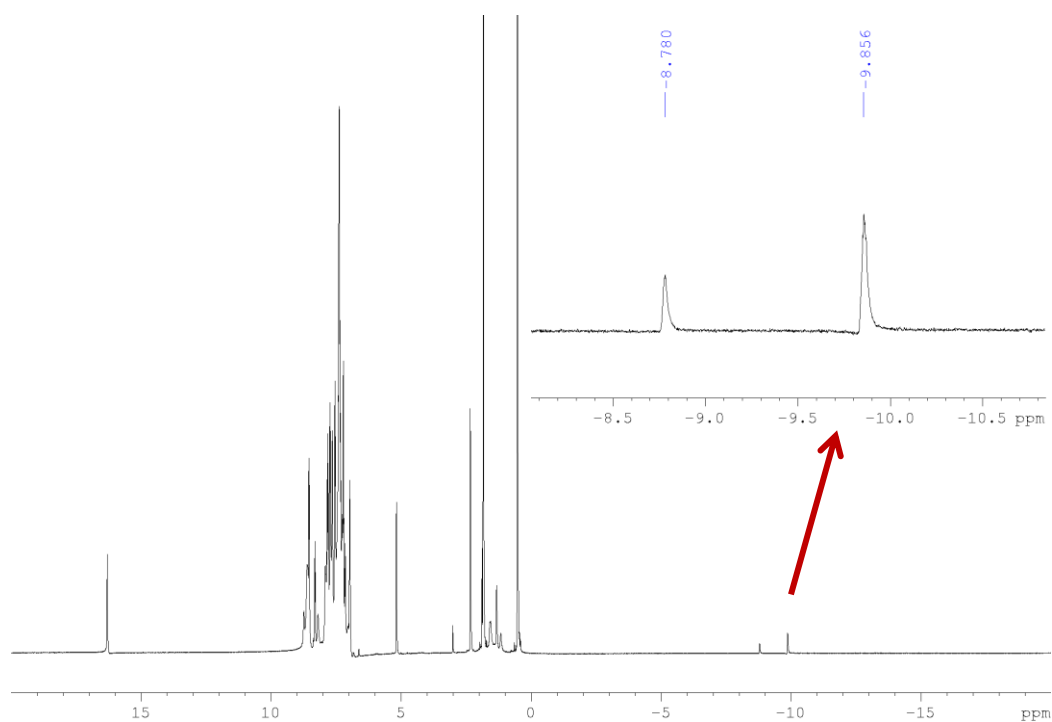


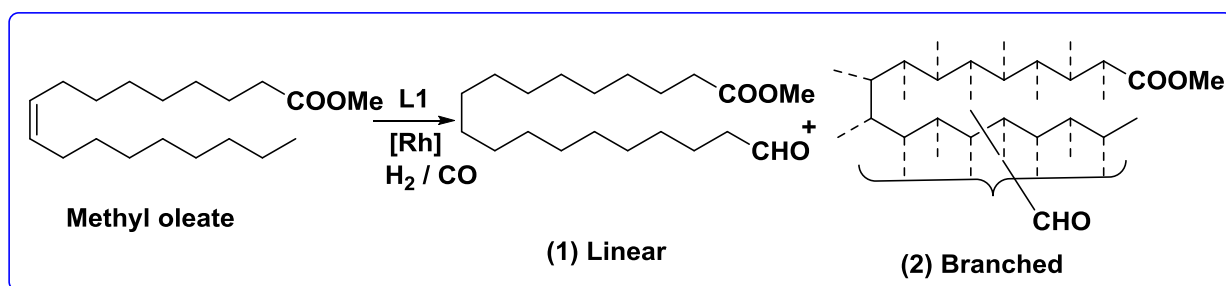
Figure 2.11: High pressure ^1H NMR spectrum of the *in-situ* generated $[\text{L1RhH}(\text{CO})_2]$ complex in Tol-d_8

2.4.5: Isomerizing hydroformylation : General procedure

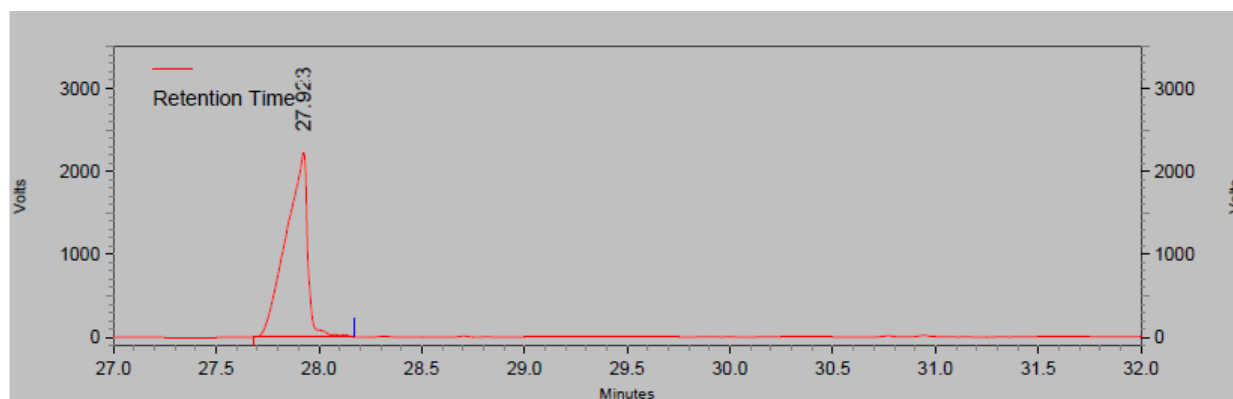
In a typical hydroformylation experiment a stainless steel autoclave (150 mL) equipped with pressure regulator and safety valves was employed. In an argon filled glove box the vials were charged with $[\text{Rh}(\text{acac})(\text{CO})_2]$ (0.002 g, 1eq.), ligand L1(0.0114 g, 2 eq.), solvent (1 ml), substrate (100 eq.) along with Teflon stirring bars. Before starting the catalytic reactions, the charged autoclave was purged three times with syngas ($\text{CO}:\text{H}_2 = 1:1$) and then pressurized to the desired pressure. After catalysis, the autoclave was cooled to $0\text{ }^\circ\text{C}$, and any excess gas vented, after which the reaction solution was analyzed directly. The conversion and regioselectivity were determined by ^1H NMR spectroscopy and by GC after evaporating the solvent.

2.4.5.1: Isomerizing hydroformylation of methyl oleate

GC analysis was carried out on an Agilent 7890B GC system using HP-05 column ($30\text{ m} \times 320\text{ }\mu\text{m} \times 0.25\text{ }\mu\text{m}$) with the following GC-method: 3 mins hold at $50\text{ }^\circ\text{C}$, heat at $8^\circ/\text{min}$ to $300\text{ }^\circ\text{C}$ and hold for 10 min. With this method, the methyl-oleate appeared at (Rt) 27.9 min. (**figure 2.12**), hydrogenated methyl-oleate at (Rt) 28.09 min. (**figure 2.13**), linear aldehyde at (Rt) 28.7 min. (**figure 2.15**) and the branched aldehydes (Rt) 30.3-31.5 min (**figure 2.17**). These retention times were further confirmed by injecting isolated linear, branched or hydrogenated products and the substrate.



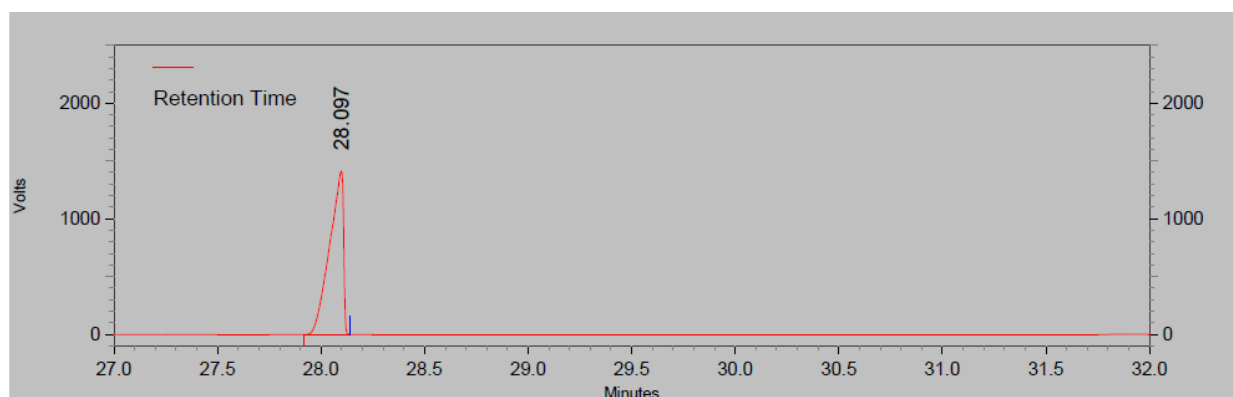
Scheme 2.5: Isomerizing hydroformylation of methyl oleate



**Back Signal
Results**

Retention Time	Area	Area %	Height	Height %
27.923	124455772	100.00	17063481	100.00
Totals	124455772	100.00	17063481	100.00

Figure 2.12: GC-chromatogram of Methyl-oleate (Rt = 27.9 mins.)



**Back Signal
Results**

Retention Time	Area	Area %	Height	Height %
28.097	50521700	100.00	10850902	100.00
Totals	50521700	100.00	10850902	100.00

Figure 2.13: GC-chromatogram of hydrogenated methyl-oleate (Rt = 28.09 mins.)

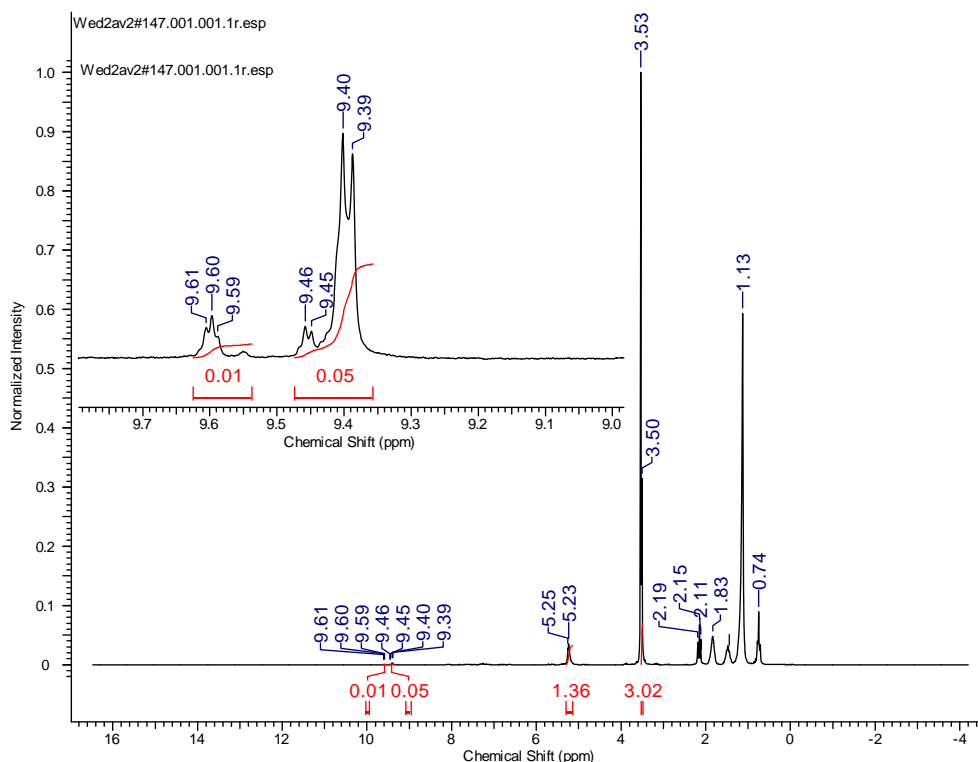
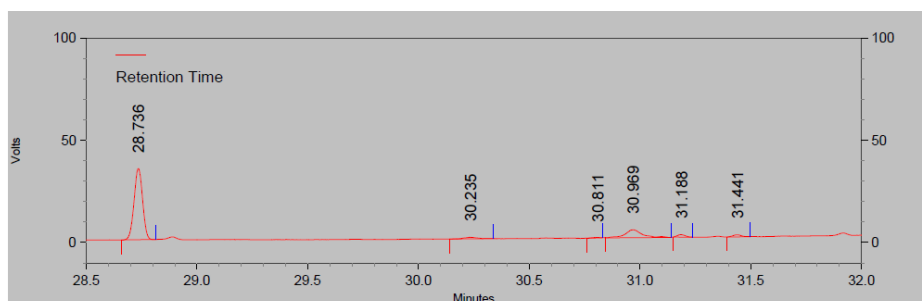


Figure 2.14: ^1H NMR spectrum of the reaction mixture after hydroformylation of methyl oleate in CDCl_3 . The triplet at 9.72 ppm can be ascribed to the linear aldehyde, while the slightly up-field (9.5-9.3) doublet/s can be assigned to all the branched aldehydes



Back Signal Results

Retention Time	Area	Area %	Height	Height %
28.736	715567	75.46	267221	83.15
30.235	24487	2.58	5801	1.81
30.811	4778	0.50	1499	0.47
30.969	160119	16.89	29611	9.21
31.188	22636	2.39	9258	2.88
31.441	20689	2.18	7978	2.48
Totals	948276	100.00	321368	100.00

Figure 2.15: GC-chromatogram of hydroformylated methyl-oleate displaying the highest linear (75%) selectivity

2.4.5.2: Separation and characterization of aldehydes

The two aldehydes were separated from the reaction mixture by using silica gel column chromatography (hexane-ethyl acetate; 95:5%).

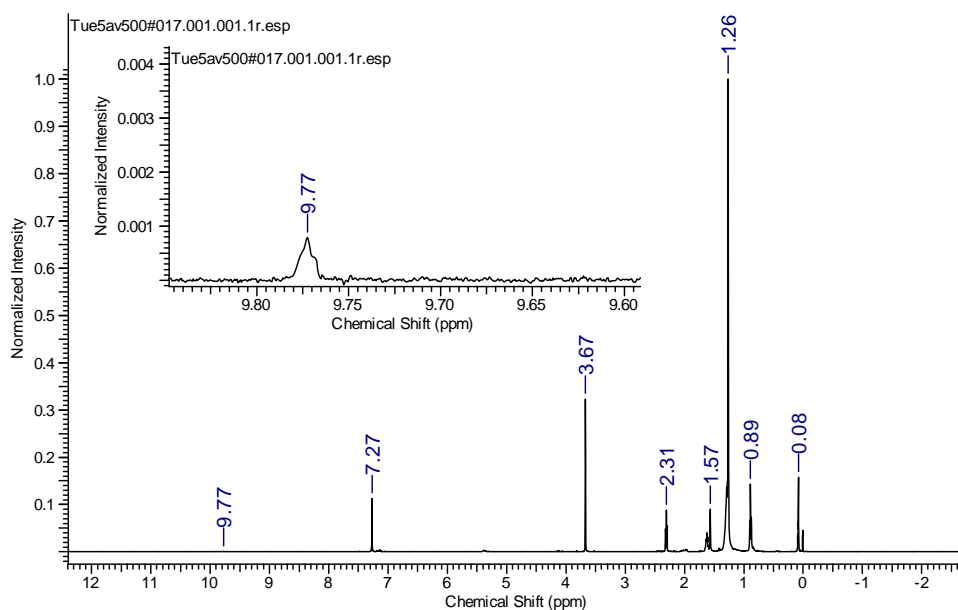
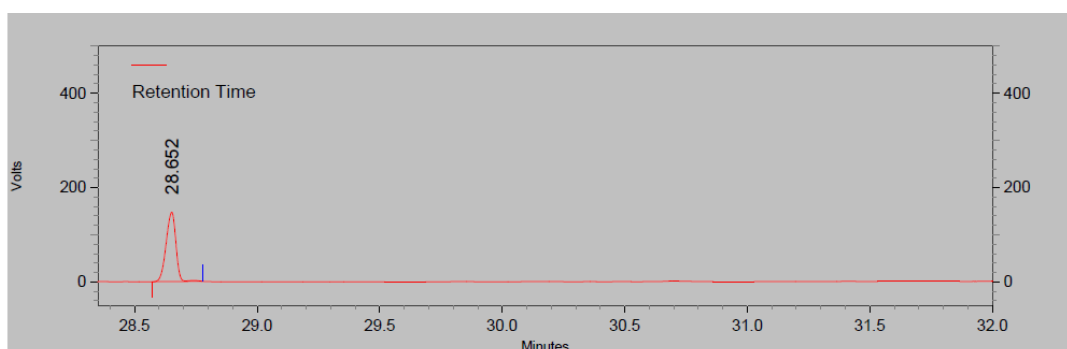


Figure 2.14 : ¹H NMR of the isolated (from branched) linear aldehyde 1 in CDCl₃ (contaminated with hydrogenated methyl-oleate)



**Back Signal
Results**

Retention Time	Area	Area %	Height	Height %
28.652	3133532	100.00	1130023	100.00
Totals	3133532	100.00	1130023	100.00

Figure 2.15: GC-chromatogram of the isolated linear aldehyde 1

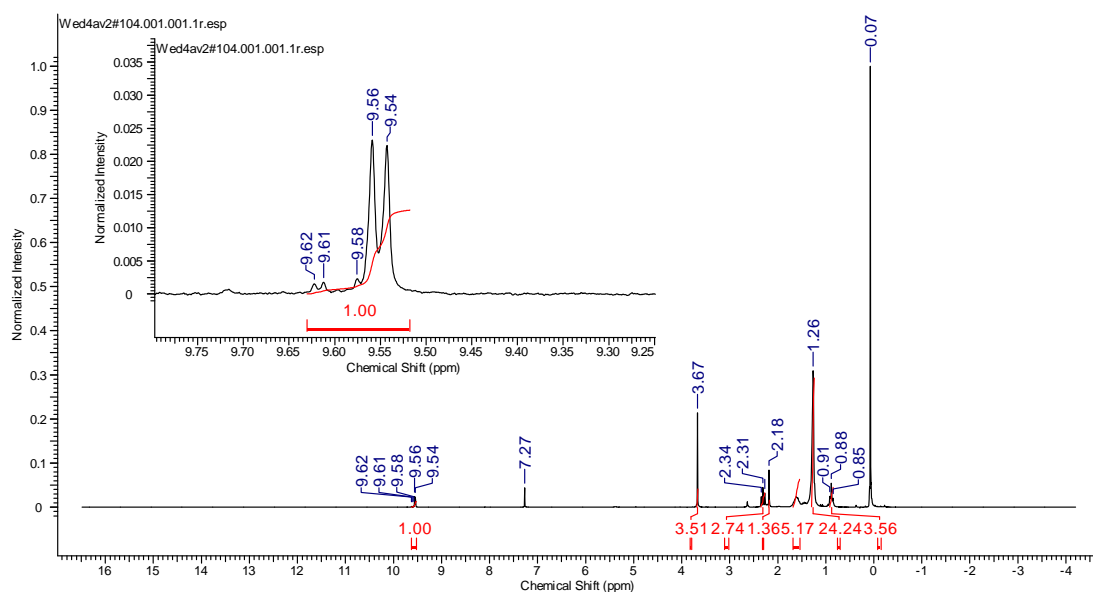
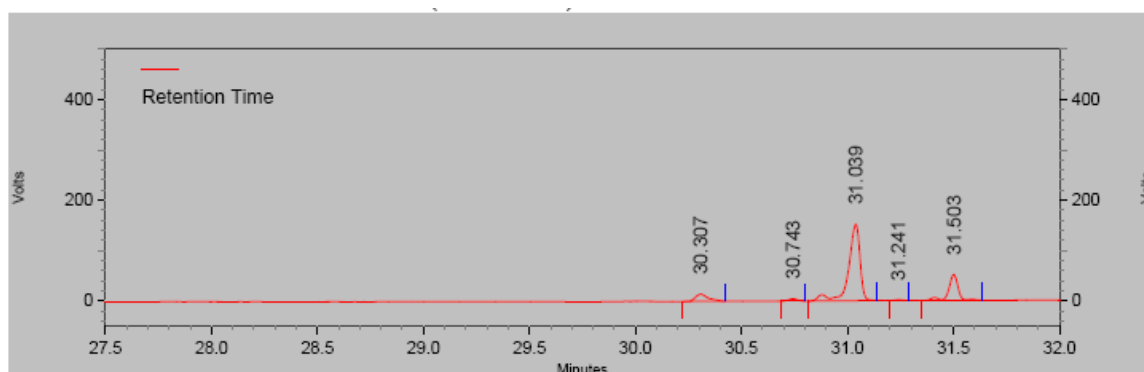


Figure 2.16: ^1H NMR spectrum of the isolated (from linear aldehyde) branched aldehyde 2 in CDCl_3



Back Signal Results

Retention Time	Area	Area %	Height	Height %
30.307	452741	7.33	108565	6.31
30.743	97081	1.57	34647	2.01
31.039	4349597	70.45	1167607	67.83
31.241	33451	0.54	13527	0.79
31.503	1241326	20.11	396920	23.06
Totals	6174196	100.00	1721266	100.00

Figure 2.17: GC-chromatogram of the isolated branched aldehyde 2

2.4.5.3: Isomerizing hydroformylation of cis-2-octene

Isomerizing hydroformylation of cis-2-octene was performed under optimized reaction conditions (**table 1, run 7**) and terminal selectivity as high as 82% was obtained. The conversion and regioselectivity were determined by ^1H NMR spectroscopy and by GC.

GC retention time for cis-2-octene was obtained as 5.2 mins (**figure 2.19**) and for linear aldehyde (nonanal) as 13.2 mins (**figure 2.20**).

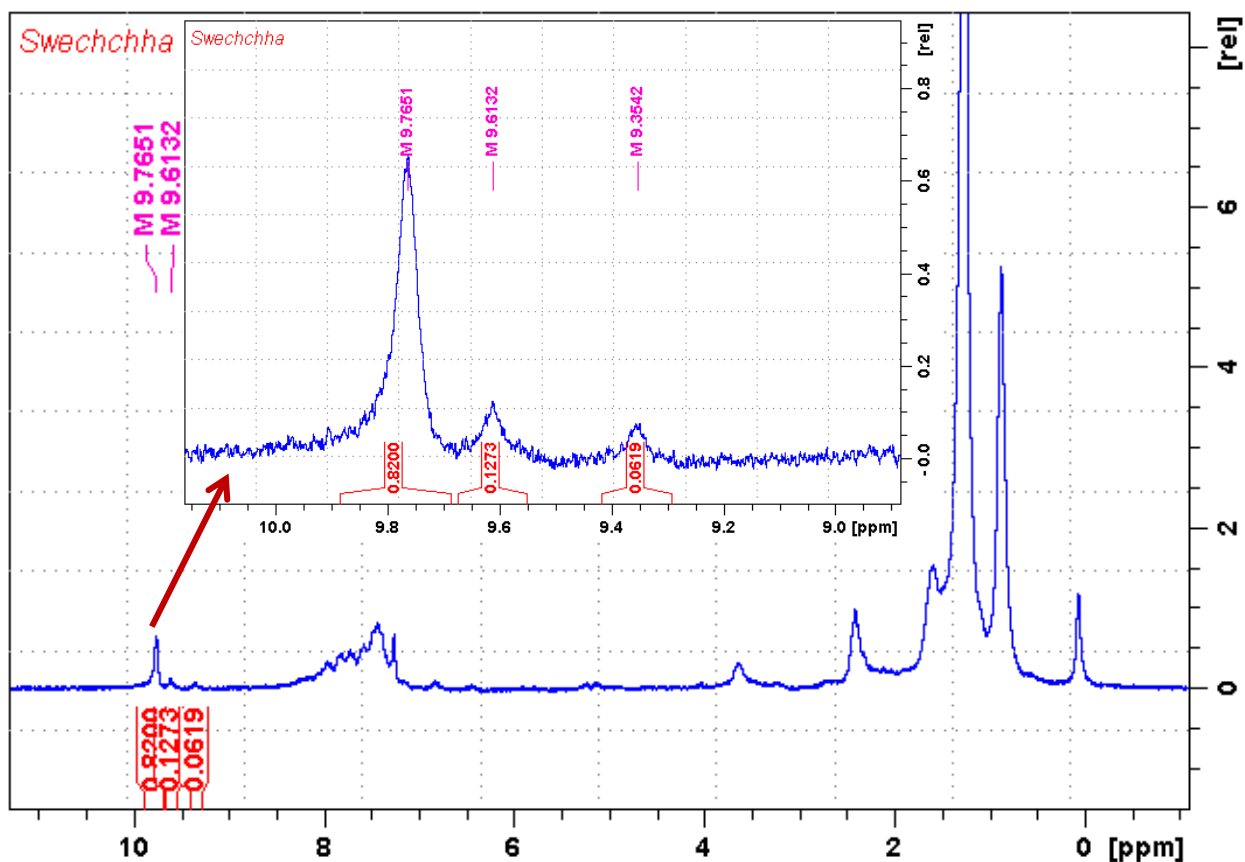
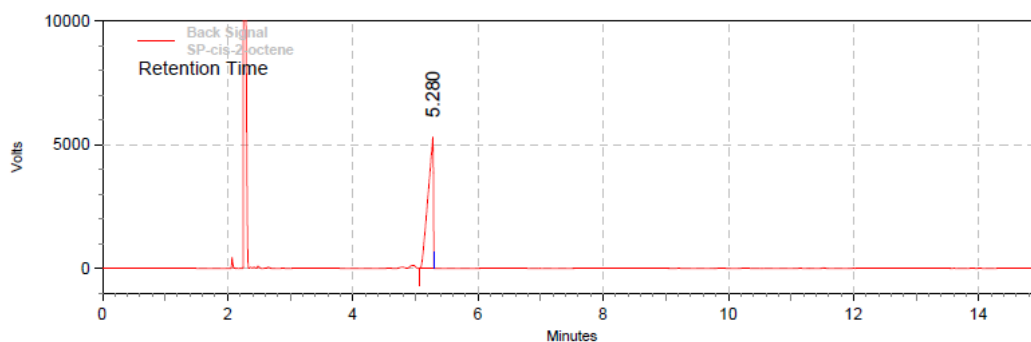
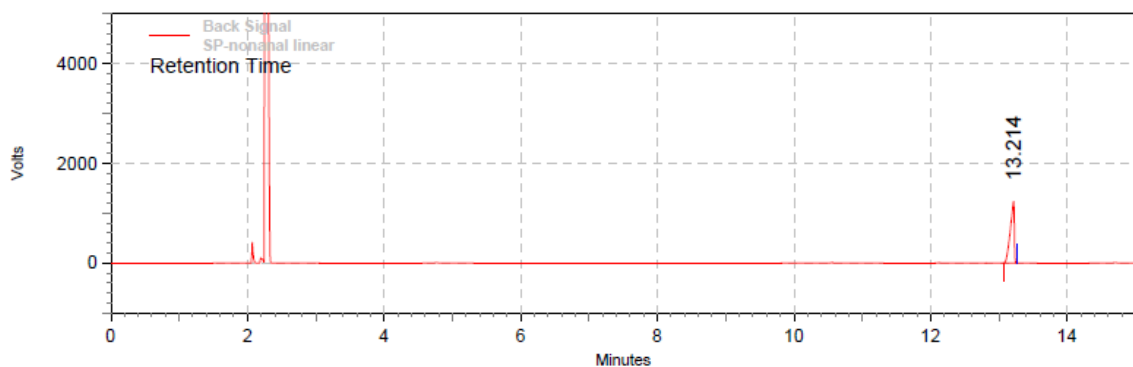


Figure 2.18: ^1H NMR spectra of reaction mixture (run 7; after evaporation of solvent) in CDCl_3 ; displaying the L/B ratio of 82:18



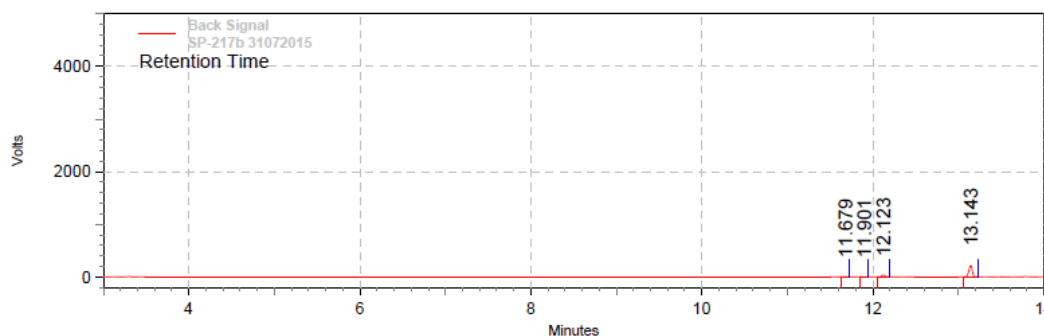
Back Signal Results				
Retention Time	Area	Area %	Height	Height %
5.280	239381783	100.00	40744269	100.00
Totals	239381783	100.00	40744269	100.00

Figure 2.19: GC-chromatogram of cis-2-octene displaying the retention time of 5.2 minutes


**Back Signal
Results**

Retention Time	Area	Area %	Height	Height %
13.214	38371651	100.00	9468786	100.00
Totals	38371651	100.00	9468786	100.00

Figure 2.20: GC-chromatogram of pure n-nonanal displaying the retention time of 13.2 minutes

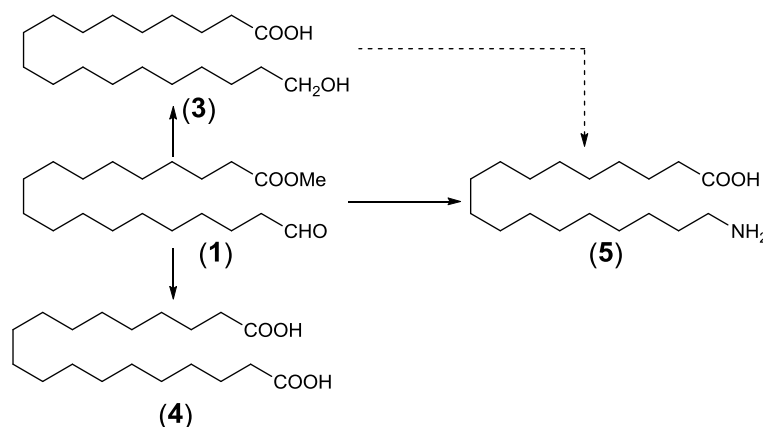

**Back Signal
Results**

Retention Time	Area	Area %	Height	Height %
11.679	73567	1.34	27347	1.35
11.901	116262	2.12	43860	2.17
12.123	772874	14.09	282296	13.97
13.143	4521688	82.45	1667193	82.51
Totals	5484391	100.00	2020696	100.00

Figure 2.21: GC-chromatogram of hydroformylated cis-2-octene displaying the highest linear (82%) selectivity

2.4.6: Functionalization of linear aldehyde

The versatile reactivity of the aldehyde can be efficiently utilized by further functionalization of 1. The linear aldehyde can be easily transformed into AA or AB type monomers and platform chemicals as depicted in scheme 2.3. We report one such attempt in section 2.4.6.1.



2.4.6.1: Reduction of linear aldehyde to hydroxy-fatty acid (3)

The linear aldehyde (232 mg, 1eq.) (contaminated with methyl oleate) was dissolved in methanol and heated to 70 °C. Next, KOH (232 mg, 4 eq.) was added to this solution and reaction mixture was refluxed for 8 hours. After 8 hours, solvent was evaporated in vacuum to get white coloured solid. Obtained solid was treated with distilled water and was acidified to pH = 2 to get white glittery residue. The residue was filtered, dried and recrystallized from toluene to obtain the anticipated compound 3.

$^1\text{H NMR}$ (500 MHz, CDCl_3 , 298 K): δ = 10.94 (br, s), 5.36 (br, t, $^3J_{\text{H-H}} = 15$ Hz), 2.32 (t, $^3J_{\text{H-H}} = 7.3$ Hz), 1.94 (m), 1.61 (m), 1.23 (m). $^{13}\text{C NMR}$ (125 MHz, CDCl_3 , 298 K): δ = 179.6, 60.6, 34.1, 32.8, 29.8, 29.4, 24.9, 22.9, 14.3. **ESI-MS**: $m/z = 297.08$ $[\text{M-OH}]^+$.⁵⁶

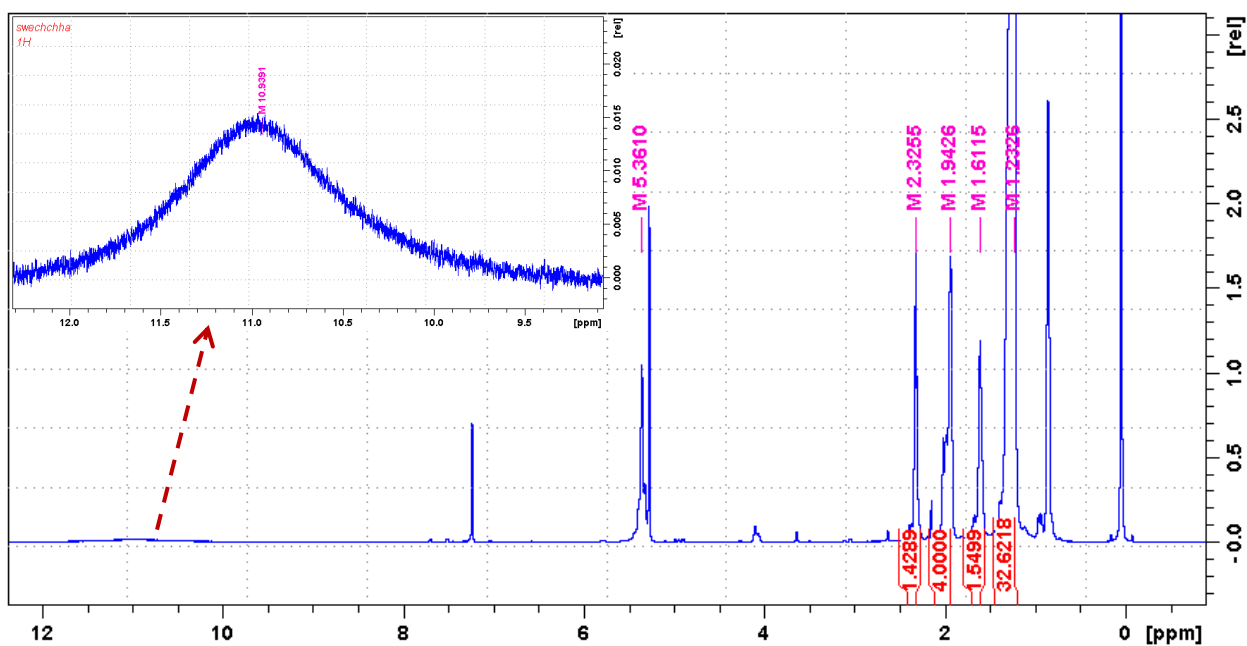


Figure 2.22: $^1\text{H NMR}$ spectra of 19-hydroxynonadecanoic acid 3 in CDCl_3 (* = CH_2Cl_2 ; # = impurity in CDCl_3)

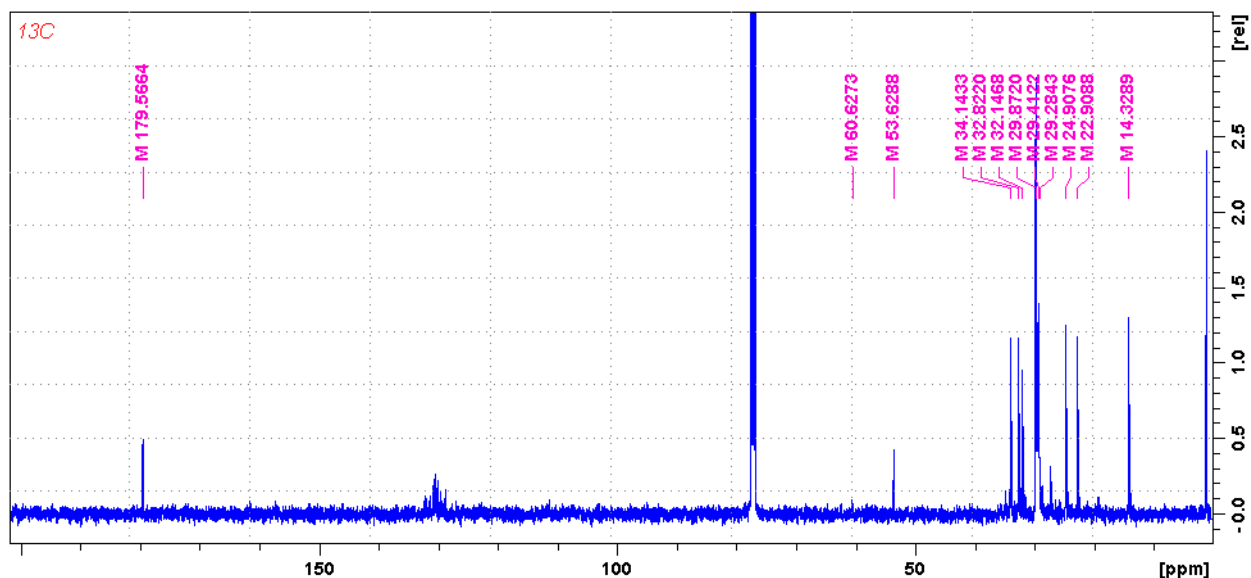


Figure 2.23: ^{13}C NMR spectrum of 19-hydroxynonadecanoic acid in CDCl_3 (* = CH_2Cl_2)

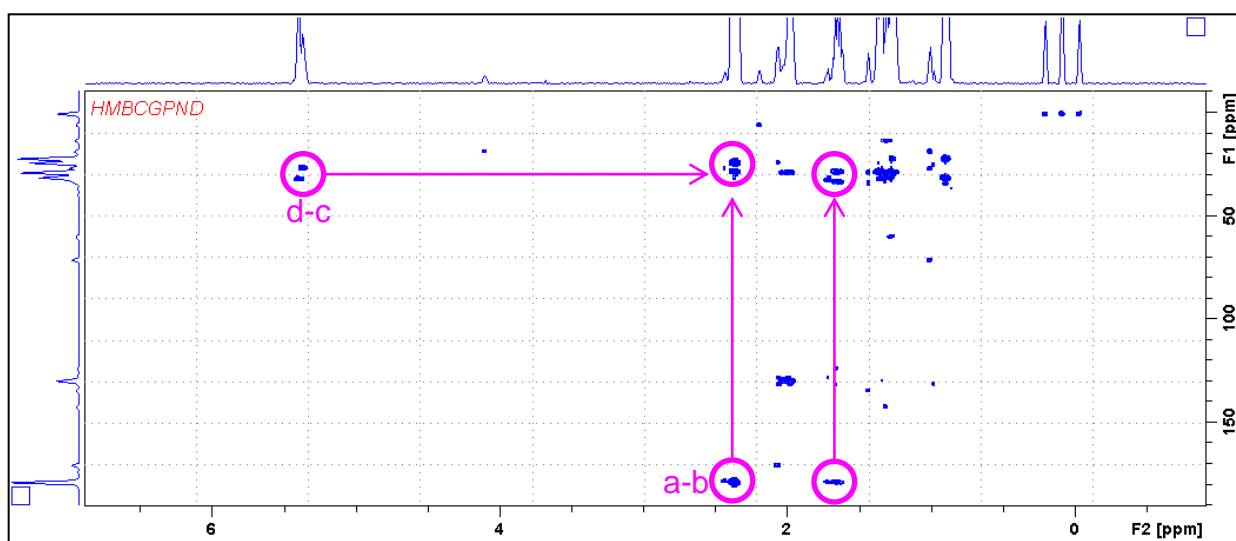
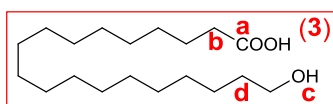


Figure 2.24: HMBC NMR spectrum of 19-hydroxynonadecanoic acid (3) in CDCl_3

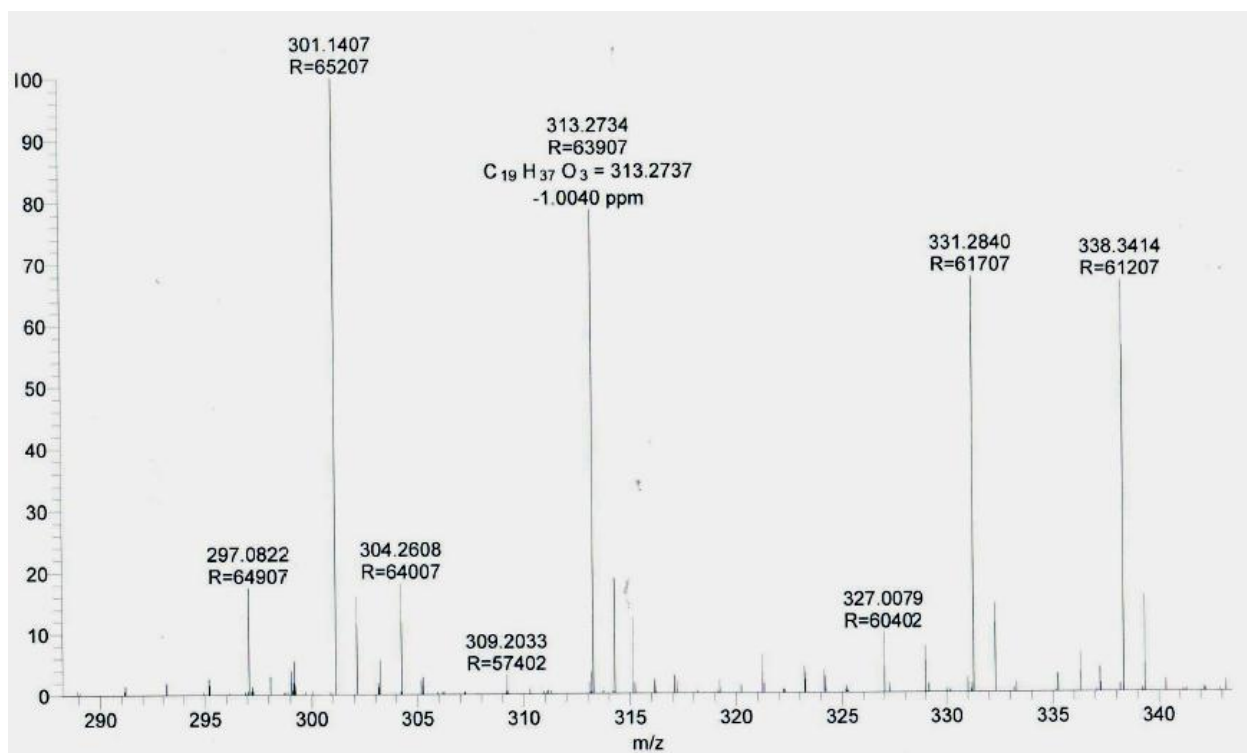


Figure 2.25: ESI-MS spectrum of 3 ($m/z = 297.08 [M-OH]^+$; $313.27 [M-H]^+$; $331.28 [M-H+H_2O]^+$; $338.34 [M-H+H_2O + Li]^+$)

2.5: Conclusion

In summary, we report synthesis of a bis-phosphite ligand that is easy to prepare. *In-situ* high pressure NMR spectroscopy revealed that the two phosphorus nuclei predominantly occupy bis-equatorial position in a trigonal bipyramidal rhodium complex. However, interestingly, the two phosphorus nuclei were found to be in-equivalent and displayed a $^1J_{\text{Rh-P}}$ coupling of 240-243 Hz. The performance of the bis-phosphite ligand L1 was evaluated in isomerizing hydroformylation of long-chain olefins. Preliminary results indicated predominant linear selective isomerizing hydroformylation of 1-Octene and cis-2-Octene. Performance of L1 was evaluated in the isomerizing hydroformylation of extremely challenging plant oil based substrate methyl-oleate. Initial screening indicated dioxane as the better solvent. Better linear selectivities were obtained at 120 °C and ambient (1 bar) syngas pressure. Thus, performing isomerizing hydroformylation of S3 using rhodium complex of L1 at 120 °C and 1 bar syngas pressure led to an unprecedented regioselectivity of 75% for the linear aldehyde. Above observations reveal that isomerization is favoured at higher temperature and terminal formylation is favoured at lower syngas pressure. These findings might guide the future developments in the field of isomerizing-hydroformylation of long-chain internal olefins to linear selective products. In addition, the synthetic utility of isomerizing-hydroformylation in organic synthesis was demonstrated by transforming the linear aldehyde (1) to 19-hydroxynonadecanoic acid (3), which is a potential AB type monomer for polyester production.

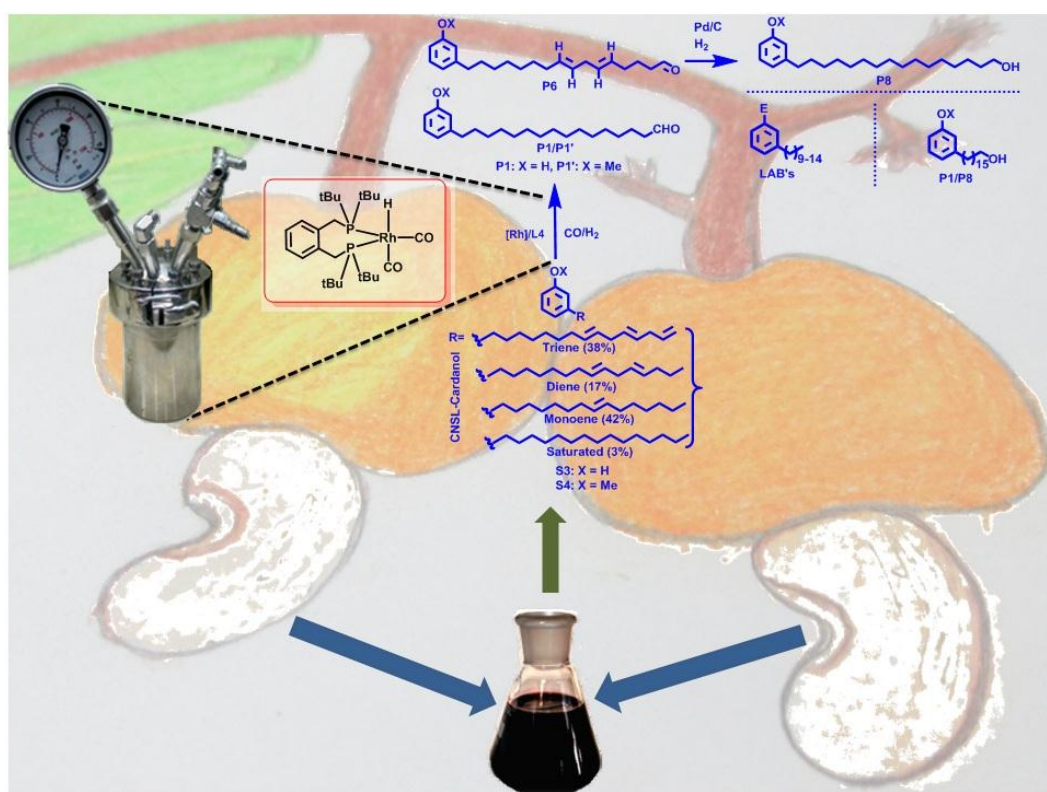
2.6: References

37. (a) Mecking, S. *Angew. Chem. Int. Ed.* **2004**, *43*, 1078-1085. (b) Biermann, U.; Bornscheuer, U.; Meier, M. A. R.; Metzger, J. O.; Schäfer, H. J. *Angew. Chem. Int. Ed.* **2011**, *50*, 3854-3871. (c) Dodds, D. R.; Gross, R. A. *Science* **2007**, *318*, 1250-1251. (d) Dapsens, P. Y.; Mondelli, C.; Perez-Ramirez, J. *ACS Catal.* **2012**, *2*, 1487-1499.
38. (a) Chheda, J. N.; Huber, G. W.; Dumesic, J. A. *Angew. Chem. Int. Ed.* **2007**, *46*, 7164-7183. (b) Huber, G. W.; Corma, A. *Angew. Chem. Int. Ed.* **2007**, *46*, 7184-7201. (c) Huber, G. W.; Iborra, S.; Corma, A. *Chem. Rev.* **2006**, *106*, 4044-4098. (d) Ragauskas, A. J.; Williams, C. K.; Davison, B. H.; Britovsek, G.; Cairney, J.; Eckert, C. A.; Frederick, W. J.; Hallett, J. P.; Leak, D. J.; Liotta, C. L. *Science* **2006**, *311*, 484-489.
39. (a) Deuss, P. J.; Barta, K.; de Vries, J. G. *Catal. Sci. Technol.* **2014**, *4*, 1174-1196. (b) Gosselink, R. W.; Hollak, S. A. W.; Chang, S. W.; van Haveren, J.; de Jong, K. P.; Bitter, J. H.; van Es, D. S. *ChemSusChem* **2013**, *6*, 1576-1594. (c) Hillmyer, M. A.; Tolman, W. B. *Acc. Chem. Res.* **2014**, *47*, 2390-2396. (d) Rajput, B. S.; Gaikwad, S. R.; Menon, S. K.; Chikkali, S. H. *Green Chem.* **2014**, *16*, 3810-3818. (e) Ciriminna, R.; Lomeli-Rodriguez, M.; Cara, P. D.; Lopez-Sanchez, J. A.; Pagliaro, M. *Chem. Commun.* **2014**, *50*, 15288-15296.
40. (a) Tullo, A. H. *Chem. Eng. News* **2011**, *89*, 10-14. (b) Tullo, A. H. *Chem. Eng. News* **2011**, *89*, 9. (c) Singhvi, M.; Gokhale, D. *RSC Adv.* **2013**, *3*, 13558-13568. (d) Hottle, T. A.; Bilec, M. M.; Landis, A. E. *Polym. Degrad. Stab.* **2013**, *98*, 1898-1907.
41. Vennestrøm, P. N. R.; Osmundsen, C. M.; Christensen, C. H.; Taarning, E. *Angew. Chem. Int. Ed.* **2011**, *50*, 10502-10509; *Angew. Chem.* **2011**, *123*, 10686-10694.
42. German Federal Ministry of Food, Agriculture and Consumer Protection, Agency of Renewable Resources, <http://www.fnr.de>.
43. Heisterberg-Moutsis, G.; Heinz, R.; Wolf, T. F.; Harper, D. J.; James, D.; Mazzur, R. P.; Kettler, V. 'Floor Coverings', in Ullmann's encyclopedia of industrial chemistry, 2001, Online Edn., WILEY-VCH Verlag GmbH & Co. KGaA, Weinheim, Germany.
44. Hydroformylation of plant oils was investigated and mere 4% of linear aldehyde was reported; see: Frankel, E. N.; Metlin, S.; Rohwedder, W. K.; Wender, I. *J. Am. Oil Chem. Soc.* **1969**, *46*, 133-138.
45. Ghebreyessus, K. Y.; Angelici, R. J. *Organometallics* **2006**, *25*, 3040-3044.
46. (a) Chikkali, S.; Mecking, S. *Angew. Chem. Int. Ed.* **2012**, *51*, 5802-5808. (b) Zerkowski, J. A. *Lipid Technol.* **2013**, *25*, 106-109. (c) Lummiss, J. A. M.; Oliveira, K. C.; Prankevicus, A. M. T.; Santos, A. G.; dos Santos, E. N.; Fogg, D. E. *J. Am. Chem. Soc.* **2012**, *134*, 18889-18891. (d) Vilela, C.; Silvestre, A. J. D.; Meier, M. A. R. *Macromol. Chem. Phys.* **2012**, *213*, 2220-2227. (e) Stempfle, F.; Ortmann, P.; Mecking, S. *Macromol. Rapid Commun.* **2013**, *34*, 47-50. (f)

- Ortmann, P.; Heckler, I.; Mecking, S. *Green Chem.* **2014**, *16*, 1816-1827. (g) Boelhauer, C.; Mol, J. C. *Progr. Lipid Res.* **1985**, *24*, 243-267.
47. (a) Zullo, J. L.; Anderson, J. C.; Kaido, H.; Pederson, R. L.; Schrodi, Y.; Sperber, W. H.; Tupy, M. J.; Wagner, E. H. (Elevance Renewable Science Inc.), US7951232B2, 2011; b) Elevance claims to have started commercial production of C18 diacid from plant oils, see: <http://www.elevance.com/platforms/engineered-polymers-and-coatings/inherent-c18-diacid/>
48. Jimenez-Rodriguez, C.; Eastham, G. R.; Cole-Hamilton, D. J. *Inorg. Chem. Commun.* **2005**, *8*, 878-881.
49. (a) Quinzler, D.; Mecking, S. *Angew. Chem. Int. Ed.* **2010**, *49*, 4306-4308. (b) Stempfle, F.; Quinzler, D.; Heckler, I.; Mecking, S. *Macromolecules* **2011**, *44*, 4159-4166. (c) Roesle, P.; Duerr, C. J.; Moeller, H. M.; Cavallo, L.; Caporaso, L.; Mecking, S. *J. Am. Chem. Soc.* **2012**, *134*, 17696-17703.
50. Roesle, P.; Caporaso, L.; Schmitte, M.; Goldbach, V.; Cavallo, L.; Mecking, S. *J. Am. Chem. Soc.* **2014**, *136*, 16871-16881.
51. (a) Selent, D.; Franke, R.; Kubis, C.; Spannenberg, A.; Baumann, W.; Kreidler, B.; Boerner, A. *Organometallics* **2011**, *30*, 4509-4514 (b) Moasser, B.; Gladfelter, W. L.; Roe, D. C. *Organometallics* **1995**, *14*, 3832-3838.
52. A relatively less intense resonance in the ^{31}P NMR and hydride region was visible, indicating existence of multiple species [LRh(acac)CO], [LRh(acac)] that are less abundant.
53. Buisman, G. J. H.; Vos, E. J.; Kamer, P. C. J.; van Leeuwen, P. W. N. M. *J. Chem. Soc. Dalton Trans.* **1995**, 409-417.
54. The protocol was adopted from Ref. 49 (b).
55. Synthesis of **3** appeared contemporarily in the following article. Witt, T.; Stempfle, F.; Roesle, P.; Haeussler, M.; Mecking, S. *ACS Catal.* **2015**, *5*, 4519-4529.
56. Apart from the positively charged species, various radical cations were observed. Formation of a radical cation in mass-spectroscopy is explained in the following text book: Gross, J. H. in *Mass Spectrometry A Text Book*, Springer, Berlin Heidelberg, **2004**, pp. 267-271.

Chapter 3

Isomerizing Hydroformylation of Non-Edible Plant Oils



This chapter has been adapted from following publication

Pandey, S.; Shinde, D. R.; Chikkali, S. H. *ChemCatChem*. **2017**, *9*, 3997-4004.

3.1: Abstract

Isomerizing hydroformylation of methyl oleate (edible plant oil) has been attempted in recent past and significant success has been achieved. However to avoid the direct competition with the food chain, it would be really attractive to utilize non-edible plant oils such as cashew nut shell liquid as renewable substrate. A small library of bisphosphorus ligands was evaluated in the rhodium-catalyzed isomerizing hydroformylation (I-HF) of cashew nut shell liquid (CNSL). Rhodium complex of 1,2-bis((di-tertbutylphosphanyl)methyl)benzene (BDTBPMB) (L4) outperformed the other bis-phosphite and bis-phosphine ligands and unveiled a moderate selectivity of 28% and 50% in the I-HF of CNSL-monoene and methoxy protected monoene respectively. The resultant aldehyde 16-(3-methoxyphenyl)hexadecanal P1' was isolated and its identity was fully established. Application of bis-phosphine ligand L4 in the I-HF of highly challenging CNSL-cardanol (S3) and methoxy protected CNSL-cardanol yielded a linear selectivity of 74%, although with reduced conversion. To demonstrate the synthetic utility of our strategy, the obtained aldehyde (derived from S3) was subjected to hydrogenation and the resultant 3-(16-hydroxyhexadecyl) phenol (P8) was isolated in 89% isolated yield. High-pressure NMR investigation revealed selective formation of bisequatorial BDTBPMB-rhodium complex which might be responsible for the excellent linear selectivity.

3.2: Introduction

Our day to day life is highly dependent on fossil fuel resources to meet the regular needs.^{37, 46a} However, the supply of fossil fuels is finite and unsustainable, which calls for long-term sustainable strategies to substitute fossil fuel resources with renewable resources.³⁸ Even partial replacement of petroleum-based raw materials by renewable resources is a major contemporary challenge in terms of both economic and environmental aspects.⁵⁷ In this context, there is a significant contribution from the scientific community, and various renewable resources have been identified.^{18,34,39} Plant oil derived fatty acids can be a suitable alternative as they have the characteristic long methylene sequence with an internal double bond.⁵⁸⁻⁶⁰ To avoid direct competition with food-chain, it is especially attractive to utilize the non-edible plant oils as a renewable resource.⁶¹ In this context, cashew nut shell liquid (CNSL)⁶² stands out as a non-edible plant sourced oil that is readily available (CNSL-450,000 metric tons per annum)⁶³ on a large scale from agricultural waste. The CNSL is equipped with a functional group at one end of the molecule and a double bond deep into the long aliphatic chain (**figure 3.1**). This internal double bond provides an excellent opportunity to further functionalize the plant sourced oil to useful chemicals and building blocks.⁶⁴ However, isomerization of internal double bond to terminal olefin is a thermodynamically unfavorable process which makes the terminal functionalization of

plant oils a challenging transformation.^{22,65}

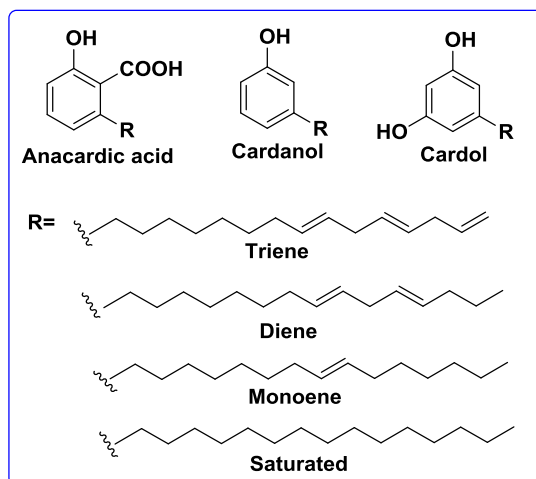


Figure 3.1: Chemical composition of CNSL

A very few attempts have been made in this regard.⁴⁴ The most successful example is isomerizing alkoxy-carbonylation (>95% terminal selectivity) of methyl oleate (from edible plant oils).^{34,48,49,50,66} Metathesis has gained significant attention however, it does not allow complete utilization of carbon chain obtained from plant oils.⁴⁷ Isomerizing-metathesis was recently investigated by Goossen and co-workers, and access to a defined distribution of metathesis products was established.⁶⁷ Isomerizing hydroboration of plant oil can provide access to boron functionalized compounds. However, the highest terminal selectivity in isomerizing-hydroboration of plant oils is moderate (45%).⁴⁵ Another approach to these functionalization's is one pot isomerizing hydroformylation (I-HF), which is a powerful tool for unsymmetrical-functionalization of plant oils along with full molecular incorporation.⁵⁵ I-HF of fatty acid methyl esters (FAMEs) was first reported by Behr and co-workers³⁵ and a terminal selectivity of 26% was achieved using a bulky bisphosphite ligand BIPHEPHOS. Later on Nozaki et al. developed a tandem isomerization-hydroformylation-hydrogenation sequence using ternary catalyst system for methyl oleate. The best yield in favor of linear alcohol from methyl oleate was 53%.³⁶ A linear selective (75%) I-HF of methyl oleate using a bulky bisphosphite ligand L1 was demonstrated by Chikkali and coworkers.⁶⁸

In contrast, very little is known about the isomerizing functionalization of non-edible plant oils (**figure 3.2**) such as CNSL.⁶⁹ Methoxycarbonylation (30 bars CO pressure, 80 °C)⁶⁹ and ethenolysis of cashew nut shell liquid has been attempted leading to the synthesis of tsetse fly attractants and oestrogenic compounds (**figure 3.2**).⁷⁰

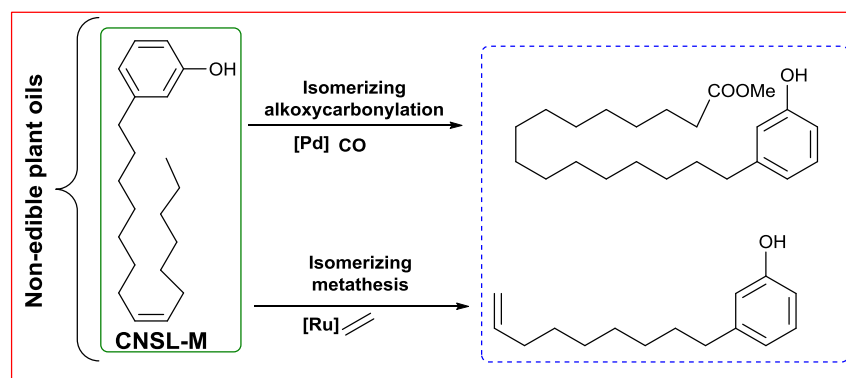


Figure 3.2: Isomerizing functionalizations of CNSL

The scientific challenges that hinder the development of isomerizing functionalization of CNSL cardanol are listed as under, although it is not a comprehensive list. i) Two transformations, namely, isomerization and terminal functionalization have to take place simultaneously without interfering with each other. ii) Either two catalysts that are compatible with each other can perform isomerization and terminal functionalization or, a rationally designed/chosen single catalyst component can perform the isomerizing functionalization reaction. iii) A catalyst must be selective only to terminal olefins to achieve highly terminal selective functionalization. Thus, new strategies to achieve terminal selective isomerizing functionalization of non-edible plant oils are highly sought.

This chapter describes an efficient methodology for isomerizing hydroformylation of cashew nut shell liquid using Rh complexes of bis-phosphorus ligands L1-L4. Regioselective I-HF of CNSLMonoene (S1), methoxy-protected CNSL-Monoene (S2), CNSL cardanol (S3), methoxy protected CNSL-cardanol (S4), and their further functionalization to unsymmetrical α,ω -difunctional building blocks and monomers is reported.

3.3: Result and Discussion

Rhodium catalyzed hydroformylation of internal alkenes to terminal aldehydes has been the subject of many investigations. Van Leeuwen and co-workers reported linear selective (86%) hydroformylation of *trans*-4-octene using xanthene-based bisphosphine ligands at low syngas pressure of 2 bars.²² Whereas, Beller and co-workers reported a linear selectivity of 70% while employing a bidentate phosphine ligand at 10 bars syngas pressure.²⁷ In contrast, Boerner and co-workers employed a phosphite ligand in the I-HF of isomeric n-octenes leading to better linear selectivity (up to 48% n-nonanal).⁷¹ Thus, a literature survey suggested that both, (bis)phosphites⁶⁸ and bisphosphine can catalyze isomerizing functionalization reactions of internal alkenes at elevated temperatures (120-140 °C).^{19,20,22,34,71,72} Among the long chain plant

oils, linear selective I-HF of methyl oleate is found to be catalyzed by bis-phosphite ligands of type L1 (**figure 3.3**).^{34,35,68}

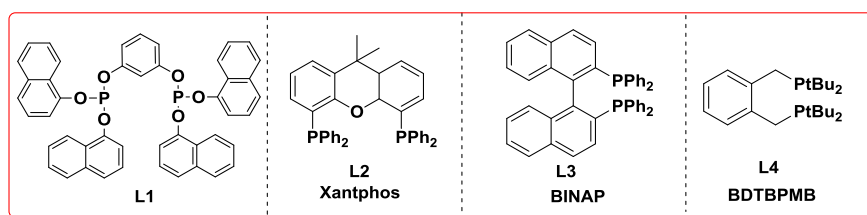
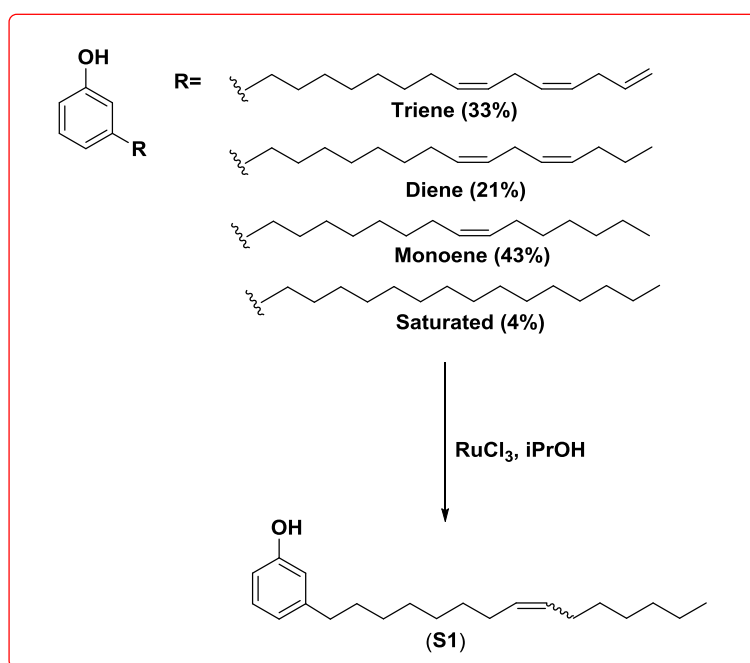


Figure 3.3: Ligands used for I-HF of cashew nut shell liquid

CNSL is a versatile byproduct of cashew industry and is a renewable and inexpensive resource.⁶³ It is obtained from spongy mesocarp of cashew nut shell. Decarboxylation of anacardic acid at 140 °C followed by vacuum distillation yields cardanol in its pure form (section 3.4, **figure 3.6**).^{72f} The relative composition of monoene, diene and triene in cardanol was established by HPLC analysis.^{70b} Diene and triene can be selectively hydrogenated to monoene when cardanol is subjected to selective hydrogenation in the presence of RuCl_3 and isopropanol (**scheme 3.1**).⁷³ The resultant monoene S1 was isolated in excellent yield (85%) and characterized using spectroscopic and analytical tools.

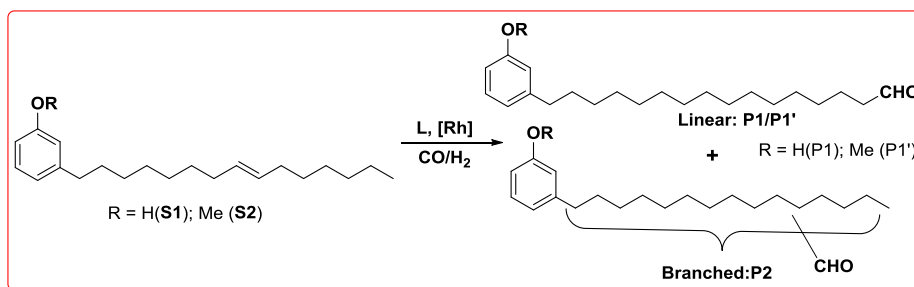


Scheme 3.1: Selective reduction of cardanol to CNSL-monoene (S1)

3.3.1: Isomerizing hydroformylation of CNSL-monoene

We began our studies with ligand screening and tested the activity of various ligands (**figure 3.3**).

The bis-phosphite ligand L1 and BINAP L3 produced only branched aldehydes, L2 led to 6% linear aldehyde, whereas application of L4 resulted in 16% linear aldehyde (**scheme 3.2**). Thus, the initial ligand screening suggested BDTBPMB (L4) as the ligand of choice (**table 3.1**).



Scheme 3.2: Isomerizing hydroformylation of CNSL-monoene

Table 3.1: Screening of various ligands in isomerizing hydroformylation of CNSL-Monoene (S1)^a

Sr. no.	L	L/M ratio	T (°C)	P (bar)	time (h.)	Conversion (%)	L:B Selectivity
01	L1	2	120	2.5	16	61	No linear
02	L2	2	120	2.5	16	53	6:94
03	L3	2	120	2.5	16	5	No linear
04	L4	2	120	2.5	16	83	16:84

^aConditions: [Rh] = [Rh(acac)(CO)₂] (2 mg), total conversion and L/B selectivities determined by ¹H NMR spectroscopy using CH₂Br₂ as an internal standard.

In our endeavor to identify the suitable solvent, we screened high boiling solvents such as toluene, xylene, mesitylene, N-methyl- 2-pyrrolidone, dimethoxyethane, and 1,4-dioxane. Solvent screening experiments supported the use of 1,4-dioxane as a better solvent (**table 3.2**). Although the selectivity for terminal aldehyde is better in *p*-xylene & mesitylene entries but overall conversion to aldehydes was less as compared to that in toluene and 1,4-dioxane (entries 2 & 3 vs. 1 & 6, **table 3.2**). Formation of terminal aldehyde was not observed in case of NMP (entry 4) while in case of DME selectivity for terminal aldehyde was 14% (entry 5). Therefore 1,4-dioxane was used as a solvent of choice for the rest of the isomerizing hydroformylation experiments.

Table 3.2: I-HF of CNSL-monoene: screening of various solvents.^a

Sr. n.o	Solvent	L/M ratio	T (°C)	P (bar)	Time (h.)	Conversion (%)	L:B Selectivity
01	Toluene	2	125	2	16	22	17:83
02	p-xylene	2	125	2	16	59	20:80
03	Mesitylene	2	125	2	16	50	20:80
04	NMP	2	125	2	16	27	No linear
05	DME	2	125	2	16	26	14:86
06	1,4-dioxane	2	125	2	16	44	20:80

^aConditions: [Rh] = [Rh(acac)(CO)₂] (2 mg), S/M = 100, total conversion and L/B selectivities determined by ¹H NMR spectroscopy using CH₂Br₂ as an internal standard.

Preliminary screening of reaction parameters led to a linear selectivity of 20% in 16 hours (**table 3.3**, run 1). Increasing the reaction time to 48 hours resulted in improved conversion but at the cost of reduced linear selectivity (entry 1 vs entry 8). Subsequently, we screened the effect of pressure on I-HF of monoene (run 2-6). Increasing the reaction pressure from 2 to 20 bars resulted in increased conversion and complete conversion of starting material was observed at 15 and 20 bars in just 4 hours (run 4-6) but the terminal selectivity dropped significantly (run 4-6 vs 1). Slight increase in reaction temperature to 125 °C resulted in improved conversion and enhanced terminal selectivity (run 1 vs. 7). A better terminal selectivity of 28% was obtained at a reaction temperature of 125 °C at 1 bar pressure (Table 1, run 7) although at the cost of reduced conversion, compared to the reaction at higher pressure. It is most likely that the rate of isomerization increases at higher temperature, whereas the rate of internal hydroformylation is suppressed at ambient pressure. The combined effect of these parameters resulted in higher terminal selectivity. To circumvent the influence of the phenoxy group, we protected free phenolic -OH group to -OMe (methoxy) by following a literature known procedure.^{70b,73} The resultant yellow oil was purified by column chromatography and the identity of S2 was established from proton and carbon (¹³C) NMR spectroscopy.⁷³ I-HF of S2 using L4 revealed linear selectivity of 50% under the optimized conditions (**table 3.3**, run 11). The resultant reaction mixture was purified by column chromatography (multiple times) to isolate the terminal aldehyde and existence of P1' was fully established using a combination of NMR, IR, Mass spectroscopy and HPLC (section 3.4, **figure 3.23-3.28**).

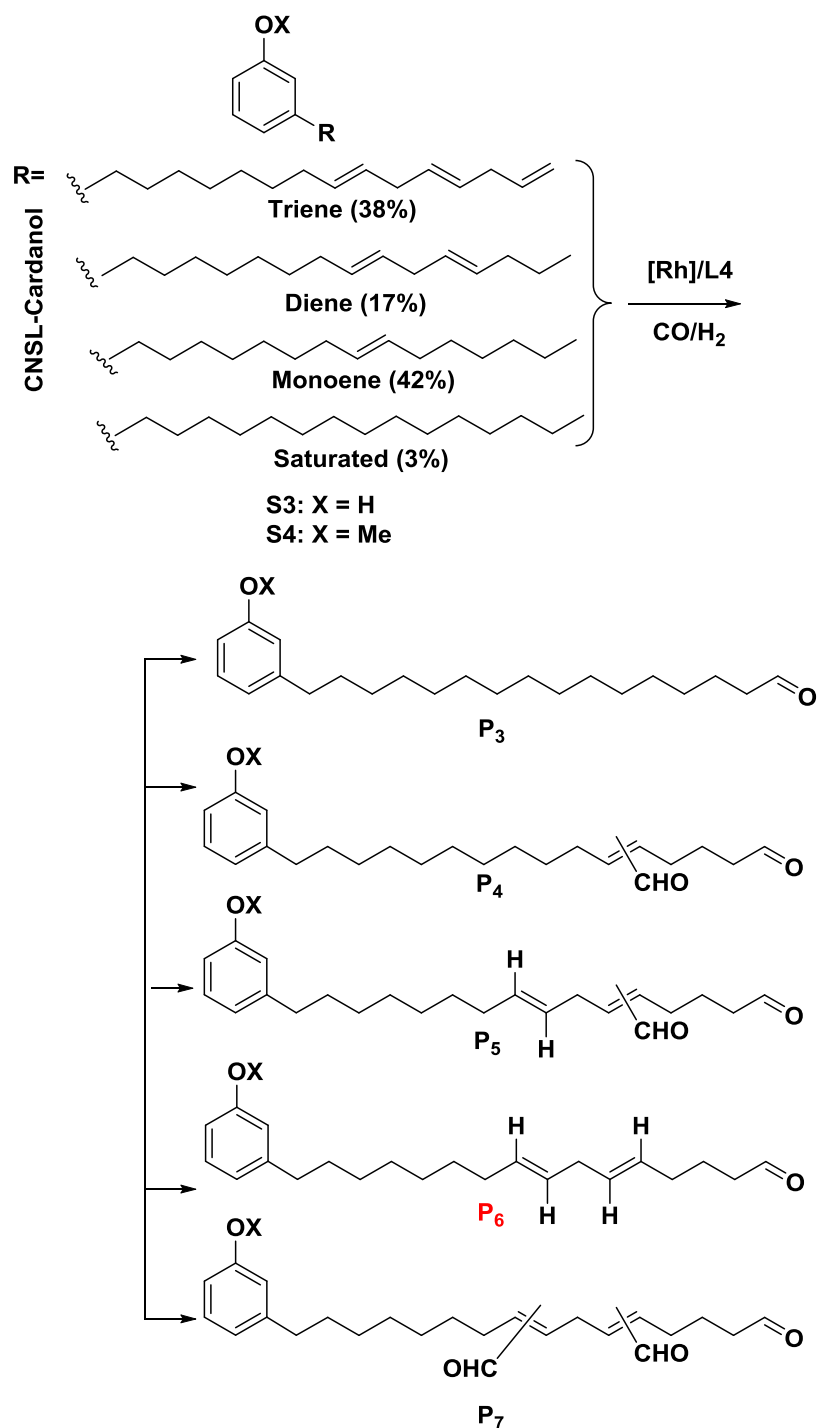
Table 3.3. I-HF of cashew nut shell liquid and short chain internal olefins.^a

Run	Subs ^b	T (°C)	P (bar)	T (h)	Conversion ^c (%)	l:b selectivity
1	S1 (1)	120	1	16	16 (7)	20:80
2	S1 (1)	125	2	16	44 (20)	20:80
3	S1 (1)	120	5	12	83 (30)	15:85
4	S1 (1)	125	10	4	99 (42)	14:86
5	S1 (1)	125	15	4	99 (63)	12:88
6	S1 (1)	125	20	4	99 (88)	10:90
7	S1 (1)	125	1	18	33 (22)	28:72
8	S1 (1)	120	1	48	89 (80)	16:84
9	S1 (1)	120	2	36	38 (37)	14:86
10	S2 (1)	120	2	36	56 (37)	18:82
11	S2 (1)	125	1	18	17 (12)	50:50
12	S2 (1)	120	5	40	51 (50)	9:91
13	S3 (2.5)	125	1	18	74 (26)	40:60
14	S3 (2.5)	120	1	10	60 (27)	52:48
15	S3 (2.5)	120	1	5	53 (16)	70:30
16	S3 (2.5)	120	1	3	50 (18)	74:26
17	S4 (2.5)	120	1	10	70 (11)	65:35
18	S4 (2.5)	120	1	5	64 (9)	68:32 ^d
19	S4 (2.5)	120	1	3	64 (6)	74:26
20	S5 (1)	120	1	16	93	37:63
21*	S5 (1)	120	1	16	99	48:52
22	S6 (1)	120	1	16	98	35:65
23*	S6 (1)	120	1	16	88	51:49

^aSubs = Substrates, S/M = 100, S1 = monoene, S2 = Me-protected monoene, S3 = CNSL-cardanol, S4 = Me protected CNSL-cardanol, S5 = *cis*-2-octene, S6 = *trans*-4-octene, [Rh] = [Rh(acac)(CO)₂] (2 mg), L/M = 2, solvent = 1,4-dioxane, total conversion and L/B selectivities determined by ¹H NMR spectroscopy using CH₂Br₂ as an internal standard. ^bThe average number of double bonds in the substrate is mentioned in bracket. ^cThis was further confirmed by HPLC, the number in the bracket indicate conversion to aldehyde out of the total conversion. ^dThese experiments were performed in duplicate, and the L/B ratio was determined by taking the average of two experiments. *Indicates that L1 was used as a ligand.

3.3.2: Isomerizing hydroformylation of CNSL-cardanol

To test the robustness of our methodology, we investigated I-HF of CNSL-cardanol. Note that CNSL-cardanol is a mixture of triene (38%), diene (17%), monoene (42%) and traces of saturated alkyl-chain. I-HF of such a mixture will not be just challenging but can lead to the mixture of aldehydes P3 to P7 (**scheme 3.3**) among others. These aldehydes P3-P7 can be either unsaturated aldehydes or saturated (if hydrogenation becomes a competing side reaction).



Scheme 3.3: Isomerizing hydroformylation of CNSL-cardanol and possible product range

Interestingly, I-HF of CNSL-cardanol (S3) under optimized conditions revealed enhanced terminal selectivity of 52% (**table 3.3**, run 14). Next, we screened the effect of time on terminal selectivity. A terminal selectivity of 74% was obtained under optimized reaction conditions (**table 3.3**, run 16) within 3 hours. However, the conversion to aldehyde was found to be only 18% of the total conversion. The improved terminal selectivity can be explained based on the fact that the CNSL-cardanol consists of a triene (about 38%) component with the readily available terminal

double bond. Thus, the I-HF of this terminal double bond adds up to the I-HF of internal double bonds and overall terminal selectivity is improved. This assumption was further corroborated by performing the I-HF of methoxy protected CNSL-cardanol S4.⁷⁴ Under the optimized conditions, I-HF of S4 displayed a terminal selectivity of 65% along with 70% overall conversion within 10 hours (**table 3.3**, run 17). Reducing the reaction time to 3 hours produced terminal selectivity of 74% with 64% overall conversion (**table 3.3**, run 19). However, conversion to the aldehyde was found to be only 6%, suggesting the limitation of the method. The performance of L1 and L4 was tested in the I-HF of short chain internal olefins such as *cis*-2-octene (S5) and *trans*-4-octene (S6), and the best results have been presented in **table 3.3**. I-HF of *cis*-2-octene under identical conditions revealed that L1 outperformed L4 and displayed 48% linear selectivity. Similarly, L1 led to 51% terminal selectivity in the I-HF of *trans*-4-octene, whereas L4 yielded 35% linear selectivity. These findings contradict the performance of L4 in the I-HF of S1-S4. As suggested by de Vries and co-workers⁷³ substrates S1-S4 might adopt a folded conformation (**figure 3.4**). In the folded conformation the phenyl ring in S1-S4 might hinder the coordination of the relatively bulky L1-catalyst to terminal-olefin and thus hamper the terminal selectivity. Whereas, relatively electron rich and less bulky L4-catalyst might still be able to coordinate to the terminal olefin, leading to better linear selectivity.

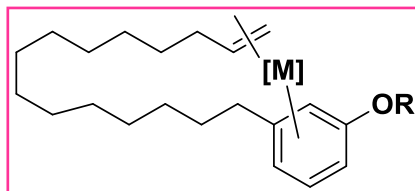
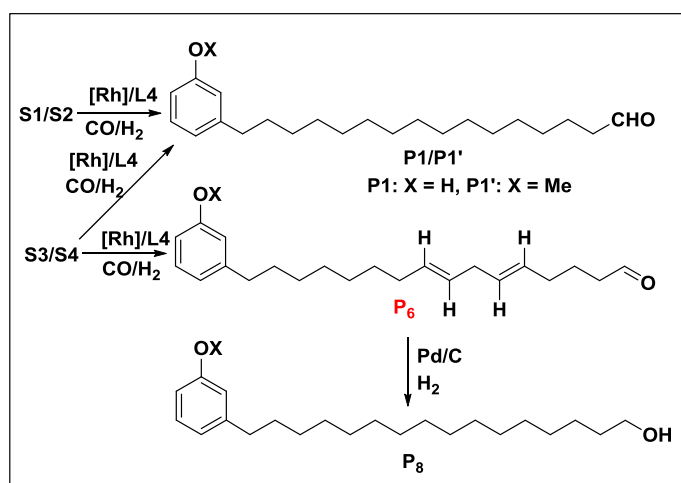


Figure 3.4: Proposed structure of folded CNSL-monoene (S1) in the presence of metal catalyst

3.3.3: Unsymmetrical α,ω -difunctional building blocks and monomers

The resultant aldehyde P6 was separated by column chromatography. The diolefinic-monoaldehyde P6 was characterized using NMR spectroscopy and was isolated in 44% yield. To demonstrate the synthetic utility of the aldehyde compounds obtained in this investigation, P6 was hydrogenated using Pd/C catalyst under mild conditions (**scheme 3.4**).



Scheme 3.4: Isomerizing hydroformylation of S1, S2, S3 and S4 to P1 and P6, and subsequent hydrogenation of P6 to P8

One pot isomerization hydroformylation-hydrogenation of S3 to P8 using Pd/C and CO:H₂ (1:4) lead to only hydrogenation with negligible aldehyde. Therefore, P6 was hydrogenated under mild conditions using Pd/C catalyst and resultant hydrogenation product P8 was isolated in 89% yield. The identity of 3-(16-hydroxyhexadecyl) phenol (P8) was fully established. The disappearance of aldehyde resonance at 9.77 ppm and consequent appearance of a hydroxy proton at 4.37 ppm and the respective methylene (-CH₂OH) proton at 3.34 ppm confirmed the existence of hydrogenated product P8. The NMR findings were corroborated by ESI-MS (+ve mode) which unveiled a positively charged ion peak at $m/z = 335.29$ [M+H]⁺ (details are given in **section 3.4**: experimental section), that exactly corresponds to the mass of P8. The thus produced unsymmetrical α,ω -difunctional molecule P8 can be utilized as AA type monomer for polycondensation.^{49b} The existence of unsymmetrical α,ω -difunctional linear aldehyde P1' (**scheme 3.4**) was confirmed by isolating the resultant aldehyde from the reaction mixture using silica gel column chromatography. A resonance at 9.77 ppm (triplet) in ¹H NMR (signals for branched aldehydes appear at 9.45-9.56 ppm as a doublet) confirmed the existence of terminal aldehyde (**figure 3.23**). The proton NMR findings were corroborated by ¹³C NMR spectroscopy that revealed a resonance at 203.3 ppm which can be assigned to aldehydic carbon (**figure 3.24-3.25**). In a 2D proton COSY NMR experiment, the aldehyde proton at 9.77 ppm revealed a cross peak to the adjacent methylene protons at 2.38 ppm (**figure 3.26**). Thus, the molecular structure of P1' was fully established using a combination of 1-2D NMR, Mass spectroscopy (**figure 3.28**) and HPLC (**figure 3.29**).

3.3.4: Coordination behavior of L4 and detection of catalyst resting state by high-pressure NMR

Phosphine as well as phosphite ligands are known to catalyze I-HF of internal olefins to linear aldehydes.³⁴ Phosphines being strong σ -donor form stable rhodium complex, whereas phosphites are good σ -donor and strong π -acceptor ligands yielding comparatively electron deficient rhodium complex. The latter are known to deliver higher activities than the former. It is well established that ligand coordination plays a pivotal role in determining the regioselectivity of a hydroformylation reaction.^{1b,1c} Therefore, establishing the coordination behavior of L4 around Rh-center and identification of the resultant catalyst resting state might shed light on the observed selectivity. Coordination behavior of L4 has been extensively studied in Pd catalyzed isomerizing alkoxy carbonylation.^{50,66,75} But coordination behavior of the same ligand around Rh and identification of resultant resting state remains unexplored. Unlike the case of palladium in isomerizing methoxycarbonylation, a bidentate ligand L4 can coordinate around trigonal bipyramidal Rh center in two different modes (**figure 3.5**): axial-equatorial (ae = C1) or equatorial-equatorial (ee = C2) or both these species may exist in equilibrium.^{29,49c}

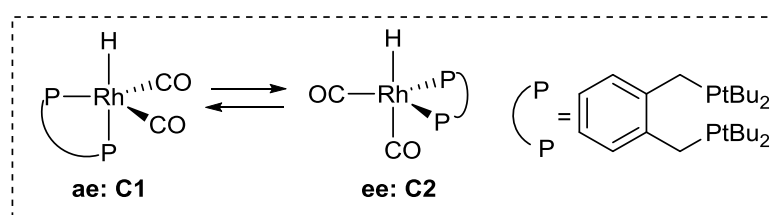


Figure 3.5: Coordination of bisphosphine ligand L4 around metal center and detection of catalyst resting states

In our pursuit to identify the active species, stoichiometric amount of L4 and $[\text{Rh}(\text{acac})(\text{CO})_2]$ were dissolved in toluene- d_8 in a high-pressure NMR tube and the mixture was pressurized with 10 bar of syngas. The high-pressure ^{31}P NMR spectrum of this solution at 90 °C revealed a doublet centered at 74.2 ppm with a $^1J_{\text{Rh-P}}$ coupling constant of 135 Hz (**figure 3.33**). The corresponding proton NMR of this solution displayed a broad doublet centered at -10.35 ppm with $J_{\text{P-H}}/J_{\text{Rh-H}}$ coupling constant of <3.5 Hz (**figure 3.34**). A doublet in the ^{31}P NMR spectrum and a fairly small $J_{\text{P-H}}$ is a characteristic of a predominantly equatorial equatorial (ee) coordination mode of the two phosphorus donors (**figure 3.5**, species C2).^{29,76} Similar results were obtained in presence of substrate (**figure 3.35 and 3.36**). Thus; these observations suggest that L4 predominantly coordinates in ee (C2) fashion. It is most likely that such exclusive formation of single isomers with $[\text{Rh}(\text{acac})(\text{CO})_2]$ at higher temperature leads to enhanced terminal selectivity.

3.4: Experimental Section

3.4.1: General methods and materials

Unless noted otherwise, all manipulations were carried out under an inert atmosphere using standard Schlenk techniques or m-Braun glove box. All solvents were distilled from sodium, sodium/benzophenone under argon atmosphere. $[\text{Rh}(\text{acac})(\text{CO})_2]$ was procured from Acros organics and used without further purification. Syngas (1:1 mixture of $\text{CO}:\text{H}_2$) was supplied by Ms. Vadilal Chemicals Ltd., Pune, India. 1,2-bis(ditertbutylphosphinomethyl)benzene ligand was purchased from Sigma Aldrich and used without further purification. Cashew nut shell liquid was received from Sunshield Chemicals Ltd. (Solvay subsidiary) and further purified to get cardanol and monoene. All other reagents/chemicals, solvents were purchased from local suppliers (Spectrochem Pvt. Ltd.; Avra Synthesis Pvt. Ltd.; Thomas Baker Pvt. Ltd. etc). The isomerizing hydroformylation was run in a Amar Equipment Pvt. Ltd. high pressure reactor equipped with pressure regulators and safety rupture valve. Solution NMR spectra were recorded on a Bruker Avance 200, 400, 500 and MHz instruments. Chemical shifts are referenced to external reference TMS (^1H and ^{13}C) or 85% H_3PO_4 ($\delta = 40.480747$ MHz, ^{31}P). Coupling constants are given as absolute values. Multiplicities are given as follows s: singlet, d: doublet, t: triplet, m: multiplet. *In-situ* high pressure NMR was recorded in Wilmad quick pressure valve NMR tube. Mass spectra were recorded on Thermo scientific Q-Exactive mass spectrometer; with Hypersil gold C18 column (150 x 4.6 mm diameter 8 μm particle size mobile phase used is 90% methanol + 10 % water +0.1 % formic acid). HPLC analyses were performed on Agilent 1260 infinity instrument equipped with UV detector at the wavelength of 273 nm. Infrared spectrum was collected on a Bruker α -T spectrophotometer in ATR mode.

3.4.2: Cashew nut shell liquid and conversion to monoene

Technical grade CNSL is a mixture of anacardic acid, cardanol, cardol and 2-methyl-cardol in smaller quantities. Decarboxylation of this mixture followed by vacuum distillation at 140 °C yielded pure cardanol from the above mixture. The decarboxylation and isolation of CNSL-cardanol is known in the literature.^{72f} It was characterized with the help of NMR and HPLC (**figure 3.6 and 3.7**). The HPLC chromatogram shows the relative composition of monoene, diene and triene in cardanol. Cardanol was selectively saturated to monoene according to the literature report.^{72f, 73} Following similar procedure, CNSL-monoene was isolated and the existence was confirmed by NMR and HPLC. The isomerizing hydroformylation of monoene to get the formyl group at the terminal position of the alkyl chain has been investigated for the first time.

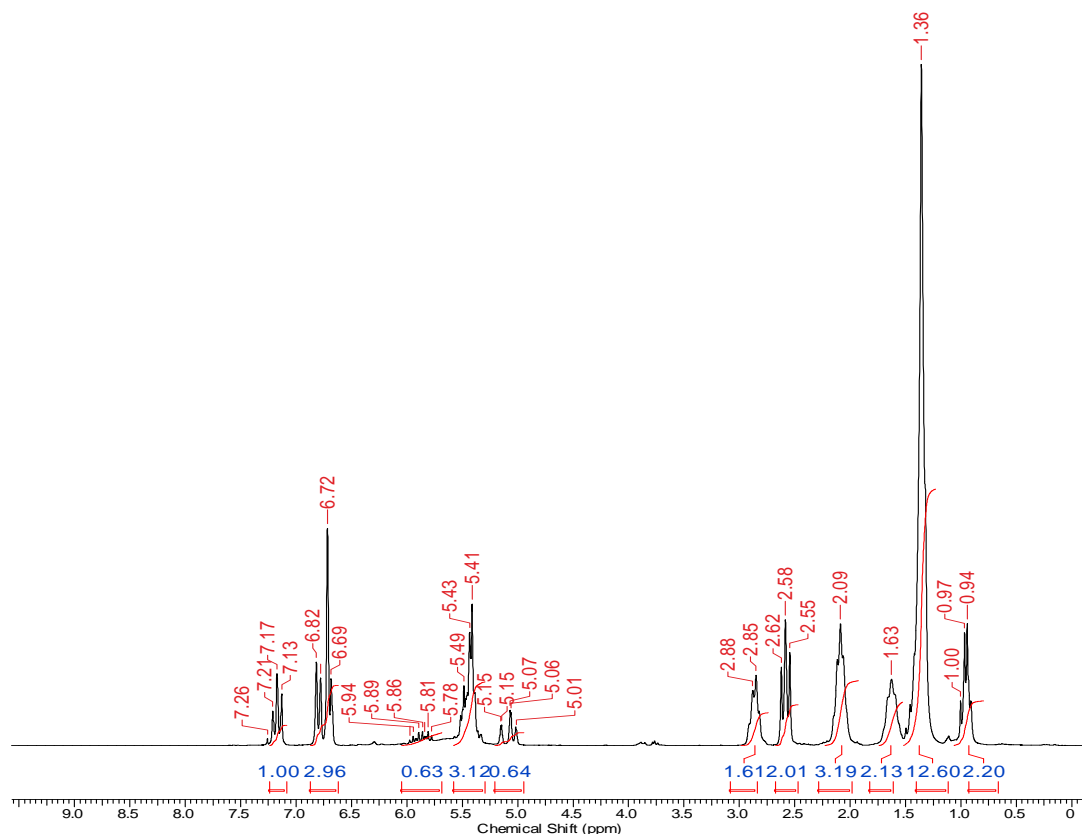
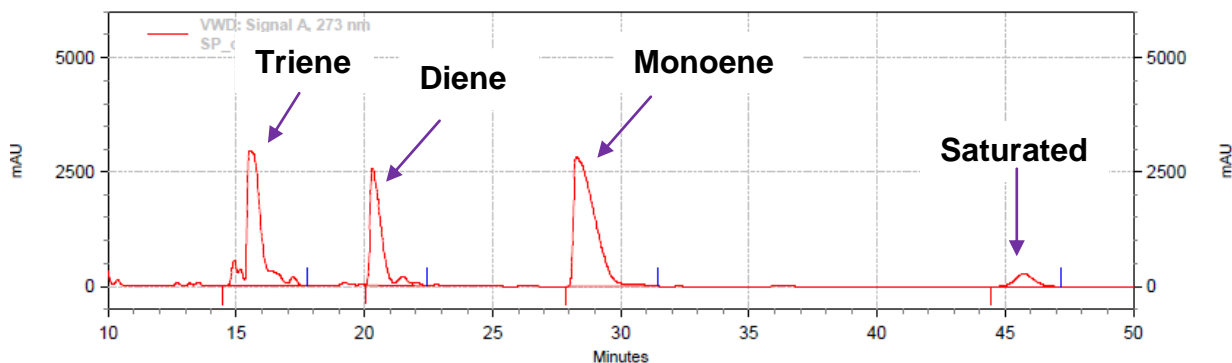


Figure 3.6: ^1H NMR spectrum of CNSL-cardanol in CDCl_3



VWD: Signal A, 273 nm Results

Retention Time	Area	Area %
15.527	2029116051	32.73
20.310	1289593678	20.80
28.273	2651425258	42.77
45.723	229314502	3.70
Totals	6199449489	100.00

Figure 3.7: HPLC chromatogram of CNSL-cardanol

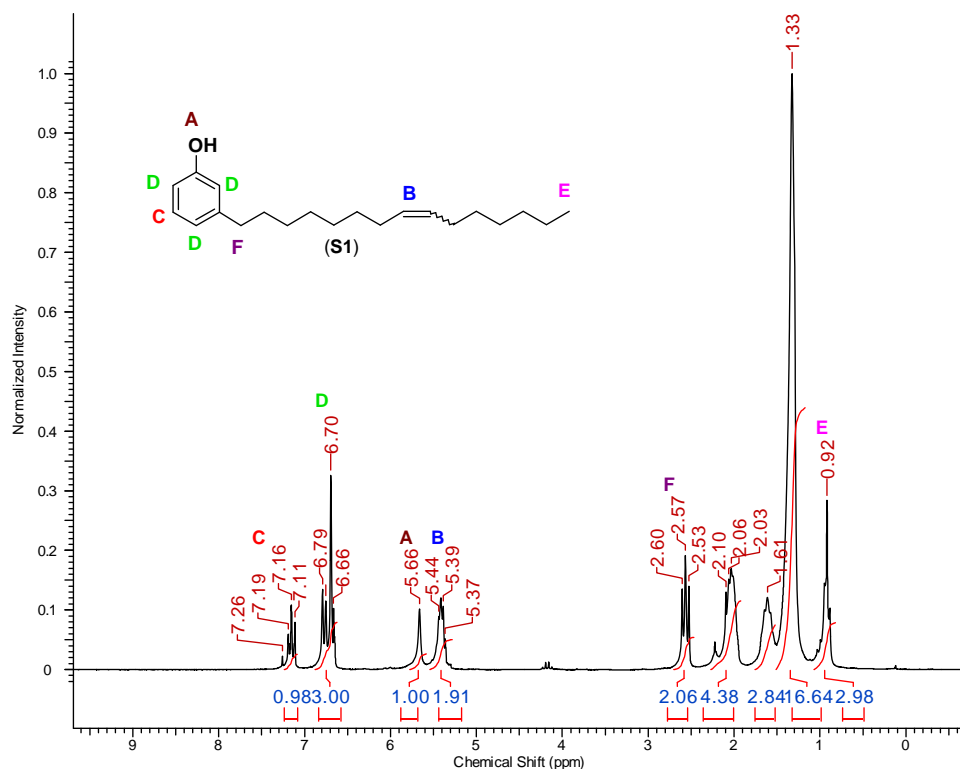


Figure 3.8: ^1H NMR spectrum of CNSL-monoene in CDCl_3

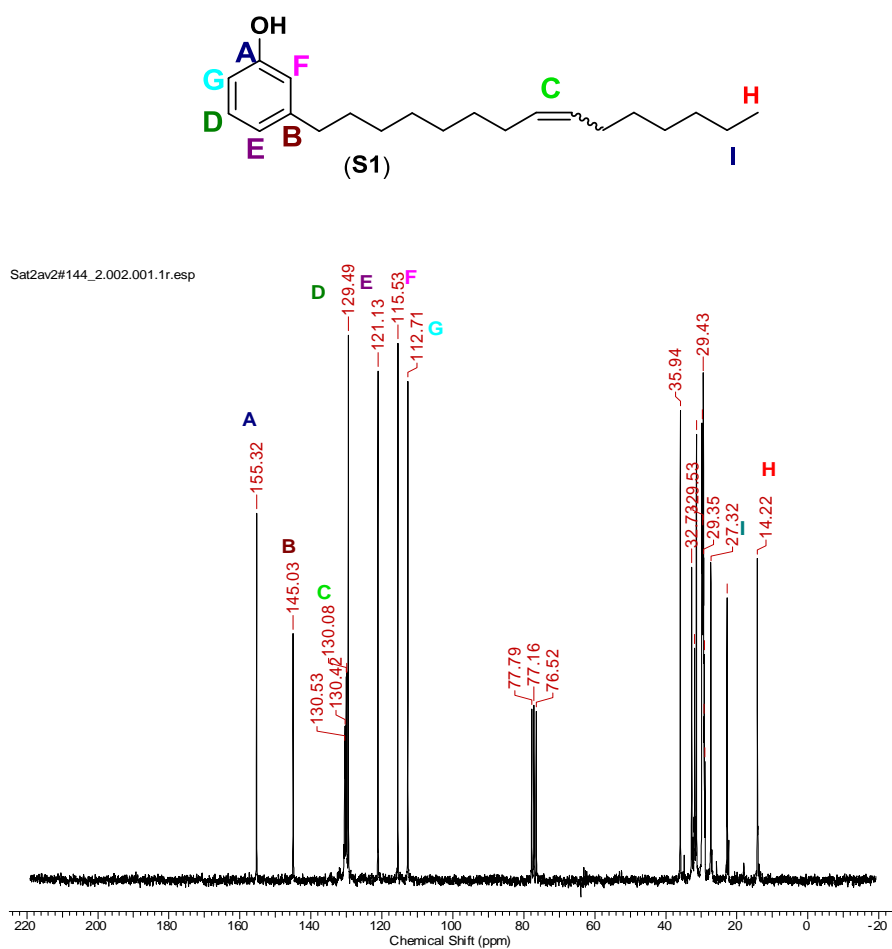


Figure 3.9: ^{13}C NMR spectrum of CNSL-monoene in CDCl_3

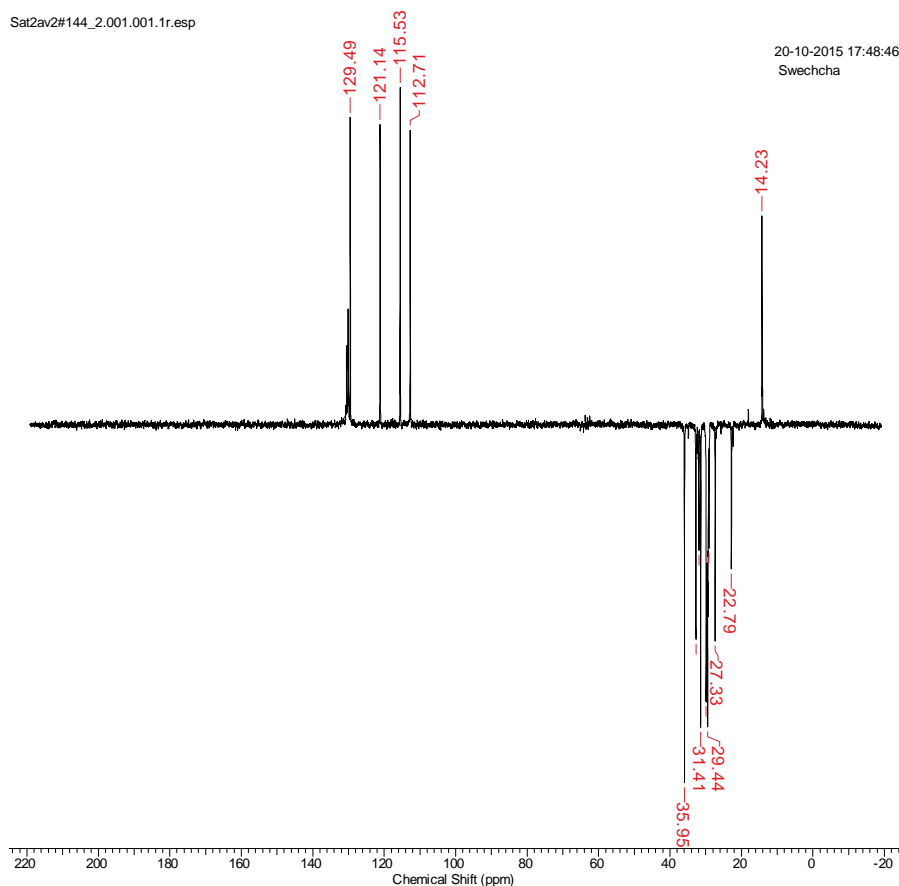
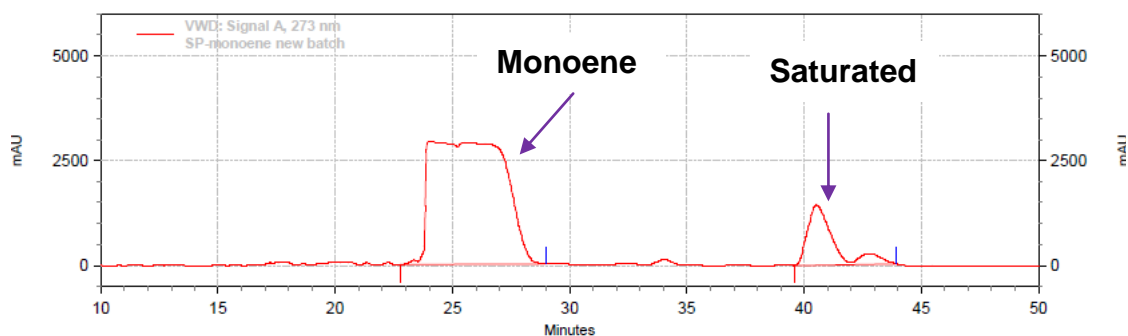


Figure 3.10: DEPT-135 spectrum of CNSL-monoene



VWD: Signal A, 273 nm Results

Retention Time	Area	Area %
24.027	11159235702	85.81
40.523	1845655629	14.19
Totals	13004891331	100.00

Figure 3.11: HPLC chromatogram of CNSL-monoene

3.4.3: Isomerizing hydroformylation of CNSL-monoene

Isomerizing hydroformylation of CNSL-monoene resulted in 28% terminal selectivity under optimized reaction conditions. The terminal selectivity and conversion was determined by NMR

using CH_2Br_2 as an internal standard. Hydrogenation of the olefin was found to be a competitive side-reaction under the optimized conditions.

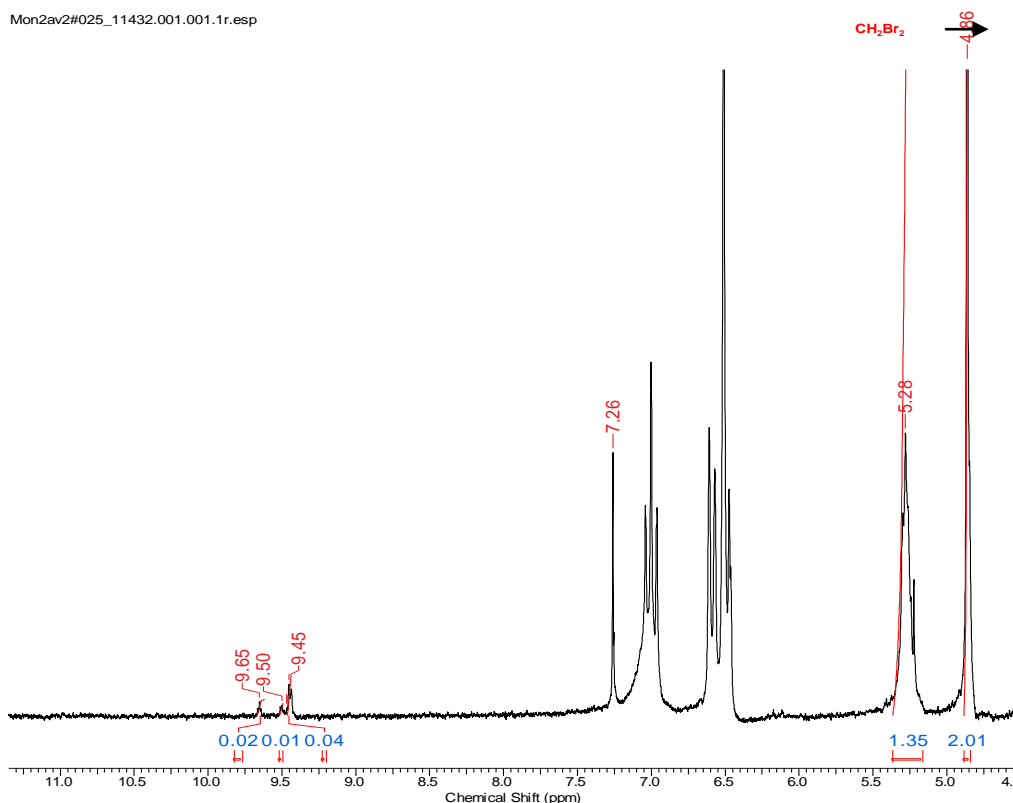


Figure 3.12: ^1H NMR spectrum of reaction mixture showing 28% terminal selectivity

3.4.4: Determination of conversion and selectivity in case of I-HF of CNSL-monoene

No. of olefinic protons present in starting material (X) = 2

Observed olefinic integration (Y) = 1.35 (see fig. 3.12) (table 3.3, run-7).

Total olefin reacted (Z) = $(X-Y)/X = (2-1.35)/2 = 0.325$

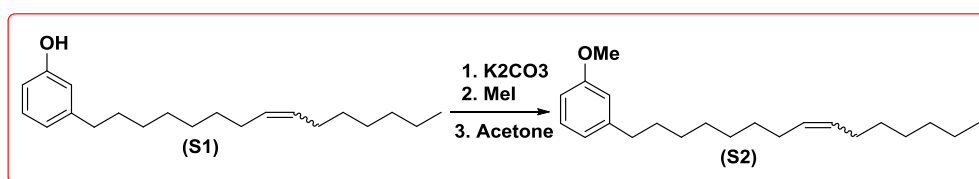
Total Conversion = $Z \times 100 = 0.325 \times 100 = 32.5\%$

Conversion to aldehyde = $(\text{Integration to aldehyde protons} / Z) \times 100 = (0.07/0.325) \times 100 = 22\%$

Terminal selectivity = $(\text{Integration to linear aldehyde} / \text{Total aldehyde integrations}) \times 100$
 $= (0.02/0.07) \times 100 = 28\%$.

3.4.5: Synthesis of Me-protected monoene (S2)

Compound S2 was synthesized by following a known literature procedure.^{70b}



Scheme 3.5: Synthesis of Me-protected monoene S2

Monoene (9.3 g, 0.0307 moles) and potassium carbonate (8.49 g, 0.0614 moles) were suspended in dry acetone. Methyl iodide (3.83 ml, 0.0614 moles) was added dropwise under inert conditions and reaction mixture was allowed to reflux for 6 hours. The reaction was then cooled to room temperature and the solvent was evaporated under reduced pressure to get white colored residue. The residue was dissolved in ethyl acetate. Now organic layer was washed with water (3* 50 ml), dried over MgSO₄, filtered and evaporated to get yellow oil. The oil was further purified over a silica column using hexane- ethyl acetate (5:1) as eluents.

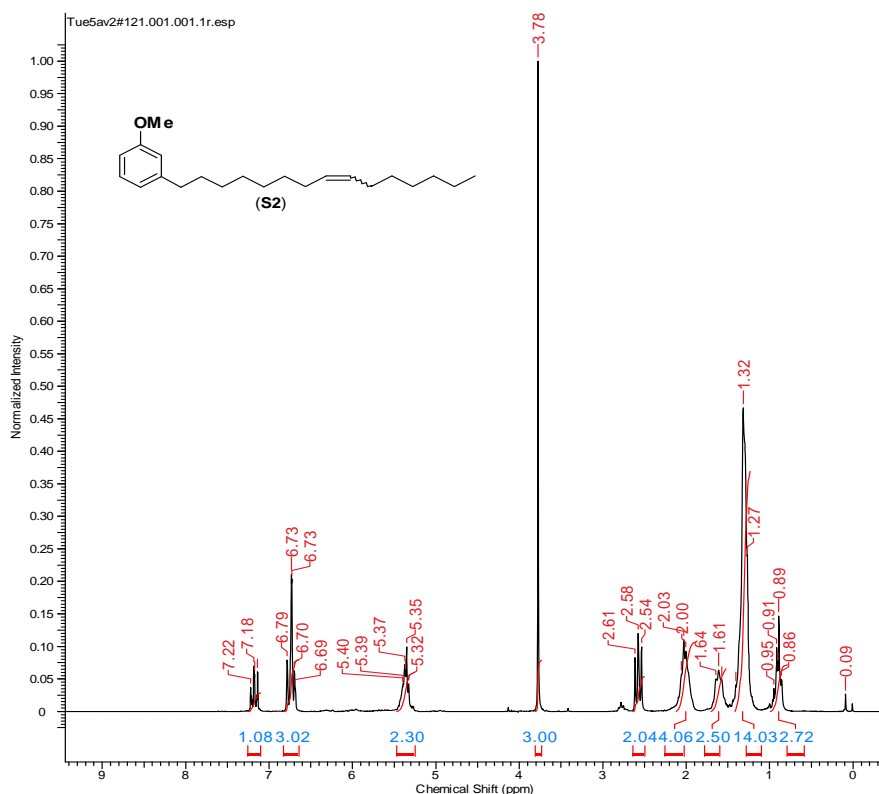


Figure 3.13: ¹H NMR spectrum of S2 in CDCl₃

3.4.6: Isomerizing hydroformylation of Me-protected monoene (S2)

Isomerizing hydroformylation of Me-protected monoene S2 revealed higher selectivity as compared to monoene under optimized reaction conditions. In this case, the terminal selectivity was improved to 50% (28% in case of monoene). Conversion and terminal selectivity was determined following a procedure described in section 3.4.4. Hydrogenation of the S2 was found to be a competitive side-reaction under the optimized conditions.

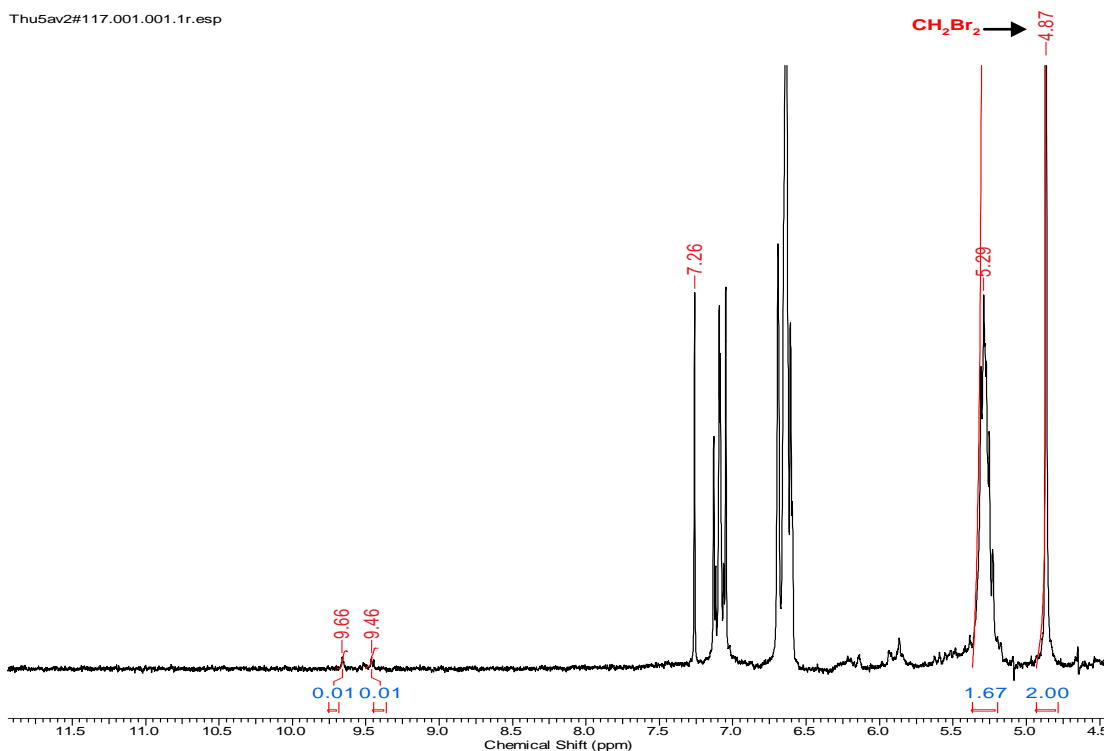


Figure 3.14: ¹H NMR spectrum of reaction mixture showing 50% terminal selectivity

3.4.7: Isomerizing hydroformylation of CNSL-cardanol

Isomerizing hydroformylation of crude cardanol proved to be highly selective than that of pure monoene. The improved terminal selectivity can be explained based on the fact that the CNSL-cardanol mixture consists of a triene component with readily available terminal double bond. Thus, the hydroformylation of this terminal double bond adds up to the isomerizing hydroformylation of internal double bonds and overall terminal selectivity is improved. However, due to presence of multiple double bonds in the starting material, formation of dialdehyde and trialdehyde along with monoaldehyde is highly favorable (**scheme 3.3**). Obtained regioselectivities were further confirmed using HPLC analysis. HPLC analyses were performed on Agilent 1260 infinity series instrument using acetonitrile + water + formic acid (93+2+5) as eluents, flow rate 0.5 ml/min., column C18, 5 μ m, 4.6*250 mm, λ_{max} = 273 nm, P6: R_t = 6.3 minutes (**figure 3.17**).

Remarkably, isomerizing hydroformylation of CNSL-cardanol led to diolefinic monoaldehyde in a selective manner. Obtained diolefinic monoaldehyde was isolated from the reaction mixture using silica gel column chromatography with pet ether and ethyl acetate (crude pet ether to ethyl acetate-90:10, isolated yield = 18 mg, 44%).

Determination of yield of P6 (scheme 3.3):

Assuming full conversion, 298.47 g of CNSL-cardanol can give 328.49 g of diolefinic monoaldehyde (P6).

Therefore, 0.23 g CNSL-cardanol should give $(328.49/298.47)*0.23 = 0.25$ g of P6.

Considering run 14 (**table 3.3**), total conversion was 60%, i.e. $(60*0.25g) / 100 = 0.15$ g of P6.

Conversion to aldehyde is 27%, therefore, $(0.15*27)/100 = 0.0405$ g of P6.

Obtained yield = 0.018 g

Therefore, % yield of P6 = $(0.018g / 0.0405 g) * 100 = 44\%$.

3.4.8: Determination of conversion & selectivity for I-HF of CNSL-cardanol

In case of CNSL-cardanol and methyl protected CNSL-cardanol the exact olefinic integrations were obtained by calibrating the NMR spectrum. Equimolar amount of CH_2Br_2 and CNSL-cardanol were dissolved in CDCl_3 (0.5 ml) and transferred to NMR tube. Proton NMR spectrum of this mixture is depicted in **figure 3.15**.

No. of olefinic protons present in starting material (X) = 5 (See fig. 3.15, $\delta = 4.99$ and 5.37).

Observed olefinic integration (Y) = 1.80 (See fig. 3.18, $\delta = 5.29$).

Total olefin reacted (Z) = $(X-Y)/X = (5-1.80)/5 = 0.64$

Total Conversion = $Z*100 = 0.64*100 = 64\%$

Conversion to aldehyde = $(\text{Integration to aldehyde protons} / Z) * 100 = (0.04/0.64)*100 = 6\%$

Terminal selectivity = $(\text{Integration to linear aldehyde} / \text{Total aldehyde integrations}) * 100$
 $= (0.03/0.04)*100 = 75\%$ (See fig. 3.18).

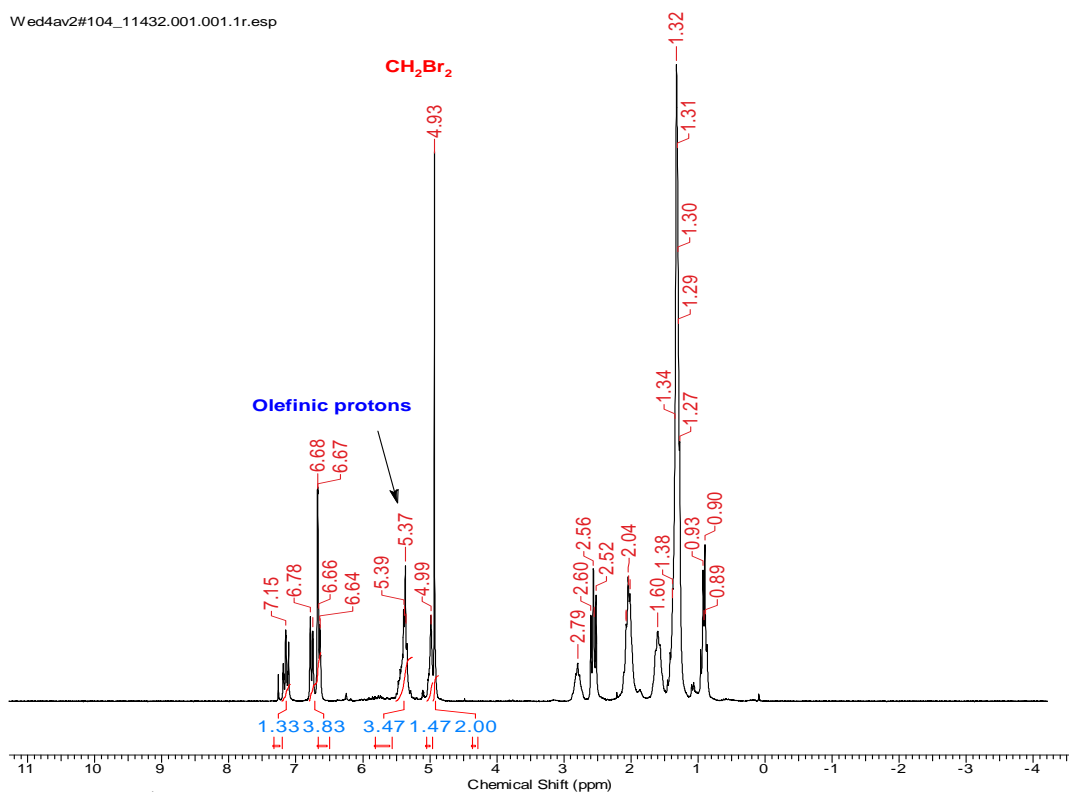


Figure 3.15: ^1H NMR spectrum of equimolar solution of cardanol and CH_2Br_2 in CDCl_3

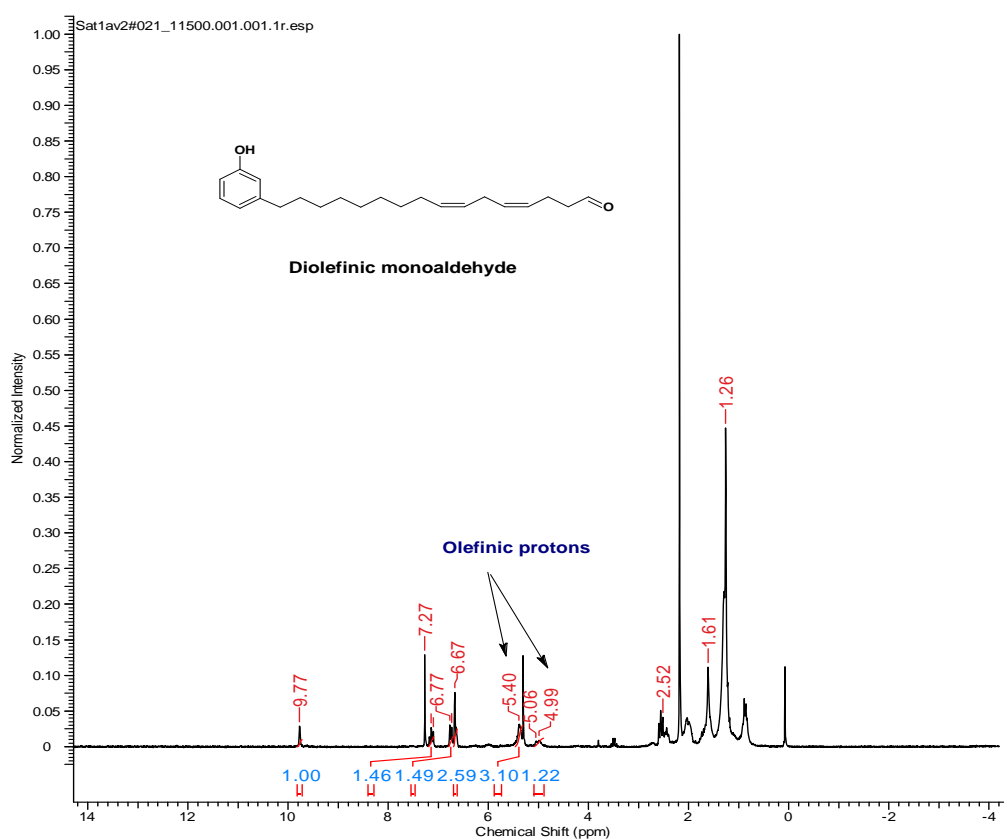
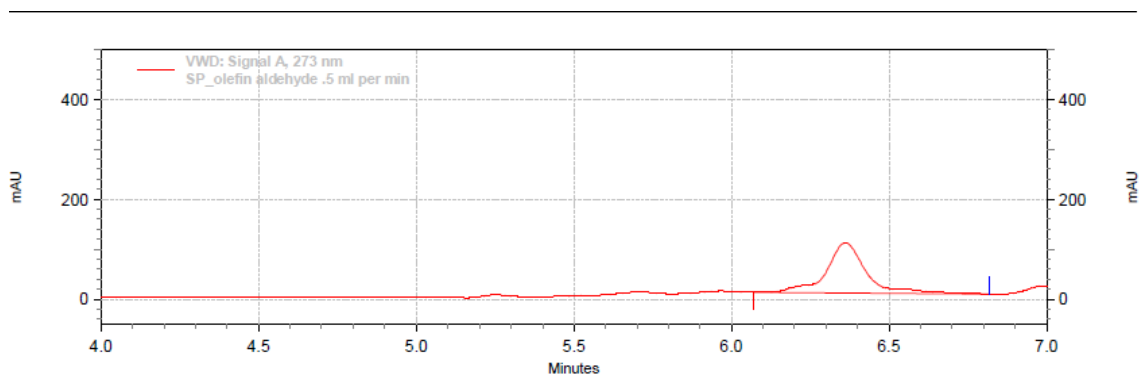


Figure 3.16: ^1H NMR spectrum of diolefinic monoaldehyde in CDCl_3

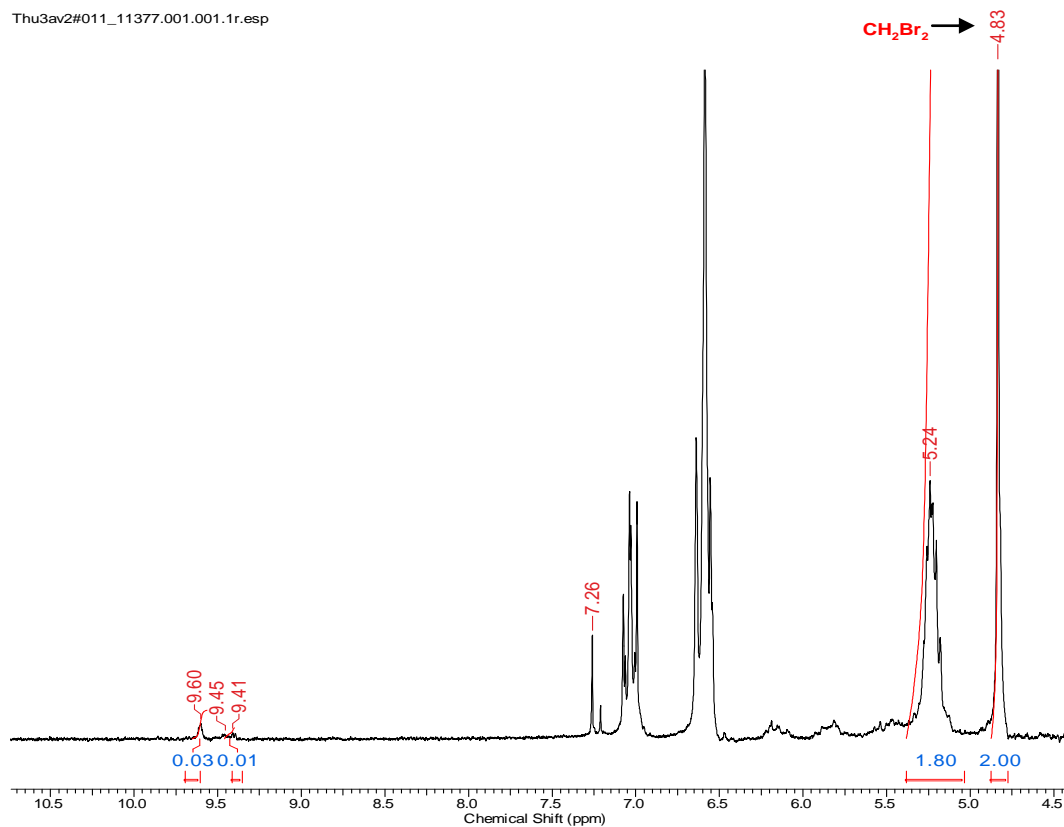


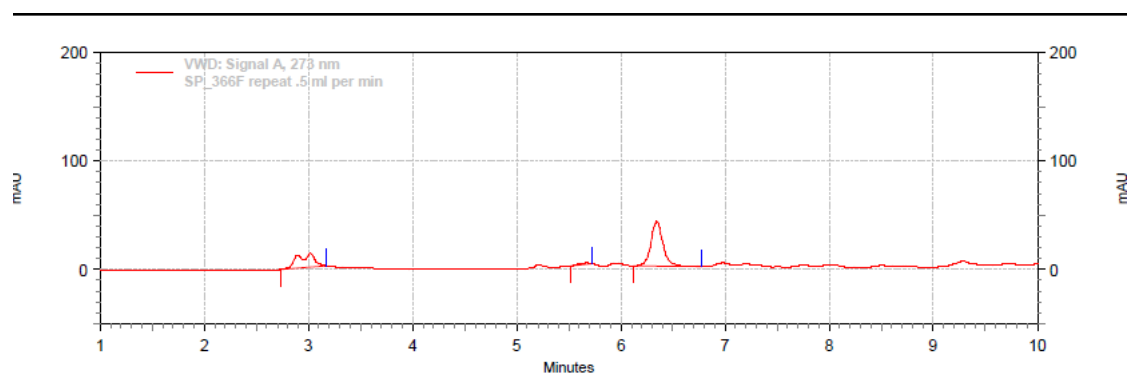
VWD: Signal A, 273 nm Results

Retention Time	Area	Area %
6.360	15009564	100.00
Totals		15009564
		100.00

Figure 3.17: HPLC chromatogram of isolated diolefin monoaldehyde

Thu3av2#011_11377.001.001.1r.esp

**Figure 3.18:** ^1H NMR spectrum of reaction mixture showing 74% terminal selectivity

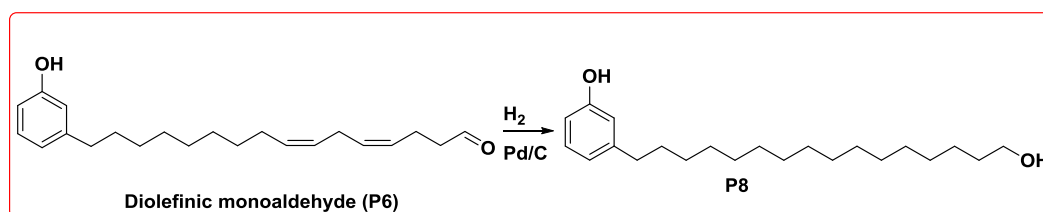


VWD: Signal A, 273 nm Results		
Retention Time	Area	Area %
3.017	2408336	29.68
5.673	191224	2.36
6.343	5514473	67.96
Totals		100.00
	8114033	

Figure 3.19: HPLC chromatogram of reaction mixture showing 68% terminal selectivity (Table 3.3, run 18)

3.4.9: Reduction of diolefinic monoaldehyde (P6)

The hydrogenation of alkenes containing aldehyde group is known in literature.⁷⁷ Similar procedure with slight modification was followed to reduce P6. Thus, subsequent reduction of monoaldehyde P6 using Pd/C led to the formation of AA type monomer P8 (scheme 3.6) with excellent conversion.



Scheme 3.6: Subsequent reduction of diolefinic monoaldehyde P6 to P8

P6 (0.020 g) and palladium on charcoal (0.025 g) were taken in a RB flask and dry methanol (5 ml) was added to it. After the desired reaction time, the reaction mixture was filtered through a pad of celite and washed with DCM. Obtained filtrate was evaporated *in vacuo* to get white colored solid (0.018 g, 89 %). Details of optimization studies are summarized in table 3.4.

Table 3.4: Optimization studies for hydrogenation of P6^a

S. No.	Solvent	Temperature (°C)	H ₂ Pressure (bar)	Reaction time (hrs.)	Conversion (%)
01	MeOH	rt	2	18	37
02	MeOH	50	10	5	85
03	MeOH	50	10	12	>99

^aConditions: P6 = 0.020g, 10% Pd on charcoal = 0.025g, MeOH = 5 ml.

¹H NMR (500 MHz, CDCl₃, 298K): δ = 7.14 (t, J_{H-H} = 7 Hz, 1H, H_f), 6.76 (d, J_{H-H} = 7.3 Hz, 1H, H_g), 6.66 (m, 2H, H_g), 4.38 (t, J_{H-H} = 4.5 Hz, 1H, H_a), 3.34 (m, 2H, H_b), 2.57 (t, J_{H-H} = 7 Hz, 2H, H_h), 1.60 (m, 6H, H_c), 1.26 (m, 22H, H_j). **¹³C NMR** (125 MHz, CDCl₃, 298K): δ = 157.2 (C_e), 145.1 (C_k), 129.5 (C_f), 121.1 (C_g), 115.4 (C_g), 112.6 (C_g), 58.7 (C_b), 36.7 (C_h), 32.1 (C_c), 29.8 (C_j), 26.3 (C_j). **ESI-MS** (+ve mode): m/z = 335.29 [M+H]⁺.

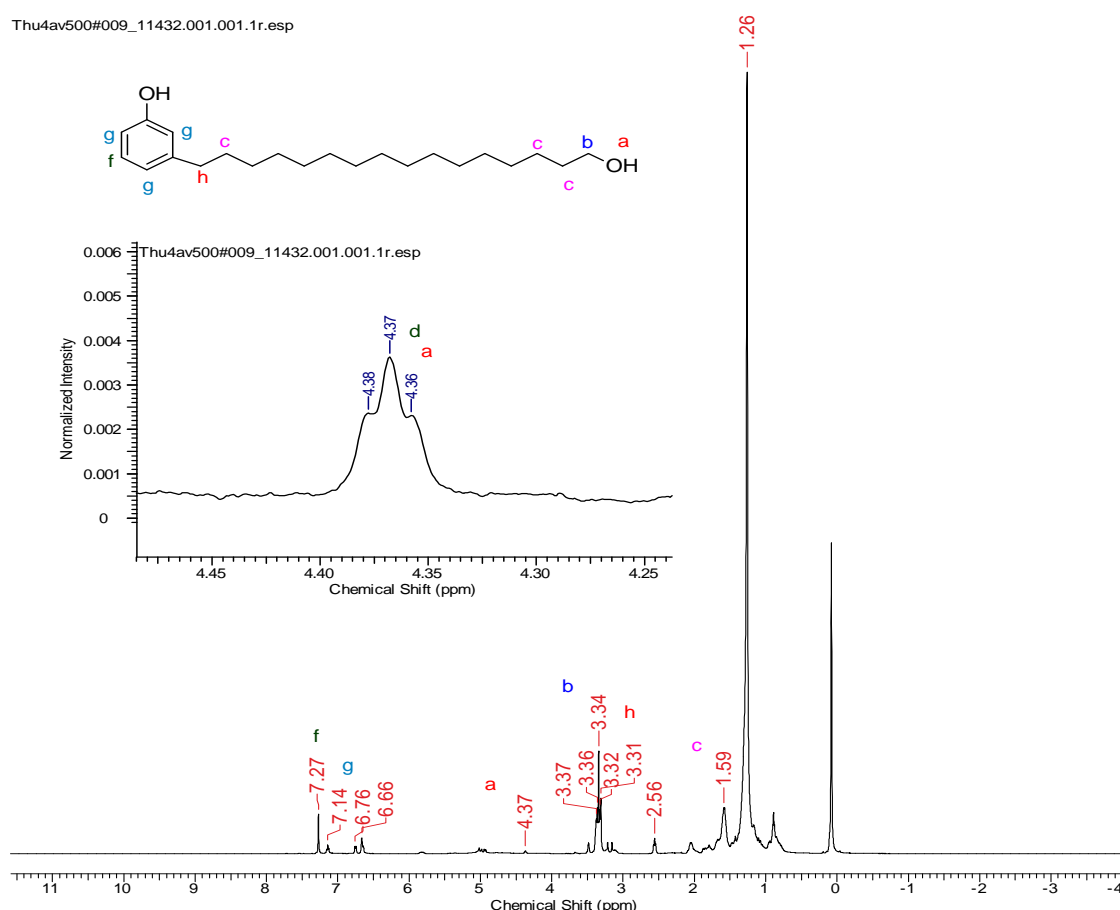
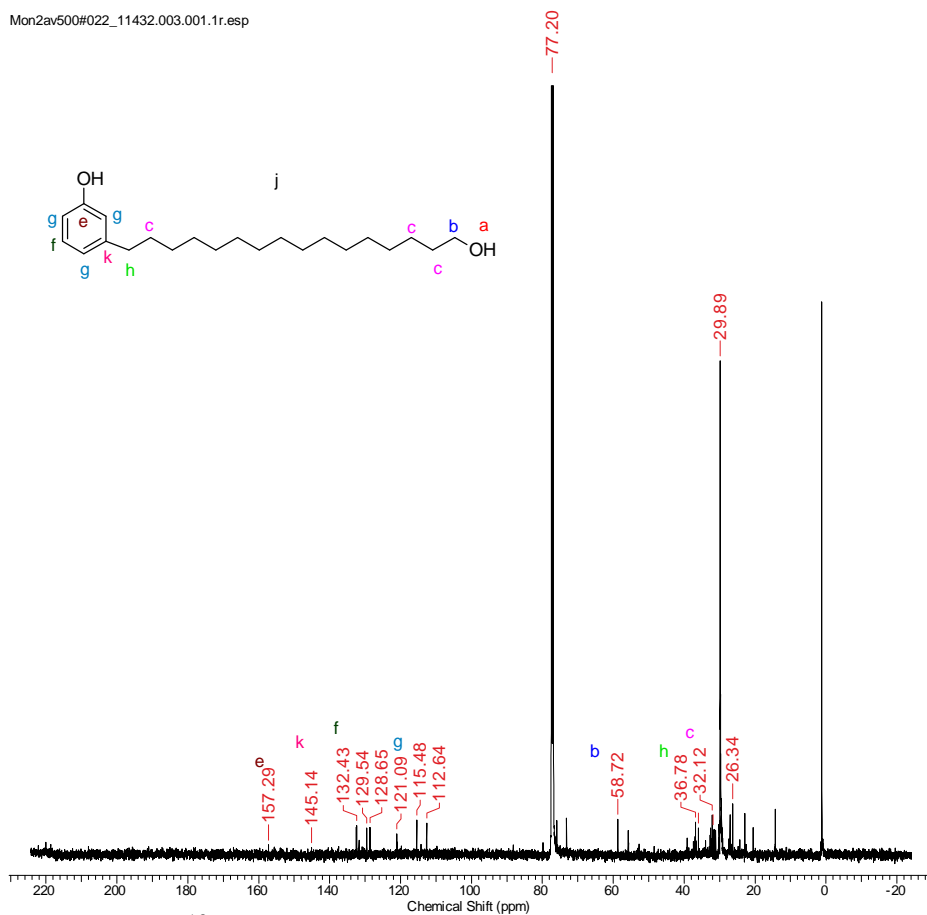
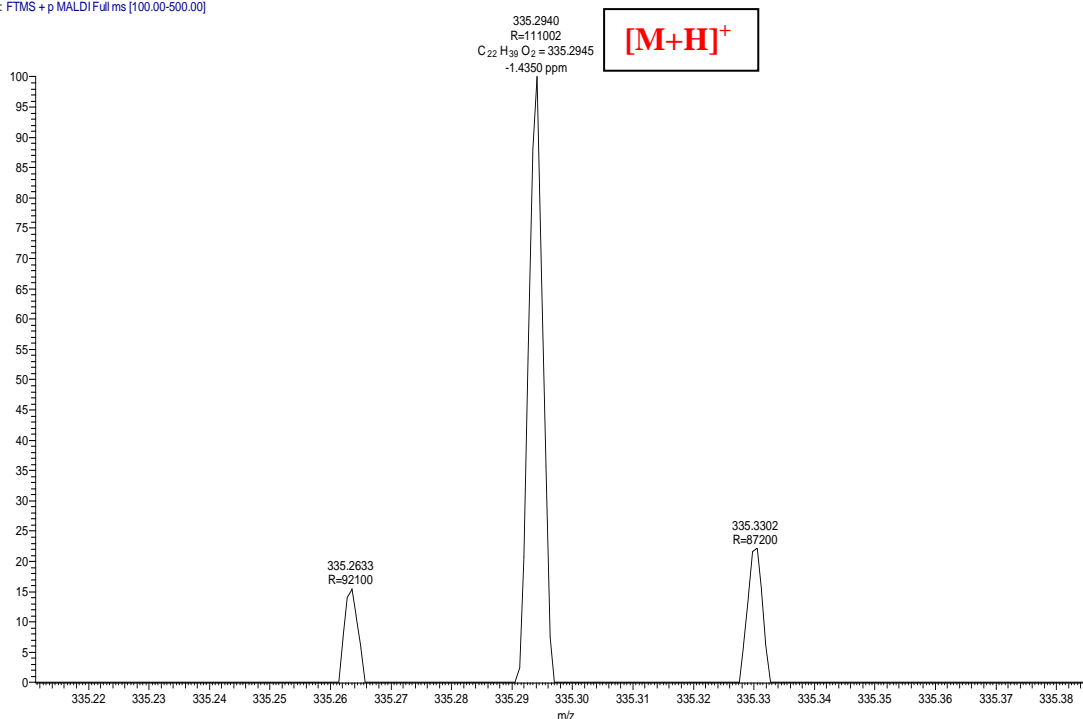


Figure 3.20: ¹H NMR spectrum of hydrogenated product P8 in CDCl₃



Data_04 #9 RT: 0.10 AV: 1 NL: 2.62E3
T: FTMS +p MALDI/Full ms [100.00-500.00]



3.4.10: Preparation, separation and characterization of linear aldehyde

To obtain reasonable amount of product, 0.48 g of Me-protected monoene was hydroformylated at 125 °C, 2 bar syngas pressure for 24 hours with 2 mol% {[Rh(acac)(CO)₂] = 4 mg} catalyst loading. As calculated by ¹H NMR, a total conversion of 64% was obtained with 46% aldehyde. After the reaction, the linear aldehyde was separated from the reaction mixture using flash silica column chromatography with hexane and diethyl ether (100:1 to 10:1) as eluents. The linear aldehyde was isolated in 10% yield as per following method.

316.52 g of Me-protected monoene (S2) gives 346.55 g of aldehydes (P1' & P2').

0.48 g Me-protected monoene (S2) should give $(346.55 \times 0.48) / 316.52 = 0.52$ g (P1' & P2').

Considering the total conversion of 64% $(64 \times 0.52 \text{ g}) / 100 = 0.33$ g (P1' & P2') (figure 3.31)

Since conversion to aldehyde is 46%,

$(0.33 \text{ g} \times 46) / 100 = 0.15$ g (P1' & P2') should be obtained.

After column 0.015 g of P1' was isolated.

Therefore, isolated % yield of P1' = $(0.015 \text{ g} / 0.15 \text{ g}) / 100 = 10\%$.

¹H NMR (500 MHz, CDCl₃, 298K): δ = 9.77 (t, 1H, H_a), 7.20 (t, 1H, H_f), 6.77 (m, 3H, H_g), 3.81 (s, 3H, H_d), 2.58 (t, 2H, H_h), 2.38 (m, 2H, H_b), 1.58 (m, 6H, H_c), 1.26 (m, 20H, H_j). ¹³C NMR (125 MHz, CDCl₃, 298K): δ = 203.2 (C_a), 159.9 (C_e), 144.6 (C_k), 129.4 (C_f), 121.0 (C_g), 114.4 (C_g), 111.0 (C_g), 55.3 (C_d), 44.1 (C_b), 36.2 (C_h), 32.3 (C_c), 31.6 (C_c), 29.9-29.6 (C_j), 26.2 (C_j). ESI-MS (+ve mode) : m/z = 347.29 [M+H]⁺.

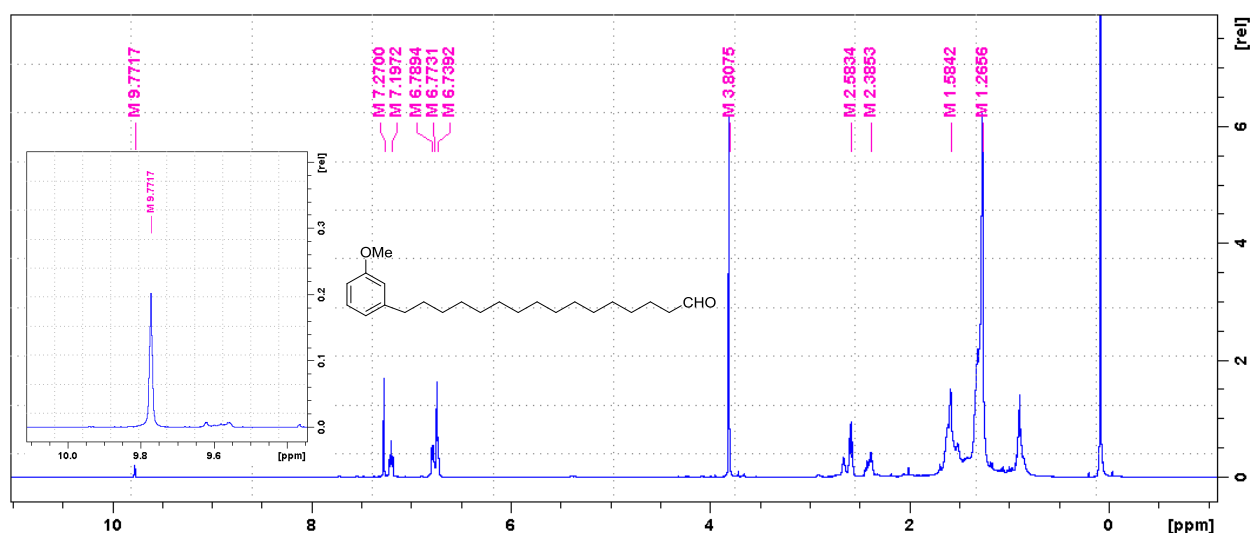


Figure 3.23: ¹H NMR spectrum of linear aldehyde (P1') in CDCl₃

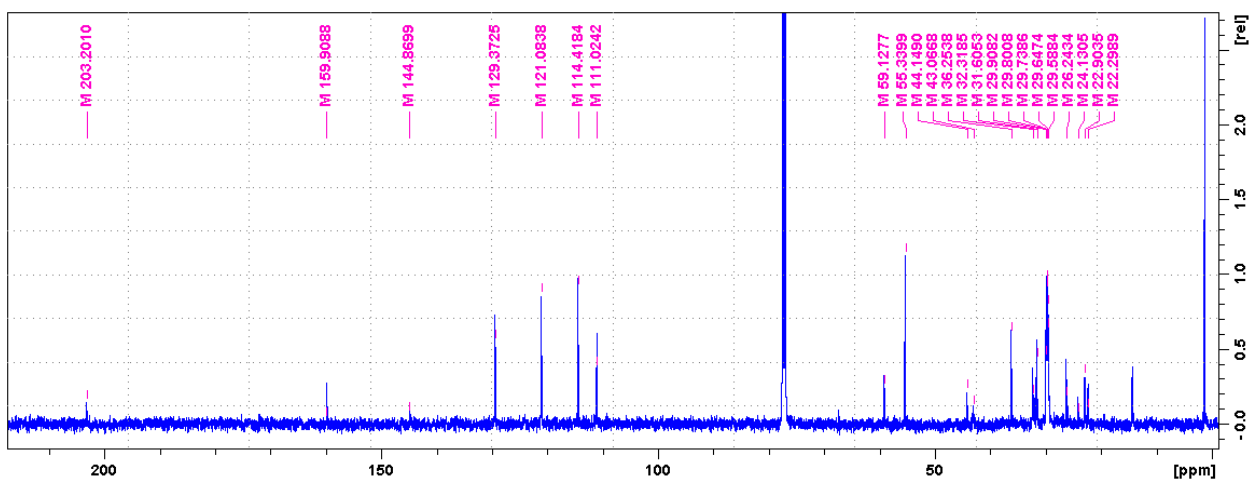


Figure 3.24: ^{13}C NMR spectrum of linear aldehyde (P1') in CDCl_3

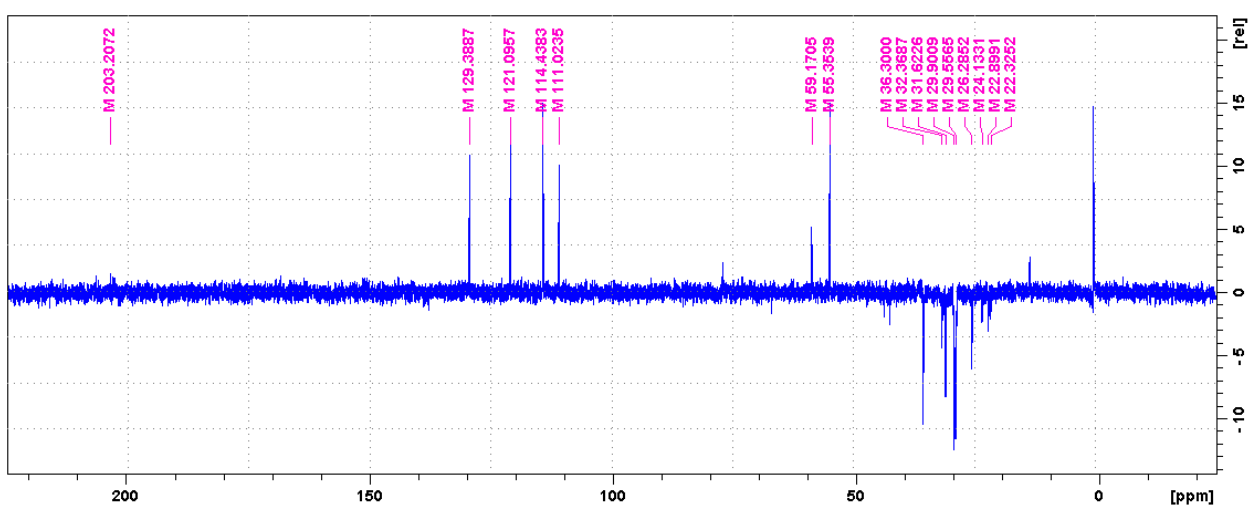


Figure 3.25: DEPT-135 NMR spectrum of linear aldehyde (P1') in CDCl_3

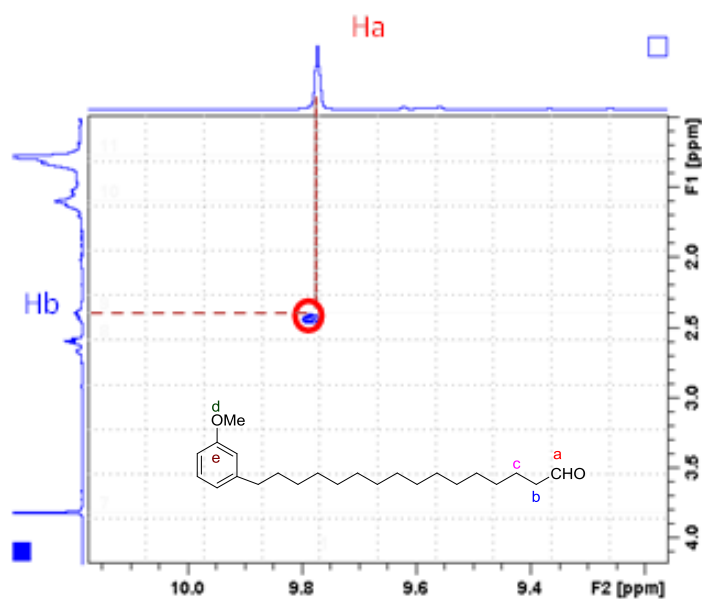


Figure 3.26: H-H correlation (COSY) spectrum of P1' displaying the connectivity between an aldehydic proton with the methylene proton.

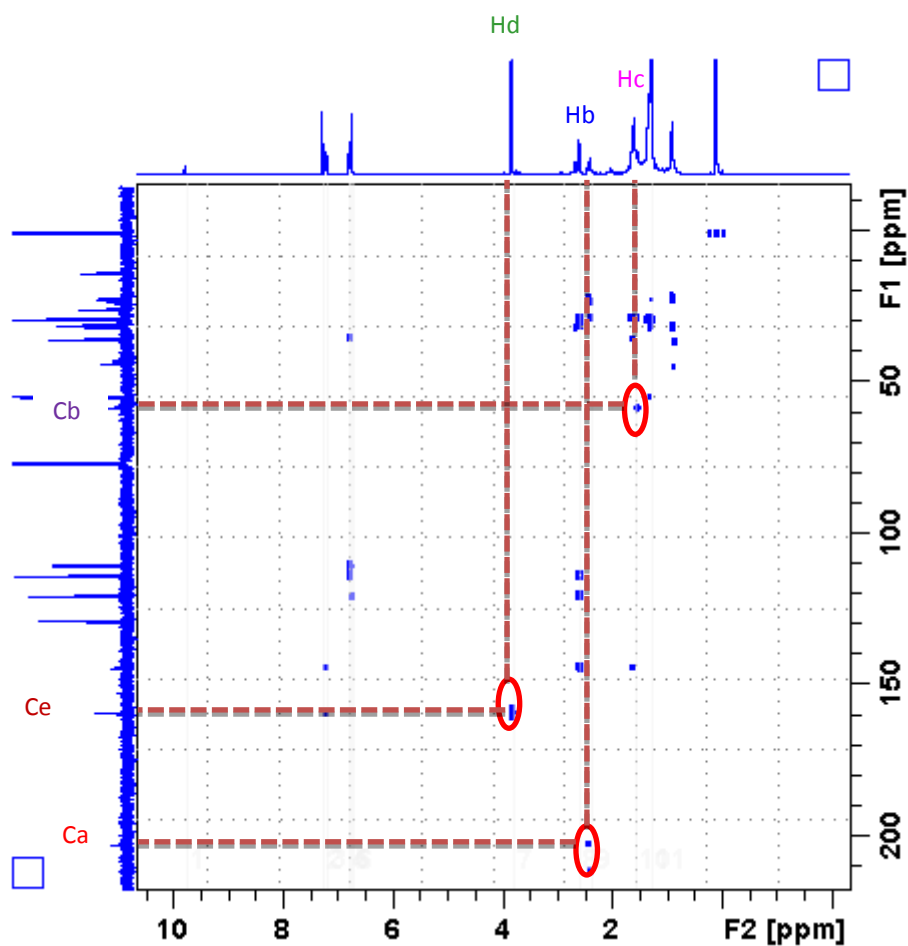


Figure 3.27: A long range C-H correlation (HMBC) spectrum of linear aldehyde (P1') in CDCl_3

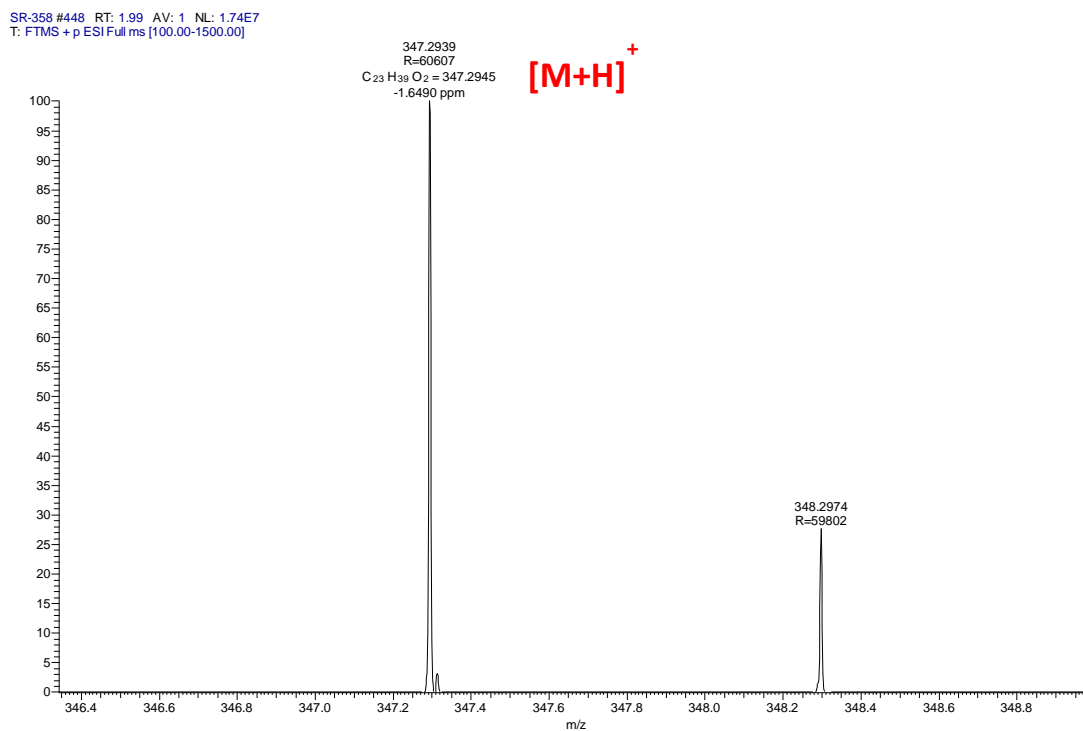
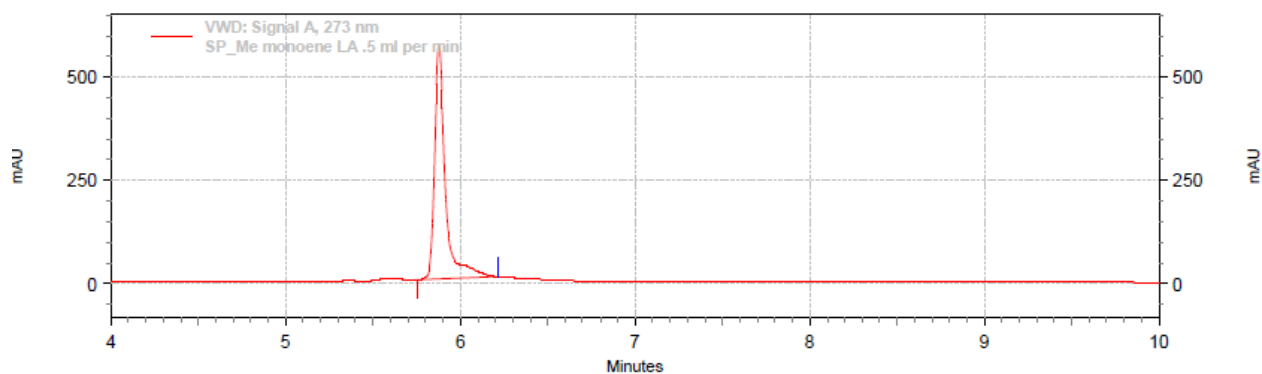


Figure 3.28: ESI-MS (positive mode) mass spectrum of linear aldehyde (P1')



VWD: Signal A, 273 nm Results

Retention Time	Area	Area %
5.877	40900831	100.00
Totals		100.00
	40900831	

Figure 3.29: HPLC chromatogram of isolated aldehyde (P1') derived from Me protected monoene

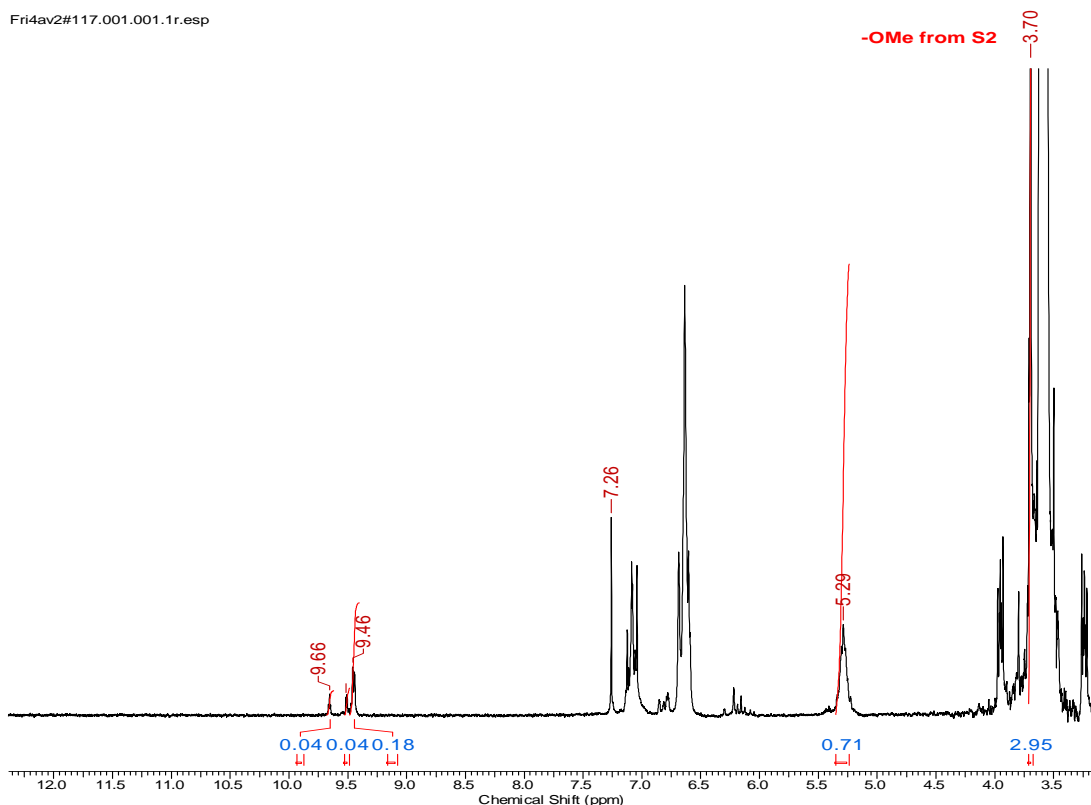


Figure 3.30: ^1H NMR spectrum of reaction mixture using S2 as substrate with a total conversion of 64% (conversion to aldehyde is 46%) in CDCl_3

3.4.11: Control experiments

3.4.11.1: In presence of conjugated diene

In a typical isomerizing-hydroformylation experiment a stainless steel autoclave (450 mL) equipped with pressure regulator and a safety valve was used. Individual vials were charged with metal precursor (0.002 g), ligand (0.0061 g), solvent (1 ml), 1,3-butadiene (0.21 ml, 100 eq.) and stirring bars in a glove box. The vials were transferred to autoclave and the autoclave was purged three times with syngas ($\text{CO}:\text{H}_2 = 1:1$) before pressurizing it to the desired pressure. The autoclave was heated at $100\text{ }^\circ\text{C}$ at 1 bar syngas pressure for 16 hours. After completion of reaction, the autoclave was cooled to $0\text{ }^\circ\text{C}$, and excess gas was vented off in a well-ventilated fume-hood. The conversion and regio-selectivity were determined by ^1H NMR spectroscopy using dibromomethane as an internal standard.

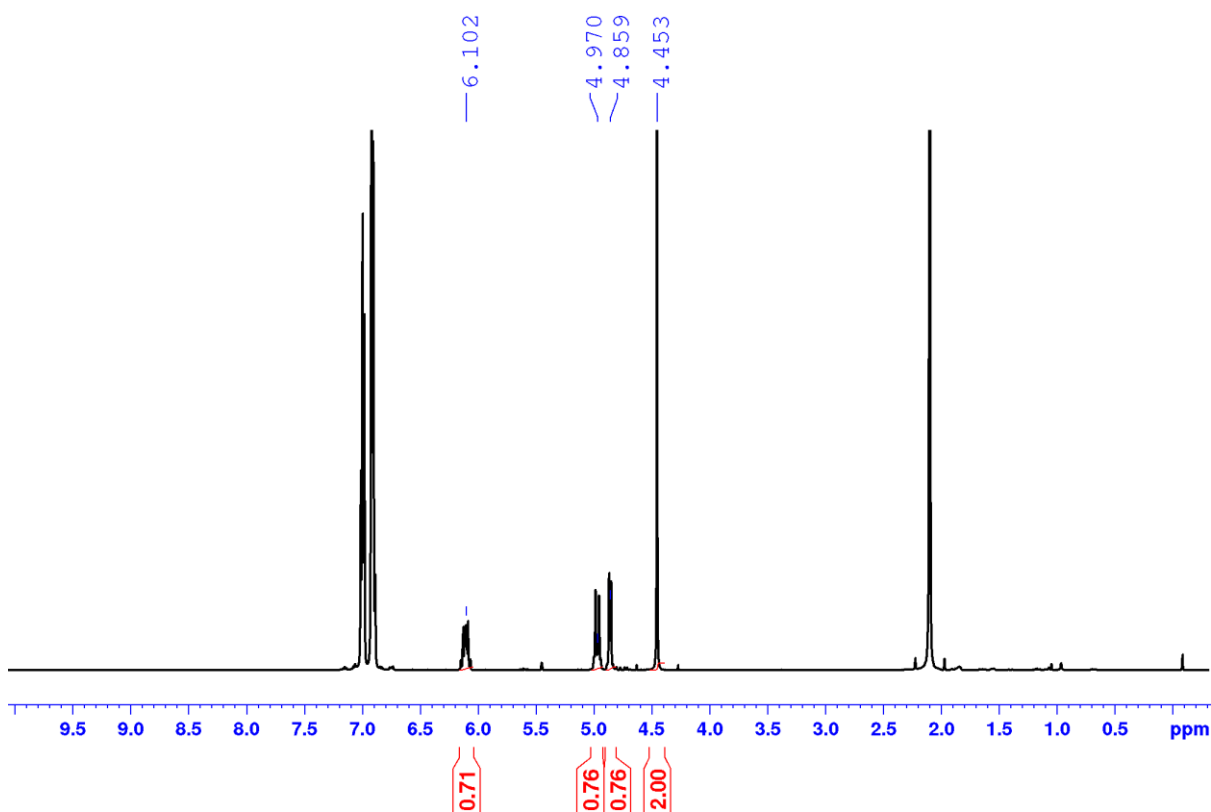


Figure 3.31: ^1H NMR of 1,3-butadiene using CH_2Br_2 (0.052 ml) as an internal standard

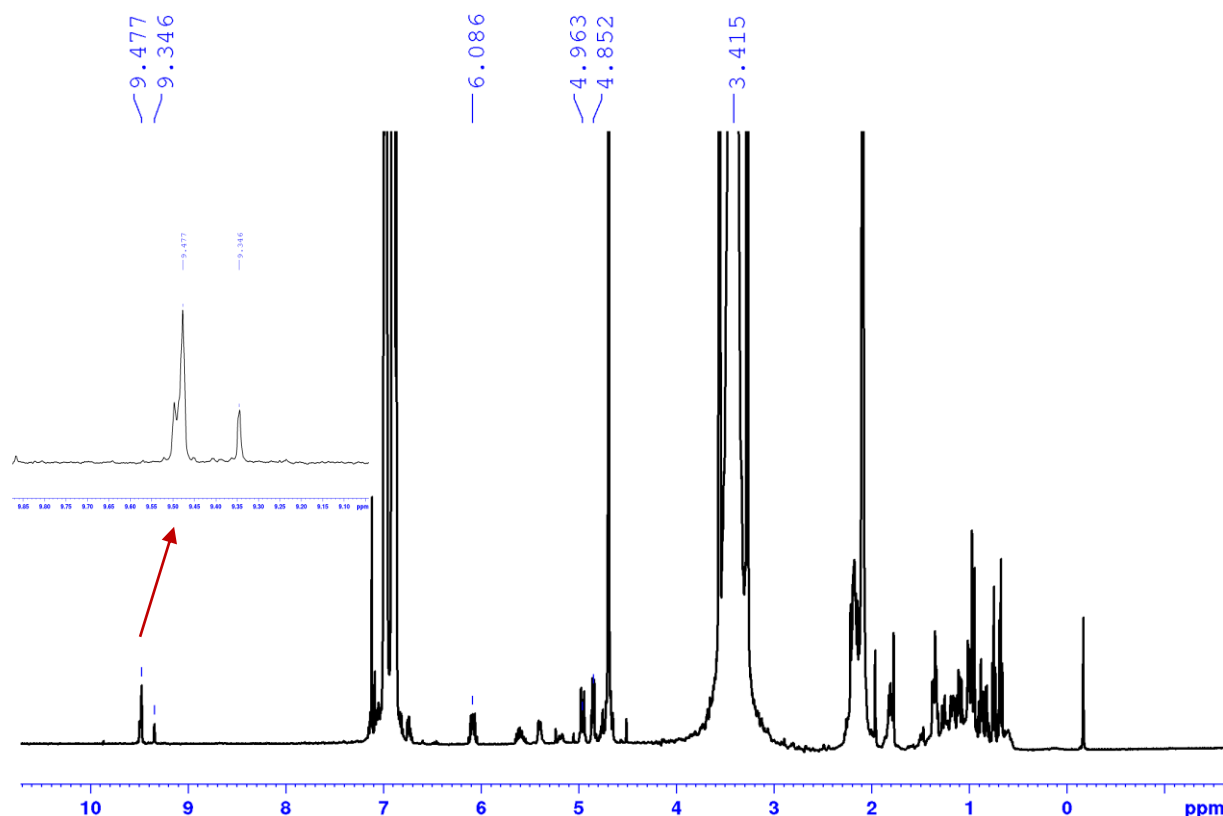


Figure 3.32: ^1H NMR spectrum of reaction mixture after I-HF of 1,3-butadiene showing partial conversion to aldehyde (expanded aldehyde region in sets)

3.4.11.2: One pot isomerization-hydroformylation-hydrogenation

A tandem one pot isomerization-hydroformylation-hydrogenation sequence was attempted and the results are presented in **table 3.5**. Substrate S3 was chosen as the representative substrate and an I-HF experiment was performed in presence of Pd/C (0.020 g) with a CO:H₂ ratio of 1:4 (table 3.5, run 1). As evident, although 68% conversion was observed, the conversion to aldehyde was negligible (only 1%). This indicates that hydrogenation become the dominant reaction and suppress hydroformylation.

Table 3.5: One pot tandem isomerization-hydroformylation-hydrogenation of S3.^a

Run	Subs ^a	T (°C)	P (bar)	CO: H ₂	T (hrs)	Conversion (%)
1	S3	120	4	1:4	16	68 (1)

^a[Rh] = [Rh(acac)(CO)₂] (2 mg), L/M = 2, solvent = 1,4-dioxane, total conversion was determined by ^1H NMR spectroscopy using CH₂Br₂ as an internal standard.

3.4.12: Mechanistic investigation: *In-situ* high pressure NMR

It is well understood that the coordination mode of ligand to the metal has a larger impact on the activity and selectivity of hydroformylation reaction. In our pursuit to investigate the coordination mode of ligand L4 and trap the resting state of the catalyst we attempted the following experiment.

3.4.12.1: Reaction of $[\text{Rh}(\text{acac})(\text{CO})_2]$ and ligand L4

$[\text{Rh}(\text{acac})(\text{CO})_2]$ (0.020 g, 0.000077 moles) and ligand L4 (0.030 g, 0.000077 moles) were dissolved in dry toluene- d_8 under inert conditions. This mixture was mixed properly to obtain a clear solution. The reaction mixture was then transferred to a high pressure NMR tube. The tube was degassed using freeze-pump-thaw cycles. Subsequently, NMR tube was purged 2-3 times with syngas and then pressurized to 10 bar and NMR was recorded between 0-90 °C. Figure 3.33 and 3.34 depict the spectrum recorded at 90 °C.

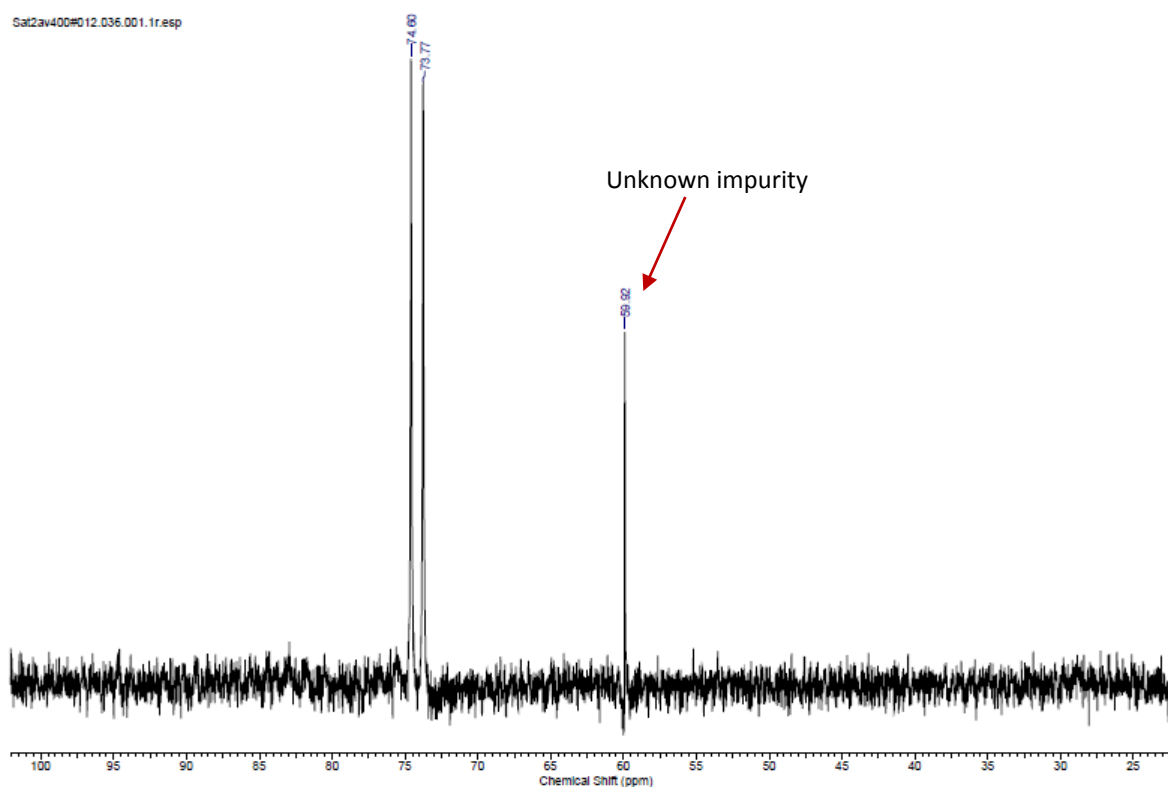


Figure 3.33: High pressure ^{31}P NMR spectrum at 90 °C showing complete coordination of ligand L4

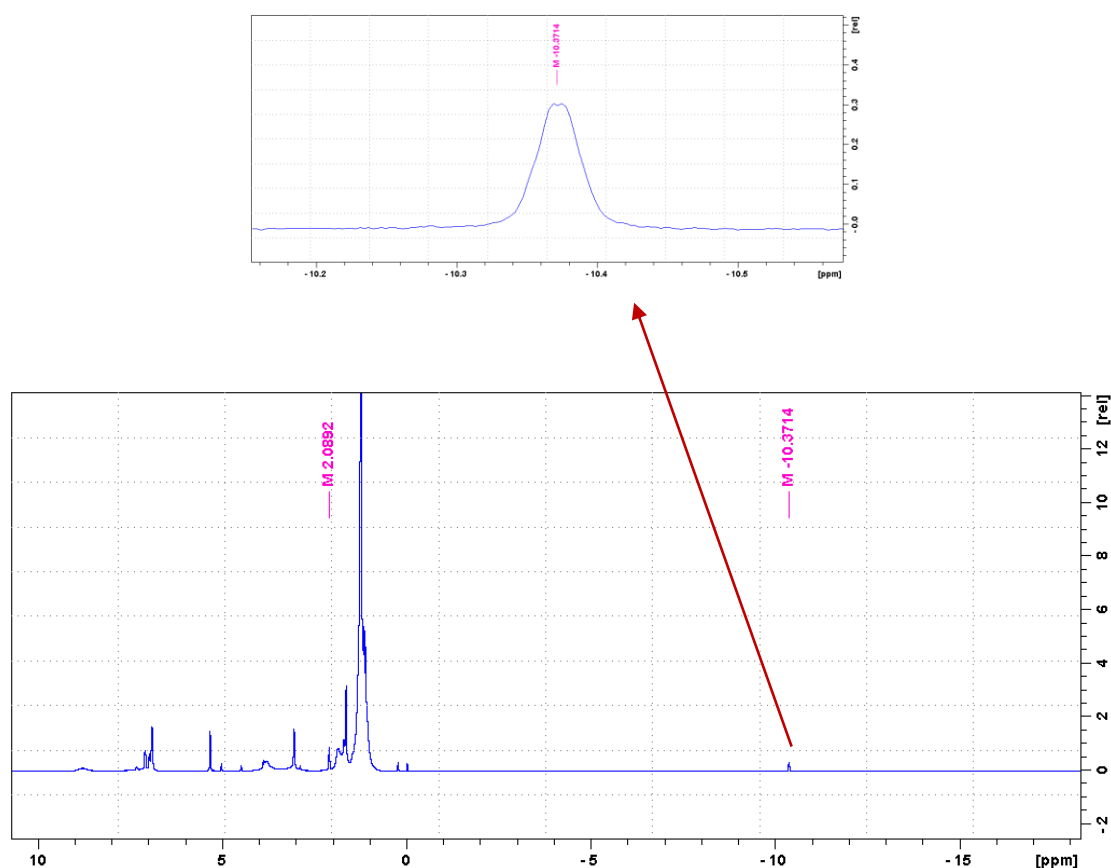


Figure 3.34: High pressure ^1H NMR spectrum at 90 °C displaying the hydride resonance at -10.37 ppm

3.4.12.2: Reaction of $[\text{Rh}(\text{acac})(\text{CO})_2]$, ligand L4 in presence of substrate

$[\text{Rh}(\text{acac})(\text{CO})_2]$ (0.030 g, 0.000116 mol) and ligand L4 (0.092 g, 0.000232 mol) were dissolved in dry toluene- d_8 (0.3 ml) under inert conditions. This mixture was mixed properly to get a clear solution. Next, *trans*-4-octene (0.018 ml, 0.000116) was added to the above solution and the reaction mixture was transferred to a high pressure NMR tube. The tube was degassed using freeze-pump-thaw cycles. Next, the NMR tube was purged 2-3 times with syngas and then pressurized to 10 bars. The tube was heated at 90°C for 4 hours. After 4 hours the reaction mixture was analyzed using high pressure and high temperature ^1H and ^{31}P NMR spectroscopy at 90 °C and the resultant spectra are depicted in figures 3.36 and 3.37.

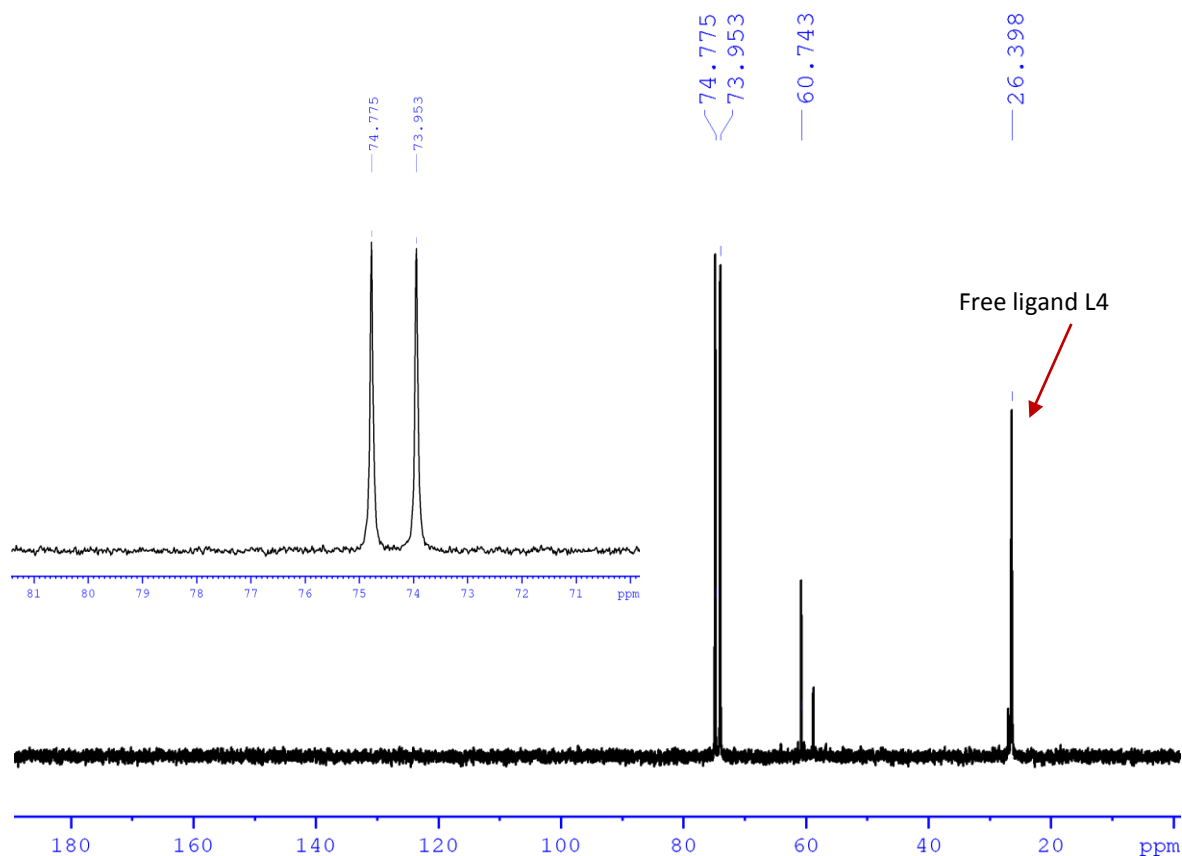


Figure 3.35: High pressure ^{31}P NMR spectrum at 90°C in toluene- d_3 under catalytic conditions (i.e. presence of substrate and excess ligand) (expanded view in sets)

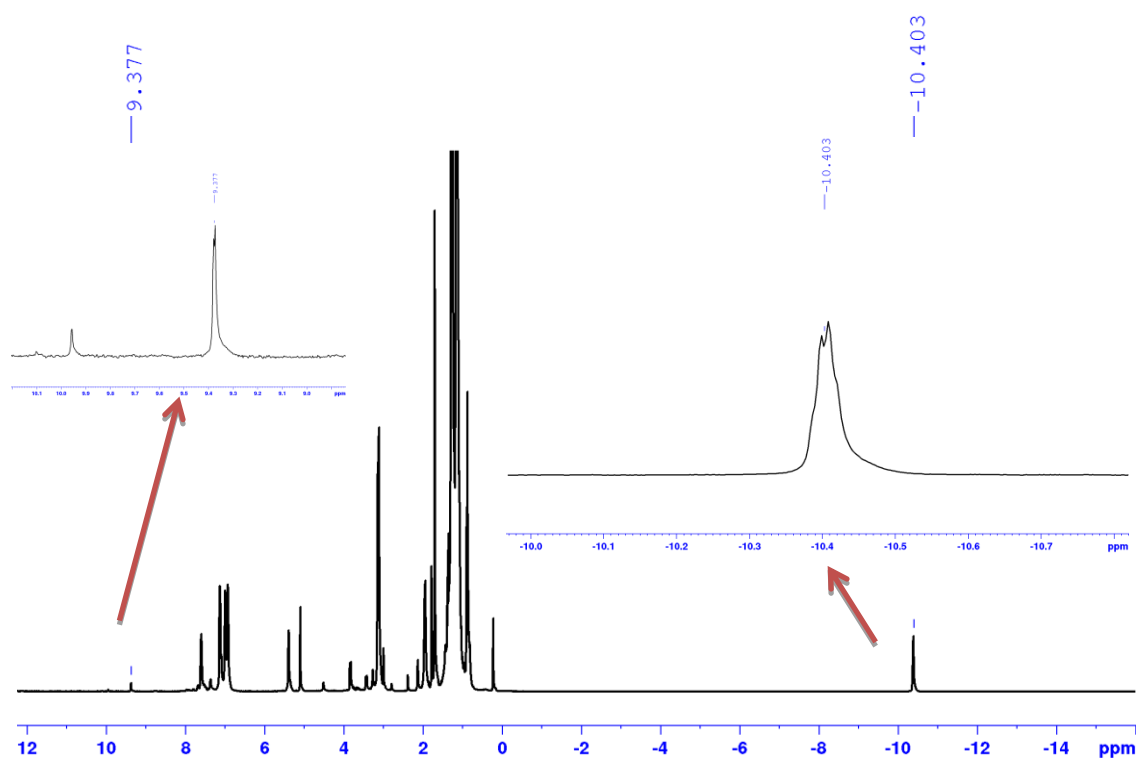


Figure 3.36: High pressure ^1H NMR spectrum at 90°C in toluene- d_3 under catalytic conditions (i.e. presence of substrate and excess ligand) (expanded view in sets)

3.5: Conclusion

In summary, unsymmetrical α,ω -difunctional molecules with the right balance of aliphatic and aromatic components are highly valuable intermediates, but usually require multi-step synthesis to access. I-HF of cashew nut shell liquid offers an opportunity to access unsymmetrical α,ω -difunctional molecules in a single step, but has not been attempted before. We now demonstrate that isomerizing-hydroformylation of CNSL-cardanol and various derivatives can yield unsymmetrical α,ω -difunctional molecules with a linear selectivity of up to 74%. A small library of bis-phosphorus ligands (L1-L4) was tested in the I-HF of CNSL-Monoene (S1), which produced terminal aldehyde with a selectivity of 28%. Moreover, a terminal selectivity of 50% was observed in the I-HF of methoxy protected monoene (S2). The resultant difunctional molecule 16-(3-methoxyphenyl)hexadecanal P1', a potential polymer precursor, was successfully isolated and fully characterized by various spectroscopic and analytical tools. I-HF of cardanol (which is a mixture of 3-4 components, along with free phenolic -OH groups) revealed a terminal selectivity of 74% (P1+P6). The resultant diolefinic monoaldehyde P6 was isolated and subjected to hydrogenation to obtain P8 in near quantitative yield. NMR spectroscopy and mass analysis confirmed formation of α,ω -difunctional molecule P8. The aldehyde P1' and the hydroxyphenol compound P8 can be used as renewable building blocks or as monomer for polycondensation chemistry. Thus, excellent linear selectivities for the I-HF of CNSL-cardanol have been achieved for the first time and direct access to unsymmetrical α,ω -difunctional molecules has been established. *In-situ* high pressure NMR investigations suggested exclusive formation of equatorial-equatorial coordination isomer at higher temperature, which might be responsible for improved selectivity offered by L4. Access to α,ω -difunctional molecules can be also obtained via isomerizing alkoxy carbonylation which delivers better selectivities compared to I-HF.

3.6: References

57. Llevot, A.; Dannecker, P.-K.; von Czapiewski, M.; Over, L. C.; Söyler, Z.; Meier, M. A. R. *Chem. – Eur. J.* **2016**, *22*, 11510-11521.
58. For plant oil derived monomers and polymers, see: Chikkali, S.; Stempfle, F.; Mecking, S. *Macromol. Rapid Commun.* **2012**, *33*, 1126-1129.
59. Montero de Espinosa, L.; Meier, M. A. R. *Eur. Polym. J.* **2011**, *47*, 837-852.
60. Rajput, B. S.; Chander, U.; Arole, K.; Stempfle, F.; Menon, S.; Mecking, S.; Chikkali, S. H. *Macromol. Chem. Phys.* **2016**, *217*, 1396-1410.
61. Atabani, A. E.; Silitonga, A. S.; Ong, H. C.; Mahlia, T. M. I.; Masjuki, H. H.; Badruddin, I. A.; Fayaz, H. *Renewable and Sustainable Energy Reviews* **2013**, *18*, 211-245.
62. Quirino, R. L.; Garrison, T. F.; Kessler, M. R.; *Green Chem.* **2014**, *16*, 1700-1715.
63. Voirin, C.; Caillol, S.; Sadavarte, N. V.; Tawade, B. V.; Boutevin, B.; Wadgaonkar, P. P. *Polym. Chem.* **2013**, *5*, 3142-3162.
64. Stempfle, F.; Ortmann, P.; Mecking, S. *Chem. Rev.* **2016**, *116*, 4597-4641.
65. (a) Breit, B.; Fuchs, E. *Chem. Commun.* **2004**, 694-695. (b) Breit, B.; Winde, R.; Mackewitz, T.; Paciello, R.; Harms, K. *Chem. –Eur. J.* **2001**, *7*, 3106-3121. (c) Kuil, M.; Soltner, T.; van Leeuwen, P. W. N. M.; Reek, J. N. H. *J. Am. Chem. Soc.* **2006**, *128*, 11344-11345. (d) Clarke, M. L. *Curr. Org. Chem.* **2005**, *9*, 701-718.
66. Christl, J. T.; Roesle, P.; Stempfle, F.; Wucher, P.; Goettker-Schnetmann, I.; Müller, G.; Mecking, S. *Chem. – Eur. J.* **2013**, *19*, 17131-17140.
67. Ohlmann, D. M.; Tschauder, N.; Stockis, J.-P.; Goossen, K. t.; Dierker, M.; Goossen, L. J. J. *Am. Chem. Soc.* **2012**, *134*, 13716-13729.
68. Pandey, S.; Chikkali, S. H. *ChemCatChem* **2015**, *7*, 3468-3471.
69. Mgaya, J. E.; Bartlett, S. A.; Mubofu, E. B.; Mgani, Q. A.; Slawin, A. M. Z.; Pogorzelec, P. J.; Cole-Hamilton, D. J. *ChemCatChem* **2016**, *8*, 751-757.
70. (a) Baader, S.; Podsiadly, P. E.; Cole-Hamilton, D. J.; Goossen, L. J. *Green Chem.* **2014**, *16*, 4885-4890. (b) Julis, J.; Bartlett, S. A.; Baader, S.; Beresford, N.; Routledge, E. J.; Cazin, C. S. J.; Cole-Hamilton, D. J. *Green Chem.* **2014**, *16*, 2846-2856.
71. Selent, D.; Wiese, K.-D.; Röttger, D.; Boerner, A.; *Angew. Chem. Int. Ed.* **2000**, *39*, 1639-1641.
72. (a) Furst, M. R. L.; Goff, R. L.; Quinzler, D.; Mecking, S.; Botting, C. H.; Cole-Hamilton, D. J.; *Green Chem.* **2012**, *14*, 472-477. (b) Jimenez-Rodriguez, C.; Foster, D. F.; Eastham, G. R.; Cole-Hamilton, D. J. *Chem. Commun.* **2004**, 1720-1721. (c) Pugh, R. I.; Drent, E.; Pringle, P. G.; *Chem. Commun.* **2001**, 1476-1477. (d) For a review on (non-isomerizing) hydroformylation of vegetable oils, see: Vanbésien, T.; Monflier, E.; Hapiot, F. *Eur. J. Lipid Sci. Technol.* **2016**, *118*,

-
- 26-35. (e) Cai, C.; Yu, S.; Liu, G.; Zhang, X.; Zhang, X. *Adv. Synth. Catal.* **2011**, *353*, 2665-2670. (f) Separation of cardanol from CNSL is explained in the following text book: Parambath Anilkumar (Eds.) in *Cashew Nut Shell Liquid A Goldfield for Functional materials*, Springer, **2017**, Chapter 9, pp-166-168.
73. Perdriau, S.; Harder, S.; Heeres, H. J.; de Vries, J. G. *ChemSusChem* **2012**, *5*, 2427-2434.
74. Detailed procedure for the synthesis of methoxy protected cardanol is described in reference 70b.
75. Goldbach, V.; Falivene, L.; Caporaso, L.; Cavallo, L.; Mecking, S. *ACS Catal.* **2016**, *6*, 8229-8238.
76. Chikkali, S. H.; Bellini, R.; de Bruin, B.; van der Vlugt, J. I.; Reek, J. N. H. *J. Am. Chem. Soc.* **2012**, *134*, 6607-6616.
77. (a) For hydrogenation of alkene and aldehyde, see: Baidossi, M.; Joshi, A. V.; Mukhopadhyay, S.; Sasson, Y. *Synth. commun.* **2004**, *34*, 643-656. (b) Felpin, F.-X.; Fouquet, E. *Chem. – Eur. J.* **2010**, *16*, 12440-12445. (c) Ide, M. S.; Hao, B.; Neurock, M.; Davis, R. J. *ACS Catal.* **2012**, *2*, 671-683.

Chapter 4

Iron Catalyzed Hydroformylation of Alkenes under Mild Conditions: Evidence of an Fe(II) Catalyzed Process



This chapter has been adapted from following publication

Pandey, S.; Vipinraj, K.; Shinde, D. R.; Vanka, K.; Kashyap, V.; Kurungot, S.; Vinod, C. P.; Chikkali, S. H. *J. Am. Chem. Soc.* **2018**, *140*, 4430-4439.

4.1: Abstract

Earth abundant, first row transition metals offer a cheap and sustainable alternative to the rare and precious metals. However, utilization of first row metals in catalysis requires harsh reaction conditions, suffers from limited activity, and fails to tolerate functional groups. Reported here is a highly efficient iron catalyzed hydroformylation of alkenes under mild conditions. This protocol operates at 10-30 bars syngas pressure below 100 °C, utilizes readily available ligands and applies to an array of olefins. Thus, the iron precursor $[\text{HFe}(\text{CO})_4(\text{Ph}_3\text{PNPPh}_3)]$ (**1**) in the presence of triphenyl phosphine catalyzes the hydroformylation of 1-hexene (S2), 1-octene (S1), 1-decene (S3), 1-dodecene (S4), 1-octadecene (S5), trimethoxy(vinyl)silane (S6), trimethyl(vinyl)silane (S7), cardanol (S8), 2,3-dihydrofuran (S9), allyl malonic acid (S10), styrene (S11), 4-methyl styrene (S12), 4-*i*Bu-styrene (S13), 4-*t*Bu-styrene (S14), 4-methoxy styrene (S15), 4-acetoxy styrene (S16), 4-bromo styrene (S17), 4-chloro styrene (S18), 4-vinylbenzotrile (S19), 4-vinylbenzoic acid (S20), and allyl benzene (S21) to corresponding aldehydes in good to excellent yields. Short chain S1 and S2 were hydroformylated at 10-20 bars syngas pressure, whereas long chain olefins S3-S5 required 30 bars syngas pressure at 100 °C for full conversion to aldehydes. Vinyl aromatics S11-S20 took 48 hours for significant conversion under identical conditions. Both electron donating and electron withdrawing substituents could be tolerated and excellent conversions were obtained for S11-S20. Remarkably, the addition of 1 mol% acetic acid promotes the reaction to completion within 16-24 hours. Detailed mechanistic investigations revealed *in-situ* formation of an iron-dihydride complex $[\text{H}_2\text{Fe}(\text{CO})_2(\text{PPh}_3)_2]$ (**A**) as an active catalytic species. This finding was further supported by cyclic voltammetry investigations and intermediacy of an Fe(0)-Fe(II) species was established. A mechanism based on an Fe(II) catalyzed hydroformylation of olefins is proposed. Identification of methyl heptanoate, derived from an iron-acyl intermediate, further authenticates the mechanistic proposal. Thus, combined experimental and computational investigations support the existence of an iron-dihydride as the catalyst resting state, which then follows a Fe (II) based catalytic cycle to produce aldehyde and regenerate the di-hydride species. To the best of our knowledge, this work represents the first example of iron catalyzed hydroformylation under mild conditions, with the underlying mechanism also elucidated.

4.2: Introduction

Transition metal catalysed hydroformylation, also known as oxo process was discovered in 1938 by German chemist Otto Roelen and is arguably the world's largest homogeneously catalyzed industrial process with the production of 12 million ton oxo-products per annum.¹ The oxo

process is a powerful synthetic tool to convert alkenes into aldehydes with perfect atom economy. It has been extensively utilized to construct an array of chemical intermediates.⁸ The first and second generation catalysts developed by BASF and ICI were based on cobalt.⁷ However, the cobalt-catalyzed process requires harsh conditions such as 100-350 bars syngas (1:1 mixture of CO:H₂) pressure and around 100-200 °C temperature. Widespread academic and industrial research to address this bottleneck led to a rhodium catalyzed low-pressure oxo-process (LPO) (10-60 bars and 80 - 135 °C),¹¹ which was developed by Union Carbide and Celanese in the mid 1970s.¹² To date, terminal alkenes, internal alkenes, cyclic olefins and aromatic alkenes have been extensively hydroformylated to pharmaceuticals, fragrances and agrochemicals using the precious rhodium metal.⁷⁸ Thus, due to technical superiority, the rhodium-based LPO is still the state of the art process practiced by industry and roughly 70% of the oxo-products are produced using this process. However the industry is increasingly being faced with the rocketing prices of rhodium due to the high demand of this metal in the automotive industry, which consumes about 80% of this metal. In addition, the natural abundance of this trace element is posing an even bigger challenge and the search for alternative metals has already begun.⁶ Iron (Fe) is an earth abundant element in contrast to precious rhodium, and its usage is justified for reasons of economic and sustainability. Iron catalyzed hydroformylation of olefins has been reported on few occasions in the past (**figure 4.1**) and suffers from some serious limitations.

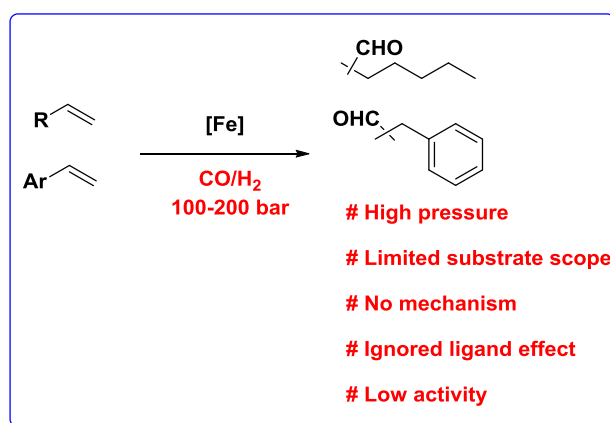
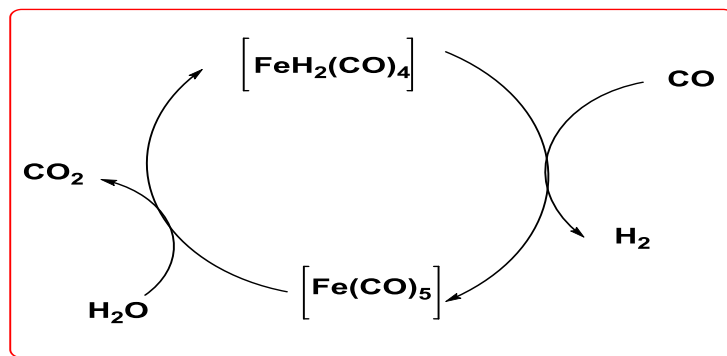


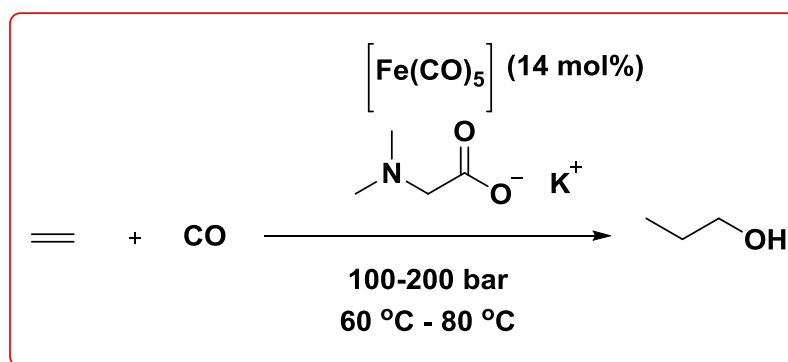
Figure 4.1: State of the art iron catalyzed hydroformylation

The first example of iron catalyzed hydroformylation was reported by Reppe and Vetter in 1953. Reppe et. al. studied the reactivity of carbonyl hydridoiron complexes. The introduction of an olefin in aqueous alkaline solution of [Fe(CO)₅] predominantly yielded higher alcohol resulting from the reduction with in situ generated hydrogen (**scheme 4.1**).⁷⁹ But the practical application of this process is limited due to the undesired formation of alkaline formates & carbonates in alkaline medium.



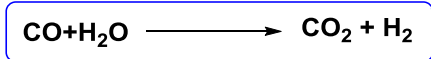
Scheme 4.1: General scheme for hydrogen evolution under Reppe conditions

Later on alkali metal hydroxides were substituted with tertiary amine bases to ensure continuous evolution of CO_2 & facilitation of reduction of aldehydes thereby resulting in enhancement of alcohol formation (**scheme 4.2**).⁸⁰

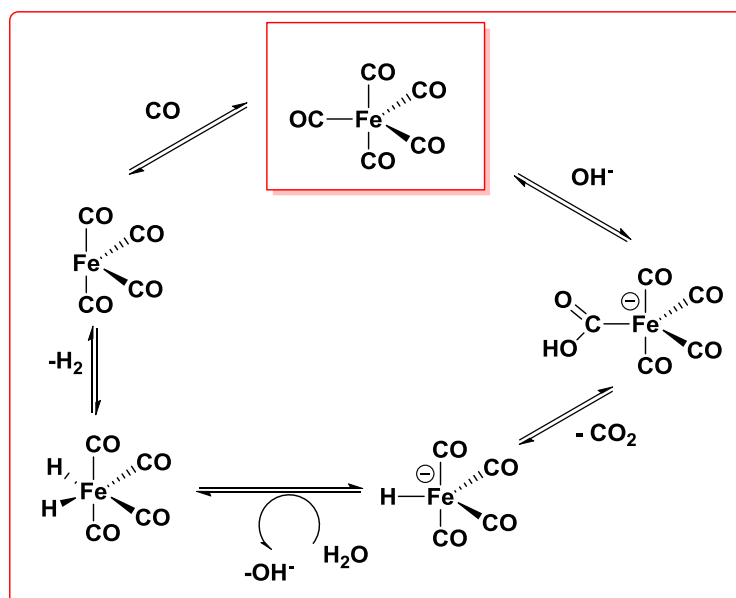


Scheme 4.2: Fe-catalyzed hydroformylation of ethylene by Reppe and Vetter

At 14% loading of $[\text{Fe}(\text{CO})_5]$, ethylene was converted to propanol under 100-200 bars of CO pressure. Note that no syngas was employed but the water gas shift (**scheme 4.3**) reaction was anticipated to deliver the hydrogen. An Fe dihydride complex $[\text{H}_2\text{Fe}(\text{CO})_4]$ was proposed to be the catalytically active species (**scheme 4.4**).



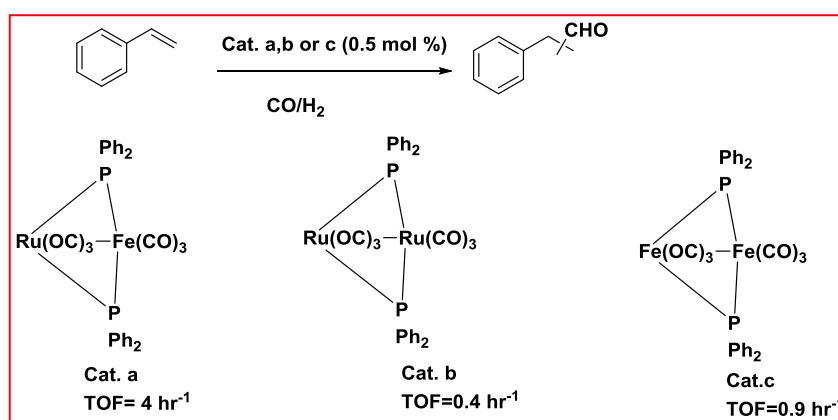
Scheme 4.3: Water gas shift reaction



Scheme 4.4: Proposed mechanism for water gas shift reaction

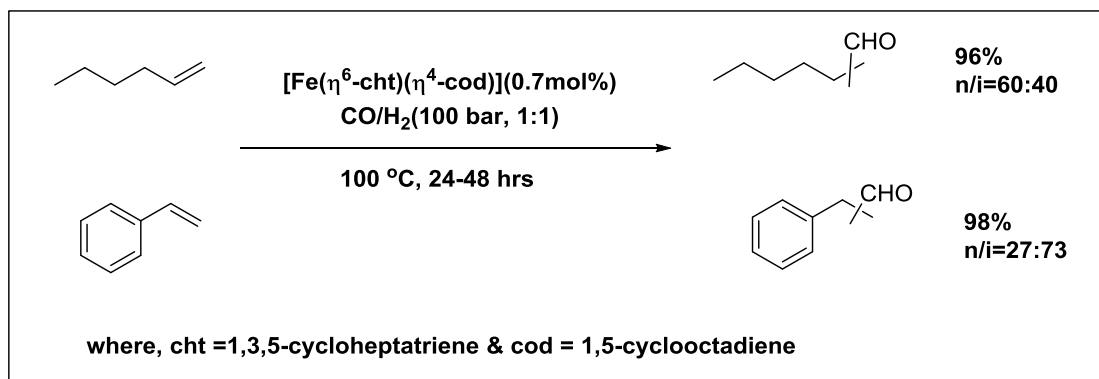
Similar attempts using 100 bar CO pressure (at 140 °C) were reported by Palagyi *et al.* after 30 years using styrene as substrate.⁸¹ The hydroformylation proceeded in the presence of $[\text{Fe}_3(\text{CO})_{12}]$, NEt_3 , and NaOH at an elevated temperature of 140° C and 100 bar CO pressure in $\text{H}_2\text{O}/\text{MeOH}$ solution. The authors noticed a strong dependence of product distribution on $\text{H}_2\text{O}/\text{MeOH}$ ratio. In this case conversion of styrene to desired oxygenated product did not exceed more than 30%.

Later on in 1992, the field was evolved in terms of applicability of mixed Ru-Fe metal clusters for hydroformylation reactions. But in such cases catalyst degradation was the major problem (**scheme 4.5**). The TOF was very low (0.4-4.0).⁸² Although it was not clear which metal was responsible for the observed hydroformylation activity, a synergistic effect between the two metals was claimed to be responsible.



Scheme 4.5: Hydroformylation of styrene catalyzed by phosphine bridged homo- and heterobimetallic complexes

The latest report in iron catalyzed hydroformylation was published in 2000 (scheme 4.6), utilizing an isolated iron complex $[\text{Fe}(\eta^6\text{-CHT})(\eta^4\text{-COD})]$, (CHT: 1,3,5-cycloheptatriene; COD: 1,5-cyclooctadiene).⁸³ Iron catalyzed hydroformylation of 1-hexene and styrene at 100 °C and 100 bars syngas pressure was investigated.



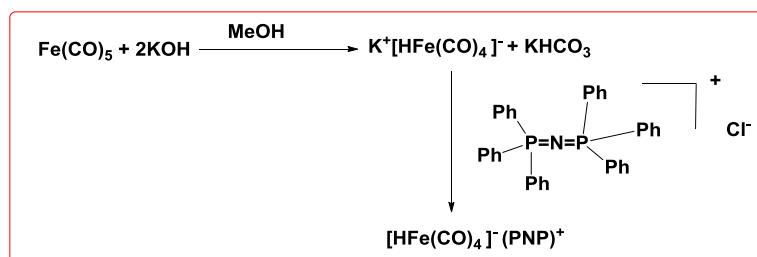
Scheme 4.6: Hydroformylation of 1-hexene and styrene catalyzed by $[\text{Fe}(\eta^6\text{-cht})(\eta^4\text{-cod})]$ as a catalyst precursor where cht = 1,3,5 cycloheptatriene & cod = 1,5 cyclooctadiene

Thus, the iron catalyzed hydroformylation is still in its infancy and suffers from serious limitations, such as high syngas pressure, limited substrate scope, lack of understanding of ligand effects and low activities. In addition, no comprehensive picture of the mechanism of Fe catalyzed hydroformylation exists, beyond the parallels drawn with Ru-catalyzed hydroformylation.

This chapter aims to overcome the limitations associated with Fe catalyzed hydroformylation of olefins and presents our attempts in developing an efficient methodology for iron catalyzed hydroformylation (HF) of olefins under mild conditions: 10-30 bars syngas pressure and below 100 °C, which falls under the purview of LPO. The generality of the approach has been demonstrated by subjecting various olefins, such as 1-octene, 1-hexene, 1-decene, 1-dodecene, 1-octadecene, trimethoxy(vinyl)silane, trimethyl(vinyl)silane, cardanol, 2,3-dihydrofuran, allyl malonic acid, styrene, 4-methyl styrene, 4-*i*Bu-styrene, 4-*t*Bu-styrene, 4-methoxy styrene, 4-acetoxy styrene, 4-bromo styrene, 4-chloro styrene, 4-vinylbenzotrile, 4-vinylbenzoic acid, and allyl benzene to iron catalyzed hydroformylation. A Fe(II) based mechanism is proposed as predicated by DFT calculations and experimental evidence. This methodology relies on commonly available reagents, does not require harsh conditions, and uses an earth abundant, non-toxic and cheap metal, which makes this approach highly suitable for practical hydroformylation of industrially important alkenes.

4.3: Result and Discussion

It is known that the hydroformylation reaction proceeds *via* a metal-hydride intermediate.⁸⁴ In our attempts to meet this criteria, we synthesized an iron-hydride complex $[\text{HFe}(\text{CO})_4][\text{PPN}]$ (1) (where PPN = Bis(triphenylphosphine)iminium) by following a known procedure (**scheme 4.7**).⁸⁵ The identity of (1) was fully established by using a combination of spectroscopic and analytical methods.

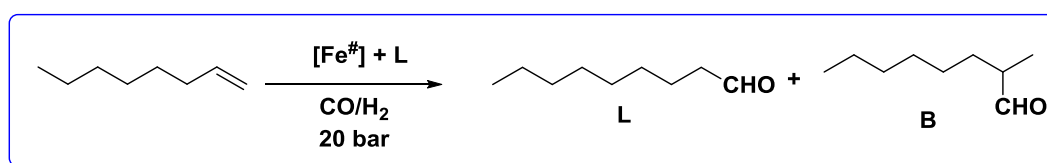


Scheme 4.7: Synthesis of $[\text{HFe}(\text{CO})_4][\text{PPN}]$ (1)

An overview of iron catalyzed reactions reported in the literature indicated that iron complexes can be activated in the presence of suitable ligands.⁸⁶ Guided by these reports, we anticipated that the best way to manipulate the reactivity of 1 would be to offer a competitive ligand to replace carbonyls and activate 1 *in situ*. Phosphorus ligands such as phosphines,⁸⁷ phosphites,⁸⁸ phosphinites,⁸⁹ diphosphines,⁹⁰ diphosphites,^{1e} phosphine-phosphonite,⁹¹ phosphine-phosphoramidite^{76, 92} and phosphine-phosphite⁹³ have been extensively utilized in rhodium catalyzed hydroformylation.

4.3.1: Hydroformylation of 1-Octene

As phosphorus ligands are the most successful candidate in hydroformylation reaction, we zeroed in on readily accessible σ -donor ligands such as phosphines and σ -donor π -acceptor ligands such as phosphites⁹⁴ to catalyze HF of model substrate 1-octene (**scheme 4.8**). The performance of precursor 1 in the presence of triphenyl phosphine (L1) and triphenyl phosphite (L2) in the iron catalyzed hydroformylation of 1-octene was evaluated and the representative catalytic data is summarized in **table 4.1**. The catalysts were prepared *in situ* by mixing a suitable amount of the iron precursor 1 and phosphorus ligands L1 or L2 in presence of syngas.



Scheme 4.8: Fe catalyzed HF of 1-octene

Preliminary screening indicated an optimal ligand to metal ratio of 2.5 (**table 4.1**, run 1-4). Remarkably, addition of triphenyl phosphine to iron precursor 1 catalyzed the hydroformylation of 1-octene to nonanal with excellent conversion (90-95%) (**table 4.1**, run 2-4), without any hydrogenation side reaction. In our attempts to identify the most suitable solvent, various solvents were screened (**table 4.1**, run 5-9). Methanol was found to be the solvent of choice and none of the other solvents were as effective as methanol. Performing the hydroformylation at lower and higher syngas pressure indicated an optimal pressure of 20 bars (run 2 vs 10-12) with 95% conversion within 24 hours, without jeopardizing the regioselectivity.

Table 4.1: Iron (1) catalyzed hydroformylation of 1-octene under mild conditions.^a

Run	L (equiv.)	Solvent	CO/H ₂ (bars)	Time (h)	Conv. (%) ^b	L:B ^b
1	L1 (1)	MeOH	20	24	47	73:27
2	L1 (2.5)	MeOH	20	24	95	66:34
3	L1 (3)	MeOH	20	24	95	64:36
4	L1 (4)	MeOH	20	24	92	64:36
5	L1 (2.5)	THF	20	24	3	NA
6	L1 (2.5)	DXN	20	24	66	73:27
7	L1 (2.5)	DCM	20	24	24	63:37
8	L1 (2.5)	EtOH	20	24	17	67:33
9	L1 (2.5)	iPrOH	20	24	20	70:30
10	L1(2.5)	MeOH	30	48	90	60:40
11	L1(2.5)	MeOH	30	24	76	70:30
12	L1(2.5)	MeOH	15	24	62	67:33
13 ^c	L1(2.5)	MeOH	20	24	85	67:33
14 ^d	L1(2.5)	MeOH	20	24	3	74:26
15	NA	MeOH	35	24	0	NA
16	L2(1)	MeOH	20	48	18	68:32
17	L2(2.5)	MeOH	20	48	47	70:30
18	L2(3)	MeOH	20	48	27	65:35
19	L2(2.5)	MeOH	30	48	92	63:37
20	L2(2.5)	MeOH	30	24	5	76:24
21	L2(2.5)	MeOH	20	24	2	NA
22 ^e	L2(2.5)	MeOH	20	24	23	68:32

^aConditions: 1: 0.0077 mmol, L/M: 2.5, Sub/Fe: 100, Solvent : 1 ml, NA: Not applicable; MeOH-Methanol, THF-Tetrahydrofuran, DXN-1,4-dioxane, DCM-Dichloromethane, EtOH-Ethanol, iPrOH-Isopropanol, hardly any (~1%)

hydrogenation product was detected. ^bDetermined by GC. ^cPerformed at 120 °C. ^dPerformed at 80 °C. ^eL2 was incubated for 24 hours before addition of 1-octene.

Increasing the temperature to 120 °C led to slightly lower conversion, but decreasing the temperature to 80 °C dramatically reduced the conversion to only 3% (**table 4.1**, runs 13-14). In a control experiment, hydroformylation of 1-octene using precursor (1), in the absence of ligand, failed to produce the corresponding nonanal (**table 4.1**, run 15). This observation clearly indicated that precursor 1 on its own is not capable of interacting with alkenes and may not be the actual active species. Thus, the control experiment accentuates the pivotal role of ligand in iron catalyzed hydroformylation, without which the iron hydride complex 1 is not active enough.

Encouraged by these results, we evaluated the performance of a readily available, σ -donor π -acceptor ligand, triphenyl phosphite (L2).⁹⁵ Initial screening in the presence of ligand L2 indicated an optimal ligand to metal ratio of 2.5 (**table 4.1**, run 16-18). However, it should be noted that a longer reaction time was required to achieve reasonable conversion under identical conditions (**table 4.1**, run 17). Notably, increasing the syngas pressure to 30 bars revealed an improved yield of 92% in 48 hours (**table 4.1**, run 19). However, performing the reaction at the same syngas pressure as in run 19 but for a shorter period of time (**table 4.1**, run 20), lead to only 5% conversion. This anomalous behavior could be due to the weak σ -donation and lower coordinating ability of L2. At a higher ligand to metal ratio, the phosphite ligands are known to be slower, leading to longer reaction times, and the behaviour noted here is in line with the previous reports.⁹⁶ Incubating L2 for 24 hours and *in situ* addition of substrate revealed slight improvement in the activity (**table 4.1**, run 22).

4.3.2: Scope of Fe Catalyzed Hydroformylation

With optimized reaction conditions in hand, the scope of the iron catalyzed hydroformylation was examined (**figure 4.2**) and about 20 substrates were evaluated. Both aliphatic and aromatic substrates were hydroformylated with good to excellent conversion to aldehydes. The aromatic substrates exhibited slightly lower reactivity. A short chain alkene, 1-hexene, was hydroformylated under further milder conditions with 50% exclusive conversion to heptanal (**figure 4.2**, P2) along with 72% linear selectivity. Hydroformylation of long-chain alkenes is even more challenging, as their reactivity decreases with increasing carbon number and the possibility of internal isomers and corresponding aldehyde products increases.⁹⁷ With increasing chain length of the olefin, the reactivity was found to decrease.⁹⁸ Thus, at 15 bars syngas pressure and 100 °C, a C10 olefin 1-decene (S3) led to only 47% yield (**figure 4.2**, P3), whereas increasing the CO/H₂ pressure to 30 bars led to an improved yield of 97% (**table 4.6**, run 2 vs 3).⁹⁹ Along the

same lines, 1-dodecene (S4) and 1-octadecene (S5) displayed 97% and 87% yield respectively (**figure 4.2**, P4 and P5) under identical conditions (**table 6**, run 4-5).^{100, 101}

With this initial success, the resilience of the catalyst was examined by subjecting functional olefins to iron catalyzed hydroformylation. The catalyst was found to tolerate trimethoxy group without any hindrance and 85% conversion to aldehyde was observed (**figure 4.2**, P6). A slight change in the silane to trimethyl(vinyl)silane led to 49% conversion to aldehyde (**figure 4.2**, P7).

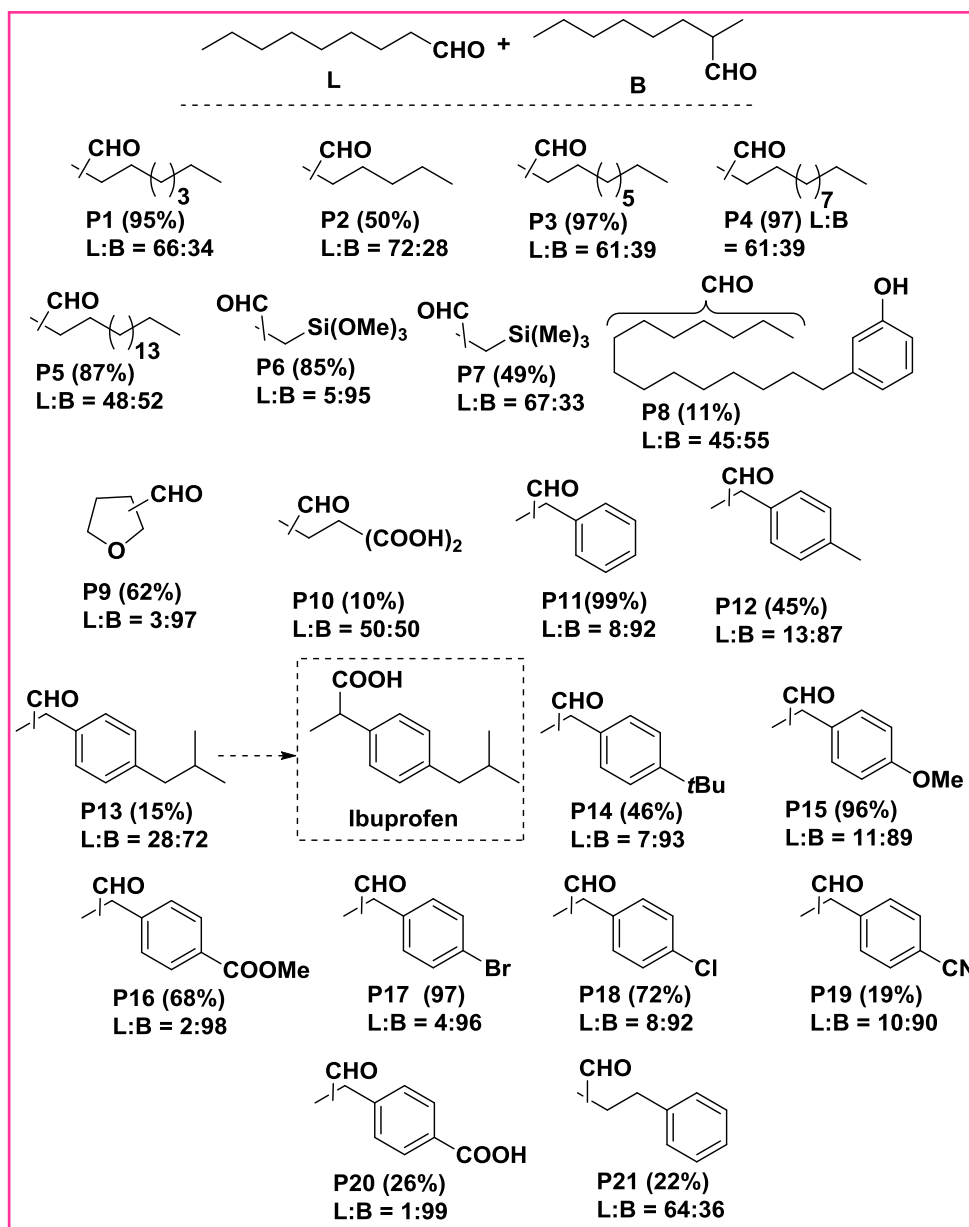


Figure 4.2: Fe catalyzed hydroformylation of various functional olefins: Conditions: 1: 0.0077 mmol, L/M: 2.5, Sub/Fe: 100, Solvent: 1 ml methanol, L:B = Linear : Branched, Yield (in bracket, %) determined by GC / ¹H NMR spectroscopy, hardly any (~1%) hydrogenation product was detected

A notoriously difficult cardanol (S8), which is a nonedible plant oil derived substrate, was tested in the iron catalyzed hydroformylation. Although only 11% aldehyde product could be observed, the fact that such a mixture (cardanol is mixture of three different internal olefins) could be hydroformylated indicates the potential that the iron catalyst holds (**figure 4.2**, P8).

A highly challenging heterocyclic olefin, 2,3-dihydrofuran (S9), was hydroformylated to yield (62%) a highly regioselective 3-carbaldehyde with 97% selectivity (**figure 4.2**, P9). Hydroformylation of 1,1-disubstituted difunctional olefin S10 (allyl malonic acid) lead to reduced activity and only 10% aldehyde could be observed (**figure 4.2**, P10) clearly indicating the limited functional group tolerance of the current catalytic system.

On an average, aliphatic olefins were hydroformylated in 24 hours, whereas aromatic substrates required 48 or more hours. Styrene was chosen as a representative benchmark substrate and iron catalyzed hydroformylation was examined.¹⁰² Under optimized conditions, a quantitative conversion was observed at 20 bars syngas pressure at 100 °C, with the preferred branched aldehyde formed with 92% selectivity (**figure 4.2**, P11). The reversal of regioselectivity is very commonly observed in styrenic substrates and monodentate phosphine ligands are known to preferably deliver the branched product.^{14c, 103} Both electron donating and electron withdrawing substituents were tolerated (**figure 4.2**, P12-20). The electron donating substrates 4-methyl styrene (S12),¹⁰⁴ 4-methoxy styrene,¹⁰⁵ 4-*tert* butyl styrene (S14) demanded 30 bars syngas pressure for 45-50% conversion. To demonstrate the practical significance of this methodology, hydroformylation of 4-isobutyl styrene (S13) was performed to yield aldehyde P13 which can be eventually oxidized to yield ibuprofen (**figure 4.2**), an anti-inflammatory drug. Whereas the electron withdrawing substituents fared better and 4-bromo styrene (S17) led to full conversion at 20 bars syngas pressure (**table 4.6**, runs 21 vs 15). S17 also revealed a high regioselectivity of 96% branched aldehyde (P17) with an excellent yield of 97%. Acetoxy, nitrile and carboxyl groups could be tolerated but at the cost of slightly reduced conversion to aldehyde (**table 4.6**, run 20, 22-23).

Thus, the above observations indicate that electron poor styrene derivatives are relatively easy to hydroformylate, whereas electron rich styrenics are slightly difficult to access. While a significant amount of literature deals with the hydroformylation of vinyl aromatics, very little is known about the hydroformylation of allyl aromatics.¹⁰⁶ The resultant aldehydes are high value pharmaceutical intermediates.¹⁰⁷ As a representative case, iron catalyzed hydroformylation of allyl benzene (S21) was investigated. Precursor 1 in the presence of L1 catalyzed the hydroformylation of allylbenzene to yield the linear selective (64%) product (P21) with a moderate conversion of 22% (**table 4.6**, run 24).

4.3.3: Acetic Acid Promoted Iron Catalyzed Hydroformylation

Having established iron catalyzed hydroformylation of various olefins, we pondered about the role of the solvent. It is to be noted that hydroformylation was found to take place in alcoholic solvents, suggesting active participation of the solvent. In this context, we postulated that the alcoholic solvents might be delivering a proton to precursor 1, to generate the active species. To test our hypothesis, we investigated the effect of acidic additives on the hydroformylation activity. To our delight, the addition of 1 mol% (AcOH : [Fe] = 1:1) acetic acid was found to dramatically promote the hydroformylation reaction.¹⁰⁸ Initial additive screening suggested that 1 equivalent (as compared to iron precursor 1) of acetic acid is sufficient to promote the reaction (**table 4.2**, run 1-3). Under optimized conditions, hydroformylation of S2 led to 49% conversion within 16 hours, which otherwise required 48 hours for similar conversion without the additive (**table 4.2**, run 1 versus **table 4.6** run 1). Remarkably, six fold increased activity was observed in the hydroformylation of styrene, which was completed (94% conversion) within 24 hours (Table 3, run 4), instead of the earlier 16% conversion (**table 4.6**, run 11). Along the same lines, accelerated hydroformylation of S12, S15 and S17 was observed in the presence of acetic acid. **Table 4.2** lists the important experiments. Thus, addition of 1 mol% (1 equivalent compared to iron precursor 1) acetic acid promotes the hydroformylation of 1-hexene, styrene and styrene derivatives and accelerated conversion could be obtained within 16-24 hours.

Table 4.2: Acetic acid promoted iron (1) catalyzed hydroformylation of 1-hexene, styrene and styrene derivatives.^a

Run	Substrate	AcOH	Time (h)	Conv. (%) ^b	L:B ^b
1 ^c	S2	1	16	49	72:28
2 ^c	S2	2	16	25	73:27
3 ^c	S2	5	16	1	NA
4	S11	1	24	94	14:76
5	S12	1	24	32	16:84
6	S15	1	24	64	16:84
7	S17	1	24	80	8:92

^aConditions: 1: 0.077 mmol, L/M: 2.5, Sub/Fe: 100, Solvent: 1 ml methanol, CO/H₂: 20 bars, Temp.: 100 °C, S2: 1-hexene, S11: styrene, S12: 4-methyl styrene, S15: 4-methoxy styrene, S17: 4-bromo styrene, NA: Not applicable;

^bDetermined by GC, °Temp.: 80 °C.

4.3.4: Mechanistic investigations

4.3.4.1: NMR Spectroscopy

Unfolding the elementary steps in the iron catalyzed hydroformylation will be of great significance for understanding the reactivity of the iron catalyst and might unlock the synthetic potential of this earth abundant metal in hydroformylation. Primitive reports on iron catalyzed HF either refer to the ruthenium based mechanism¹⁰⁹ or cite the Reppe process, which proposes the CO deficient $[\text{H}_2\text{Fe}(\text{CO})_3]$ as an active intermediate.¹¹⁰ However, direct experimental or theoretical evidence for iron catalyzed HF is largely missing.

In our attempts to trap key intermediates, precursor 1 was treated with triphenyl phosphine at 45 °C and the progress of the reaction was monitored by phosphorus NMR spectroscopy. The ^{31}P resonances at 82.3 and 71.5 ppm indicated coordination of L1 to the metal and the presence of intermediate (i) (**figure 4.3**) (see experimental section **figure 4.33**). The above phosphorus chemical shifts fall within the range of mononuclear iron-phosphine complexes reported earlier.¹¹¹

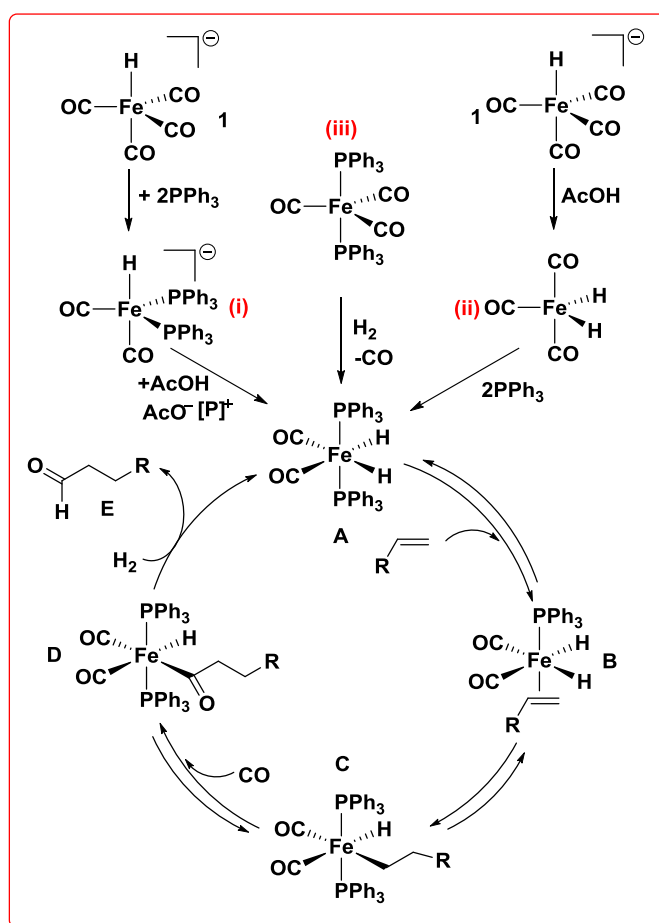


Figure 4.3: Proposed catalytic cycle for iron catalyzed hydroformylation. The orientation of ligands around the metal is only for the sake of understanding and does not mean that this is the final spatial arrangement of the ligands

Beller and co-workers in their investigation on iron catalyzed hydrogen production using formic acid reported that the coordinated phosphorus in $[\text{Fe}(\text{CO})_3(\text{PPh}_3)_2]$ complex appear at 82.5 and 70.6 ppm.¹¹¹ Therefore, the resonance at 82.3 and 71.5 ppm observed in our investigation can be assigned to coordinated L1. It should be noted that the phosphine coordination was observed at an elevated temperature of 45 °C. In an ideal situation, addition of acetic acid at 45 °C would lead to the generation of intermediate A (**figure 4.3**). However, addition of acetic acid to the above NMR tube and recording proton NMR did not show any hydride resonance. This is most likely due to release of H_2 from intermediate (A) at elevated temperature.

To arrest the hydrogen release, the NMR tube with added L1 was first heated for 16 hours at 45 °C, and then the tube was cooled to 0 °C. At this temperature, acetic acid was added to the NMR tube and a proton and ^{31}P NMR was recorded. Thus, the addition of acetic acid led to the appearance of a very weak hydride signal at -12.28 ppm (**figure 4.36**), but the intensity of the signal was so weak (even after large number of scans) that it demanded further support. In the hope of capturing intermediate A, compound 1 was treated with triphenyl phosphine and acetic acid was added at room temperature without heating the reaction mixture. Immediately a proton NMR was recorded, which revealed a doublet centered at -9.50 ppm (**figure 4.39**). This chemical shift can be assigned to complex A, which is consistent with literature reports.¹¹² Similar results were obtained when deuterated acetic acid (CD_3COOD) was used (**figure 4.41**). This is most likely due to fast H-D exchange between added deuterated acetic acid and the protic solvent (methanol). In a second route to trap intermediate species A (**figure 4.3**), 1 was treated with acetic acid to reveal a hydride resonance at -15.3 ppm (**figure 4.43**). Observation of the hydride resonance confirmed the formation of species (ii). However, addition of L1 did not show any coordination at room temperature and heating the sample to obtain the desired coordination led to elimination of H_2 . Therefore, species A could not be generated by following this route.¹¹³ In a third protocol, formation of A was accessed by synthesizing the known iron-phosphine complex (iii). Isolated complex (iii) was treated with hydrogen gas in a high pressure NMR tube and the tube was heated to 60 °C for 16 hours. The progress of the reaction was monitored by proton and phosphorus NMR spectroscopy. ^{31}P NMR of the resultant mixture revealed a resonance at 83.1 ppm (**figure 4.45**) and the corresponding proton NMR displayed two broad singlets at -8.91 and -9.02 ppm (**figure 4.44**). These resonances can be tentatively assigned to an iron complex that would be similar to species A; perhaps with a different spatial arrangement of the two hydrides. Thus, the above spectroscopic investigations suggest formation of species A, which might be the potential active species for hydroformylation. The intermediate thus prepared is highly unstable and only *in situ* characterization has been attempted.

4.3.4.2: Cyclic Voltammetry

The interconversion of Fe(0) to Fe(II) species was further supported by cyclic voltammetry (CV) investigations. The cyclic voltamogram (CVs) of the iron precursor (1) was recorded before and after the addition of acetic acid in the electrolyte medium (**figure 4.4**).¹¹⁴ Initial reduction potential for the compound (1) was found to be 0.43 V (*vs* Pt), which was shifted to 0.33 V (*vs* Pt) after acetic acid addition. Similarly, a shift in the oxidation peak of the precursor 1 was noted from 0.55 to 0.40 V (*vs* Pt). The above shift in the peak potential clearly indicates that the initial Fe (0) species in precursor 1 is being converted to the iron-dihydride species after the addition of acetic acid. To verify these results further, control experiments were conducted under analogous conditions. Ferrocene, ferrocene carboxylic acid, $[\text{Fe}(\text{CO})_3(\text{PPh}_3)_2]$ and $[\text{Fe}(\text{CO})_5]$ were selected as control samples. As can be seen in **figure 4.49**, the ferrocene and ferrocene carboxylic acid, wherein iron is in the +2 oxidation state, displayed separate peak positions for oxidation and reduction. The shift in the peak position is related to the carboxylic group attached to the cyclopentadienyl ring.

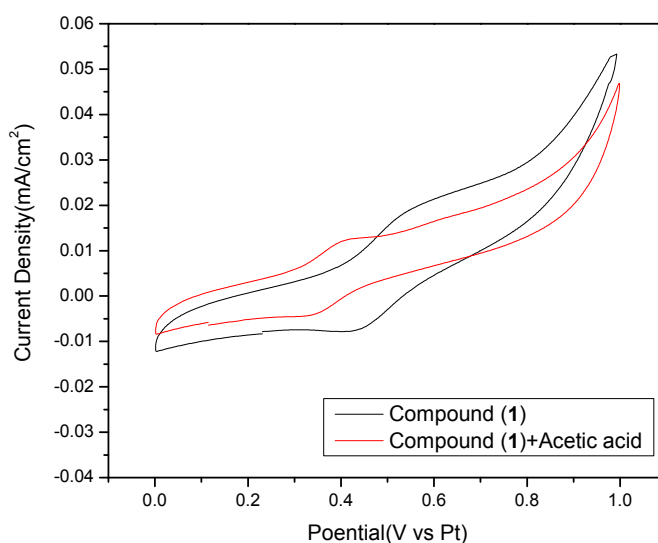


Figure 4.4: Cyclic voltamograms of iron precursor (1) (black line) and (1) + acetic acid (red line), recorded at 50mV/s with an electrode rotation rate of 900 rpm in 0.1 M LiClO₄ (solution in methanol)

Further, we recorded the CVs of the iron(0) compounds such as $[\text{Fe}(\text{CO})_3(\text{PPh}_3)_2]$ and $[\text{Fe}(\text{CO})_5]$. The CV of $[\text{Fe}(\text{CO})_3(\text{PPh}_3)_2]$ revealed an oxidation and reduction peak at higher potential against the iron(+2) ferrocene and ferrocene carboxylic acid, whereas no peak for $[\text{Fe}(\text{CO})_5]$ could be identified in the analogous potential range (**figure 4.50**). The anomalous behavior of the $[\text{Fe}(\text{CO})_5]$ could be because of the homogenous ligand surrounding the metal. As evident from the

control experiments outlined above, it is most likely that the Fe (0) precursor 1 is converted to Fe (II) after the addition of acetic acid. The reduction peak of the acetic acid treated compound 1 was in close resemblance with Ferrocene (0.26 V vs Pt), i.e. iron (2+). Whereas precursor 1 (0.43 V vs Pt) without acetic acid treatment resembles $[\text{Fe}(\text{CO})_3(\text{PPh}_3)_2]$ (0.46 V vs Pt), i.e. Fe (0).

4.3.4.3: Computational and Additional Experimental Evidence

The existence of A was investigated by computational methods and complex A was found to be the lowest energy isomer (**table 4.8**) among the six possible geometrical isomers. Based on the computational investigations, it is proposed that the *in situ* generated active species A forms a π -bond with the olefin to yield species B (**figure 4.3**), which inserts into the Fe-H bond to give the metal-alkyl complex C. The next step is the formation of the acyl intermediate D. Upon addition of H_2 , D releases the aldehyde and regenerates the active species A. In our attempts to trap the acyl intermediate, a reaction between 1 and 1-hexene was conducted at 0 °C to obtain the acyl intermediate D. The acyl complex D was then treated with iodine in methanol to obtain methyl heptanoate, which was characterized by NMR (**figure 4.46**), ESI-MS (**figure 4.47**) and GCMS (**figure 4.48**). The observation of methyl heptanoate confirms the intermediacy of species D. Similar evidence was presented for the cobalt catalyzed hydroformylation mechanism by Heck and Breslow.¹¹⁵ Thus, formation and intermediacy of A has been demonstrated by various experimental methods and it is therefore reasonable to believe that complex A is the actual active species. The observation of the methyl heptanoate further supports the proposed mechanism.

A radical mechanism with a potential radical species $[\bullet\text{Fe}(\text{CO})_4^-]$ has also been evoked in the past.^{79, 116} However, the existence of the radical mechanism seems unlikely based on three experimental pieces of evidence. (a) Two control experiments were performed in the presence of excess (150 times) radical scavengers 2,2,6,6-Tetramethylpiperidinyloxy (TEMPO) and galvinoxyl (**section 4.4.3.6.5: Control Experiments**). In both these cases, the aldehyde product was obtained. If a radical mechanism had been operating, the radical would have been scavenged by TEMPO or galvinoxyl and there would not have been any aldehyde formation. Thus, the formation of aldehyde in the presence of the radical scavenger rules out the possibility of a radical mechanism. (b) *In situ* NMR investigations could be performed without any paramagnetic NMR resonances. The absence of a paramagnetic species further supports the absence of a radical mechanism. (c) CV experiments indicated two electron processes and, therefore, intermediacy of one electron transformations is unlikely.

To obtain detailed insight into the iron catalyzed hydroformylation reaction, full quantum chemical calculations have been performed with density functional theory (DFT) at the

PBE/TZVP level of theory. It is well known that an octahedral complex with a general formula $MA_2B_2C_2$ has six different stereoisomers,¹¹⁷ and from the calculations, it is found that A is the most favorable stereoisomer for $[Fe(CO)_2(H)_2(PPh_3)_2]$ (**figure 4.5**). The insertion of olefin from the π -complex intermediate B can follow two pathways: 1,2-insertion (Path A) or 2,1-insertion (Path B) (**figure 4.5**). The former would lead to the linear aldehyde 7a, while the latter would produce the branched aldehyde 7b. The energy barriers for this particular step (insertion or hydride transfer) suggested that the 1,2-insertion is more favorable (by 1.3 kcal/mol) (**figure 4.6**, bottom) for 1-hexene. However, an opposite trend is seen in the case of styrene, where the 2,1-insertion is favored (by 1.7 kcal/mol) (**figure 4.6**, bottom). These computational findings complement the experimental observations, wherein higher amount of branched product was observed for styrene (**table 4.6**, run 12) and the linear product was seen to be the major one for 1-hexene (**table 4.6**, run 1).

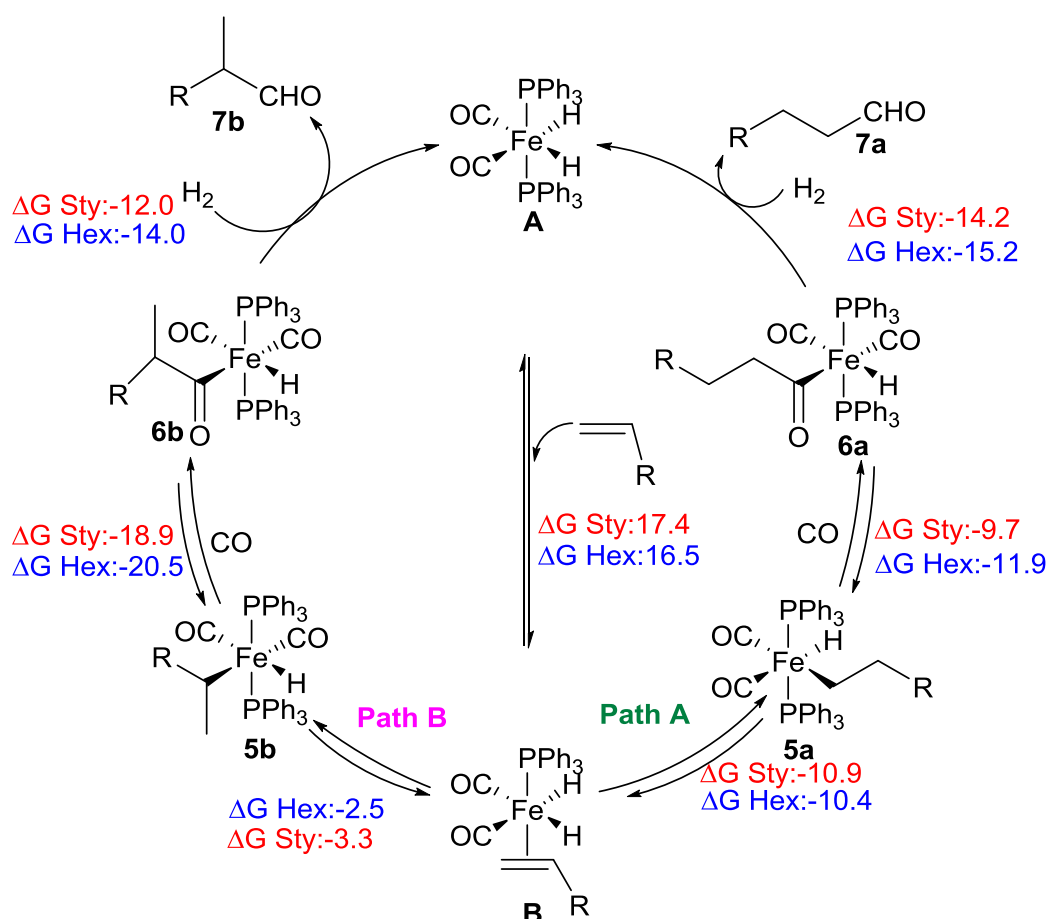


Figure 4.5: The reaction mechanism for the hydroformylation of olefins calculated at the PBE/TZVP level of theory. ΔG (in kcal/mol) represents Gibbs free energy of reaction

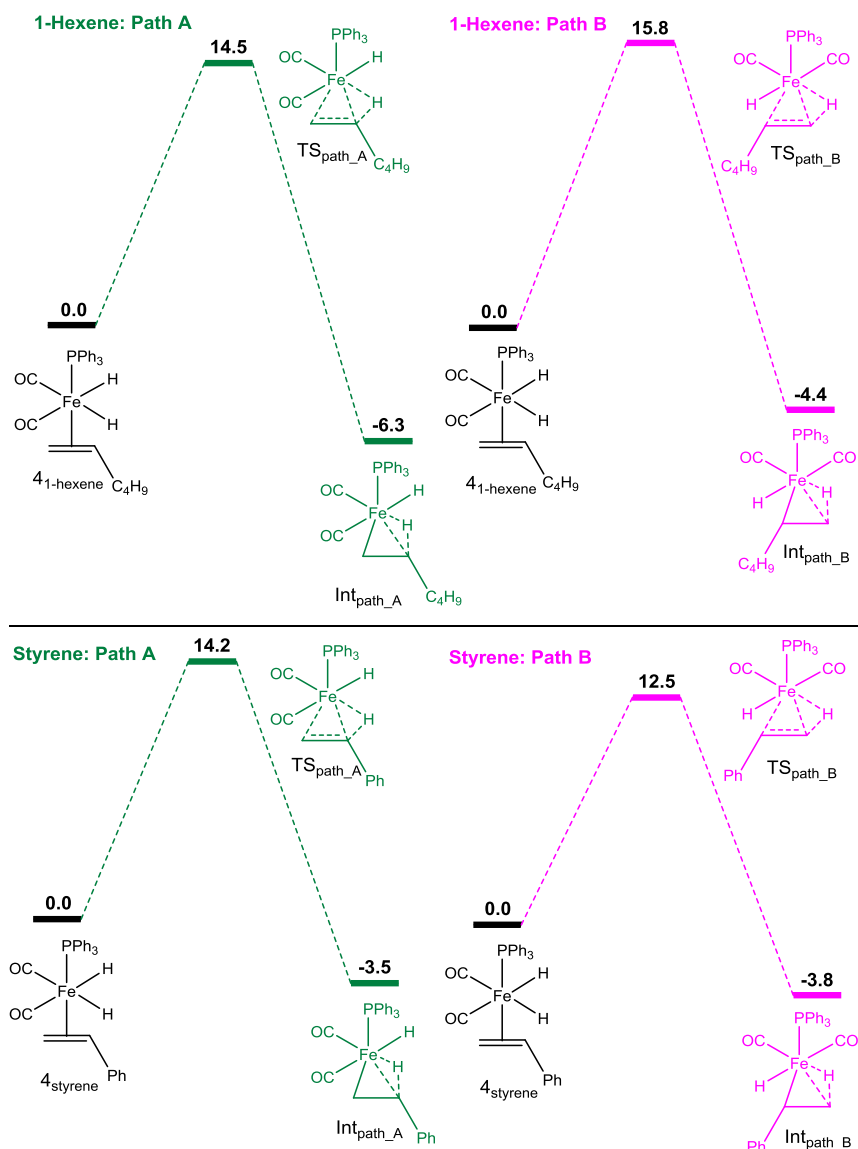


Figure 4.6: Free energy profile for the hydride transfer step in path A and path B. The free energy values are in kcal/mol

4.3.4.4: Is it Iron or Rhodium?

Iron catalyzed cross-coupling reactions such as “arylation” were reported to be influenced by presence of copper impurities in the Iron precursor FeCl_3 .¹¹⁸ In this context; we pondered about the possible role of rhodium impurities in our iron precursor. Thus, a three prong approach was used to establish if it is Iron or Rhodium that is catalyzing the hydroformylation reaction. i) In the first approach, commercially available iron precursor $[\text{Fe}_2(\text{CO})_9]$ was evaluated in the hydroformylation of 1-octene, in presence and absence of phosphine ligand under identical conditions and the results are presented in **table 4.3**. As evident, no hydroformylation was observed with $[\text{Fe}_2(\text{CO})_9]$ and a meager 1% hydroformylation product (**figure 4.52**) was observed in presence of triphenyl phosphine ligand. Had there been any rhodium impurity in the commercial precursor $[\text{Fe}_2(\text{CO})_9]$, it would have catalyzed the HF in presence of triphenyl

phosphine ligand. Thus, the lack of hydroformylation in the above experiment suggests that the impurities in the commercial precursor do not catalyze hydroformylation. ii) In the catalyst preparation step, $[\text{Fe}_2(\text{CO})_9]$ was converted into $[\text{Fe}(\text{CO})_5]$, which is subsequently utilized for the synthesis of complex 1. In order to further investigate the role of rhodium impurity in this intermediate, $[\text{Fe}(\text{CO})_5]$ catalyzed hydroformylation of 1-octene with and without triphenyl phosphine under identical conditions was examined. In this case as well, almost no hydroformylation was observed (**figure 4.53**). These observations rule out the possible hydroformylation by rhodium impurities and support the assumption that the reaction is most likely catalyzed by Iron. iii) In our attempts to detect the rhodium, the iron precursor $[\text{Fe}_2(\text{CO})_9]$ and complex 1 were subjected to bulk analyses using atomic absorption/emission spectroscopy and surface analysis using XPS. Both of these analyses revealed absence of rhodium in the precursor (see **section 4.4.3.6.7.2**). Thus, it is most likely that the hydroformylation is catalyzed by iron and it is highly unlikely that the rhodium impurity that is beyond the detection limits (0.01 ppm) is responsible for the observed HF.

Table 4.3: Hydroformylation of 1-octene with iron in presence and absence of ligand.^a

Run	Fe-precursor	Ligand	L:M	Conv. (%) ^b
1	$[\text{Fe}_2(\text{CO})_9]$	NA	2.5	0
2	$[\text{Fe}_2(\text{CO})_9]$	PPh ₃	2.5	~1
3	$[\text{Fe}(\text{CO})_5]$	NA	2.5	0
4	$[\text{Fe}(\text{CO})_5]$	PPh ₃	2.5	0

^aConditions: $[\text{Fe}_2(\text{CO})_9]$: 0.0109 mmol, $[\text{Fe}(\text{CO})_5]$: 0.0204 mmol, Sub/Fe: 100, Solvent: 1 ml methanol, CO/H₂: 20 bars, Temp.: 100 °C, Time : 24 hours; NA: Not added; ^bDetermined by GC.

4.4: Experimental Section

4.4.1: General Methods and Materials

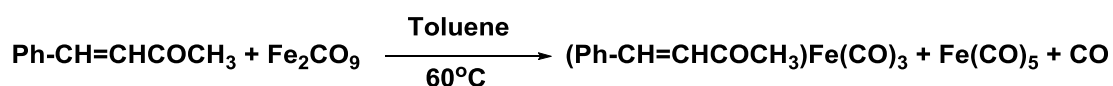
Unless noted otherwise, all manipulations were carried out under an inert atmosphere of argon using standard Schlenk line techniques or M-Braun glove box. Tetrahydrofuran was distilled from sodium/benzophenone under argon atmosphere. Methylene chloride was distilled on calcium-hydride. Methanol, ethanol, and isopropanol were dried on magnesium cake. Magnesium turning, triphenyl phosphine, triphenyl phosphite were purchased from Sigma-Aldrich and used without further purification. 1-hexene, 1-octene, 1-decene, 1-dodecene, 1-octadecene, styrene, 4-chloro styrene, trimethoxy(vinyl)silane, trimethyl(vinyl)silane, allyl malonic acid, 4-*t*Bu-styrene, 4-acetoxy styrene, 4-vinylbenzotrile, 4-vinylbenzoic acid and allyl benzene were purchased from Sigma-Aldrich and used after passing through a plug of neutral alumina followed by distillation.

Cashew nut shell liquid was received from Sunshield Chemicals Limited (subsidiary of Solvay) and was further purified to obtain cardanol. 4-*iso*-butyl-styrene was prepared by following a known procedure.¹¹⁹ $[\text{Fe}_2(\text{CO})_9]$, 4-methoxy styrene, 4-methyl styrene, 4-bromo styrene were obtained from Alfa Aesar. Complex $[\text{HFe}(\text{CO})_4][\text{PPN}]$ (1) was synthesized by modifying literature procedure.⁸⁵ $[(\text{PPh}_3)_2\text{Fe}(\text{CO})_3]$ (iii) was prepared by following a reported procedure.¹¹¹ Other chemicals like methylene chloride, methanol, ethanol, isopropanol, 1,4-dioxane, tetrahydrofuran, toluene, chloroform, calcium hydride, 2,3-dihydrofuran, etc. were purchased from local suppliers. Acetic acid (glacial) was purchased from Qualigens Fine Chemicals and was dried by adding acetic anhydride (7:3). The syngas and hydrogen gas were supplied by Ms. Vadilal Chemicals Ltd, Pune, India. The hydroformylation of α -olefins was run in an Amar Equipment Pvt. Ltd. high pressure reactor equipped with pressure regulators and safety rupture valve. The hydroformylation of 1-octene with incubation was run in an Amar Equipment Pvt. Ltd. high pressure reactor equipped with additional high pressure liquid charging chamber, pressure regulators and safety rupture valve. NMR spectra were recorded on Bruker 200, 400, and 500 MHz instruments. Chemical shifts are referenced to external reference TMS (^1H and ^{13}C) or 85% H_3PO_4 ($\Xi = 40.480747$ MHz, ^{31}P). Coupling constants are given as absolute values. Multiplicities are given as follows s: singlet, d: doublet, t: triplet, m: multiplet. *In-situ* high pressure NMR was recorded in Wilmad quick pressure valve NMR tube. Mass spectra were recorded on Thermo scientific Q-Exactive mass spectrometer; with Hypersil gold C18 column (150 x 4.6 mm diameter 8 μm particle size mobile phase used is 90% methanol + 10 % water + 0.1 % formic acid). IR spectrum was recorded on Bruker alpha-T spectrometer in liquid state. Sample was dissolved in chloroform and spectrum was obtained using sodium chloride window. GC analyses for 1-hexene, 1-octene, 1-decene, 1-dodecene, 1-octadecene, styrene, 4-methoxy styrene, 4-bromo styrene, 4-methyl styrene, other styrenic substrates and allyl benzene were carried out on an Agilent 7890B GC system. GC-MS analysis was carried out on a Varian 3800 GC-MS (Saturn 2000MS) with VF-5 capillary column (5% phenyl, 95% dimethyl polysiloxane). The column oven program used is same as that for GC analysis. Headspace GC analysis was performed on an Agilent 7890A GC system equipped with Porapak column and thermal conductivity detector. Inlet temperature was maintained at 150 °C, column flow = 14 ml/min. Detector temperature was maintained at 200 °C. Temperature program: starting at 60 °C with hold time of 5 mins. Ramp 1: @ 10 °C to 100 °C, hold for 21 mins. Retention time for H_2 = 1.5 mins. The XPS measurements were carried out using Thermo Scientific Kalpha+ spectrometer using a monochromatic Al $\text{K}\alpha$ (1486.6 eV) x-ray source. The base pressure of the spectrometer was 2×10^{-9} mbar. The wide area and narrow region scans were acquired using 100 eV and 50 eV pass energy respectively. The bulk analyses for the detection of rhodium impurity was carried out at three different places using; Varian

atomic absorption spectrometer, model- 220fs (NCL), SPECTRO Analytical Instruments GmbH, Germany, model-ARCOS, Simultaneous ICP Spectrometer (IIT Bombay), and Agilent model-4100 MP-AES. A Bio-Logic electrochemical workstation was used to perform the electrochemical analysis. In a typical setup a three electrode cell was employed which comprises of a glassy carbon (0.196 cm² geometrical surface area) as working electrode, graphite rod as counter electrode and Pt-wire as reference electrode. The methanolic solution of LiClO₄ (0.1 M) served as the electrolyte purpose. For recording the cyclic voltamogram of the compounds, a 0 to 1 V potential range was applied with a scan rate of 50 mV/s. Further, in order to maintain the reactant flow over the glassy carbon electrode a 900 rpm was given to the working electrode.

4.4.2: Synthesis of iron complexes [Fe(CO)₅] and [HFe(CO)₄][PPN]

We began with the synthesis of [Fe(CO)₅] following a known literature procedure (**scheme 4.9**).¹²⁰ 2.01 g (0.0137 mol) of benzylideneacetone, 5 g (0.0137 mol) of [Fe₂(CO)₉] were suspended in dry toluene (30 ml) in a Schlenk flask. The above suspension was heated at 60 °C for 5 hours, after which volatiles were evaporated under vacuum. The resultant volatiles were collected and subjected to low temperature precipitation at -45 °C to obtain [Fe(CO)₅] as straw yellow colored precipitate. The supernatant toluene was syringed out and the resultant solid (64% yield) was used for next step. Subsequently, the solid was allowed to warm up to room temperature, leading to a straw yellow color liquid.



Scheme 4.9: Synthesis of [Fe(CO)₅]

5 g (0.0255 mol) of [Fe(CO)₅] was treated with 2.86 g (0.051 mol) of KOH in methanol (40 ml) to obtained the desired metal precursor [HFe(CO)₄]⁻[K]⁺.⁸⁵ A saturated solution of bis-triphenylphosphine iminium chloride (1 g in 10 ml methanol) was added to above [HFe(CO)₄]⁻[K]⁺ salt to obtain pale yellow colored precipitate (**scheme 4.7**). The thus obtained precipitate was further recrystallized from 1:1 hot solution of ethanol: ethyl acetate to obtain [HFe(CO)₄][PPN]⁺ (**1**) [where [PPN]⁺ = Bis(triphenylphosphine)iminium cation] in 46% yield.

Key resonances for (**1**):

¹H NMR (500 MHz in CD₃OD): δ = -8.52 (s, 1H, Fe-H). ¹³C NMR (125 MHz in CD₃OD): δ = 161.5 (C=O), 135.0, 133.6, 130.8, 128.3. ³¹P NMR (500 MHz in CD₃OD): δ = 21.02. IR (cm⁻¹) = 1870 (C=O). ESI-MS (-ve mode): m/z = 168.91 [M]⁻.

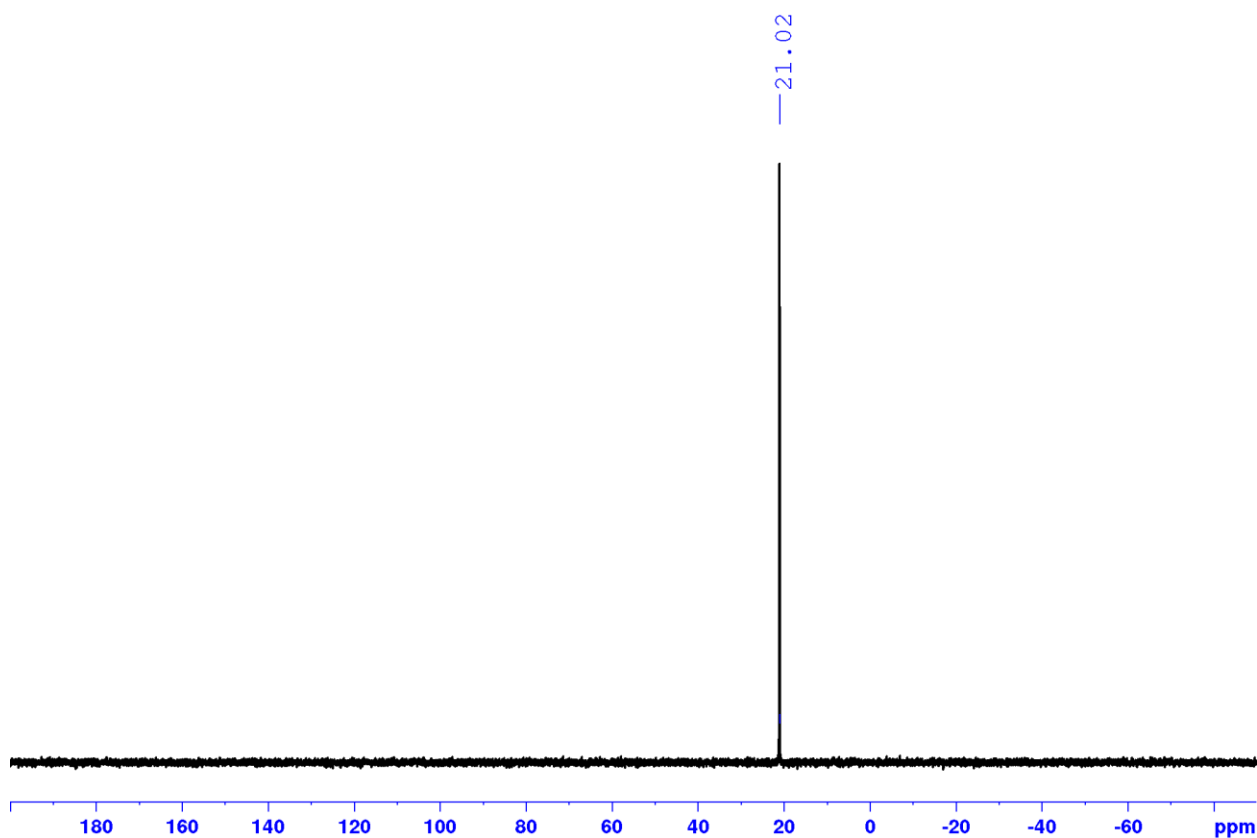


Figure 4.7: ^{31}P NMR spectrum of hydrido-tetracarbonyl ferrate bis(triphenylphosphine)iminium

(1)

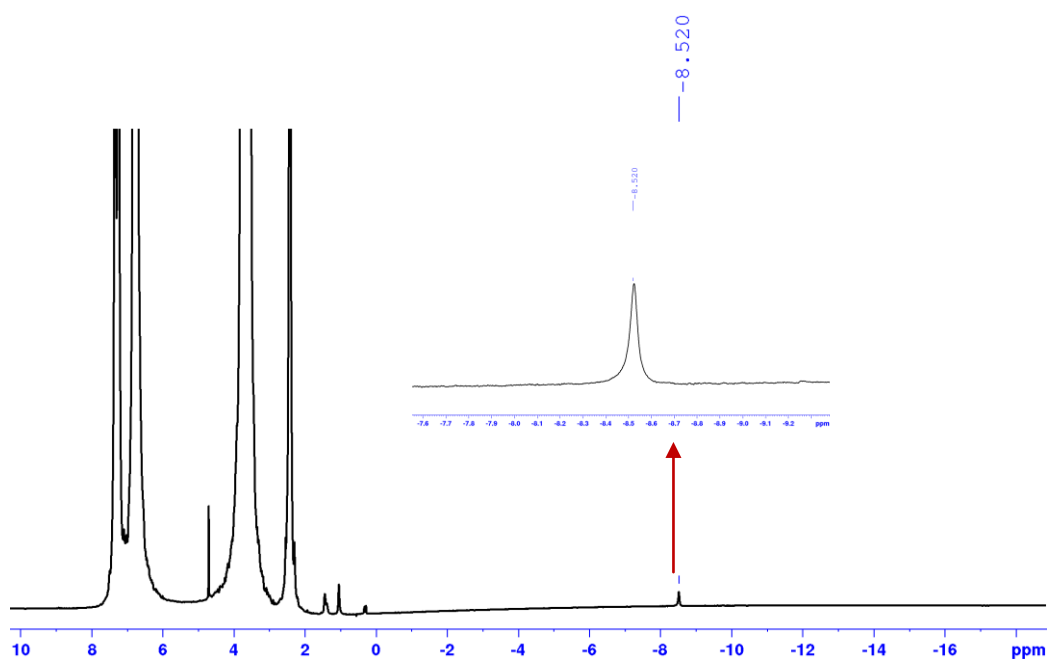


Figure 4.8: ^1H NMR spectrum of hydrido-tetracarbonyl ferrate bis(triphenylphosphine)iminium

(1)

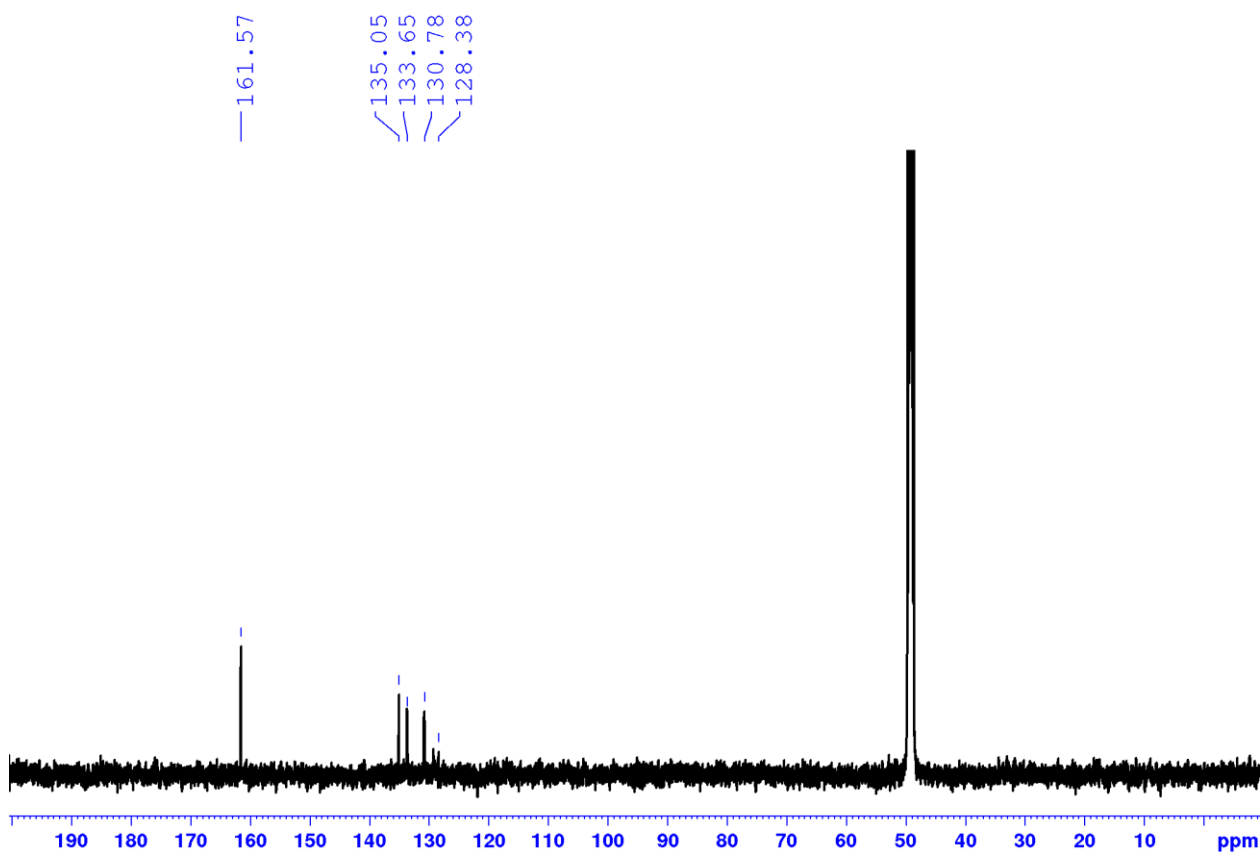


Figure 4.9: ^{13}C NMR spectrum of hydrido-tetracarbonyl ferrate bis(triphenylphosphine)iminium

(1)

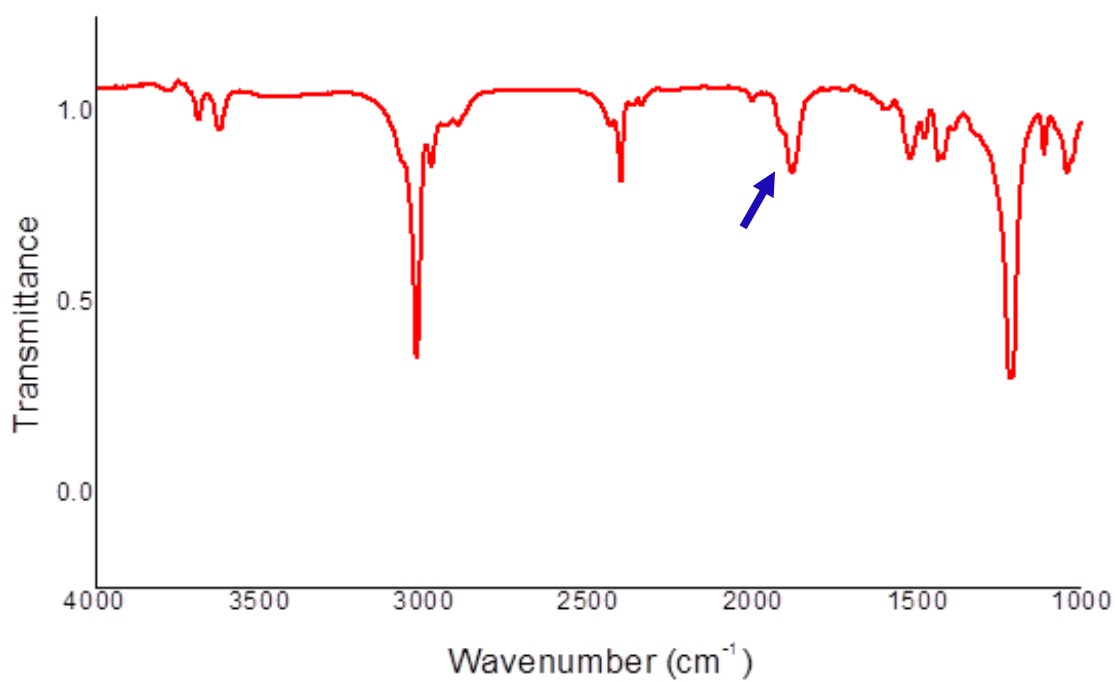


Figure 4.10: IR spectrum of hydrido-tetracarbonyl ferrate bis(triphenylphosphine)iminium (1)

SP-1 #149 RT: 0.67 AV: 1 NL: 2.78E4
T: FTMS - p ESI Full ms [100.00-1500.00]

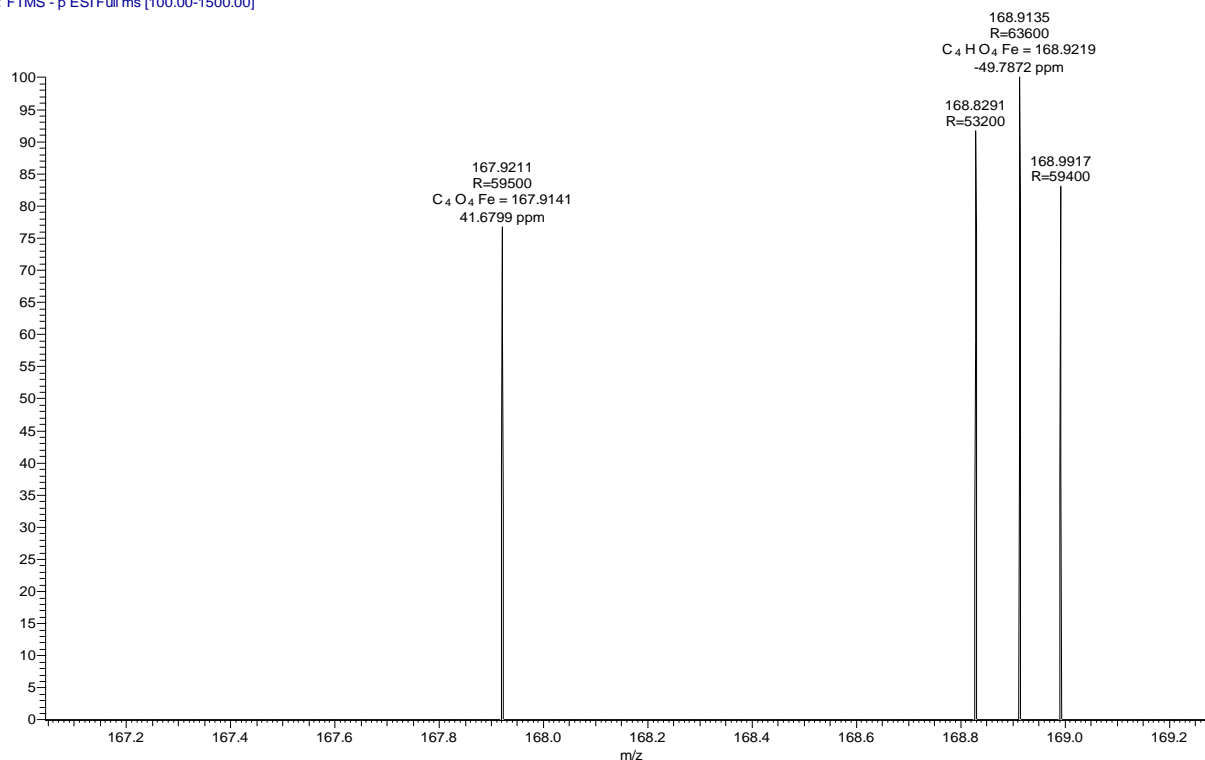


Figure 4.11: ESI-MS (negative mode) spectrum of hydrido-tetracarbonyl ferrate bis(triphenylphosphine)iminium (1)

4.4.3: General Procedure for Hydroformylation

In a typical hydroformylation experiment a stainless steel autoclave (450 mL) equipped with 50 ml high pressure liquid charging chamber, pressure regulator and a safety valve was used. Individual vials were charged with metal precursor $[HFe(CO)_4]^- [PPN]^+$ (1) (5.5 mg, 0.0077 mmol), ligand (as in **table 4.1-4.3**), solvent (1 ml), substrate (100 equiv.) and stirring bars in a glove box. The vials were transferred to autoclave and the autoclave was purged three times with syngas ($CO:H_2 = 1:1$) before pressurizing it to the desired pressure. Suitable temperature and pressure was maintained during the reaction. After completion of the reaction, the autoclave was cooled to $0^\circ C$, and excess gas was vented off in a well-ventilated fume-hood. The conversion and regio-selectivity were determined by using gas chromatography (GC).

4.4.3.1: Iron Catalyzed Hydroformylation of 1-Octene

Hydroformylation of 1-octene was carried out as reported in the general procedure and the results are summarized in **table 4.1**.

GC analysis for 1-octene was carried out on an Agilent 7890B GC system using HP-05 column ($30\text{ m} \times 320\ \mu\text{m} \times 0.25\ \mu\text{m}$), split ratio 30:1, column pressure 10 psi, injector temperature of 260

°C, detector temperature of 330 °C, argon carrier gas. Temperature program: Initial temperature 70 °C, hold for 1 min.; ramp 1: 4 °C/min. to 120 °C; ramp 2: 10 °C/min. to 250 °C; ramp 3: 20 °C/min. to 320 °C, hold for 2 min. Retention time for ; 1-octene = 2.7 min.; hydrogenated product (octane) = 2.8 min.; branched aldehydes = 7.02 min.; linear aldehyde = 8.1 minute (**figure 4.12**).

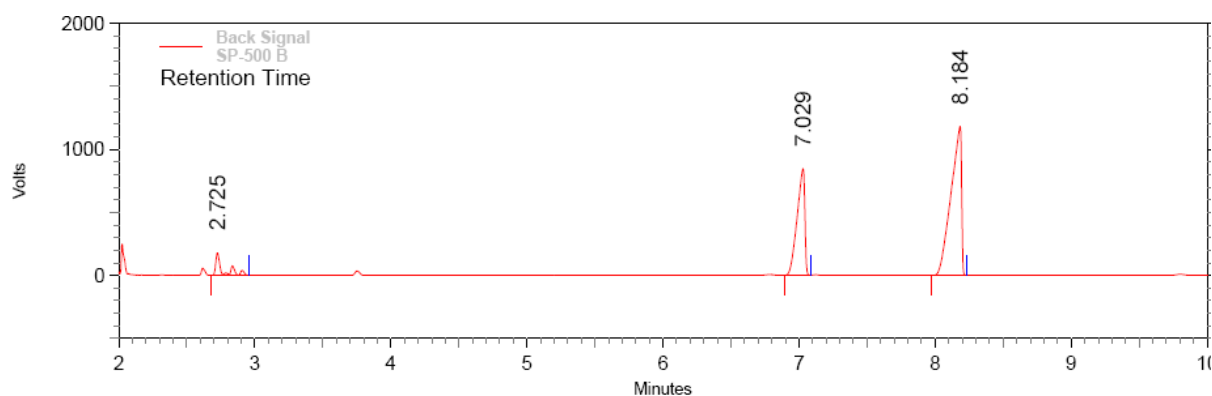
Determination of regioselectivity: Regioselectivity was determined according to the following equation:

Linear selectivity = (area under peak for linear aldehyde/ sum of the area for linear and branched aldehydes)*100.

For example, in the fig. 4.12, area under peak for linear aldehyde = 61.85%

Total peak area for aldehydes = (32.47+61.85) = 94.32%

Linear selectivity = (61.85/94.32)*100 = 66%



Back Signal Results

Retention Time	Area	Area %	Height	Height %
2.725	4471477	5.68	1368813	8.08
7.029	25562508	32.47	6502004	38.37
8.184	48698423	61.85	9074305	53.55
Totals	78732408	100.00	16945122	100.00

Figure 4.12: GC chromatogram for 1-octene (table 4.1, run 02)

4.4.3.2: Iron Catalyzed Hydroformylation of 1-Hexene

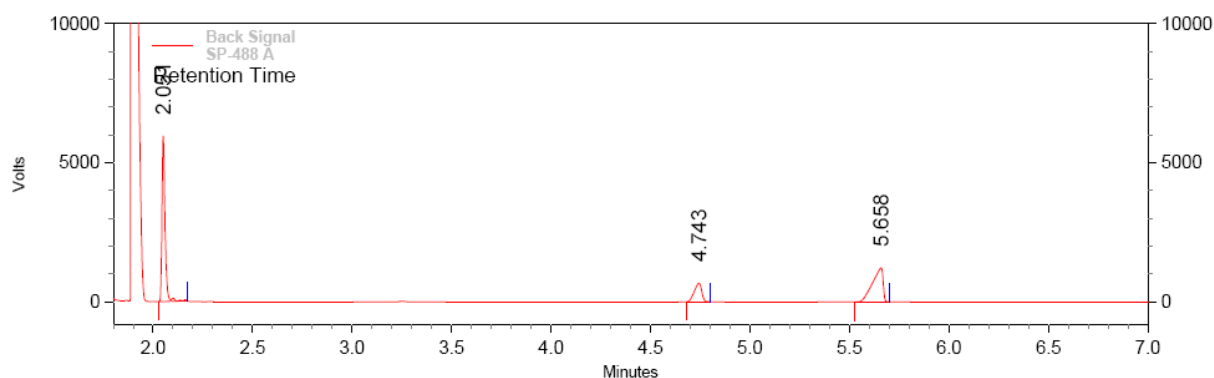
Hydroformylation of 1-hexene was performed following the general procedure reported earlier and the results are summarized in **table 4.4**.

Table 4.4: Iron catalyzed hydroformylation of 1-hexene.^a

Run	Temp. (°C)	CO/H ₂ (bars)	Time (h)	Conv. ^b (%)	L:B ^b
01.	100	20	24	-----	-----
02.	80	20	24	28	74:26
03.	70	20	24	5	74:26
04.	80	10	24	20	75:25
05.	80	10	48	50	72:28

^aConditions: 1: 0.0077 mmol, Sub/Fe: 100, Methanol: 1 ml, NA: Not applicable; ^bDetermined by GC.

GC analysis for 1-hexene was carried out on an Agilent 7890B GC system using HP-05 column (30 m × 320 μm × 0.25 μm), split ratio 30:1, column pressure 10 psi, injector temperature of 260 °C, detector temperature of 330 °C, argon carrier gas. Temperature program: Initial temperature 50 °C, hold for 1 min.; ramp 1: 4 °C/min. to 120 °C; ramp 2: 20 °C/min. to 250 °C; ramp 3: 20 °C/min. to 320 °C, hold for 2 min. Retention time for 1-hexene = 2.05 min.; hydrogenated product (n-hexane) = 2.07 min.; branched aldehydes = 4.74 min.; linear aldehyde = 5.65 minute (**figure 4.13**).



Back Signal Results

Retention Time	Area	Area %	Height	Height %
2.051	48686364	50.43	45667088	75.85
4.743	13322454	13.80	5140612	8.54
5.658	34526226	35.77	9396930	15.61
Totals	96535044	100.00	60204630	100.00

Figure 4.13: GC chromatogram for 1-hexene (table 4.4, run 5)

Determination of regioselectivity: Regioselectivity was determined according to the following equation:

Linear selectivity = (area under peak for linear aldehyde/ sum of the area for linear and branched aldehydes)*100.

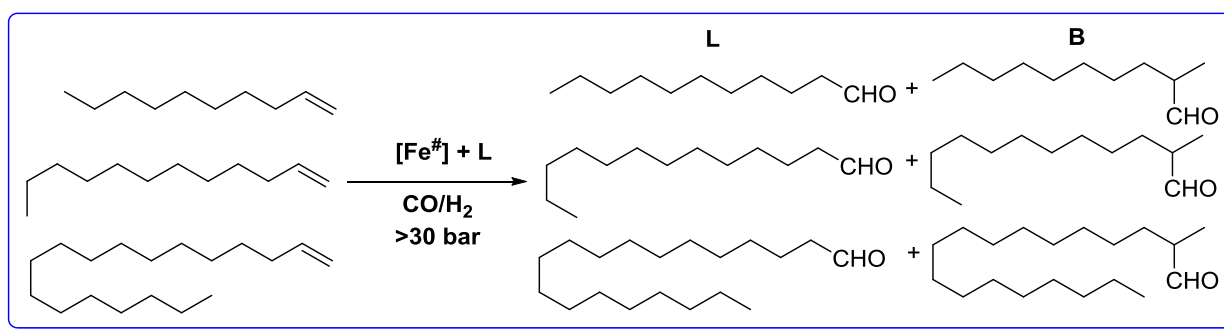
For example, in the fig. 4.13, area under peak for linear aldehyde = 35.77%

Total peak area for aldehydes = (35.77+13.80) = 49.57%

Linear selectivity = (35.77/49.57)*100 = 72%

4.4.3.3: Iron Catalyzed Hydroformylation of Long Chain Olefins

Hydroformylation of long chain olefins such as 1-decene, 1-dodecene and 1-octadecene (**scheme 4.10**) was performed following the general procedure reported earlier and the results are summarized in **table 4.5**.



Scheme 4.10: Iron catalyzed hydroformylation of long chain olefins

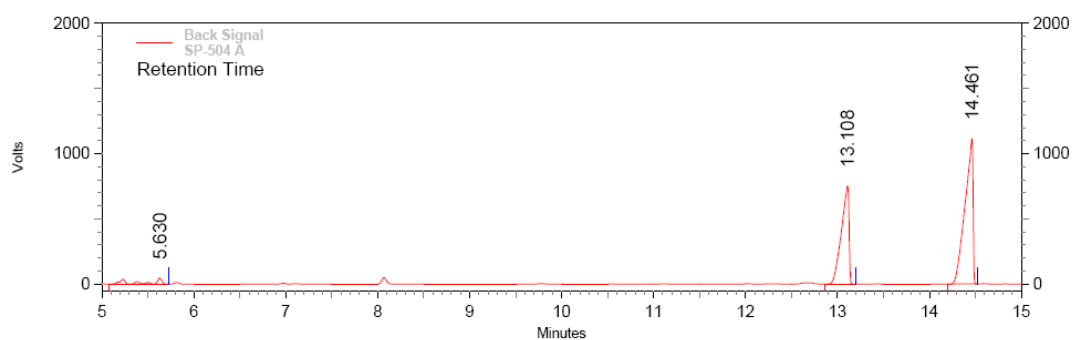
Table 4.5: Iron catalyzed hydroformylation of long chain olefins.^a

Run	Substrate	Temp. (°C)	CO/H ₂ (bars)	Time (h)	Conv. (%) ^b	L:B ^b
1	1-decene	100	15	24	47	74:26
2	1-decene	100	30	24	97	61:39
3	1-decene	120	20	24	85	61:39
4	1-decene	80	20	24	2	ND
5	1-dodecene	100	30	24	97	61:39
6	1-octadecene	100	30	24	87	48:52

^aConditions: 1: 0.0077 mmol, Sub/Fe: 100, Methanol: 1 ml, ND: Not determined; ^bDetermined by GC.

GC analysis for 1-decene, 1-dodecene and 1-octadecene was carried out on an Agilent 7890B GC system using HP-05 column (30 m × 320 μm × 0.25 μm), split ratio 30:1, column pressure 10 psi., injector temperature of 260 °C, detector temperature of 330 °C, argon carrier gas.

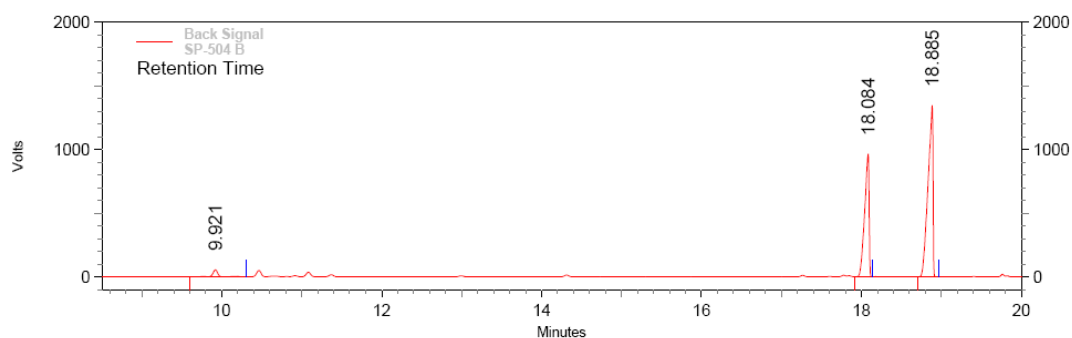
Temperature program: Initial temperature 70 °C, hold for 1 min.; ramp 1: 4 °C/min. to 120 °C; ramp 2: 10 °C/min. to 250 °C; ramp 3: 20 °C/min. to 320 °C, hold for 2 min. Retention time for 1-decene = 5.4 min.; hydrogenated product (n-decane) = 5.7 min.; branched aldehydes = 13.1 min.; linear aldehyde = 14.4 minute (**figure 4.14**). Retention time for 1-dodecene = 9.9 min.; hydrogenated product (n-dodecane) = 11.2 min.; branched aldehydes = 18.0 min.; linear aldehyde = 18.8 min. (**figure 4.15**). Retention time for 1-octadecene = 22.4 min.; branched aldehydes = 26.0 min.; linear aldehyde = 26.5 min. (**figure 4.16**).



Back Signal Results

Retention Time	Area	Area %	Height	Height %
5.630	3095654	3.51	346720	2.36
13.108	33195501	37.63	5774030	39.36
14.461	51917560	58.86	8548925	58.28
Totals	88208715	100.00	14669675	100.00

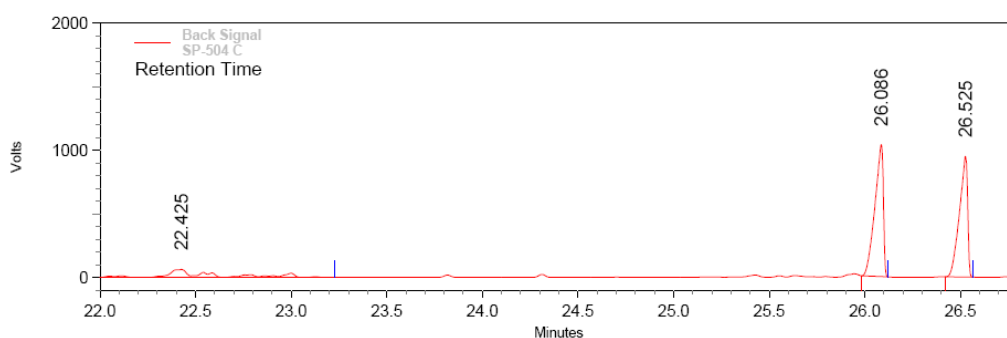
Figure 4.14: GC chromatogram for 1-decene (table 4.5, run 2)



Back Signal Results

Retention Time	Area	Area %	Height	Height %
9.921	1983764	2.66	426359	2.35
18.084	28310408	37.96	7399529	40.77
18.885	44281072	59.38	10322538	56.88
Totals	74575244	100.00	18148426	100.00

Figure 4.15: GC chromatogram for 1-dodecene (table 4.5, run 5)



Back Signal Results				
Retention Time	Area	Area %	Height	Height %
22.425	7297451	13.62	483534	3.07
26.086	24509375	45.73	7969080	50.64
26.525	21791023	40.66	7284725	46.29
Totals				
	53597849	100.00	15737339	100.00

Figure 4.16: GC chromatogram for 1-octadecene (table 4.5, run 6)

4.4.3.4: Iron Catalyzed Hydroformylation of Functional Olefins

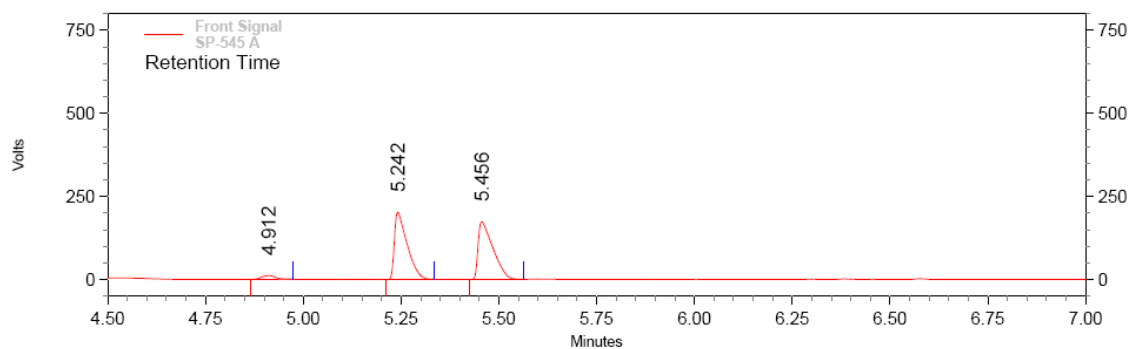
Hydroformylation of functional olefins such as trimethoxy(vinyl)silane, trimethyl(vinyl)silane, cardanol, allyl malonic acid and 2,3-dihydrofuran (**figure 4.2**) was performed following the general procedure reported earlier and the results are summarized in **table 4.6**.

GC Method for 2,3-dihydrofuran : 2-carbaldehyde = 4.9 min.; 3-carbaldehydes = 5.2 minutes and 5.4 minutes (**figure 4.17**).⁷⁶ Conversion and regioselectivity for trimethoxy(vinyl) silane (**figure 4.18**), trimethyl(vinyl) silane (**figure 4.19**), cardanol (**figure 4.20**) and allyl malonic acid (**figure 4.21**) was determined by proton NMR using CH_2Br_2 as an internal standard.

Table 4.6: Scope for iron catalyzed hydroformylation of olefins.^a

Run	Subs.	Temp. (°C)	CO/H ₂ (bars)	Time (h)	Conv. (%) ^b	L:B ^b
1	S2	80	10	48	50	72:28
2	S3	100	15	24	47	74:26
3	S3	100	30	24	97	61:39
4	S4	100	30	24	97	61:39
5	S5	100	30	24	87	48:52
6	S6 ^c	100	30	24	85	5:95
7 ^d	S7 ^c	100	30	24	99	67:33
8 ^e	S8 ^c	100	30	48	43	45:55
9	S9	70	25	24	62	3:97
10 ^f	S10 ^c	100	30	48	82	50:50
11	S11	100	20	24	16	11:89
12	S11	100	20	48	99	8:92
13	S12	100	20	48	14	15:85
14	S12	100	30	48	45	13:87
15	S13	100	30	48	15	28:72
16	S14	100	30	48	46	7:93
17	S15	100	20	48	41	18:82
18	S15	100	30	48	96	11:89
19	S16	100	25	48	68	2:98
20	S17	100	20	48	97	4:96
21	S18	100	30	48	72	8:92
22	S19	100	25	48	19	10:90
23 ^g	S20 ^c	100	30	48	99	0:99
24	S21	100	35	48	22	64:36

^aConditions: 1: 0.0077 mmol, L/M: 2.5, Sub/Fe: 100, Solvent: 1 ml methanol, S2: 1-hexene, S3: 1-decene, S4: 1-dodecene, S5: 1-octadecene, S6: trimethoxy(vinyl)silane, S7: trimethyl(vinyl)silane, S8: Cardanol, S9: 2,3-dihydrofuran, S10: Allyl malonic acid, S11: styrene, S12: 4-methyl styrene, S13: 4-*t*Bu-styrene, S14: 4-*t*Bu-styrene, S15: 4-methoxy styrene, S16: 4-acetoxy styrene, S17: 4-bromo styrene, S18: 4-chloro styrene, S19: 4-vinylbenzotrile, S20: 4-vinylbenzoic acid, S21: allyl benzene; NA: Not applicable; ^bDetermined by GC. ^c Yields determined by ¹H NMR with CH₂Br₂ as an internal standard, ^dconversion to aldehyde is 49%; ^econversion to aldehyde is 11%; ^fconversion to aldehyde is 10%; ^gconversion to aldehyde is 26%.



**Front Signal
Results**

Retention Time	Area	Area %	Height	Height %
3.568	4448576	38.14	723167	19.55
4.912	213467	1.83	88760	2.40
5.242	3498534	29.99	1550336	41.92
5.456	3504459	30.04	1336132	36.13
Totals	11665036	100.00	3698395	100.00

Figure 4.17: GC chromatogram of hydroformylated 2,3-dihydrofuran showing 3:97 (2-carbaledehyde:3-carbaledehyde selectivity) (table 4.6, run 9)

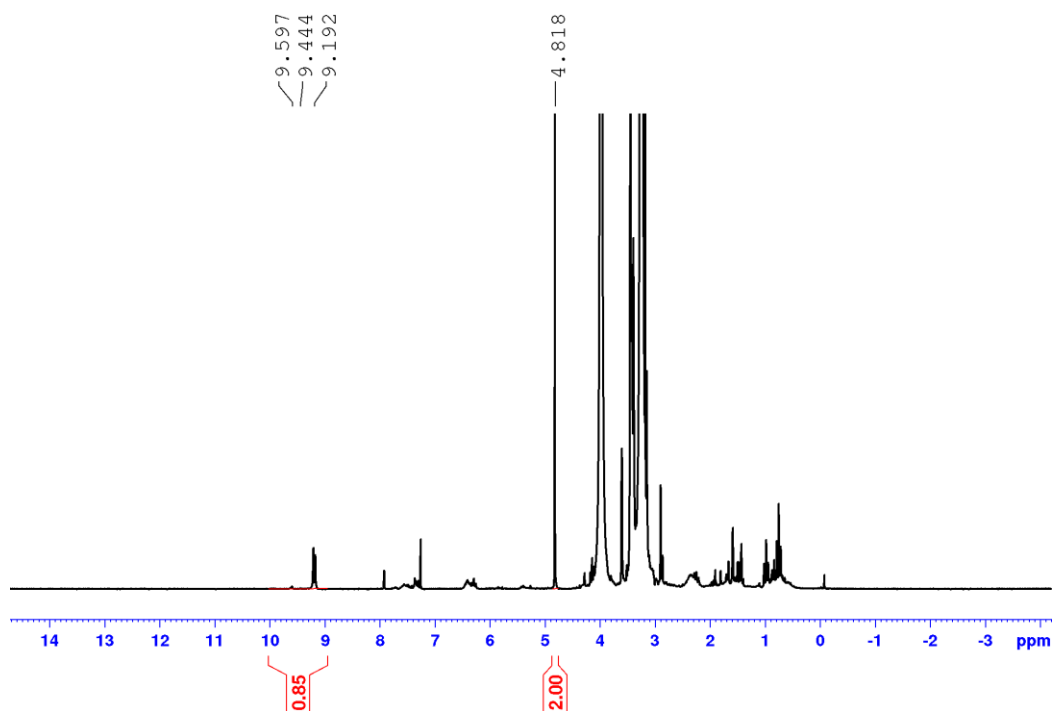


Figure 4.18: ¹H NMR spectrum (CH₂Br₂ as internal standard) of reaction mixture of trimethoxy(vinyl)silane

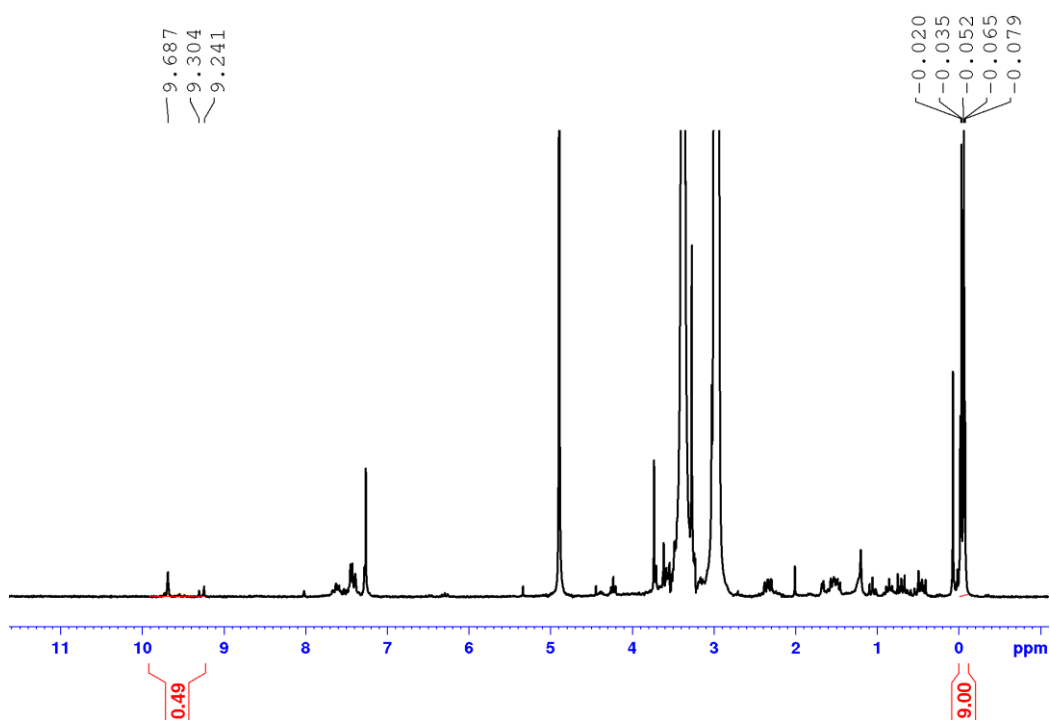


Figure 4.19: ¹H NMR spectrum (CH₂Br₂ as internal standard) of reaction mixture of trimethyl(vinyl)silane

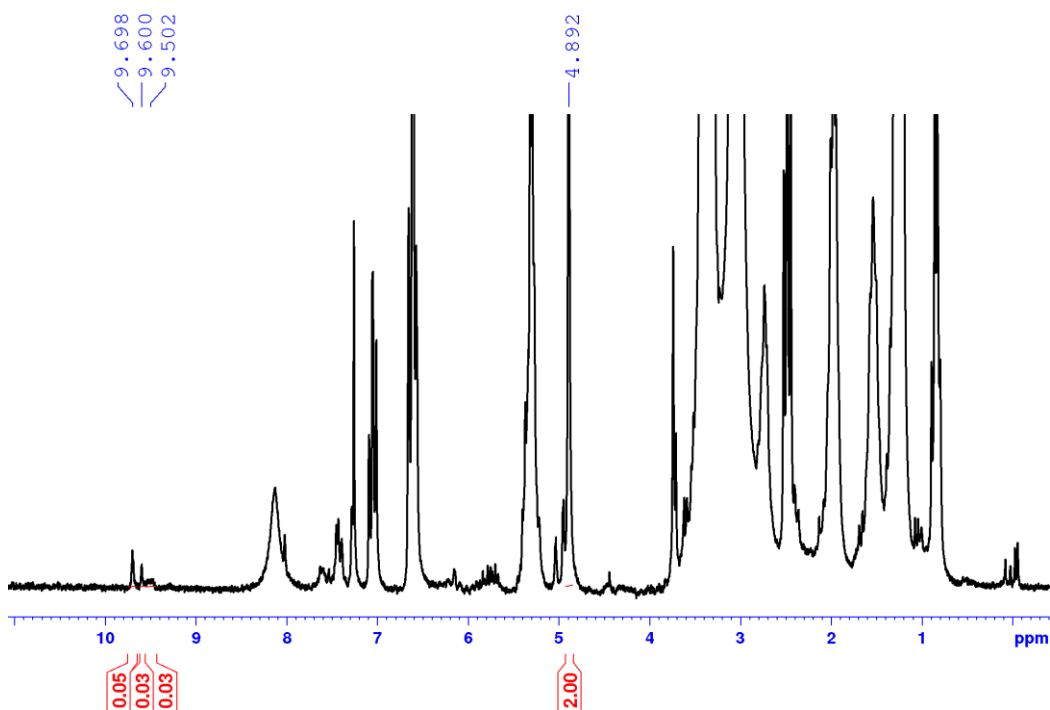


Figure 4.20: ¹H NMR spectrum (CH₂Br₂ as internal standard) of reaction mixture of cardanol

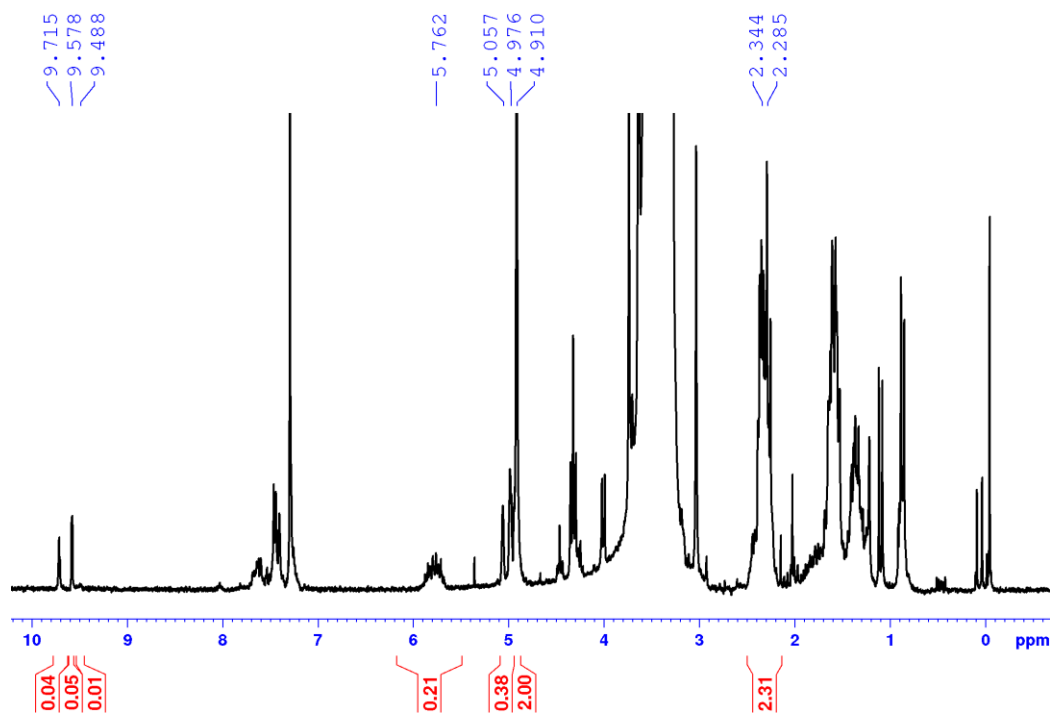


Figure 4.21: ^1H NMR spectrum (CH_2Br_2 as internal standard) of reaction mixture in case of HF of allyl malonic acid

4.4.3.5: Iron catalyzed hydroformylation of styrene and styrene derivatives

Hydroformylation of styrene and styrene derivatives (**scheme 4.11**) was performed as reported in the general procedure and important runs are presented in **table 4.6**. GC analysis for styrene and styrene derivatives was carried out on an Agilent 7890B GC system using Supelco β -dex 225 (30 m* 0.25 mm * 0.25 μm), split ratio 30:1, column pressure 10 psi., injector temperature of 220 $^\circ\text{C}$, detector temperature of 300 $^\circ\text{C}$, argon carrier gas. Temperature program for S11: styrene, S12: 4-methyl styrene: Initial temperature 100 $^\circ\text{C}$, hold for 2 min.; ramp 1: 2 $^\circ\text{C}/\text{min.}$ to 160 $^\circ\text{C}$; ramp 2: 20 $^\circ\text{C}/\text{min.}$ to 210 $^\circ\text{C}$; hold for 2 min. Retention time R_t for styrene = 7.3 mins. for hydrogenated product (Ethyl benzene) = 6.3 mins. n-dodecane = 14.7 min. (internal standard), for branched aldehydes = 17.0 mins. for linear aldehyde = 23.4 mins. (**figure 4.22**).

Retention time R_t for 4-methyl styrene = 10.3 mins. for branched aldehydes = 22.0 mins. for linear aldehyde = 27.7 mins. (**figure 4.23**).

Temperature program for S13: 4-*i*Bu-styrene, S14: 4-*i*Bu-styrene, S15: 4-methoxy styrene, S16: 4-acetoxy styrene, S17: 4-bromo styrene, S18: 4-chloro styrene, S19: 4-vinylbenzotrile, S21: allyl benzene: Initial temperature 100 $^\circ\text{C}$, hold for 2 min.; ramp 1: 2 $^\circ\text{C}/\text{min.}$ to 160 $^\circ\text{C}$; ramp 2: 10 $^\circ\text{C}/\text{min.}$ to 210 $^\circ\text{C}$; hold for 2 min.

Retention time R_t for 4-isobutyl styrene = 20.7 mins. for branched aldehydes = 32.6 mins. for linear aldehyde = 37.1 mins. (**figure 4.24**).

Retention time R_t for 4-tertbutyl styrene = 19.9 mins. for branched aldehydes = 33.3 mins. for linear aldehyde = 36.2 mins. (**figure 4.25**).

Retention time R_t for 4-methoxy styrene = 20.5 mins. for branched aldehydes = 33.3 mins. for linear aldehyde = 36.0 mins. (**figure 4.26**).

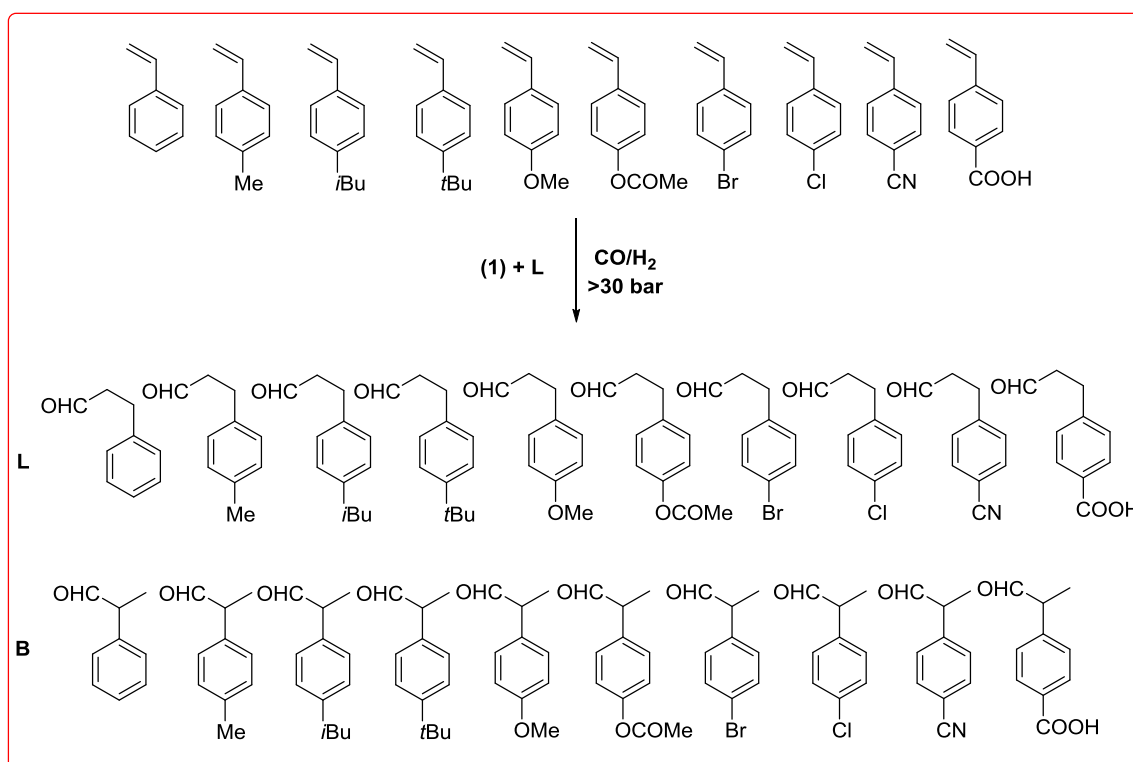
Retention time R_t for 4-acetoxy styrene = 30.0 mins. for branched aldehydes = 32.9 mins. for linear aldehyde = 38.44 mins. (**figure 4.27**).

Retention time R_t for 4-bromo Styrene = 19.3 mins. for branched aldehydes = 35.4 mins. for linear aldehyde = 38.5 mins. (**figure 4.28**).

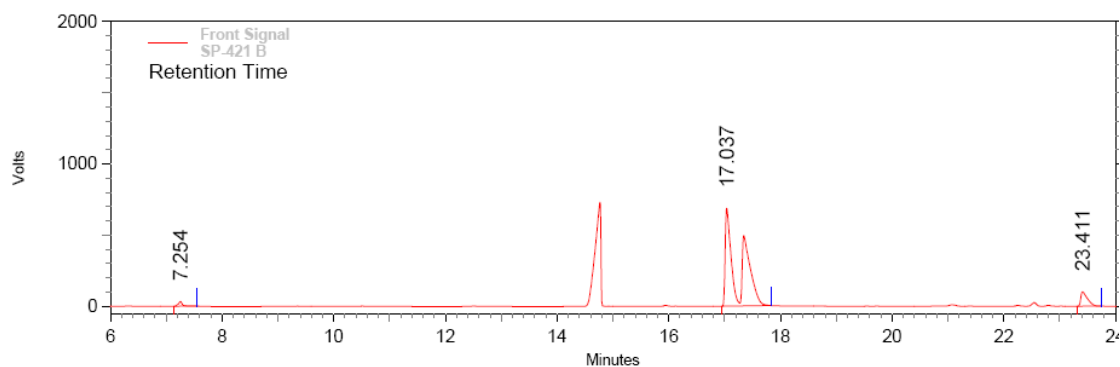
Retention time R_t for 4-chloro styrene = 14.4 mins. for branched aldehydes = 31.4 mins. for linear aldehyde = 36.0 mins. (**figure 4.29**).

Retention time R_t for 4-vinylbenzotrile = 28.3 mins. for branched aldehydes = 37.0 mins. for linear aldehyde = 38.5 mins. (**figure 4.30**).

Retention time R_t for Allyl benzene = 8.4 mins. for branched aldehydes = 24.3 mins. for linear aldehyde = 29.2 mins. (**figure 4.32**).



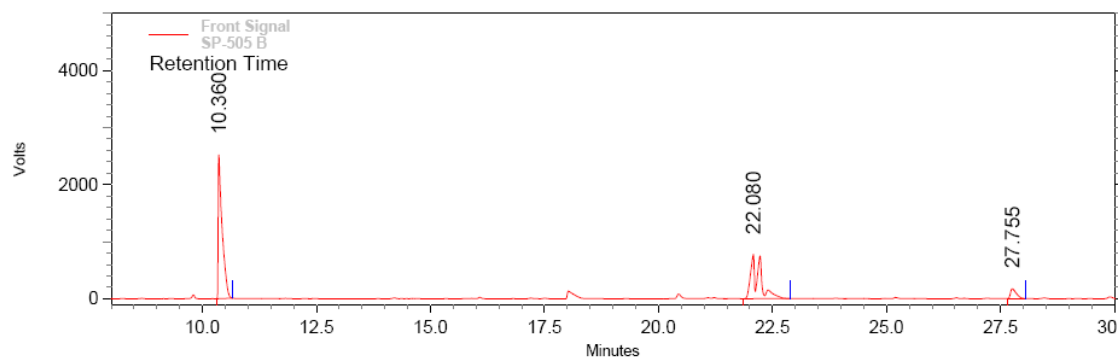
Scheme 4.11: Iron catalyzed hydroformylation of styrene and styrene derivatives



**Front Signal
Results**

Retention Time	Area	Area %	Height	Height %
7.254	1295618	1.53	252679	4.01
17.037	76812390	90.87	5280267	83.77
23.411	6424519	7.60	770678	12.23
Totals	84532527	100.00	6303624	100.00

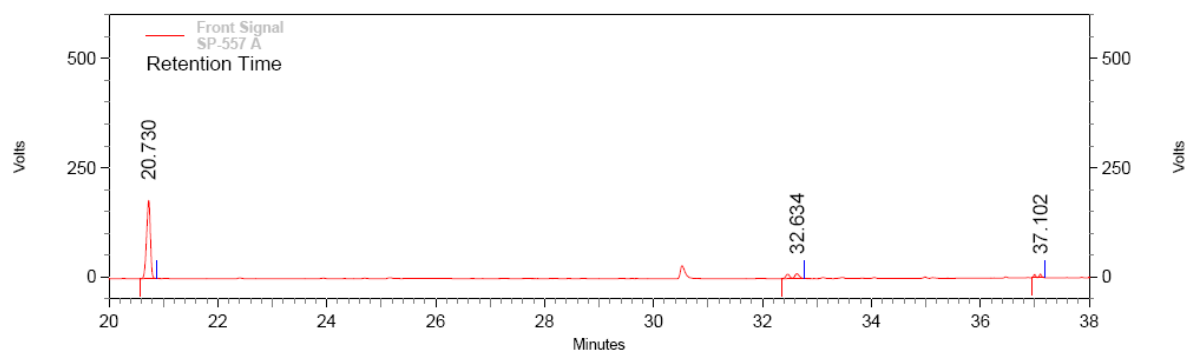
Figure 4.22: Hydroformylation of styrene- GC chromatogram of reaction mixture showing l:b selectivity of 8:92 (table 4.6, run 12)



**Front Signal
Results**

Retention Time	Area	Area %	Height	Height %
10.360	115400871	54.98	19326340	72.54
22.080	82649308	39.37	5979093	22.44
27.755	11857308	5.65	1337346	5.02
Totals	209907487	100.00	26642779	100.00

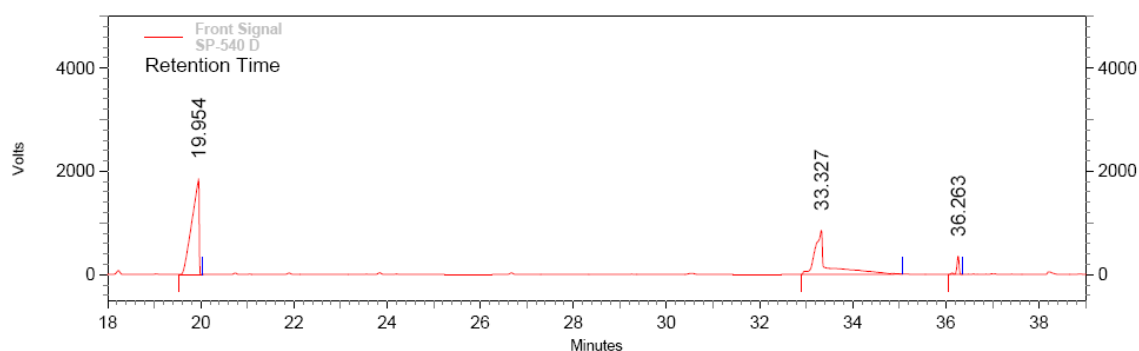
Figure 4.23: Hydroformylation of 4-methyl styrene- GC chromatogram of reaction mixture showing l:b selectivity of 13:87 (table 4.6, run 14)



**Front Signal
Results**

Retention Time	Area	Area %	Height	Height %
20.730	6639516	85.17	1369616	90.43
32.634	835584	10.72	84012	5.55
37.102	320910	4.12	60936	4.02
Totals	7796010	100.00	1514564	100.00

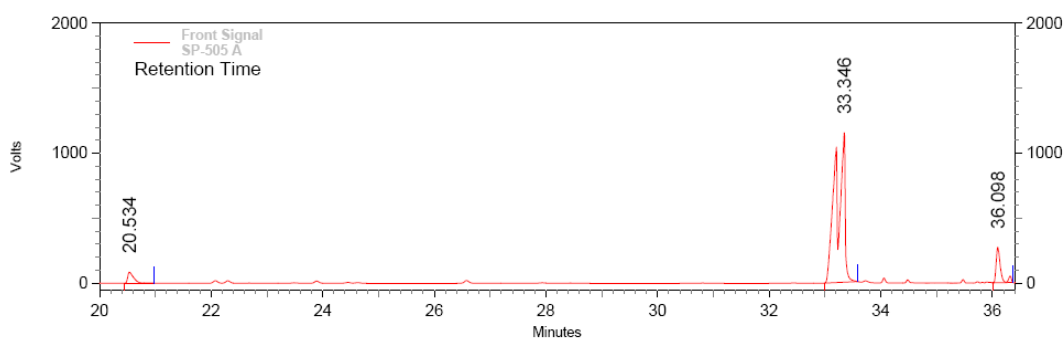
Figure 4.24: Hydroformylation of 4-*iso*-butyl styrene- GC chromatogram of reaction mixture showing l:b selectivity of 28:72 (table 4.6, run 15)



**Front Signal
Results**

Retention Time	Area	Area %	Height	Height %
19.954	154416065	54.55	14238639	60.61
33.327	119880981	42.35	6545527	27.86
36.263	8792908	3.11	2706305	11.52
Totals	283089954	100.00	23490471	100.00

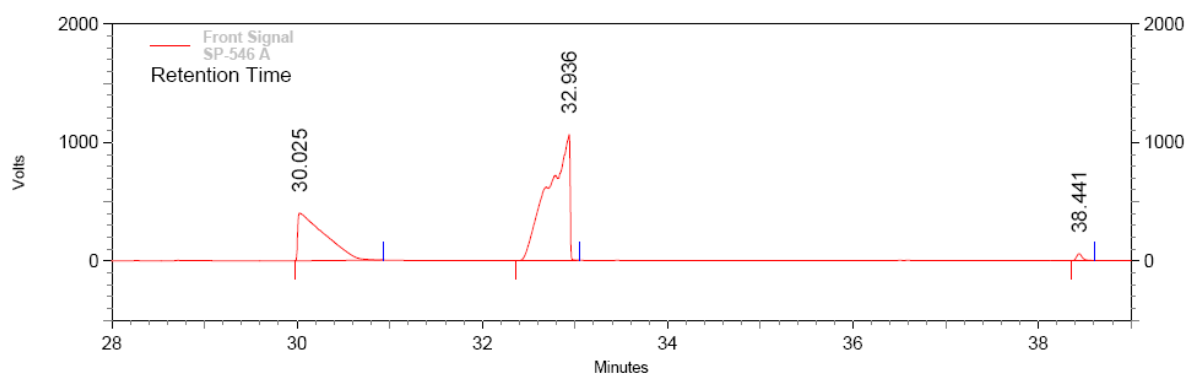
Figure 4.25: GC chromatogram of HF of 4-*tert*-butyl styrene showing 7:93 (l:b selectivity, table 4.6, run 16)



**Front Signal
Results**

Retention Time	Area	Area %	Height	Height %
20.534	4759768	4.19	651609	5.63
33.346	97257904	85.70	8827623	76.28
36.098	11469795	10.11	2094081	18.09
Totals	113487467	100.00	11573313	100.00

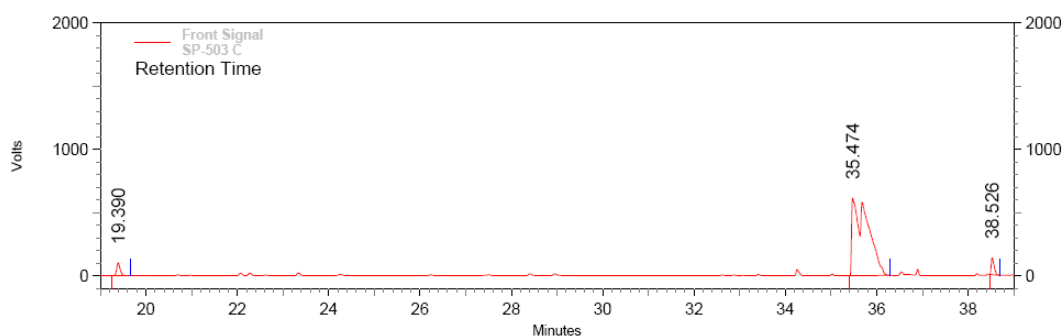
Figure 4.26: Hydroformylation of 4-methoxy styrene- GC chromatogram of reaction mixture showing l:b selectivity of 11:89 (table 4.6, run 18)



**Front Signal
Results**

Retention Time	Area	Area %	Height	Height %
30.025	62512569	32.08	3100612	26.48
32.936	130455547	66.95	8155983	69.64
38.441	1885508	0.97	454626	3.88
Totals	194853624	100.00	11711221	100.00

Figure 4.27: GC chromatogram of hydroformylation product of 4-acetoxystyrene showing regioselectivity of 2:98 (l:b selectivity, table 4.6, run 19)

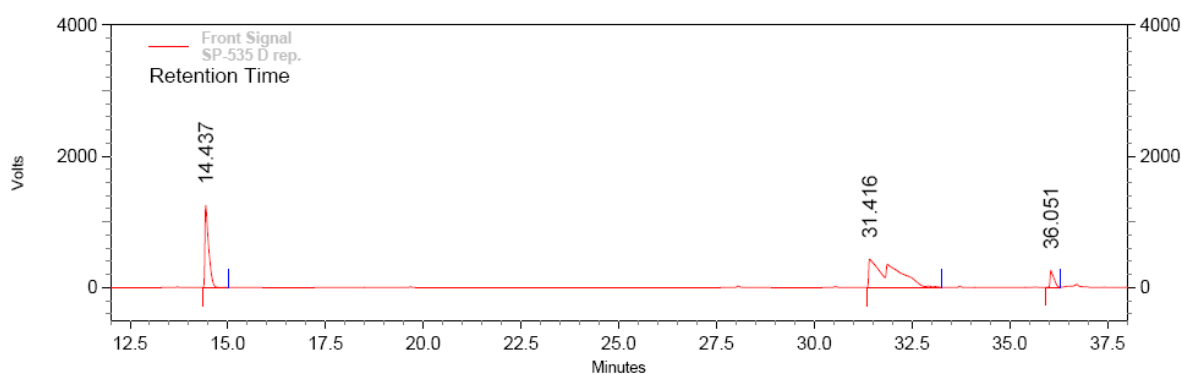


**Front Signal
Results**

Retention Time	Area	Area %	Height	Height %
19.390	4058019	3.33	780763	12.02
35.474	113220691	93.04	4693753	72.26
38.526	4411773	3.63	1021514	15.73

Totals	121690483	100.00	6496030	100.00
--------	-----------	--------	---------	--------

Figure 4.28: Hydroformylation of 4-bromo styrene- GC chromatogram of reaction mixture showing l:b selectivity of 4:96 (table 4.6, run 20)

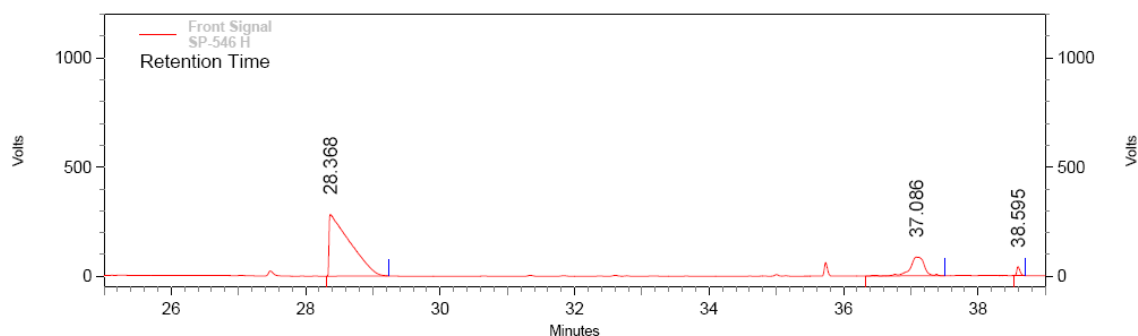


**Front Signal
Results**

Retention Time	Area	Area %	Height	Height %
14.437	63462931	28.43	9624588	64.50
31.416	146656410	65.71	3318935	22.24
36.051	13070603	5.86	1979218	13.26

Totals	223189944	100.00	14922741	100.00
--------	-----------	--------	----------	--------

Figure 4.29: GC chromatogram of hydroformylation product of 4-chloro styrene showing regioselectivity of 8:92 l:b selectivity (table 4.6, run 21)


**Front Signal
Results**

Retention Time	Area	Area %	Height	Height %
28.368	46845251	81.42	2174989	69.07
37.086	9667520	16.80	656576	20.85
38.595	1022776	1.78	317601	10.09
Totals	57535547	100.00	3149166	100.00

Figure 4.30: GC chromatogram of HF of 4-vinylbenzotrile showing 10:90 l:b selectivity (table 4.6, run 22)

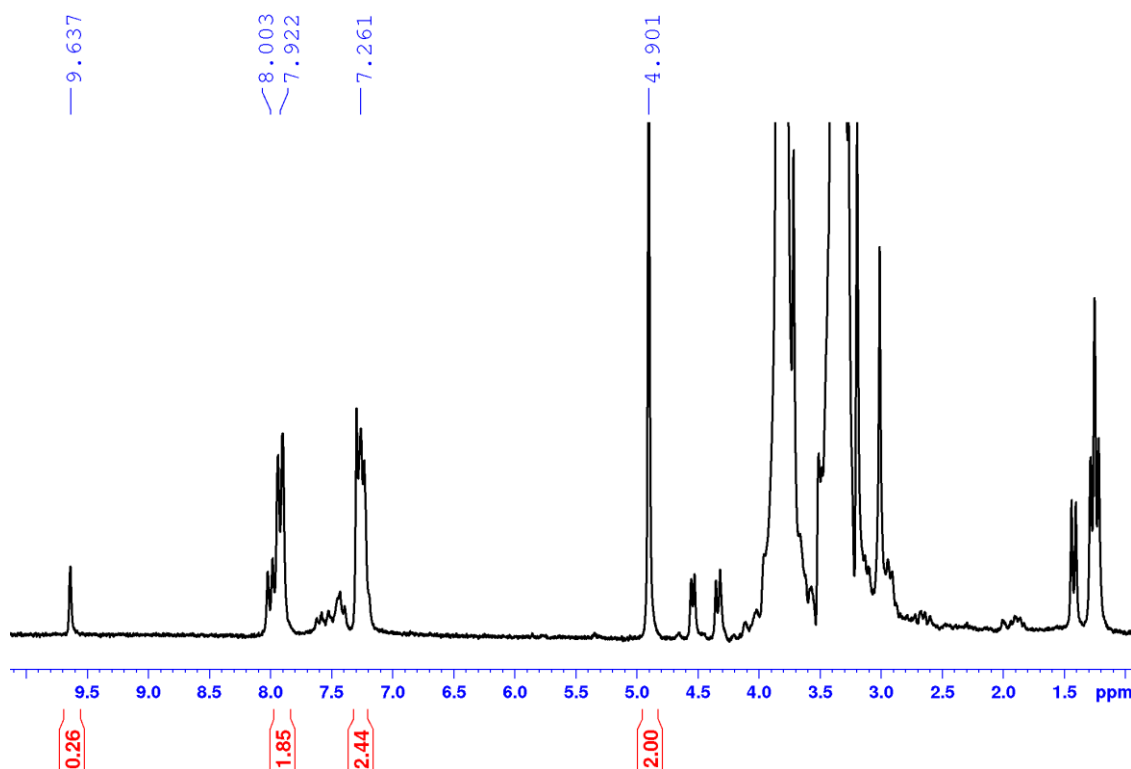
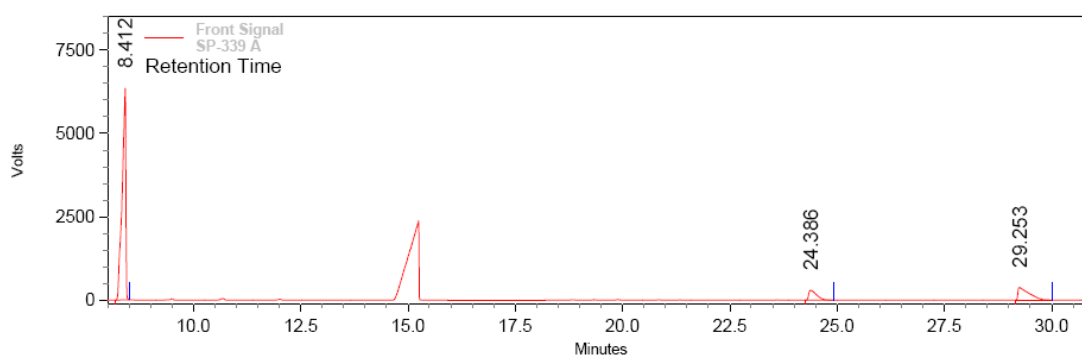


Figure 4.31: ^1H NMR spectrum (CH_2Br_2 as internal standard) of hydroformylation product of 4-vinylbenzoic acid showing >99% selectivity towards branched product (table 4.6, run 23)



Front Signal Results				
Retention Time	Area	Area %	Height	Height %
8.412	289089964	78.36	48700866	90.38
24.386	28342223	7.68	2245412	4.17
29.253	51503358	13.96	2937163	5.45
Totals				
	368935545	100.00	53883441	100.00

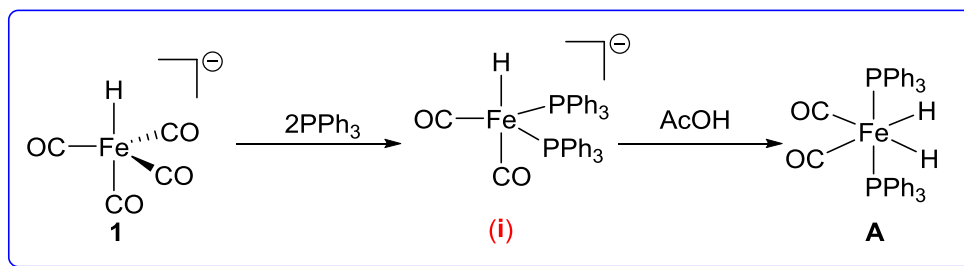
Figure 4.32: Hydroformylation of allyl benzene- GC chromatogram of reaction mixture showing l:b selectivity of 64:36 (table 4.6, run 24)

4.4.3.6: Mechanistic Investigations

In our attempts to under pin the catalyst resting state, three different pathways (i), (ii), (iii) (**figure 4.3**) were investigated and the reaction was tracked using *in-situ* NMR spectroscopy.

4.4.3.6.1: Coordination of Ligand followed by Generation of Dihydride Species

Method A: Coordination behaviour of triphenyl phosphine with the iron precursor $[\text{HFe}(\text{CO})_4][\text{PPN}]$ (1) was investigated (**scheme 4.12**). In a dried and argon cooled Schlenk tube 0.010 g (0.0000138 moles) of 1 was dissolved in 0.4 ml CDCl_3 and 2 equivalent (0.0073 g, 0.0000277 moles) of triphenyl phosphine (L1) was added to above mixture and the resultant solution was transferred to a high pressure NMR tube. The above mixture was heated to 50 °C and ^{31}P NMR was recorded after 45 minutes at 45 °C. The phosphorus NMR revealed a singlet resonance at 82.3 and 71.5 ppm along with the counter cation signal at 21 ppm and free triphenyl phosphine at -5 ppm. Next, the NMR tube was heated to 45 °C for 16 hours and a ^{31}P NMR was recorded. After 16 hours, 50% coordination of triphenyl phosphines was observed (**figure 4.34**). The new resonance at 82.3 and 71.5 ppm can be ascribed to coordinated triphenyl phosphine as depicted in species (i), which is in line with the reported chemical shifts for a triphenyl phosphine coordinated iron complex.¹¹¹



Scheme 4.12: Coordination behaviour of L1 with iron precursor 1

Having observed L1 coordination, the NMR tube was allowed to freeze in liq. N₂ bath. Now acetic acid (50 μL) (0.87 mmol) was added to above NMR tube under frozen condition and a proton NMR was immediately recorded at 0 °C. A very weak resonance at -12.2 ppm appeared (**figure 4.36**) in a proton NMR spectrum. The new hydride signal can be attributed to a di-hydride species (A).

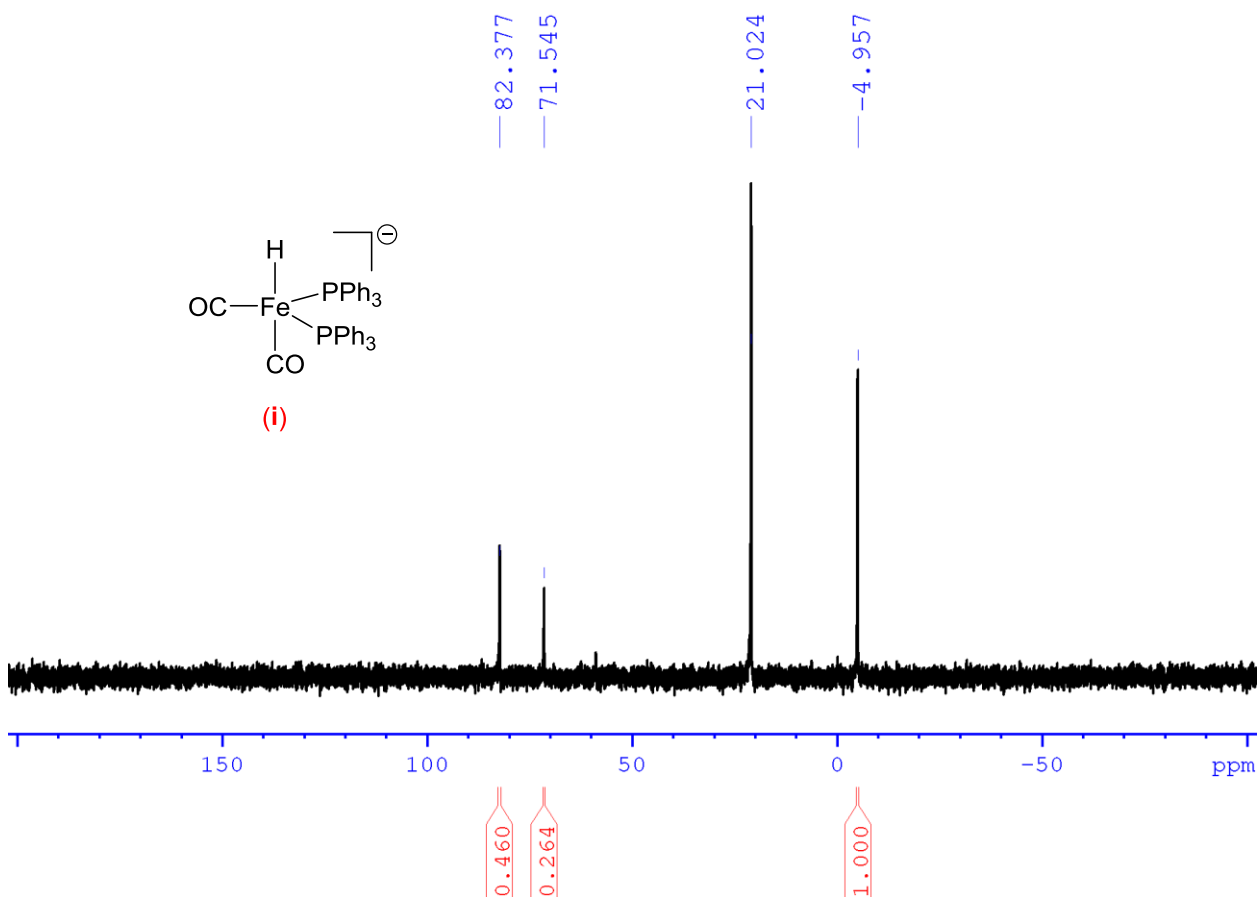


Figure 4.33: ³¹P NMR spectrum of a reaction mixture of L1 and (i) after heating at 50 °C for 45 minutes

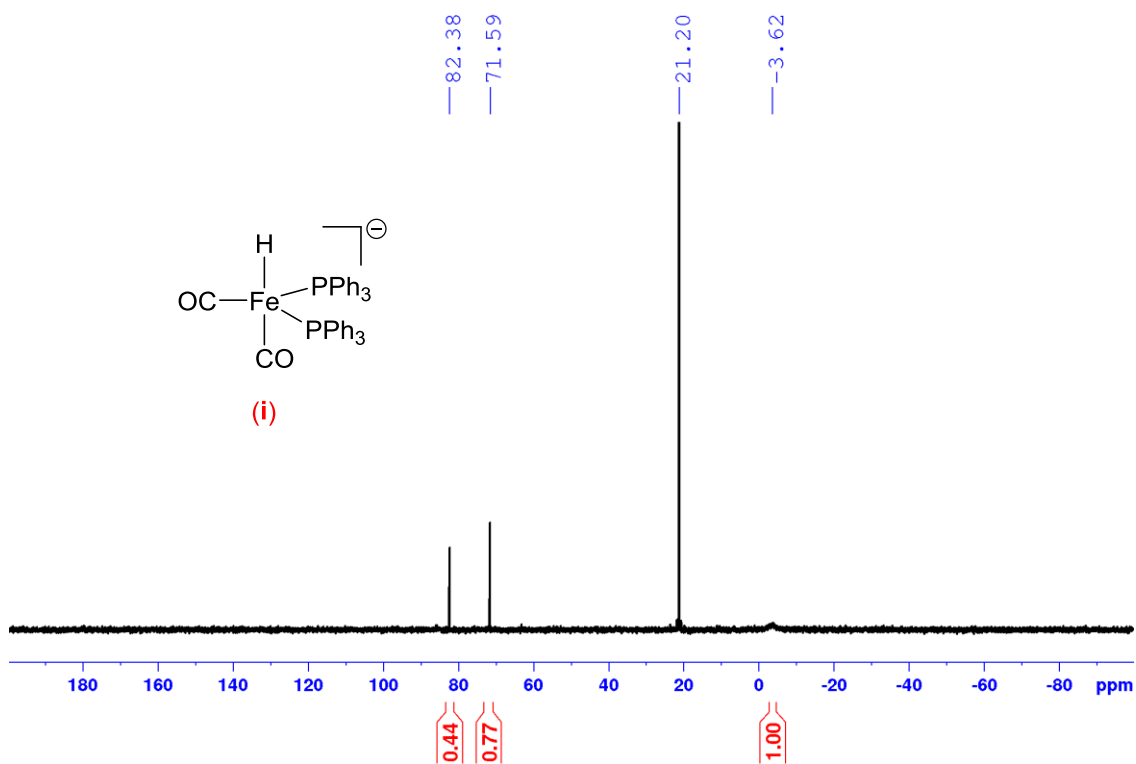


Figure 4.34: ^{31}P NMR spectrum of a reaction mixture of L1 and (1) after heating at 45 °C for 16 hours

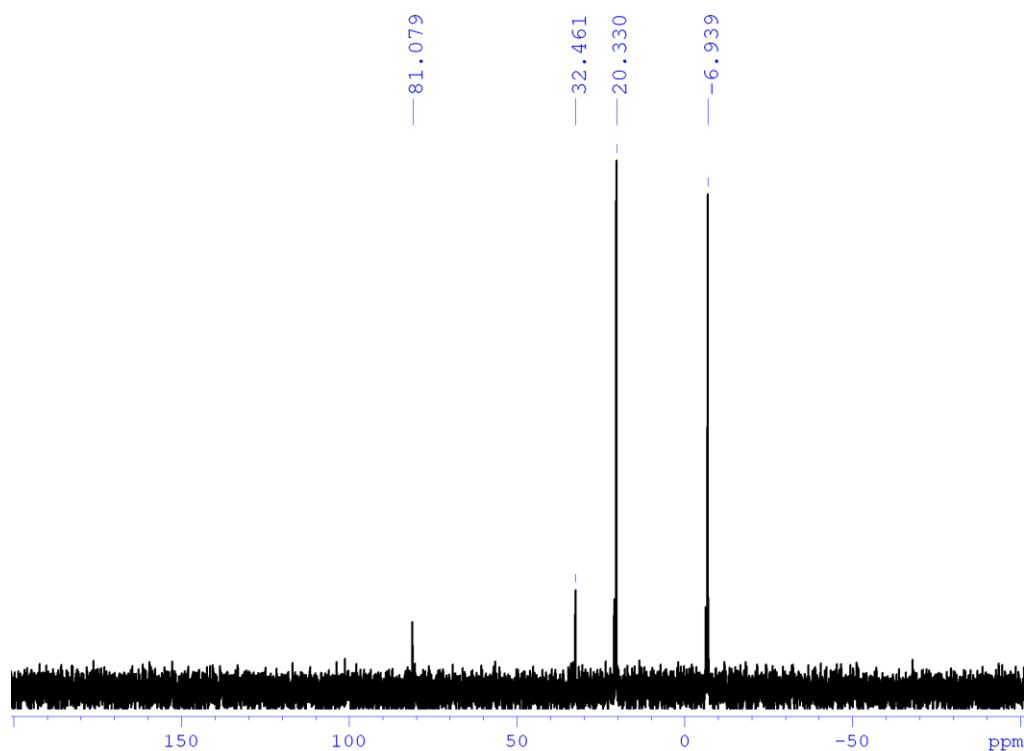


Figure 4.35: ^{31}P NMR spectrum of a reaction mixture of L1 + (1) after addition of acetic acid at 0 °C

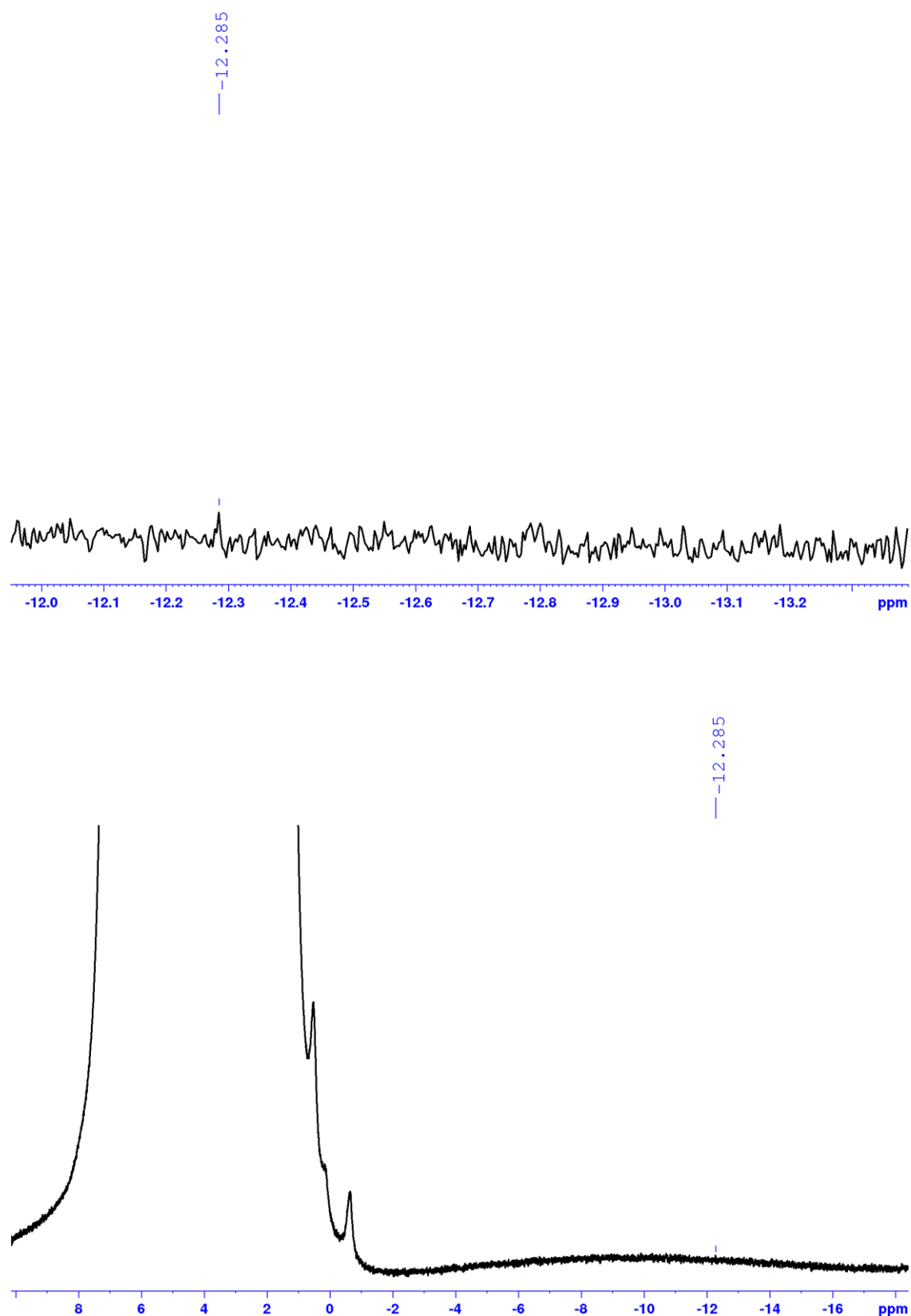


Figure 4.36: ^1H NMR spectrum of a reaction mixture of L1 + (1) after addition of acetic acid at 0 $^{\circ}\text{C}$

Method B: In a NMR tube, 0.014 g (0.0000194 moles) of **1** and triphenyl phosphine (L1) (0.010 g, 0.0000388 moles) were dissolved in 0.4 ml of dry methanol to get a clear solution. D₂O capillary was added to it as an internal lock. Now the NMR of the reaction mixture was recorded at room temperature (**figure 4.37**). Next, acetic acid (75 μ L) was added to the above NMR tube and NMR was immediately recorded at room temperature. Proton NMR spectrum revealed a doublet at -9.50 ppm (**figure 4.39**) with a $^2J_{P-H}$ of 43 Hz. Similar chemical shift has been reported for diphosphine iron-dihydride complexes in the literature.¹¹² The corresponding phosphorus NMR displayed a single peak at 71.5 ppm confirming the coordination of the phosphine ligand L1 (**figure 4.38**).

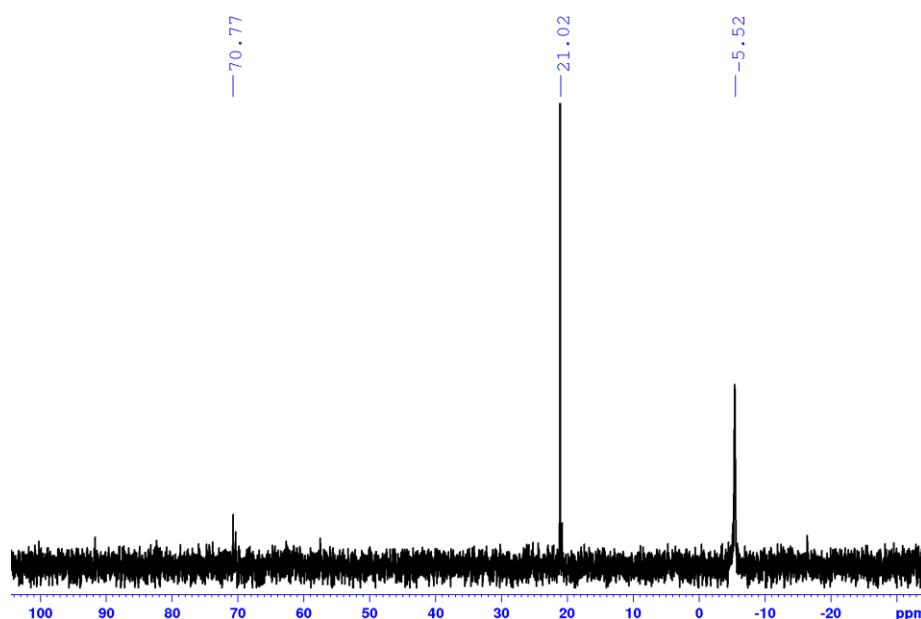


Figure 4.37: ³¹P NMR spectrum of a reaction mixture of L1 and **1** at room temperature

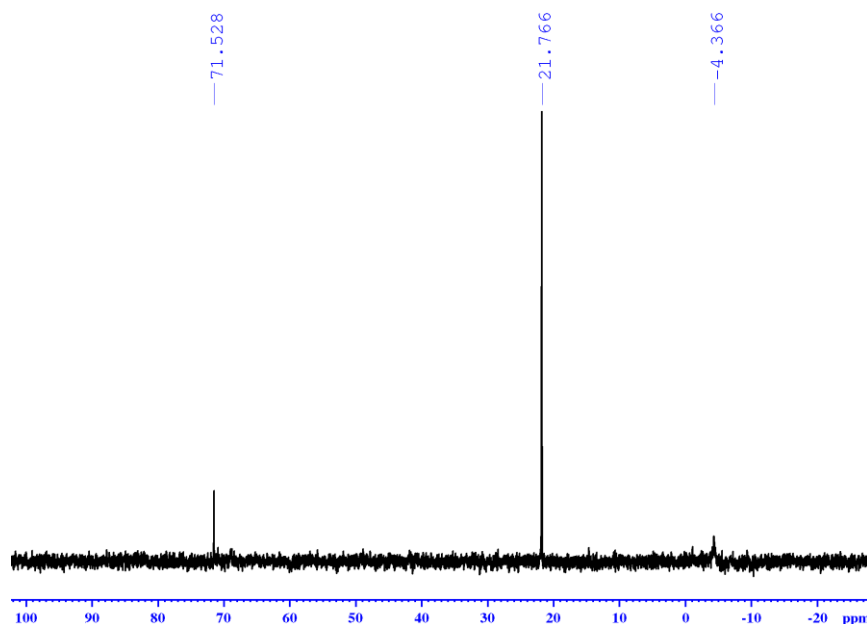


Figure 4.38: ³¹P NMR spectrum of a reaction mixture of L1 and **1** immediately after addition of acetic acid at room temperature.

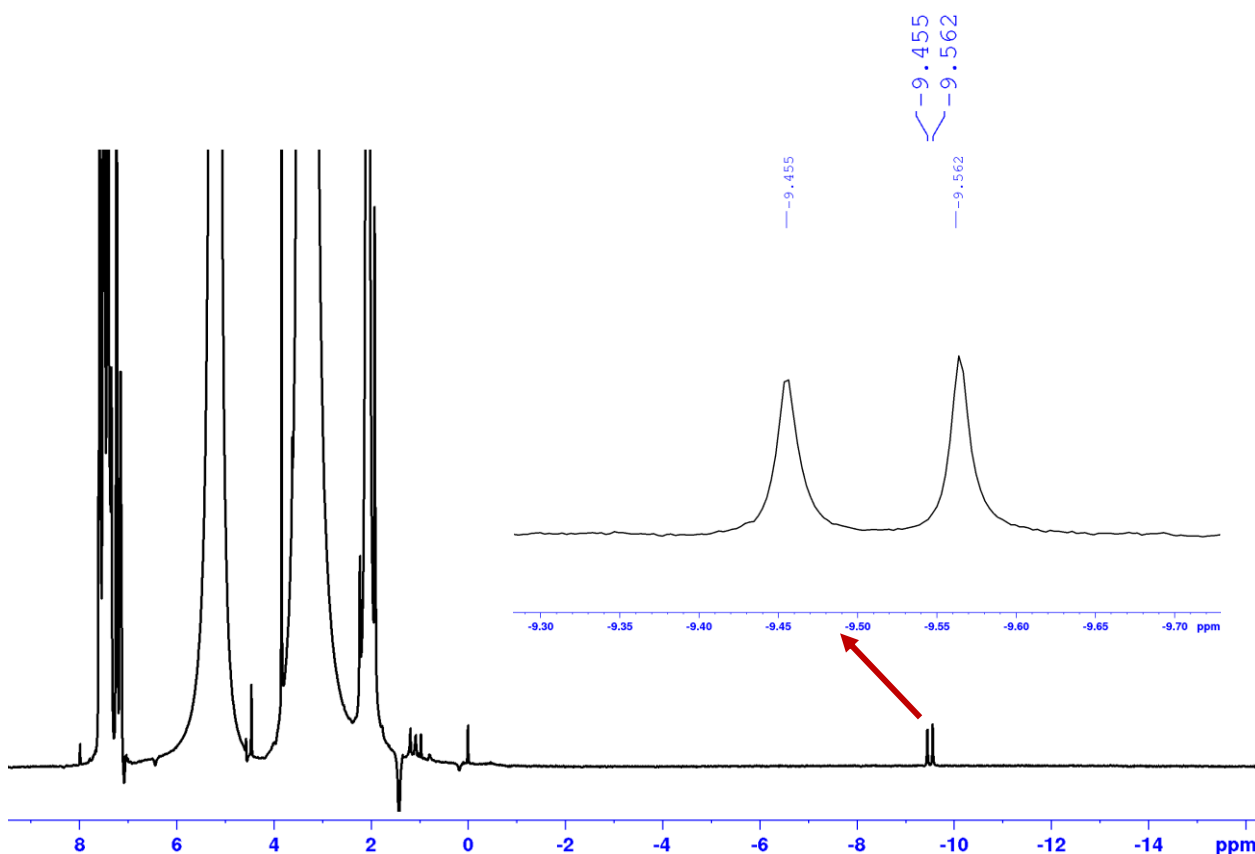


Figure 4.39: ¹H NMR spectrum of a reaction mixture of L1 and 1 immediately after addition of acetic acid at room temperature displaying the dihydride peak (expanded view in sets)

Method B in presence of CD₃COOD: The above NMR experiment was repeated by using CD₃COOD and the details are as under. In a NMR tube, 0.014 g (0.0000194 moles) of 1 and triphenyl phosphine (L1) (0.010 g, 0.0000388 moles) were dissolved in 0.4 ml of dry methanol to get a clear solution. D₂O capillary was added to it as an internal lock. Now the NMR of the reaction mixture was recorded at room temperature. Next, deuterated acetic acid (75 μL) was added to the above NMR tube and NMR was immediately recorded at room temperature. This experiment essentially produced the same results and a doublet was clearly seen in the hydride region in a proton NMR spectrum (**figure 4.41**). This could be due to excess methanol, which will exchange its proton with the CD₃COOD, eventually giving CD₃COOH. Along the same line, a proton decoupled ³¹P NMR indicated a resonance at 83.01, 71.55 ppm, along with a broad multiplet at 69.17 ppm (**figure 4.40**)

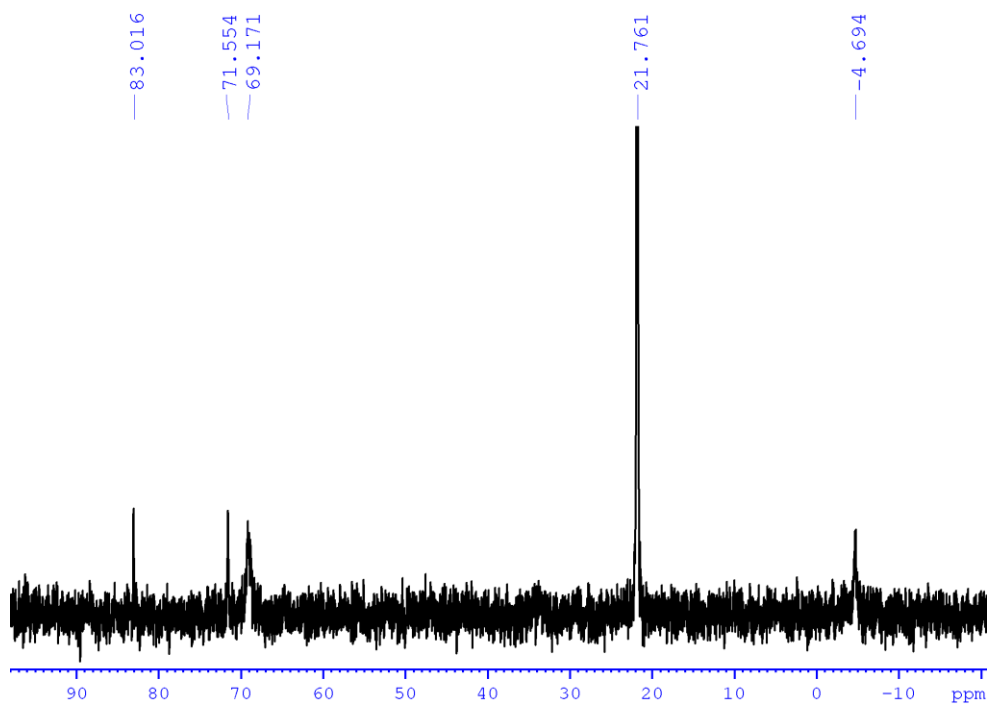


Figure 4.40: ^{31}P NMR spectrum of a reaction mixture of L1 and 1 immediately after addition of CD_3COOD at room temperature

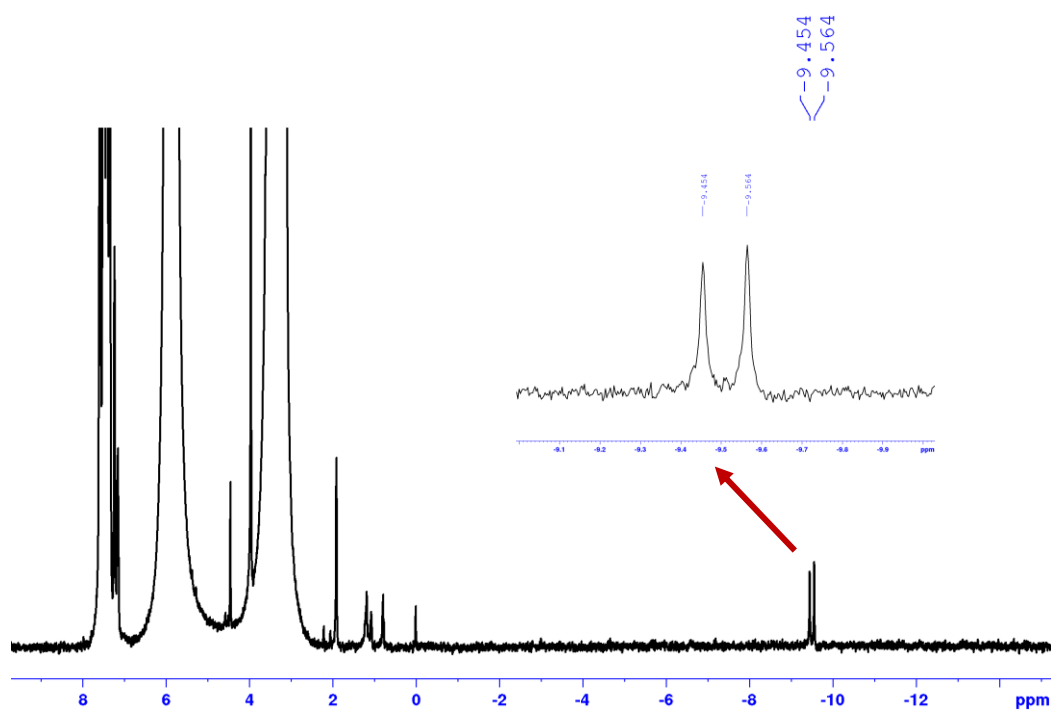


Figure 4.41: ^1H NMR spectrum of a reaction mixture of L1 and 1 immediately after addition of CD_3COOD at room temperature displaying the dihydride peak (expanded view in sets)

Detection of H₂ Using Headspace GC

The dihydride seems to be highly unstable and H₂ gas is released. In our attempts to detect the released H₂, we performed the following experiment and as shown in **figure 4.42**, H₂ was detected.

Experimental procedure: In a vial, [HFe(CO)₄][PPN] (0.100 g, 0.000138 mol) and PPh₃ (0.072 g, 0.000276 mol) were weighed in a glove box. It was dissolved in CDCl₃: MeOH (0.3 ml:0.1ml). Next, acetic acid (0.3 ml, 0.00524 mol) was added to the tightly sealed vial immediately before recording the sample. Sample was taken from the closed vial using a gas syringe and was injected in headspace GC.

Headspace GC analysis was performed on an Agilent 7890A GC system equipped with Porapak column and thermal conductivity detector. Inlet temperature was maintained at 150 °C, column flow = 14 ml/min. Detector temperature was maintained at 200 °C. Temperature program: starting at 60 °C with hold time of 5 mins. Ramp 1: @ 10 °C to 100 °C, hold for 21 mins. Retention time for H₂ = 1.5 mins.

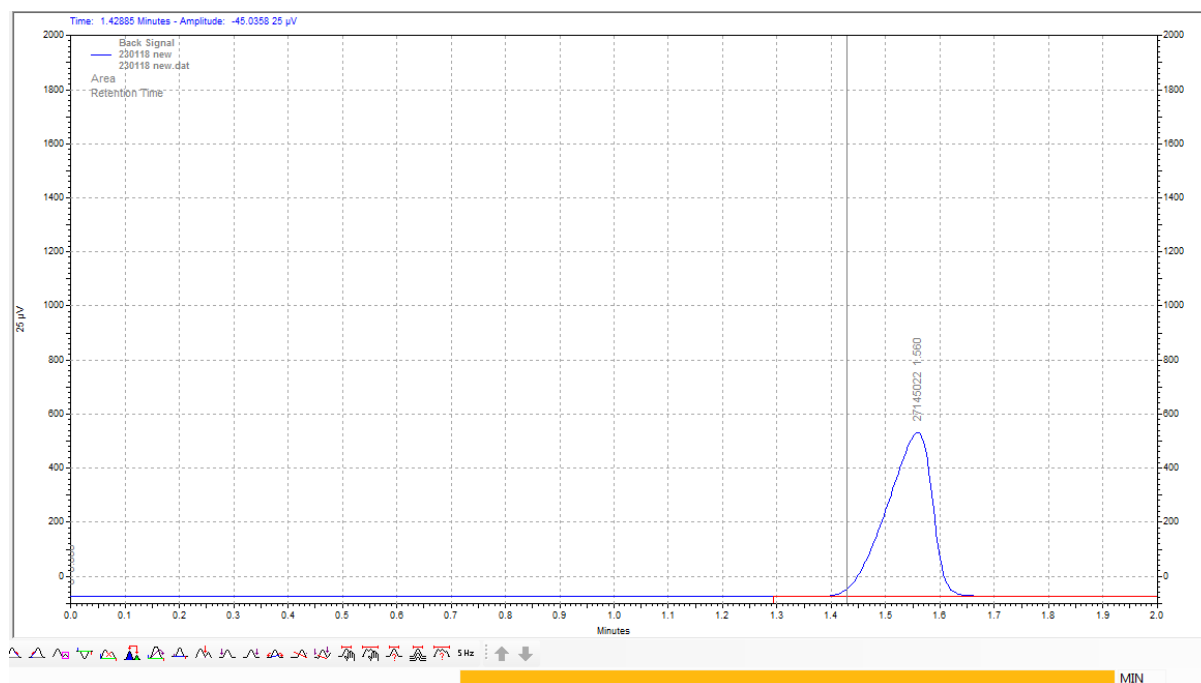
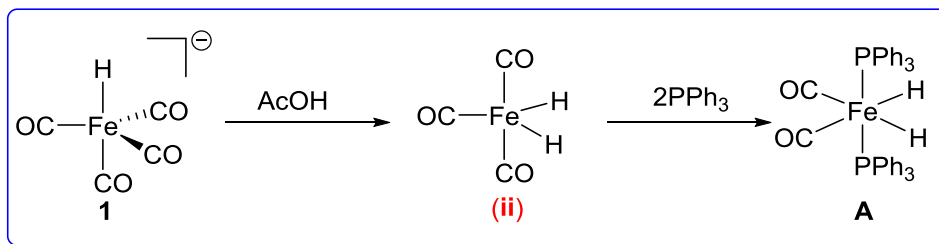


Figure 4.42: Detection of released H₂ using headspace GC

4.4.3.6.2: Formation of Dihydride Complex followed by Ligand Coordination

In a reversed protocol; first formation of dihydride iron complex, followed by ligand coordination was investigated (scheme 4.13).



Scheme 4.13: Coordination behaviour of L1 with iron precursor 1

The iron precursor $[\text{HFe}(\text{CO})_4][\text{PPN}]$ (**1**) (0.016 g, 0.000022 moles) was dissolved in 0.6 ml $\text{CDCl}_3:\text{MeOH}$ (3:1) mixture in an NMR tube and the tube was cooled to liquid nitrogen temperature. Excess (50 μL , 0.87 mmol) of acetic acid was added to above solution at -196°C . The NMR tube was taken out from the liquid nitrogen bath just before inserting it in the magnet and recording the NMR spectrum. The hydride resonance at -15.38 ppm can be attributed to the iron dihydride as depicted in species (ii) (figure 4.43). This was followed by addition of 2 equivalent (0.0115 g, 0.000044 moles) triphenyl phosphine and a phosphorus NMR was recorded. However, addition of L1 did not show any coordination at room temperature and heating the sample to obtain the desired coordination led to elimination of H_2 . Therefore, species A could not be generated by following this route.¹¹³

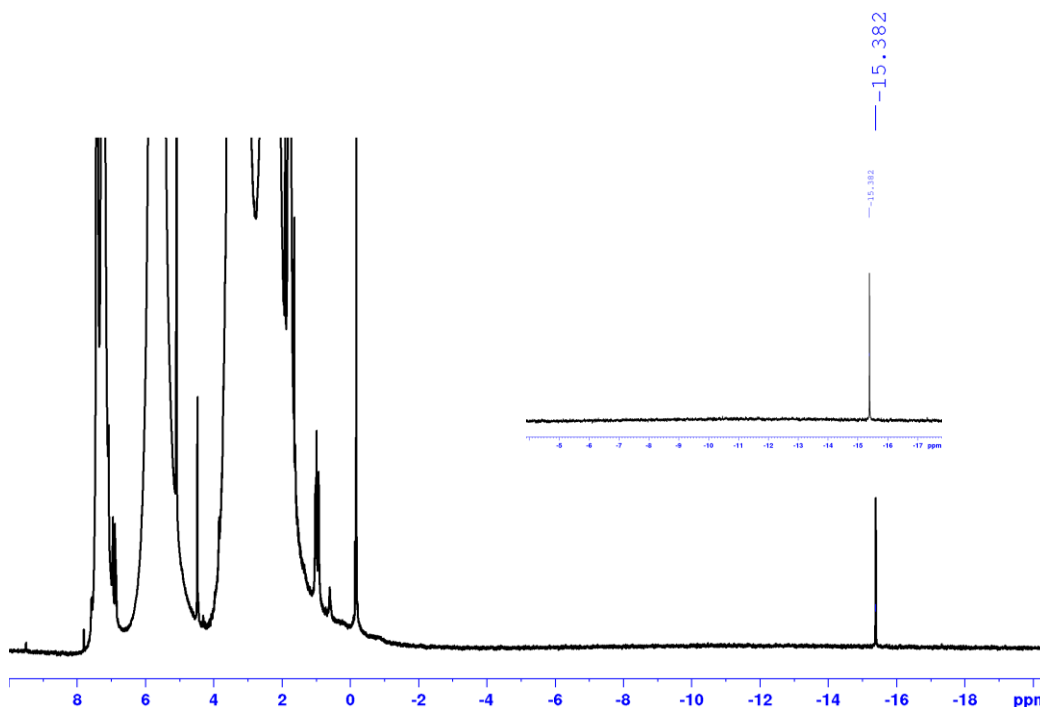
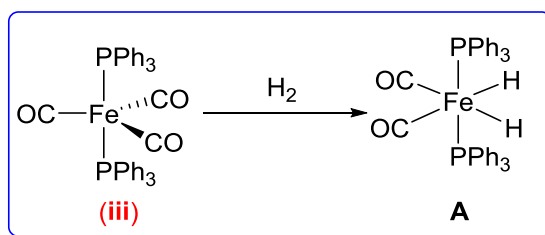


Figure 4.43: ^1H NMR spectrum of species (ii) displaying the formation di-hydride immediately (expanded view is presented in set)

4.4.3.6.3: From $[\text{Fe}(\text{CO})_3(\text{PPh}_3)_2]$ to Iron Dihydride Complex

The starting compound (iii) was prepared by following a literature procedure (scheme 4.14).¹¹¹



Scheme 4.14: Synthesis of $[\text{Fe}(\text{CO})_3(\text{PPh}_3)_2]$

0.010 g (0.0000150 moles) of $[\text{Fe}(\text{CO})_3(\text{PPh}_3)_2]$ was taken in a high pressure NMR tube and toluene- d_8 (0.3 ml) was added to it. The above NMR tube was pressurized with hydrogen gas (10 bars) and a NMR was recorded. A proton NMR of this reaction mixture revealed a hydride resonance at -8.90 and -9.02 ppm (**figure 4.44**), suggesting existence of a di-hydride species. Although the exact identity of the di-hydride product could not be fully established, it is most likely that an iron di-hydride species of type (A) with different coordination environment is generated.^{Error! Bookmark not defined.} The corresponding ^{31}P NMR displayed the coordinated phosphine resonance at 83.1 ppm (with a minor resonance at -5.23 ppm which can be ascribed to free triphenyl phosphine) (**figure 4.45**).

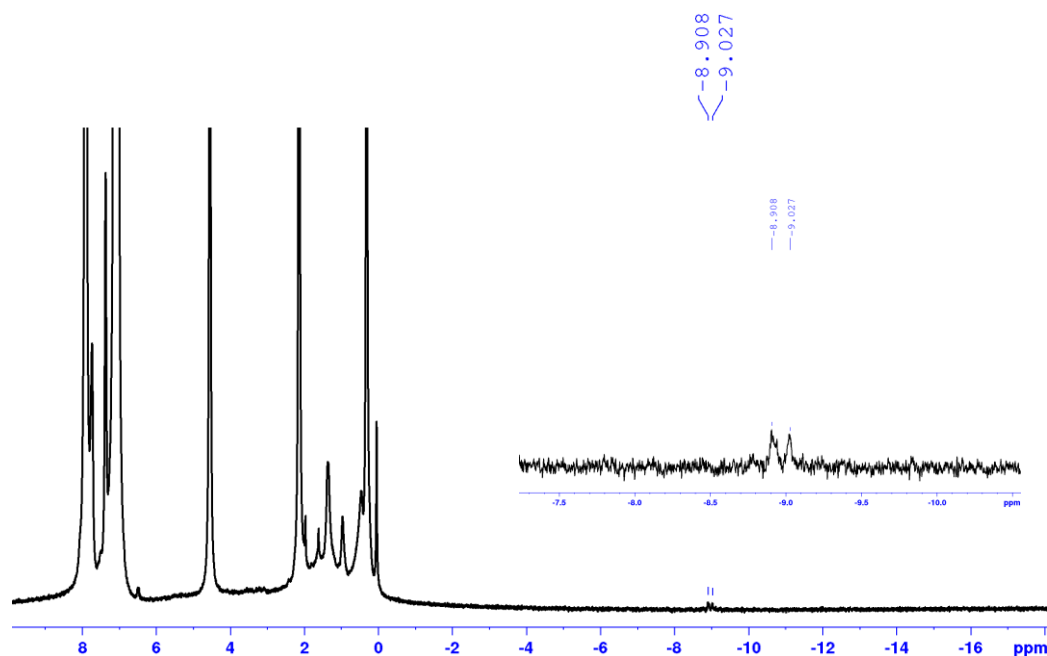


Figure 4.44: High pressure ^1H NMR spectrum of $[\text{Fe}(\text{CO})_3(\text{PPh}_3)_2]$ after treatment of H_2

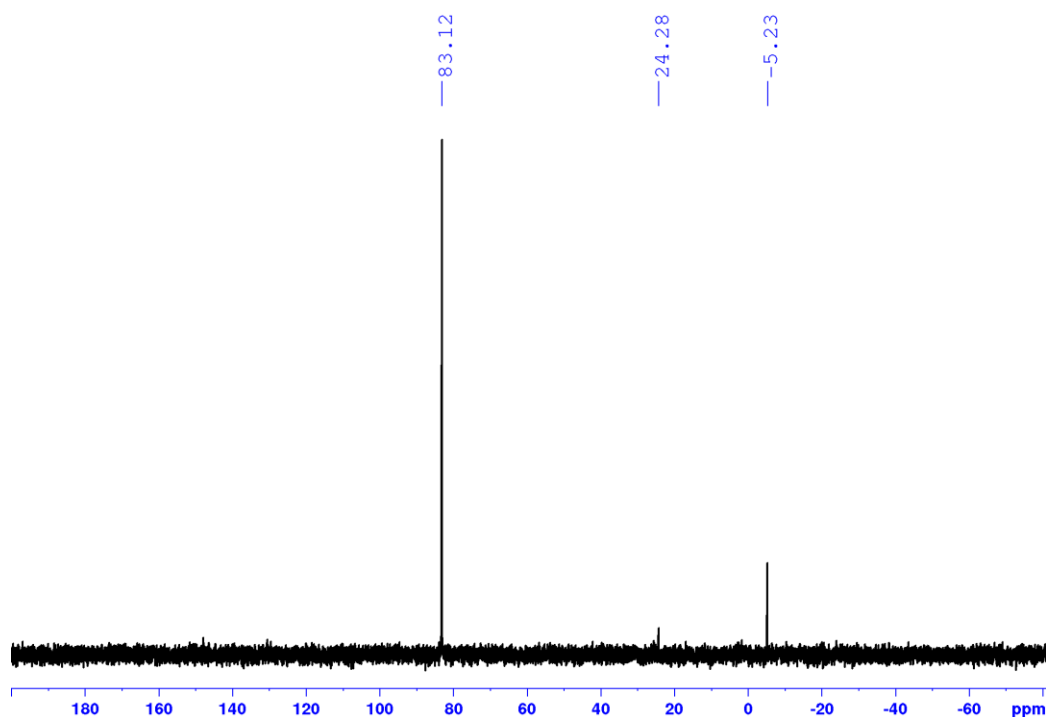


Figure 4.45: High pressure ^{31}P NMR spectrum of $[\text{Fe}(\text{CO})_3(\text{PPh}_3)_2]$ after treatment of H_2

4.4.3.6.4: Trapping Iron-Acyl Intermediate D

0.010 g (0.0000138 moles) of iron precursor 1, 0.0073 g (0.000027 moles) of triphenylphosphine, and 1-hexene (0.15 ml, 0.00124 moles) were dissolved in a Schlenk tube containing 3 ml of methanol. This mixture was cooled to $0\text{ }^\circ\text{C}$ and 0.1 ml acetic acid was added to it. The reaction mixture was stirred at this temperature for 1 hour before quenching it by adding 0.035 g of iodine. The resultant solution was passed through a small plug of silica and subjected to proton NMR, ESI-MS and GC-MS analysis. The appearance of methoxy peak at 3.49 ppm and the remaining resonances confirm formation of methyl heptanoate (**figure 4.46**). A positive mode ESI-MS revealed a peak at $m/z = 167$ Da (**figure 4.47**), that can be assigned to sodium salt of methyl heptanoate ($\text{C}_8\text{H}_{16}\text{NaO}_2$). Methyl heptanoate is obtained after the cleavage of iron-acyl species D and thus represent the direct observation of species D. ESI-MS observation were further supported by GC-MS analysis that displayed fragments of methyl heptanoate (**figure 4.48**). These fragments are consistent with literature reports (**chart C1**).¹²¹ The existence of methyl heptanoate directly confirms the intermediacy of species D (**figure 4.3**).

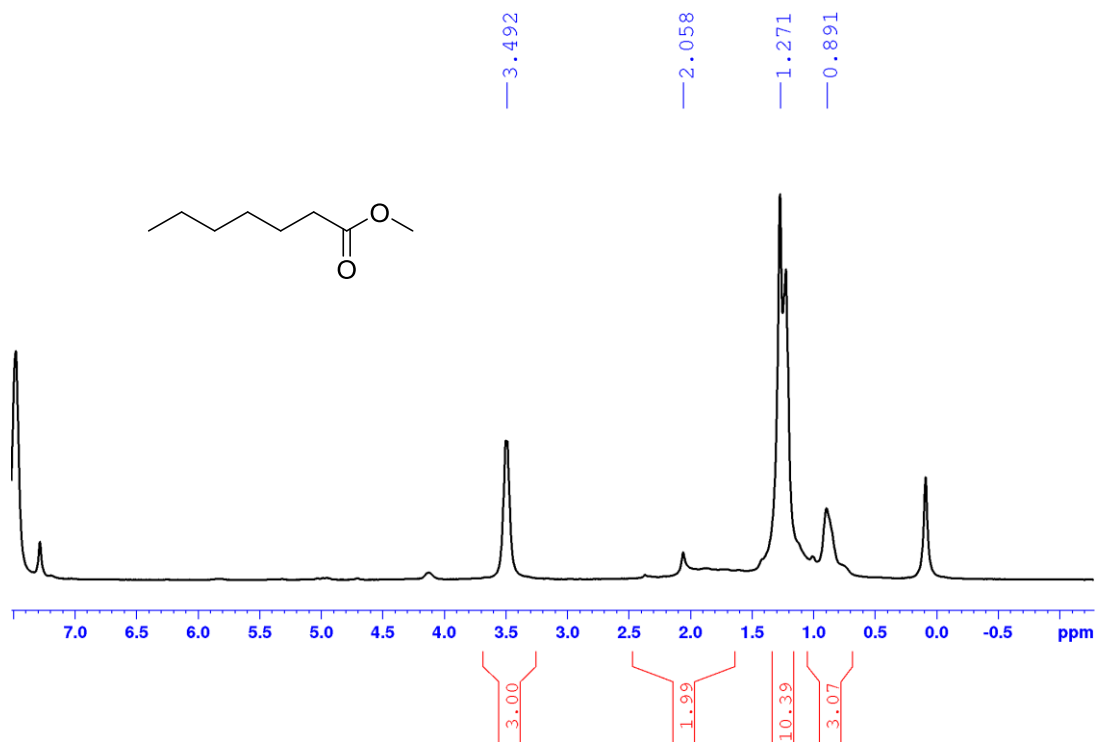


Figure 4.46: ^1H NMR spectrum of methyl heptanoate

SP-548 #244 RT: 1.09 AV: 1 NL: 1.19E6
T: FTMS + p ESI Full ms [100.0000-1500.0000]

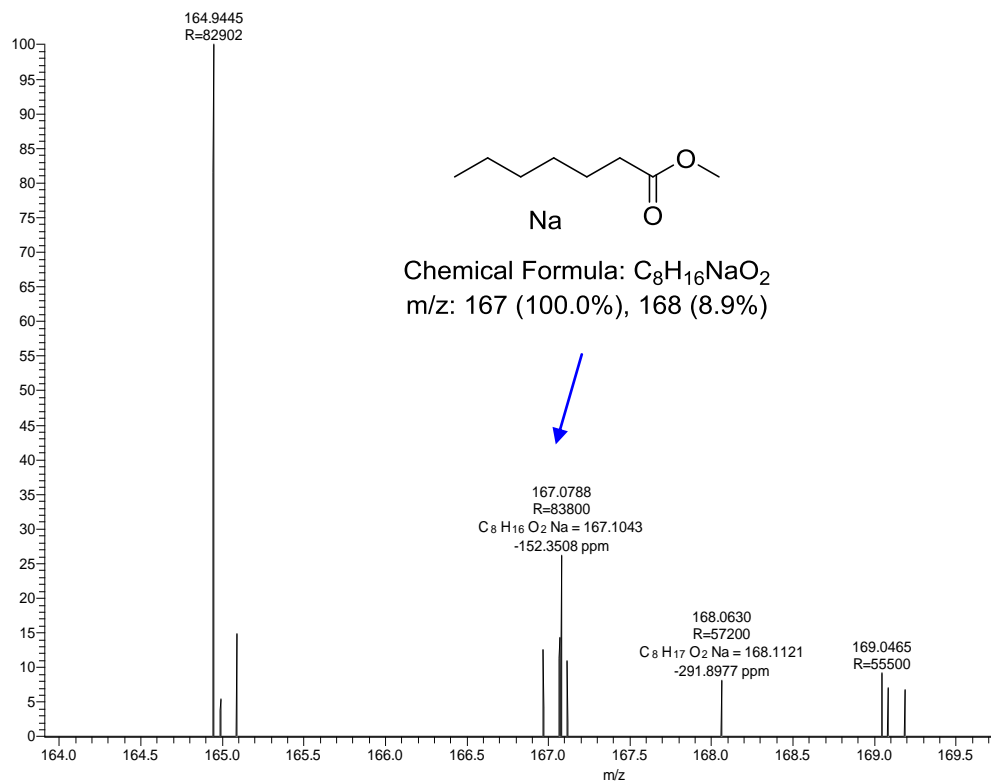


Figure 4.47: ESI-MS (+ve mode) spectrum of the methyl heptanoate, $\text{C}_8\text{H}_{16}\text{O}_2\text{Na} = 167$ $[\text{M}+\text{Na}]^+$

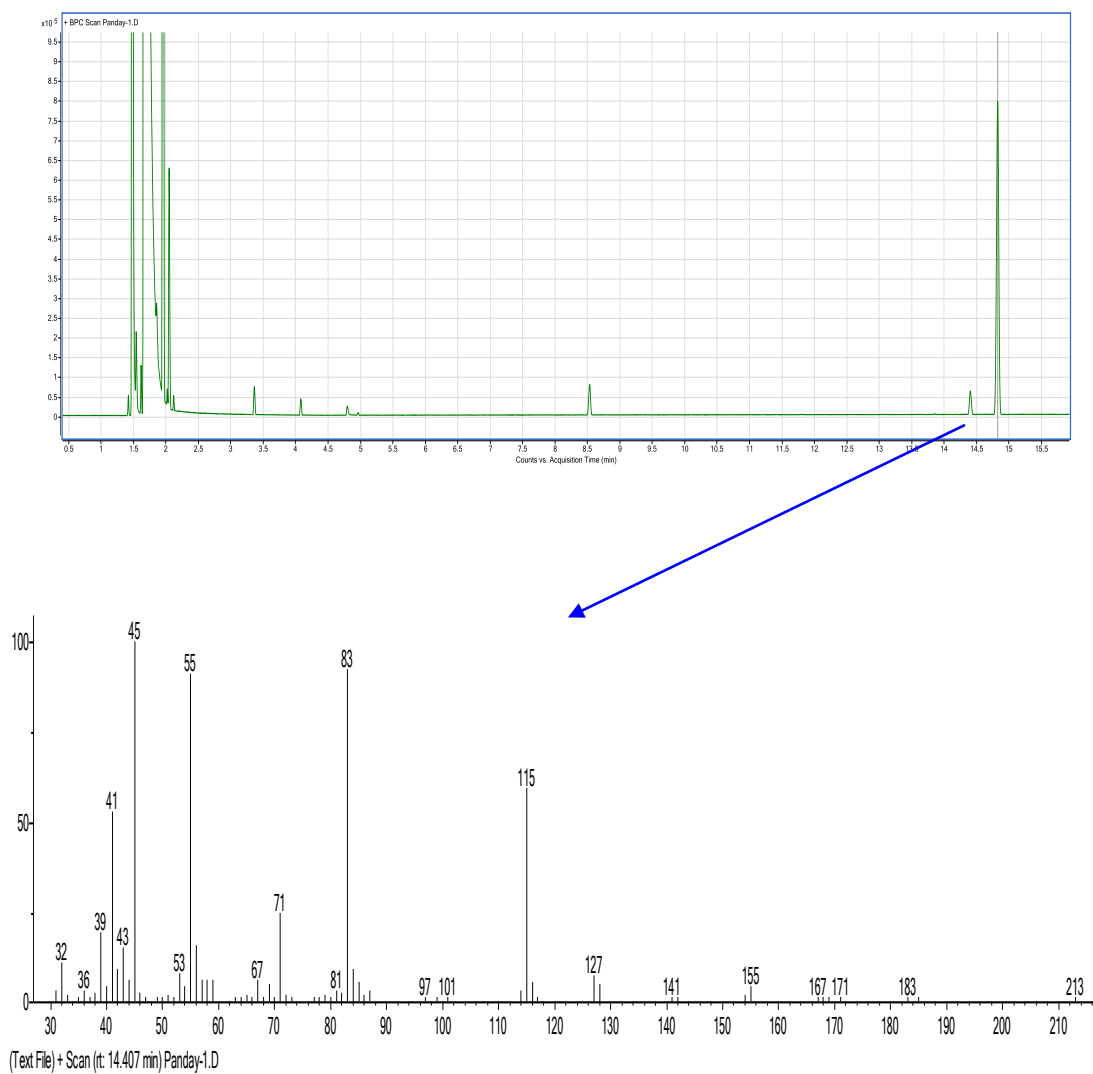
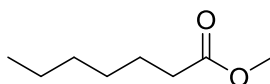


Figure 4.48: GC-MS plot of the methyl heptanoate

Chemical Formula: $C_8H_{16}O_2$

Exact Mass: 144.1150

Molecular Weight: 144.2140

Sr. No	Mass	Fragment	Structure
01.	115	$C_6H_{11}O_2$	 Chemical Formula: $C_6H_{11}O_2^+$ Exact Mass: 115.0754 Molecular Weight: 115.1515
02.	101	$C_5H_9O_2$	 Chemical Formula: $C_5H_9O_2^+$ Exact Mass: 101.0597 Molecular Weight: 101.1245
03.	83	C_5H_7O	 Chemical Formula: $C_5H_7O^+$ Exact Mass: 83.0491 Molecular Weight: 83.1095

Chart C1: Fragments of methyl heptanoate that can be observed by GC-MS

4.4.3.6.5: Cyclic Voltammetry

A Bio-Logic electrochemical workstation was used to perform the electrochemical analysis. In a typical setup a three electrode cell was employed which comprises of a glassy carbon (0.196 cm² geometrical surface area) as working electrode, graphite rod as counter electrode and Pt-wire as reference electrode. The methanolic solution of LiClO₄ (0.1 M) served as the electrolyte purpose. For recording the cyclic voltamogram of the compounds, a 0 to 1 V potential range was applied with a scan rate of 50 mV/s. Further, in order to maintain the reactant flow over the glassy carbon electrode a 900 rpm was given to the working electrode.

The cyclic voltamogram (CVs) of the compound was recorded before and after addition of the acetic acid in the electrolyte medium (**figure 4.4**). Initial reduction potential for the compound was at 0.43 V (*vs* Pt) which after acetic acid addition shifted to 0.33 V (*vs* Pt). Similarly, a shift in the oxidation peak of the compound was noted from 0.55 to 0.40 V (*vs* Pt). The above shift in the peak potential clearly indicates the role of acetic acid in converting iron monohydride to dihydride species. Further to verify our results, control experiments were conducted under the

analogous conditions. Ferrocene, ferrocene carboxylic acid, $[\text{Fe}(\text{CO})_3(\text{PPh}_3)_2]$ and $[\text{Fe}(\text{CO})_5]$ were selected as control samples. As can be seen in the **figure 4.49** the ferrocene and ferrocene carboxylic acid where iron is in +2 oxidation state, show separate peak position for oxidation and reduction. The shift in the peak position is related to the carboxylic group attached to the cyclopentadienyl ring.

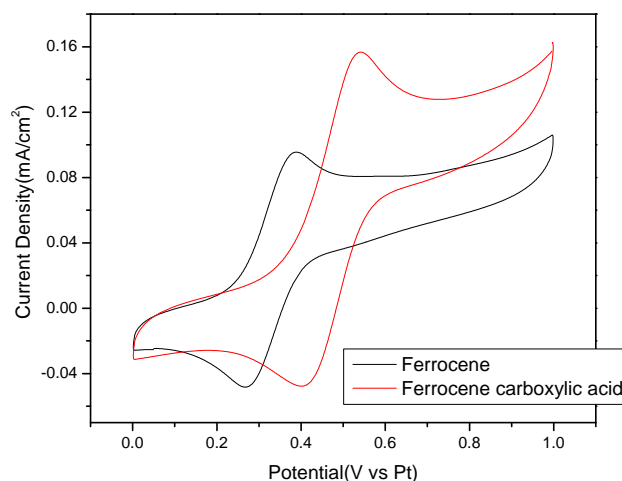


Figure 4.49: Cyclic Voltammogram of the ferrocene and ferrocene carboxylic acid recorded in 0.1 M LiClO_4 (solution in methanol) with a sweep of 50 mV/s and a rotation of 900 rpm

Further we recorded the CVs of the iron(0) compounds such as $[\text{Fe}(\text{CO})_3(\text{PPh}_3)_2]$ and $[\text{Fe}(\text{CO})_5]$ (**figure 4.50**). The CV of the $[\text{Fe}(\text{CO})_3(\text{PPh}_3)_2]$ show oxidation and reduction peak at higher potential against the iron(+2) ferrocene and ferrocene carboxylic acid, whereas no peak for $[\text{Fe}(\text{CO})_5]$ could be identified in the analogous potential range. The anomalous behaviour of the $[\text{Fe}(\text{CO})_5]$ could be because of the homogenous ligand surrounding to the metal.

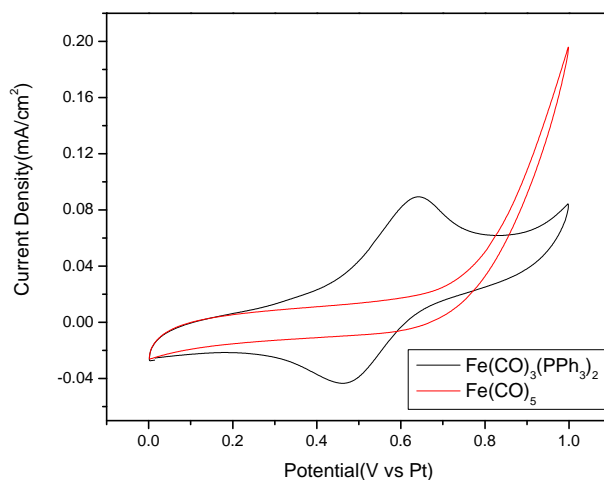


Figure 4.50: Cyclic voltammograms (CVs) of $[\text{Fe}(\text{CO})_3(\text{PPh}_3)_2]$ and $[\text{Fe}(\text{CO})_5]$ compound recorded in 0.1 M LiClO_4 (solution in methanol) with a sweep of 50mV/s and a rotation of 900 rpm

From the above control experiments it can be clearly identified that after acetic acid addition, the iron monohydride changes to the iron-dihydride. The reduction peak of the acetic acid treated compound was in close resemblance with ferrocene (0.26 V vs Pt), i.e. iron (+2); whereas the one without acetic acid matched to $[\text{Fe}(\text{CO})_3(\text{PPh}_3)_2]$ (0.46 V vs Pt) that is, iron(0) compound.

4.4.3.6.5: Control Experiments

A radical mechanism with a potential radical species $[\bullet\text{Fe}(\text{CO})_4^-]$ has been proposed in the past⁸¹ or a mechanism based on organic radical has been proposed very recently.¹¹⁶ In order to probe the possibility of radical mechanism in the iron catalyzed hydroformylation, we performed hydroformylation in presence of excess (150 times) amount of radical scavengers, namely, 2,2,6,6-Tetramethylpiperidinyloxy (TEMPO) and galvinoxyl.¹²² If a radical mechanism is followed, these scavengers will trap the radical and stop hydroformylation, without producing any aldehyde.

In a typical control experiment, a stainless steel autoclave (450 mL) equipped with pressure regulator and a safety valve was used. Individual vials were charged with metal precursor $\{[\text{HFe}(\text{CO})_4]^-[\text{PPN}]^+\}$ (5.5 mg, 0.0077 mmol), triphenyl phosphine (as in table 6), radical scavenger (150 equivalents, compared to precursor 1) and stirring bars in a glove box. The vials were transferred to a wide neck Schlenk container and methanol (1 ml), and substrate (100 equiv.) was added. The vials were immediately transferred to autoclave and the autoclave was purged three times with syngas ($\text{CO}:\text{H}_2 = 1:1$) before pressurizing it to the desired pressure. Suitable temperature and pressure was maintained during the reaction. After completion of the reaction, the autoclave was cooled to 0 °C and excess gas was vented off in a well-ventilated fume-hood. The conversion and regio-selectivity were determined by gas chromatography (GC).

As evident from **table 4.7**, even in presence of large excess (150 times) TEMPO, 48% conversion was observed, while 65% conversion was achieved in presence of 150 equivalents of galvinoxyl. Therefore, it is most unlikely that a radical mechanism is operative in the investigated iron catalyzed hydroformylation.

Table 4.7: Hydroformylation of 1-octene in presence of radical scavengers.^a

S.No.	Subs.	Radical Scavenger	Temp. (°C)	Syngas (Bar)	Time (h)	Conv. ^b (%) ^b	l:b ^b
01.	1-octene	TEMPO	100	20	24	48	71:29
02.	1-octene	Galvinoxyl	100	20	24	65	72:28

^aConditions: **1**: 0.0077 mmol, PPh_3 : 0.0192 mmol, L1/Fe: 2.5, Sub/Fe: 100, TEMPO/Fe: 150, Galvinoxyl/Fe: 150, Solvent: 1 ml Methanol; ^bDetermined by GC.

4.4.3.6.6: Computational Investigations

Full quantum chemical calculations have been performed with density functional theory (DFT) at the PBE/TZVP level of theory in order to understand the regioselectivity in the hydroformylation reaction by an octahedral iron catalyst A (see **table 4.8** and fig. 4.5). It is well known that an octahedral complex with a general formula $MA_2B_2C_2$ has six different stereoisomers,¹¹⁷ and from the calculations it is found that A is the most favourable stereoisomer for the complex $[\text{Fe}(\text{CO})_2(\text{H})_2(\text{PPh}_3)_2]$ (see **table 4.8**).

Table 4.8: The relative free energies of six possible stereoisomers for the intermediate $[\text{Fe}(\text{CO})_2(\text{H})_2(\text{PPh}_3)_2]$ (values are in kcal/mol)

Stereoisomers						
Relative free energy (ΔG)	0	3.1	10.5	5.4	4.4	2.4

The proposed reaction mechanism for the hydroformylation reaction is shown in the **figure 4.5**. From the π -complex B, there are two possibilities; either the hydride can transfer to the secondary carbon (path A) or to the primary carbon (path B). Path A eventually leads to a linear product 7a, while path B leads to a branched product 7b.

In order to understand the effect of kinetics on the regioselectivity, we have calculated energy barrier for one particular step (hydride transfer from π -complex B), where the regioselectivity originates (see **figure 4.6**). The calculations suggested that, the path B is more favourable (by 1.7 kcal/mol) than the path A for styrene. But an opposite trend is seen in the case of 1-hexene, where the path A is more favourable (by 1.3 kcal/mol) than the path B. These computational results exactly corroborate with experimental observations.

4.4.3.6.7: Who Catalyses the HF: Is It Iron or Rhodium?

4.4.3.6.7.1: Hydroformylation Using the Precursors

It has been observed that impurities present in the iron precursors sometimes catalyzed cross-coupling reactions. For example, copper impurities were found to catalyze the arylation reactions.¹¹⁸ In our attempt to examine the possible role of rhodium impurities in our iron precursors, we performed the hydroformylation of 1-octene using the commercially available precursor $[\text{Fe}_2(\text{CO})_9]$. The results are summarized in **table 4.3**. There was hardly any nonanal observed in presence and absence of triphenyl phosphine ligand (**figure 4.51** and **4.52**).

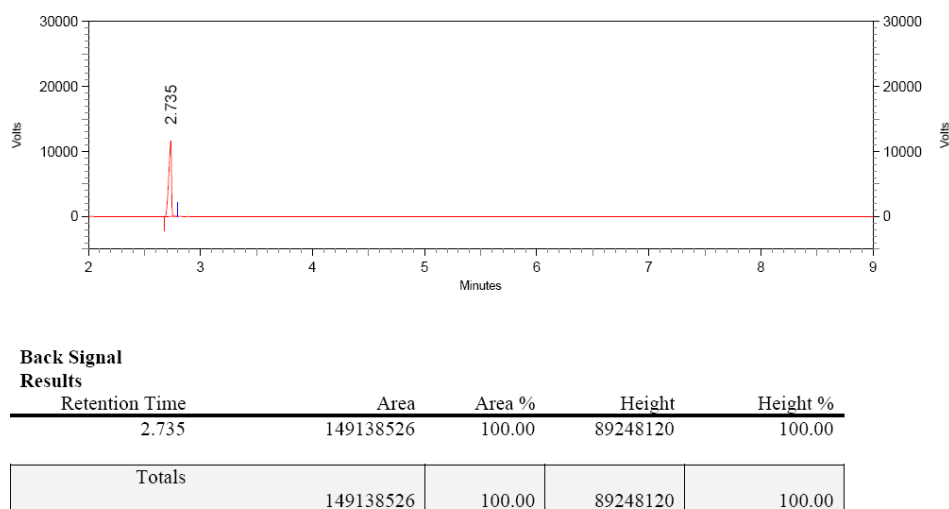


Figure 4.51: GC chromatogram of HF of 1-octene using $[\text{Fe}_2(\text{CO})_9]$ as metal precursor (in absence of ligand) (table 4.3, run 1)

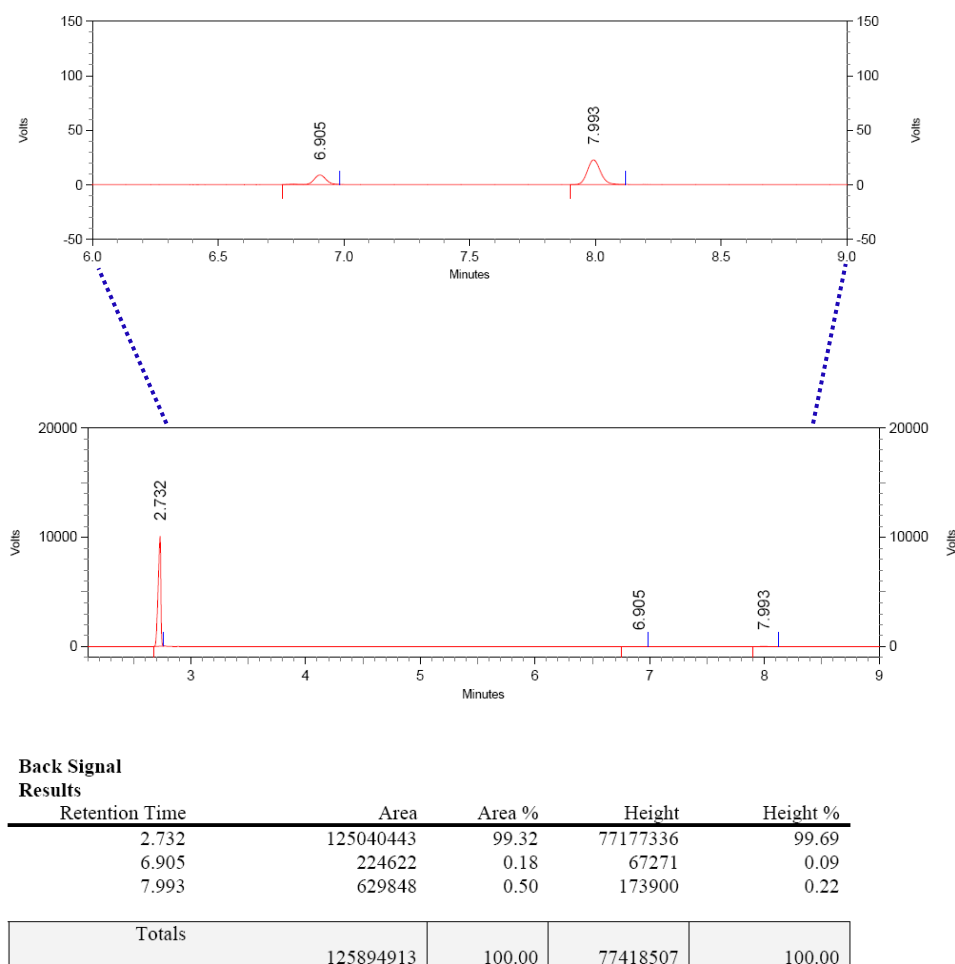


Figure 4.52: GC chromatogram of HF of 1-octene using $[\text{Fe}_2(\text{CO})_9]$ in presence of PPh_3 as a ligand (table 4.3, run 2) (expanded view in the top)

Similar trend was witnessed in the hydroformylation of 1-octene using $[\text{Fe}(\text{CO})_5]$ (**figure 4.53**). Thus, it is reasonable to conclude that the hydroformylation reaction is most likely catalyzed by iron and not by rhodium impurities present in the commercial precursor or the intermediate.

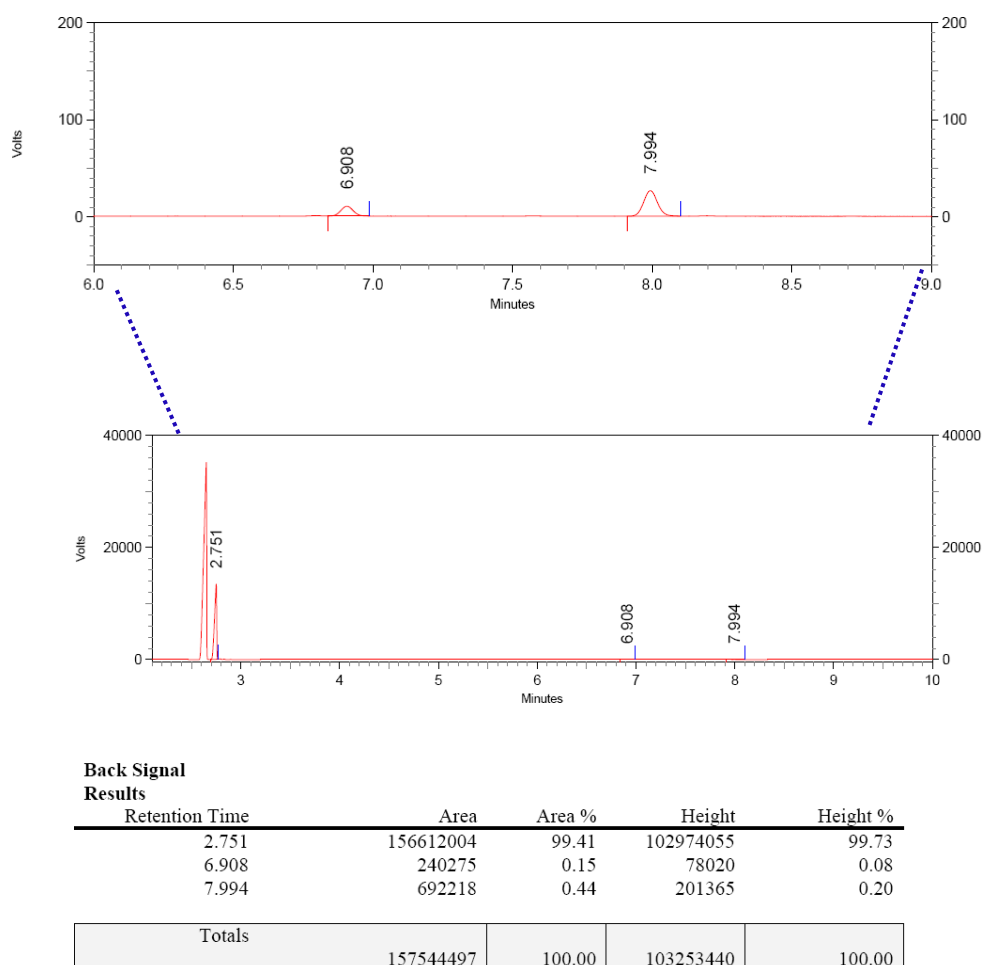


Figure 4.53: GC chromatogram of HF of 1-octene using $[\text{Fe}(\text{CO})_5]$ in presence of PPh_3 as a ligand (table 4.3, run 4) (expanded view in the top)

4.4.3.6.7.2: Bulk and Surface Analyses

A) XPS: To figure out the purity and composition of the precursor $[\text{Fe}_2(\text{CO})_9]$ and the catalyst 1, XPS was carried out and the results are shown in **Figure 4.54** and **4.55**. The measurements were carried out using Thermo Scientific Kalpha+ spectrometer using a monochromatic $\text{AlK}\alpha$ (1486.6 eV) x-ray source. The base pressure of the spectrometer was 2×10^{-9} mbar. The wide area and narrow region scans were acquired using 100 eV and 50 eV pass energy respectively. **Figure 4.54** show the wide area scan from the precursor and the major peaks are indexed. As it can be seen, the sample mainly consists of Fe, C, O and various core-levels and Auger peaks resulting from these elements are indexed. One of the contaminants which can contribute to the background activity is the presence of Rhodium. Rh3d in photoelectron spectrum comes at 307.6 eV for

metallic species and 308.8 eV for native oxide.¹²³ These regions which are marked in the wide area scan showed no obvious presence of Rh. To prove the complete absence of Rh, the narrow region spectrum of Rh3d and Rh3p (496 eV) were recorded and the corresponding plots are given in figure 4.56a and 4.56b. Both these spectra gives further indication that Rh is absent in the precursor material.

Further, the compound 1 was also analysed by XPS and the wide area scan is shown in figure 4.55, which shows the constituent elements present in the sample. The wide area scan is again conspicuous with the absence of Rh and the narrow scan of Rh3d and Rh3p (figure 4.57a and 4.57b) shows this very clearly.

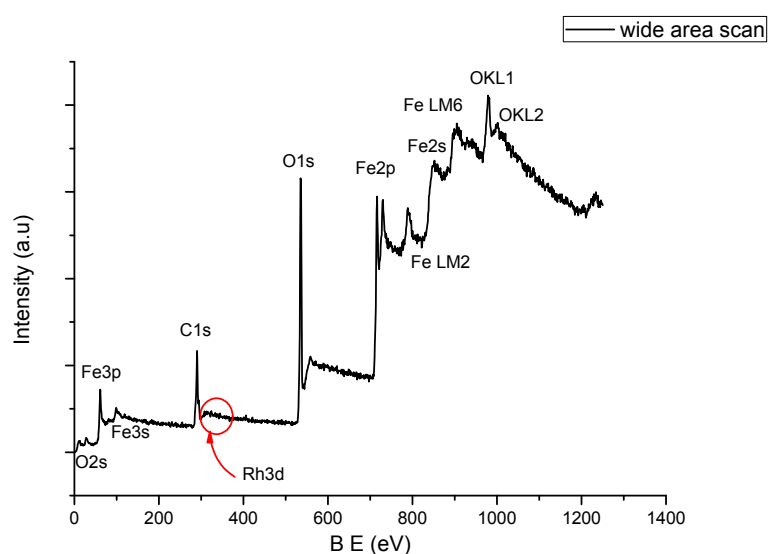


Figure 4.54: Wide area XPS spectrum of $[\text{Fe}_2(\text{CO})_9]$ sample showing the elemental distribution.

Red circle shows the area where Rh3d should be appearing

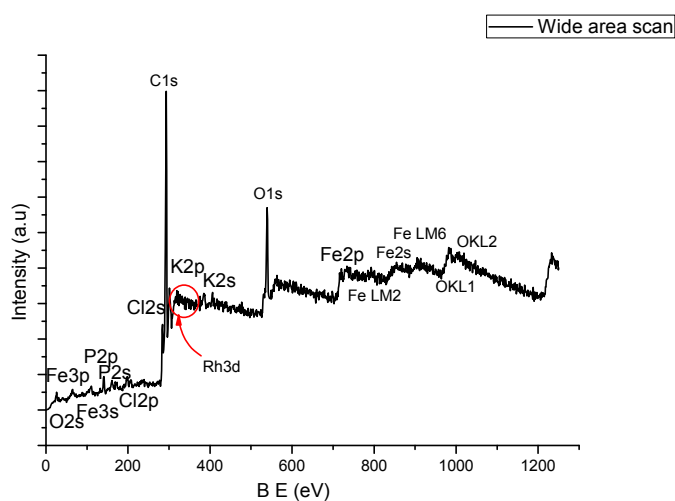


Figure 4.55: Wide area XPS spectrum of compound 1 showing the elemental distribution. Red

circle shows the area where Rh3d should be appearing

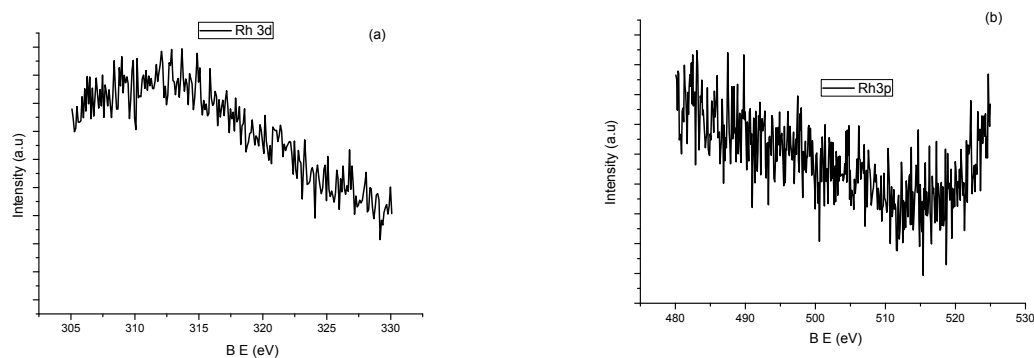


Figure 4.56: (a) Rh 3d and (b) Rh 3p XPS spectrum collected from $[\text{Fe}_2(\text{CO})_9]$ sample

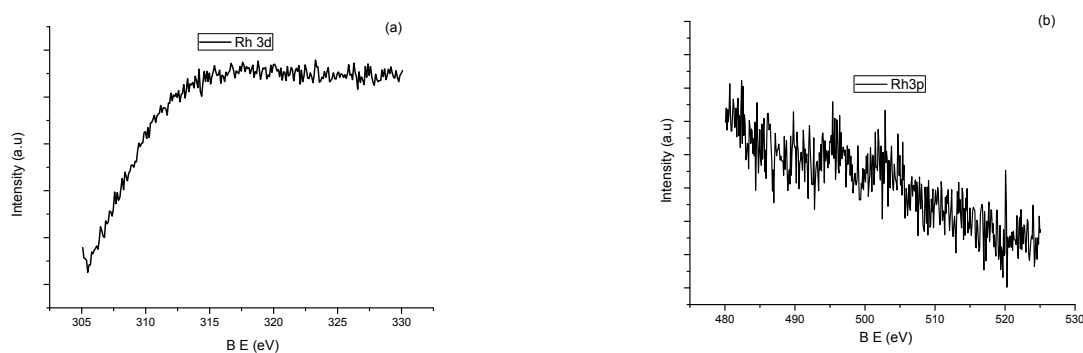


Figure 4.57: (a) Rh 3d and (b) Rh 3p XPS spectrum collected from compound 1

B) AAS: The bulk analyses of the iron precursor $[\text{Fe}_2(\text{CO})_9]$ and compound **1** was carried out using atomic absorption spectroscopy (AAS), ICP-AES and MP-AES. The results are presented in **table 4.9**. AAS: Varian atomic absorption spectrometer, model-220fs (NCL), ICP-AES: SPECTRO Analytical Instruments GmbH, Germany, model-ARCOS, Simultaneous ICP Spectrometer (IIT Bombay) MP-AES: Agilent model-4100 MP-AES. **Figure 4.58** depicts the representative analysis method.

Table 4.9. Bulk analysis of Iron precursors using AAS, ICP-AES and MP-AES.^a

Run	Method	Fe-precursor	Rh content (ppm)*
1	AAS	$[\text{Fe}_2(\text{CO})_9]$	Less than 1
2		1	Less than 1
3	ICP-AES	$[\text{Fe}_2(\text{CO})_9]$	Less than 0.01
4		1	Less than 0.01
5	MP-AES	$[\text{Fe}_2(\text{CO})_9]$	Less than 0.01
6		1	Less than 0.01

*Means less than 0.01 ppm or below detection limit

Results

Date Time	Label	Element Label (nm)	Conc	%RSD	Unadjusted Conc	Intensity	%RSD
2/1/2018 12:34:10	Blank	Rh (343.489 nm)	0.00 (ppm)	N/A	0.00 (ppm)	0.00	> 100.00
2/1/2018 12:34:59	Standard 1	Rh (343.489 nm)	0.01 (ppm)	N/A	0.01 (ppm)	80.44	11.47
2/1/2018 12:35:50	Standard 2	Rh (343.489 nm)	0.02 (ppm)	N/A	0.02 (ppm)	268.46	5.74
2/1/2018 12:36:41	Standard 3	Rh (343.489 nm)	0.05 (ppm)	N/A	0.05 (ppm)	570.94	1.69
2/1/2018 12:37:33	Standard 4	Rh (343.489 nm)	0.10 (ppm)	N/A	0.10 (ppm)	1180.54	1.36
2/1/2018 12:38:26	Standard 5	Rh (343.489 nm)	0.20 (ppm)	N/A	0.20 (ppm)	2214.71	0.11
2/1/2018 12:40:23	180201_Fe2CO9	Rh (343.489 nm)	-0.01 u (ppm)	15.35	-0.01 u (ppm)	-117.17	14.58
2/1/2018 12:41:41	180201_HFe(CO)4P+	Rh (343.489 nm)	-0.01 u (ppm)	13.24	-0.01 u (ppm)	-101.70	12.48

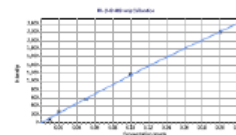
Calibration Curves

Rh (343.489 nm)

Intensity = (12001.93174443 * Concentration - 5.84597444) / (1 + 0.40556264 * Concentration)

Correlation coefficient: 0.99956

Standards	Intensity	Method Concentration	Calculated Concentration	% Error
Blank	0.00	0.00	0.00	N/A
Standard 1	80.44	0.01	0.01	27.91
Standard 2	268.46	0.02	0.02	15.32
Standard 3	570.94	0.05	0.05	1.99
Standard 4	1180.54	0.10	0.10	2.98
Standard 5	2214.71	0.20	0.20	0.01

**Figure 4.58:** MP-AES analyses data for [Fe₂(CO)₉] and compound 1 with calibration

4.5: Conclusion

In summary, the current work unveils a new iron catalyst for the hydroformylation of aliphatic and aromatic olefins under mild conditions. An iron hydride precursor 1, in combination with readily available phosphine or phosphite ligand and syngas generates the catalytically active species (which is believed to be **A**) and delivers hydroformylation of 1-hexene, 1-octene, 1-decene, 1-dodecene, 1-octadecene, trimethoxy (vinyl)silane, trimethyl(vinyl)silane, cardanol, 2,3-dihydrofuran, allyl malonic acid, styrene, 4-methyl styrene, 4-*i*Bu-styrene, 4-*t*Bu-styrene, 4-methoxy styrene, 4-acetoxy styrene, 4-bromo styrene, 4-chloro styrene, 4-vinylbenzotrile, 4-vinylbenzoic acid, and allyl benzene. The reaction operates under relatively mild conditions of 100 °C and 10-30 bars syngas pressure within 24-48 hours. Initial optimization studies with 1-octene indicated an optimal ligand to metal ratio of 2.5, methanol as the most suitable solvent, and a temperature of 100 °C. Short chain 1-hexene could be hydroformylated at 10 bars syngas pressure and 80 °C. While long-chain olefins S3-S5 (C10-C18) required slightly higher syngas pressure of 30 bars to achieve excellent conversion to corresponding aldehydes. The scope of iron catalyzed hydroformylation was extended to functional olefins, cyclic olefins, vinyl aromatics and the hydroformylation S1-S21 was examined. Compared to the aliphatic olefins, vinyl aromatics required longer reaction times. The catalyst tolerated electron donating as well as electron withdrawing functional groups and displayed good to excellent yields. Notable branched selectivity was observed for styrenic substrates (S11-S20), along with significant yields. The addition of 1 mol% of acetic acid was found to promote the hydroformylation reaction and the reaction time for vinyl aromatics could be reduced to 24 hours. Combined experimental and computational investigations indicate that the di-hydride species **A** is the actual active catalytic species. The identity of species **A** was established by multiple NMR experiments, which indicated coordination of ligand L1 and formation of the iron-dihydride complex. Cyclic voltammetry results revealed a Fe(0) to Fe(II) interconversion, explaining the accelerating effect of acetic acid. Control experiments with externally added radical scavengers ruled out the possibility of a radical or an Fe(I) to Fe(III) mechanism. The experimental findings were further corroborated by DFT calculations. Among the six possible stereoisomers of iron-dihydride complex, species **A** was found to be the most favorable. Transition state calculations for 1-hexene insertion revealed that 1,2-insertion was favored by 1.3 kcal/mol, whereas styrene preferred 2,1-insertion by 1.7 kcal/mol. Thus, experimental and computational investigations establish that the iron catalyzed hydroformylation follows a Fe(II) catalytic cycle, as depicted in **figure 4.3**. The role of rhodium impurities in catalyzing the hydroformylation of alkenes was investigated. These studies established that the reported hydroformylation is catalyzed by iron and it is highly unlikely that the rhodium impurities are responsible for the observed hydroformylation.

4.6: References

78. Whiteker, G. T.; Cobley, C. J. *Top. Organomet. Chem.* **2012**, *42*, 35-46.
79. Note that syngas was not used in this reaction, only CO was used, and H₂ was produced in situ. For details, see: Reppe, V. W.; Vetter, H. *Justus Liebigs Ann. Chem.* **1953**, *582*, 133-161.
80. (a) Kang, H. C.; Mauldin, C. H.; Cole, T.; Slegeir, W.; Cann, K.; Pettit, R. *J. Am. Chem. Soc.* **1977**, *99*, 8323 – 8325. (b) Sternberg, H.W.; Markby, R.; Wender, I. *J. Am. Chem. Soc.* **1957**, *79*, 6116 – 6121.
81. Palagyi, J.; Marko, L. *J. Organomet. Chem.* **1982**, *236*, 343-347.
82. (a) He, Z.; Lugan, N.; Neibecker, D.; Mathieu, R.; Bonnet, J.- J. *J. Organomet. Chem.* **1992**, *426*, 247-259. (b) Along the same lines, a Rh-Fe bimetallic complex was claimed to be responsible for the hydroformylation of 1-hexene, see: Trzeciak, A. M.; Mieczynska, E.; Ziolkowski, J. J. *Topics Catal.* **2000**, *11/12*, 461-468. (c) Attali, S.; Mathieu, R. *J. Organomet. Chem.* **1985**, *291*, 205-211. (d) Richmond, M.G. *J. Mol. Catal.* **1989**, *54*, 599-204.
83. Breschi, C.; Piparo, L.; Pertici, P.; Maria Caporusso, A.; Vitulli, G. *J. Organomet. Chem.* **2000**, *607*, 57-63.
84. (a) Bianchini, C.; Lee, H. M.; Meli, A.; Vizza, F. *Organometallics* **2000**, *19*, 849-853. (b) van der Slot, S. C.; Kamer, P. C. J.; van Leeuwen, P. W. N. M.; Iggo, J. A.; Heaton, B. T. *Organometallics* **2001**, *20*, 430-441. (c) Hettersheid, D. G. H.; Chikkali, S. H.; de Bruin, B.; Reek, J. N. H. *ChemCatChem* **2013**, *5*, 2785-2793.
85. (a) Smith, M. B.; Bau, R. *J. Am. Chem. Soc.* **1973**, *7*, 2388-2389. (b) Brunet, J. J.; Chauvin, R.; Diallo, O.; Kindela, F.; Leglaye, P.; Neibecker, D. *Coord. Chem. Rev.* **1998**, *178-180*, 331-351.
86. Fuerstner, A. *ACS Cent. Sci.* **2016**, *2*, 778-789.
87. For recent reports on monodentate phosphines in hydroformylation, see: (a) Mormul, J.; Mulzer, M.; Rosendhal, T.; Romiger, F.; Limbach, M.; Hofmann, P. *Organometallics* **2015**, *34*, 4102-4108. (b) Alsalahi, W.; Grzybek, R.; Trezeciak, A. M. *Catal. Sci. Technol.* **2017**, *7*, 3097 - 3103.
88. (a) For review, see reference 1e. (b) Saidi, O.; Ruan, J.; Vinci, D.; Wu, X.; Xiao, J. *Tetrahedron Lett.* **2008**, *49*, 3516-3519.
89. Deshmukh, S. S.; Gaikwad, S. R.; Pandey, S.; Mali, P.; Chikkali, S. H. *J. Chem. Sci.* **2017**, *129*, 1143-1152.
90. van Leeuwen, P. W. N. M.; Kamer, P. C. J.; Reek, J. N. H.; Dierkes, P. *Chem. Rev.* **2000**, *100*, 2741-2769.
91. Chikkali, S. H.; Bellini, R.; Berthon-Gelloz, G.; van der Vlugt, J. I.; de Bruin, B.; Reek, J. N. H. *Chem. Commun.* **2010**, *46*, 1244-1246.

92. (a) How, R. C.; Hembre, R.; Ponasik, J. A.; Tolleson, G. S.; Clarke, M. L. *Catal. Sci. Technol.* **2016**, *6*, 118-124. (b) For a general review on this class of ligands in catalysis, see: Chen, X.-S.; Hou, C.-J.; Hu, X.-P. *Synth. Commun.* **2016**, *46*, 917-941.
93. (a) Noonan, G. M.; Fuentes, J. A.; Cobley, C. J.; Clarke, M. L. *Angew. Chem. Int. Ed.* **2012**, *51*, 2477-2480. (b) Robert, T.; Abiri, Z.; Wassenaar, J.; Sandee, A. J.; Romanski, S.; Neudorfl, J.-M.; Schmalz, H.-G.; Reek, J. N. H. *Organometallics* **2010**, *29*, 478-483. (c) Arribas, I.; Vargas, S.; Rubio, M.; Suarez, A.; Domene, C.; Alvarez, E.; Pizzano, A. *Organometallics* **2010**, *29*, 5791-5804. (d) Rubio, M.; Suarez, A.; Alvarez, E.; Bianchini, C.; Oberhauser, W.; Peruzzini, M.; Pizzano, A. *Organometallics* **2007**, *26*, 6428-6436. (e) Slagt, V. F.; Roder, M.; Kamer, P. C. J.; van Leeuwen, P. W. N. M.; Reek, J. N. H. *J. Am. Chem. Soc.* **2004**, *126*, 4056-4057. (f) Arena, C. G.; Faraone, F.; Graiff, C.; Tiripicchio, A. *Eur. J. Inorg. Chem.* **2002**, 711-716. (g) Beghetto, V.; Scrivanti, A.; Matteoli, U. *Catal. Commun.* **2001**, *2*, 139-143. (h) Deerenberg, S.; Kamer, P. C. J.; van Leeuwen, P. W. N. M. *Organometallics* **2000**, *19*, 2065-2072. (i) Nozaki, K.; Sakai, N.; Nanno, T.; Higashijima, T.; Mano, S.; Horiuchi, T.; Takaya, H. *J. Am. Chem. Soc.* **1997**, *119*, 4413-4423.
94. Many of the commercial plants for hydroformylation use these simple ligands.
95. For a review on the role of phosphites in hydroformylation, see: Dieguez, M.; Pamies, O.; Claver, C. *Tetrahedron: Asymmetry*, **2004**, *15*, 2113-2122.
96. (a) Foca, C. M.; Barros, H. J. V.; dos Santos, E. N.; Gusevskaya, E. V.; Bayon, J. C. *New J. Chem.* **2003**, *27*, 533-539. (b) Janecko, H.; Trzeciak, A. M.; Ziolkowski, J. J. *J. Mol. Catal.* **1984**, *26*, 355-361. (c) Pittman-Jr., C. U.; Honnick, W. D. *J. Org. Chem.* **1980**, *45*, 2132-2139.
97. For hydroformylation of 1-decene, see: (a) Hamerla, T.; Rost, A.; Kasaka, Y.; Schomacker, R. *ChemCatChem* **2013**, *5*, 1854-1862. (b) Markert, J.; Brunsch, Y.; Munkelt, T.; Kiedorf, G.; Behr, A.; Hamel, C.; Seidel-Morgenstern, A. *Appl. Catal. A: Gen.* **2013**, *462-463*, 287-295.
98. Hydroformylation of higher alkenes is a challenging task, see: (a) Kunene, T. E.; Webb, P. B.; Cole-Hamilton, D. J. *Green Chem.* **2011**, *13*, 1476-1481. (b) Potier, J.; Menuel, S.; Monflier, E.; Hapoit, F. *ACS Catal.* **2014**, *4*, 2342-2346.
99. For recent reports on hydroformylation of 1-decene, see: (a) Divekar, S. S.; Deshpande, R. M.; Chaudhari, R. V. *Catal. Lett.* **1993**, *21*, 191-200. (b) Takahashi, K.; Yamashita, M.; Ichihara, T.; Nakano, K.; Nozaki, K. *Angew. Chem. Int. Ed.* **2010**, *49*, 4488-4490. (c) Takahashi, K.; Yamashita, M.; Tanaka, Y.; Nozaki, K. *Angew. Chem. Int. Ed.* **2012**, *51*, 4383-4387.
100. For hydroformylation of 1-dodecene, see: (a) Yuan, M.; Chen, H.; Li, R.; Li, Y.; Li, X. *Catal. Lett.* **2004**, *94*, 15-16. (b) Bhang, B. M.; Divekar, S. S.; Deshpande, R. M.; Chaudhari, R. V. *J. Mol. Catal. A: Chem.* **1997**, *115*, 247-257.

101. Hydroformylation of 1-octadecene is rarely reported, see: Koch, T. J.; Desset, S. L.; Leitner, W. *Green Chem.* **2010**, *12*, 1719-1721.
102. For rhodium catalyzed hydroformylation of styrene, see: (a) Nelsen, E. R.; Landis, C. R. *J. Am. Chem. Soc.* **2013**, *135*, 9636-9639. (b) Brezny, A. C.; Landis, C. R. *J. Am. Chem. Soc.* **2013**, *139*, 2778-2785. (c) Tonks, I. A.; Froese, R. D.; Landis, C. R. *ACS Catal.* **2013**, *3*, 2905-2909. (d) Boymans, E.; Janssen, M.; Mueller, C.; Lutz, M.; Vogt, D. *Dalton Trans.* **2013**, *42*, 137-142. (e) Jing, Q.; Kazlauskas, R. *J. ChemCatChem* **2010**, *2*, 953-957.
103. For linear selective hydroformylation of styrene, see: Kranenberg, M.; van der Burgt, Y. E. M.; Kamer, P. C. J.; van Leeuwen, P. W. N. M.; Goubitz, K.; Fraanje, J. *Organometallics* **1995**, *14*, 3081-3089 and the reference therein.
104. For recent representative example of hydroformylation of 4-methyl styrene, see: Doro, F.; Reek, J. N. H.; van Leeuwen, P. W. N. M. *Organometallics* **2010**, *29*, 4440-4447.
105. For hydroformylation of 4-methoxy styrene, see: Kadyrov, R.; Heller, D.; Selke, R. *Tetrahedron: Asymmetry* **1998**, *9*, 329-340.
106. Kollar, L.; Farkas, E.; Batiu, J. *J. Mol. Catal. A: Chem.* **1997**, *115*, 283-288.
107. Siegel, H.; Himmele, W. *Angew. Chem. Int. Ed.* **1980**, *19*, 178-183.
108. Additive effect was evaluated with an additive to [Fe] ratio of 1, 2, 5. 1 equivalent acetic acid was found to promote the hydroformylation, while excess acetic acid seems to have deleterious effect.
109. See reference 79, 81 and Sanchez-Delgado, R. A.; Bradley, J. S.; Wilkinson, G. *J. Chem. Sci. Dalton Trans.* **1976**, 399-404.
110. Bellagamba, V.; Ercoli, R.; Gamba, A. *J. Organomet. Chem.* **1982**, *235*, 201-214.
111. Boddien, A.; Loges, B.; Gartner, F.; Torborg, C.; Fumino, K.; Junge, H.; Ludwig, R.; Beller, M. *J. Am. Chem. Soc.* **2010**, *132*, 8924-8934.
112. The observed chemical shifts are consistent with those reported for [H₂Fe(CO)₂(dppe)], [H₂Fe(CO)₂(PPh₃)₂], [H₂Fe(CO)₂{P(OR)₃}₂], see: (a) Schubert, U.; Knorr, M. *Inorg. Chem.* **1989**, *28*, 1765-1766. (b) Cenini, S.; Porta, F.; Pizzotti, M. *Inorg. Chima. Acta.* **1976**, *20*, 119-126. (c) Porta, F.; Cenini, S.; Giordano, S.; Pizzotti, M. *J. Organomet. Chem.* **1978**, *150*, 261-271. (d) Brunet, J. J.; Kindela, F. B.; Labroue, D.; Neibecker, D. *Inorg. Chem.* **1990**, *29*, 4152-4153.
113. In this step, heating to 50 °C is involved, so as to obtain reasonable phosphine coordination. It is most likely that due to heating, H₂ gas is released leaving no hydride on the metal.
114. It was observed that addition of acetic acid accelerates the hydroformylation reaction; therefore acetic acid was chosen to investigate the change in oxidation state of iron precursor (1).
115. Heck, R.; Breslow, D. *J. Am. Chem. Soc.* **1961**, *83*, 4023-4027.

116. An organo-catalytic hydroformylation with a radical intermediate has been recently reported, see: Huang, H.; Yu, C.; Zhang, Y.; Zhang, Y.; Mariano, P. S.; Wang, W. *J. Am. Chem. Soc.* **2017**, *139*, 9799-9802.
117. M. North, in *Principles and applications of stereochemistry*, Stanley Thornes (publishers) Ltd, Cheltenham, UK, 1998.
118. (a) Buchwald, S. L.; Bolm, C. *Angew. Chem. Int. Ed.* **2009**, *48*, 5586-5587. (b) Plenio, H. *Angew. Chem. Int. Ed.* **2008**, *47*, 6954-6956.
119. Movahhed, S.; Westphal, J.; Dindaroglu, M.; Falk, A.; Schmalz, H.-G. *Chem. Eur. J.* **2016**, *22*, 7381-7384.
120. Domingos, A. J. P.; Howell, J. A. S.; Johnson, B. F. G.; Lewis, J.; Grice, N.; Pettit, R. in *Inorganic Syntheses: Reagents for Transition Metal Complex and Organometallic Syntheses* (Eds. Angelici, R. J.) John Wiley and Sons Inc. New York, USA, Vol. 28, 2007.
121. Mass spectrum of methyl heptanoate is available from a common organic compound database, SDBS, see: http://sdb.sdb.aist.go.jp/sdb/cgi-bin/direct_frame_top.cgi
122. TEMPO and Galvinoxyl are the two well know radical scavengers, see: Zhao, M.; Chen, D.; Shi, Y.; Yang, W.; Fu, Z. *Macromol. Chem. Phys.* **2013**, *214*, 1688-1698.
123. Abe Y.; Kato, K.; Kawamura, M.; Sasaki, K. *Surf. Sci. Spectra* **2001**, *8(2)*, 117-125.

Chapter 5

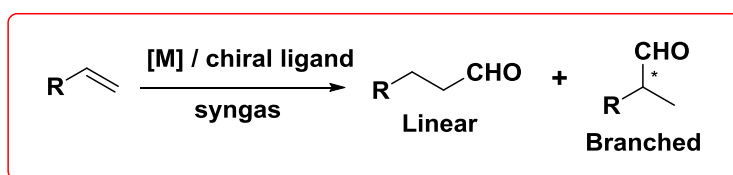
Iron Catalyzed Asymmetric Hydroformylation of Olefins

5.1: Abstract

Asymmetric hydroformylation is one of the powerful synthetic tool to synthesize a large variety of enantiomerically rich compounds and pharmaceutical intermediates in single step. Significant advancements have been made in the field of Rh catalyzed asymmetric hydroformylation using rationally designed catalytic systems. Apart from Rh, other transition metals such as Ru, Pd, Pt have also been used to catalyze this industrially relevant transformation. However it is highly desirable to substitute these precious and rare transition metals with earth abundant first row transition metals such as Fe. Reported here is an unprecedented methodology for Fe catalyzed asymmetric hydroformylation of olefins under mild conditions. This protocol is applicable for an array of olefins such as styrene derivatives as well as functional heterocyclic olefins. The reaction operates at low syngas pressure 10-30 bar and below 100 °C. The iron precursor $[\text{HFe}(\text{CO})_4][\text{Ph}_3\text{PNPh}_3]$ (1) in presence of chiral bidentate ligands such as (*R,R*)-DIOP and (*S*)-tBu-Josiphos catalyze the asymmetric hydroformylation of heterocyclic olefin such as 2,3-dihydrofuran with reasonable conversion and results in 99% enantiomeric excess (ee) under optimized reaction conditions.

5.2: Introduction

Transition metal catalyzed hydroformylation, also known as oxo process, allows formation of aldehydes starting with an olefin (either terminal or internal). However, when prochiral olefin is used as a substrate, it results in highly valuable chiral aldehydes in presence of chiral catalytic systems and the process is termed as asymmetric or enantioselective hydroformylation (A-HF)¹²⁴ (**scheme 5.1**). There is close relationship between absolute configuration of a chiral compound and its biological or pharmaceutical activity hence the demand for enantiomerically pure compound is rapidly increasing. Due to which there is always a need of synthetic processes that can yield chiral products in a simple and efficient manner.



Scheme 5.1: General representation of asymmetric hydroformylation

Asymmetric hydroformylation holds the potential of synthesizing chiral aldehydes, a versatile synthetic intermediates from prochiral olefins in a single step.¹²⁵ One of the successful example in this regard is synthesis of NSAID (non-steroidal anti-inflammatory drug) such as Ibuprofen,

Naproxen, Fenoprofen (**figure 5.1**) from asymmetric hydroformylation of vinyl arenes followed by oxidation of resultant aldehyde.¹²⁶

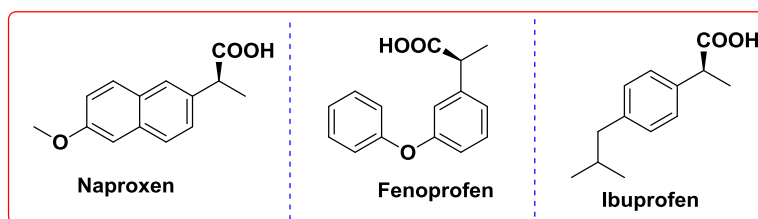


Figure 5.1: NSAIDs synthesized using asymmetric hydroformylation followed by oxidation

Apart from vinyl arenes, heterocyclic olefins such as dihydrofurans and pyrrolines are considered as attractive substrates for asymmetric hydroformylation as corresponding aldehydes are important building blocks in organic synthesis and medicinal chemistry.⁷⁶ The carbaldehydes of dihydrofuran and pyrrolines are known to be very important precursors for the syntheses of versatile pharmaceuticals, natural products, and amino-acids.^{8,127} One example is the 4-formyl derivative of cholest-4-ene, which is a valuable intermediate of potent drugs for the treatment of prostatic cancer and other androgen-dependent diseases.

The success of an asymmetric hydroformylation reaction rely heavily on designed or selected ligand system and till now several chiral ligands such as chiral diphosphines,⁸ diphosponites,^{1d} or diphosphites^{1e} were found to be promising candidates. Not only symmetrical bidentate ligands but also some hybrid ligand systems such as phosphine-phosphite,⁹³ phosphine-phosphinite¹²⁸ and phosphine-phosphoramidite ligands^{76,92} are known to catalyze this reaction in an efficient manner. In most of the cases, asymmetric hydroformylation is catalyzed by Rh complexes. However other transition metals such as Co, Pt, Pt-Sn have also been investigated for the same.

5.2.1: Co Catalyzed Asymmetric Hydroformylation

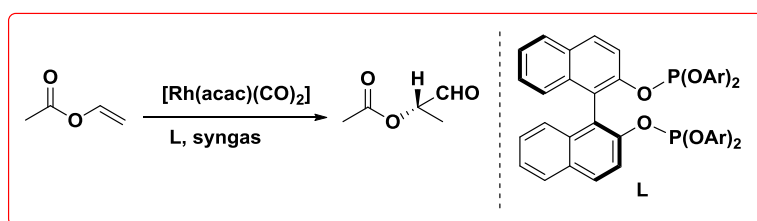
The first report of asymmetric hydroformylation dealt with Co based catalytic system modified by a chiral Schiff base and styrene as substrate.¹²⁹ However, the main reaction observed was hydrogenation to ethyl benzene (~52 %) and the best branched vs normal (b/l) ratio for the aldehydes was 59/41. Moreover, optical yields obtained were very low (<3% ee).

In general, Co based systems suffer from poor chemo and regioselectivity and a preference for commercially less important linear aldehyde. Co catalyzed hydroformylation leads to poor enantioselectivities possibly due to harsh reaction conditions employed in the hydroformylation. Harsh reaction conditions also demand for high investment costs thereby limiting its commercialization.^{1e,130}

5.2.2: Rh Catalyzed Asymmetric Hydroformylation

In the early 1970s Rh based systems attracted significant attention from scientific community. The first asymmetric hydroformylation using Rh and DIOP as ligand was reported in 1973 for aromatic olefins such as styrene. The best b/l ratio obtained was 69/31 and enantioselectivities upto 23% were achieved.¹³¹ After this several DIOP derivatives were investigated to improve enantioselectivities in the AHF of styrene, cis-2-butene, vinyl acetate and N-vinyl succinimide. However, the results obtained were still moderate. In 1990s two new type of ligands were discovered that led to high enantiomeric excess (ee) namely diphosphites and phosphine-phosphite ligands.

Unfortunately, the first asymmetric hydroformylation using diphosphites did not result in any asymmetric induction.¹³² However in 1992, vinyl acetate was successfully hydroformylated and enantioselectivity upto 50% was obtained (**scheme 5.1**) by Takaya et.al.¹³³ upon employing an axially chiral bisphosphite ligand.



Scheme 5.1: Asymmetric hydroformylation of vinyl acetate

A major breakthrough was observed in same year when Babin and Whiteker described in a Union Carbide patent the most significant early work on asymmetric hydroformylation, using bulky bisphosphite ligands (**figure 5.2**).¹³⁴ The Babin and Whiteker patent describes rhodium complexes of bisphosphite ligands derived from homochiral (2*R*,4*R*)-pentane-2,4-diol that catalyze the hydroformylation of styrene at moderate pressures with 98% selectivity for the branched product with 98% enantiomeric excess.

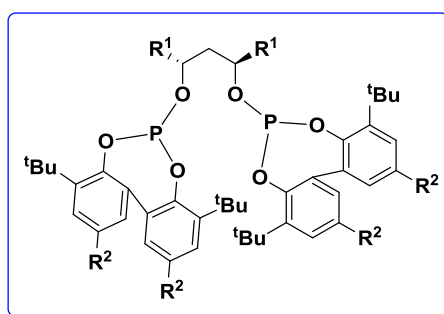


Figure 5.2: UCC's bulky homochiral bisphosphite ligand

Later on, Van Leeuwen and co-workers studied the influence of the bridge length, bulky substituents and cooperativity of chiral centres on the performance of the catalyst.¹³⁵ They concluded that three-carbon linker in the diol backbone with stereocenters at 1- and 3-positions is important for high selectivity due to restricted rotation. They also proposed that the highest enantioselectivities in the hydroformylation reaction will be obtained with ligands co-ordinating in an equatorial-equatorial fashion to the rhodium $[\text{RhH}(\text{L})(\text{CO})_2]$ with retention of C_2 symmetry in the catalysts. Coordination of substrate to a vacant equatorial position with the diphosphite ligand coordinating in the same plane may give rise to the most effective interaction between substrate and ligand. The low enantioselectivities obtained in some cases where ligand is bis-equatorially coordinated might be due to the fluxional behavior of these complexes.

A series of related bisphosphite systems based on commercially available optically active 1,2 and 1,4-diols, 1,2:5,5-diisopropylidene-D-mannitol, L- $\alpha,\alpha,\alpha,\alpha$ -tetramethyl-1,3-dioxalan-4,5 dimethanol and L-diethyl tartrate, were first used in the asymmetric hydroformylation of styrene by van Leeuwen¹³⁶ and Clever.¹³⁷ In this case, the relative stereochemistry at the ring carbon and carbon-5 of the sugar backbone were important. Likewise, sterically demanding *tert*-butyl substituents in the *ortho* position and electron-donating *p*-methoxy substituents in the *para* position of the aryl groups create the most selective catalysts for asymmetric hydroformylation of styrene to form > 98% branched product with 90% ee.

Most of the early bisphosphite ligands employed were C_2 symmetric. Thus, a major breakthrough was the use of mixed phosphite-phosphine ligands by Nozaki, Takaya, and co-workers.¹³⁸ The C_1 symmetric atropisomeric ligand (*S,R*)-BINAPHOS (**figure 5.3**) generated a rhodium complex that catalyzed the hydroformylation of vinylarenes with high branched-to-linear selectivities and high enantiomeric excess.

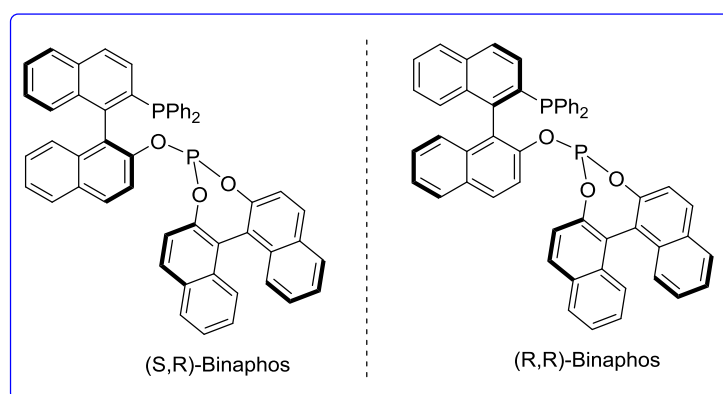
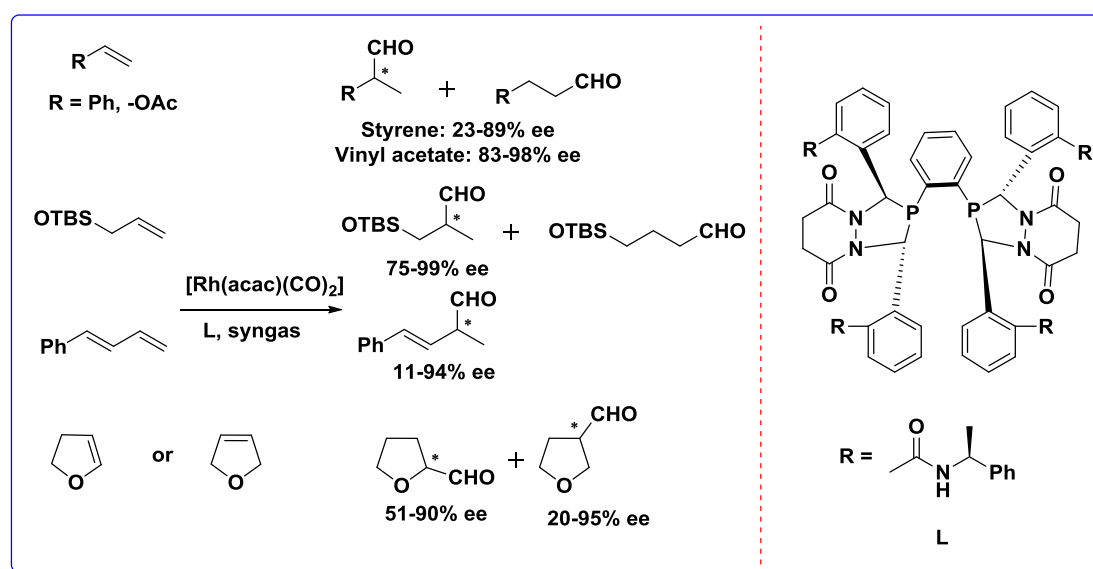


Figure 5.3: Takaya's phosphine-phosphite ligand for asymmetric hydroformylation

With vinylarenes, vinyl acetate, and vinyl phthalimide, the percent of branched aldehyde was typically 85% or higher, and the ee of the product was between 83% and 97%. Many reactions, particularly those of vinylarenes, yielded 92-95% ee.

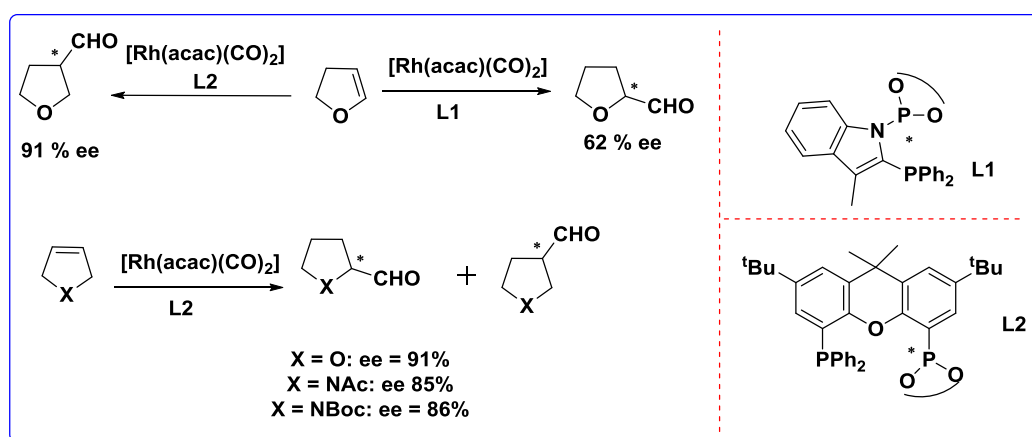
Initial studies using BINAPHOS revealed that two diastereomeric catalysts containing the opposite relative stereochemistry of the two binaphtholate groups react with much different enantioselectivity. The (*R,S*)-BINAPHOS ligand (and its enantiomer) generate catalysts that react with high enantioselectivity, but the (*R,R*)-BINAPHOS ligand (**figure 5.3**, right) generates a catalyst that leads to low enantioselectivity. The aryl group on the phosphine also has an effect on enantioselectivity, and the complexes generated from ligands containing *meta*-methoxyphenyl substituents on phosphorus react with the highest enantioselectivity.^{93i, 139} For this type of ligands the absolute configuration of the product obtained is the same as that of the absolute configuration of the binaphthyl (biphenyl) bridge. Thus, it seems that the binaphthyl bridge directs the position of the diphenylphosphino fragment. Remarkably, the best combination was obtained when the absolute configurations for the binaphthyl and bisnaphthol moieties are opposite (i.e. *S,R* or *R,S* diastereomers). Enantioselectivities were much lower with (*R,R*)-ligands. *R,R* diastereomer still gives the R-aldehyde in excess, but the ee is low (26%).¹⁴⁰

Significantly enhanced efficiency was achieved for wide range of substrates such as allyl cyanide, vinyl acetate and styrene with a series of bisphospholane and bisdiazaphospholane ligands discovered by Dow pharma and Dow Chemical¹⁴¹ in cooperation with Landis's group¹⁴² with good regio and enantioselectivity (**scheme 5.2**). Interestingly, catalysts generated from these ligands exhibit even faster rates of hydroformylation than those containing either (*R,S*)-BINAPHOS or Chiraphite. Moreover, the scope of the hydroformylation catalyzed by this ligand is unusually broad.



Scheme 5.2: Bisdiazaphospholane catalyzed asymmetric hydroformylation of various olefins

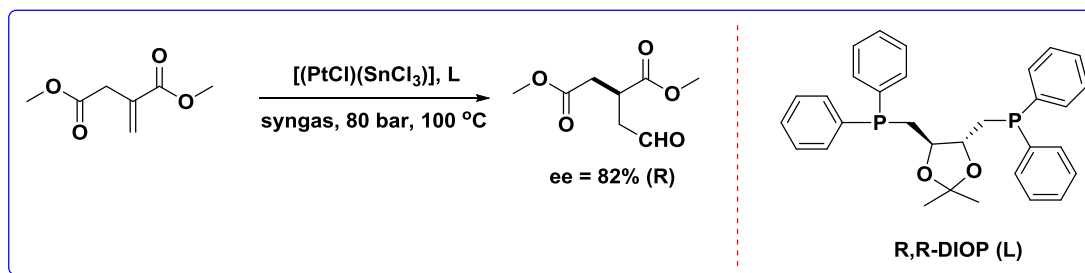
In 2012, Chikkali et.al.⁷⁶ reported a new family of chiral hybrid phosphine-phosphoramidite and phosphine-phosphonite ligands and utilized them for asymmetric hydroformylation of heterocyclic olefins (**scheme 5.3**) to get excellent enantioselectivities. The effect of ligand bite angle on observed ee's was also studied and it was concluded that indole based ligands (small bite angle) preferably binds in equatorial-axial (ea) coordination and xanthene based ligands (large bite angle) gives predominant equatorial-equatorial (ee) coordination leading to higher ee's.



Scheme 5.3: Asymmetric hydroformylation of heterocyclic olefins using chiral hybrid ligands

5.2.3: Pt Catalyzed Asymmetric Hydroformylation

Pt complexes are not very extensively used in asymmetric hydroformylation due to their lower reaction rates and low chemoselectivity compared to that of Rh complexes. However there are some reports that deal with Pt catalyzed asymmetric hydroformylation. DIOP was the first chiral ligand used in case of Pt-Sn catalyzed hydroformylation.¹⁴³ Early stage of research on Pt catalyzed hydroformylation involves some irreproducible and contradictory results on hydroformylation of butenes and vinyl aromatics.¹⁴⁴ However, DIOP-PtCl₂-SnCl₂ systems are characterized by a rather good catalytic activity compared to other platinum-based systems. Nevertheless, aldehyde formation is usually accompanied by hydrogenation, and sometimes extensive isomerization or polymerization of the substrate. The regioselectivity of hydroformylation is strictly dependent on the nature of the substrate. The asymmetric hydroformylation of an itaconate derivative occurs with the highest selectivity in the presence of platinum catalysts (**scheme 5.4**).¹⁴⁵ However, the chemical yields of branched aldehydes from reactions catalyzed by platinum catalysts are typically low. Although with this system 82% ee was observed for itaconate derivative, it could not exceed 26% for vinyl aromatics such as styrene.



Scheme 5.4: Pt catalyzed asymmetric hydroformylation of itaconate derivative

A significant increase in the regio and the enantioselectivity was observed during hydroformylation of butenes^{144c} and styrenes¹⁴⁶ when DBP-DIOP (**figure 5.4**) was used as ligand in place of DIOP. This catalytic system could successfully be applied to variety of olefins such as vinyl acetate, norbornene, and N-vinylphthalimide and ee's upto 70% could be obtained.¹⁴⁷

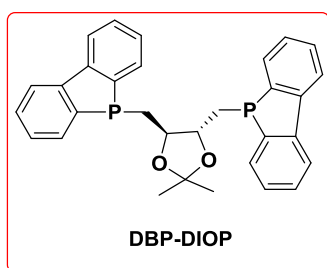


Figure 5.4: DBP-DIOP ligand for asymmetric hydroformylation

Although significant literature is available on asymmetric hydroformylation using late transition and noble metals such as Rh and Pt, there is hardly any report on asymmetric hydroformylation using first row transition metals such as Fe. This chapter describes first methodology of Fe catalyzed asymmetric hydroformylation of heterocyclic olefins such as 2,3-dihydrofuran and 2,5-dihydrofuran.

5.3: Result and Discussion

Encouraged by the success achieved in case of non-chiral version of Fe catalyzed hydroformylation¹⁴⁸ (**chapter 4**), we thought of extending this methodology further to prochiral olefins leading to chiral aldehydes. Fe precursor (1) was used along with various chiral bidentate phosphine ligands (**figure 5.5**) and an efficient methodology for enantioselective hydroformylation of heterocyclic olefins has been developed for the first time.

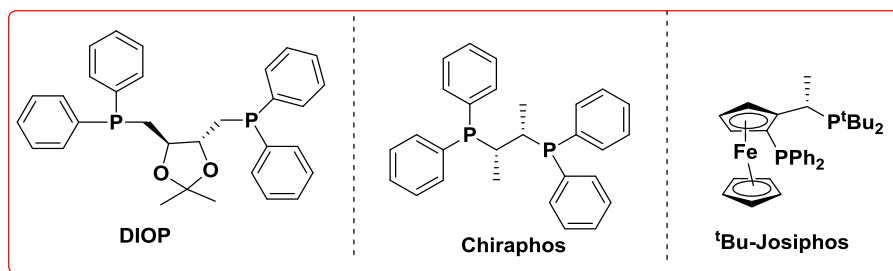
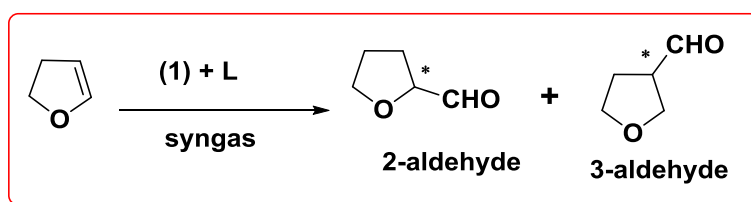


Figure 5.5: Ligands used for Fe catalyzed A-HF

5.3.1: Fe Catalyzed A-HF of 2,3-DHF

Guided by our previous report on Fe catalyzed hydroformylation of olefins, we started with Fe precursor $[\text{HFe}(\text{CO})_4]^- (\text{PPN})^+$ designated as (1) and various chiral bidentate ligands (**figure 5.6**) were evaluated. 2,3-dihydrofuran was chosen as a representative substrate (**scheme 5.5**) and several optimization experiments were performed. Significant findings have been summarized in **table 5.1**.



Scheme 5.5: Fe catalyzed A-HF of 2,3-dihydrofuran

Table 5.1: Fe catalyzed A-HF of 2,3-dihydrofuran^a

Run	Ligand	L:M	T (°C)	CO/H ₂ (bar)	Time (h)	Conv. (%) ^b	2:3 Selectivity ^b	ee (%) ^b
01.	(<i>R,R</i>)-DIOP	1.2	70	20	24	----	----	----
02.	(<i>R,R</i>)-DIOP	1.2	80	20	72	7	0:99	11
03.	(<i>R,R</i>)-DIOP	1.5	80	30	72	34	0:99	----
04.	(<i>R,R</i>)-Chiraphos	1.5	80	30	72	10	0:99	----
05.	(<i>S</i>)- <i>t</i> Bu josiphos	1.5	80	30	72	12	0:99	8
06.	(<i>S</i>)- <i>t</i> Bu josiphos	1.2	100	20	72	30	50:50	98 (2)
07.	(<i>S</i>)- <i>t</i> Bu josiphos	1.2	100	20	96	50	49:51	99 (2) 88(3)

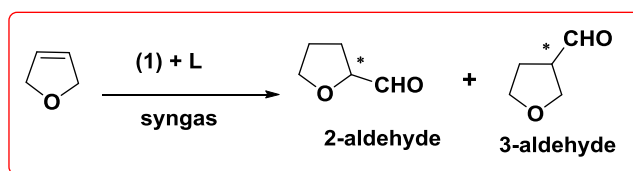
^aConditions: 1: 0.0077 mmol, Sub/Fe: 100, Solvent : MeOH 1 ml, ^bDetermined by GC.

Initial screening experiment for 24 hours did not result in aldehyde formation (**table 5.1**, run 1). However, upon carrying out the reaction for longer time led to 7% conversion to aldehyde (**table**

5.1, run 2). Increasing syngas pressure to 30 bar resulted in improved conversion but at the cost of enantioselectivity (**table 5.1**, run 2 vs 3). Another bisphosphine ligand chiraphos led to only 10% conversion and yielded racemic product (run 4). Changing the ligand to (*S*)-*t*-butyl josiphos under optimized reaction conditions resulted in 12% conversion and 8% ee (run 5). However, an improved conversion to 30% and ee upto 98% was observed when temperature was increased to 100 °C (**table 5.1**, run 5 vs 6). This is possibly due to the better coordination of chiral bidentate ligand at higher temperature. Further, the conversion was improved to 50% upon carrying out the reaction for longer time (**table 5.1**, run 7).

5.3.2: Fe Catalyzed A-HF of 2,5-DHF

Asymmetric hydroformylation of 2,5-dihydrofuran was observed to be slower compared to that of 2,3-DHF. Significant findings have been reported in **table 5.2**.



Scheme 5.6: Fe catalyzed A-HF of 2,5-dihydrofuran

Table 5.2: Fe catalyzed A-HF of 2,5-dihydrofuran^a

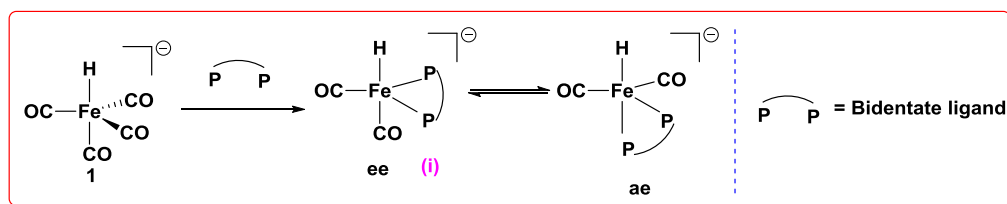
Run	Ligand	L:M	T (°C)	CO/H ₂ (bar)	Time (h)	Conv. (%) ^b	2:3 Selectivity ^b	ee (%) ^b
01.	(<i>R,R</i>)-DIOP	1.2	70	20	24	---	---	---
02.	(<i>R,R</i>)-DIOP	1.2	80	20	96	5	26:74	99 for 2 10 for 3
03.	(<i>R,R</i>)-DIOP	1.2	80	20	72	2	0:99	68
04.	(<i>S</i>)- <i>t</i> Bu josiphos	1.2	100	20	72	5	50:50	8 (2) 16 (3)

^aConditions: 1: 0.0077 mmol, Sub/Fe: 100, Solvent : MeOH 1 ml, ^bDetermined by GC.

5.3.3: Coordination studies

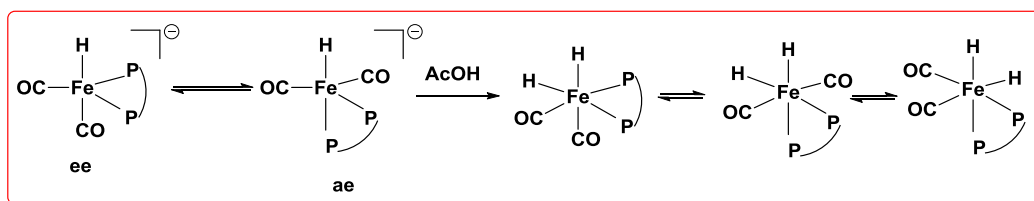
It is well known that the coordination mode of the ligand influences the selectivity in an asymmetric hydroformylation reaction.^{1c} In our pursuit to study the coordinating ability of bidentate phosphine ligands such as (*R,R*)-DIOP and (*S*)-*t*Bu-josiphos around Fe metal center, *in-situ* NMR experiments were conducted. Both of these ligands can coordinate to Fe metal

precursor in two different binding modes (**scheme 5.7**) : axial-equatorial (ea) or equatorial-equatorial (ee) or both the species may be in equilibrium with each other.



Scheme 5.7: Coordination mode of bidentate ligand around Fe metal center

Species (i) upon acetic acid treatment can lead to active Fe-dihydride intermediate (**scheme 5.8**).



Scheme 5.8: Protonation to get active dihydride intermediate

In order to generate active dihydride intermediate Fe metal precursor (1) was treated with 1 eq. of bisphosphorus ligands DIOP and tBu-josiphos individually, followed by addition of acetic acid to get the dihydride species. The progress of the reaction was monitored using *in-situ* ^1H and ^{31}P NMR spectroscopy.

5.3.3.1: Reaction of (*R,R*)-DIOP with Fe Precursor (1)

In a NMR tube, 0.010 g (0.0000138 moles) of 1 and (-) DIOP (0.0069 g, 0.0000138 moles) were dissolved in 0.4 ml of dry methanol to get a clear solution. D_2O capillary was added to it as an internal lock. Now the NMR of the reaction mixture was recorded at room temperature. Next, acetic acid (50 μL) was added to the above NMR tube and NMR was immediately recorded at room temperature. Proton NMR spectrum revealed a broad doublet at centered at -10.7 ppm (**figure 5.6**) which could possibly be assigned to Fe-dihydride complex. The corresponding phosphorus NMR did not show signal corresponding to free ligand (-22.6 ppm)¹⁴⁹ and displayed a single peak at 66.5 ppm confirming the coordination of DIOP (**figure 5.7**).¹¹²

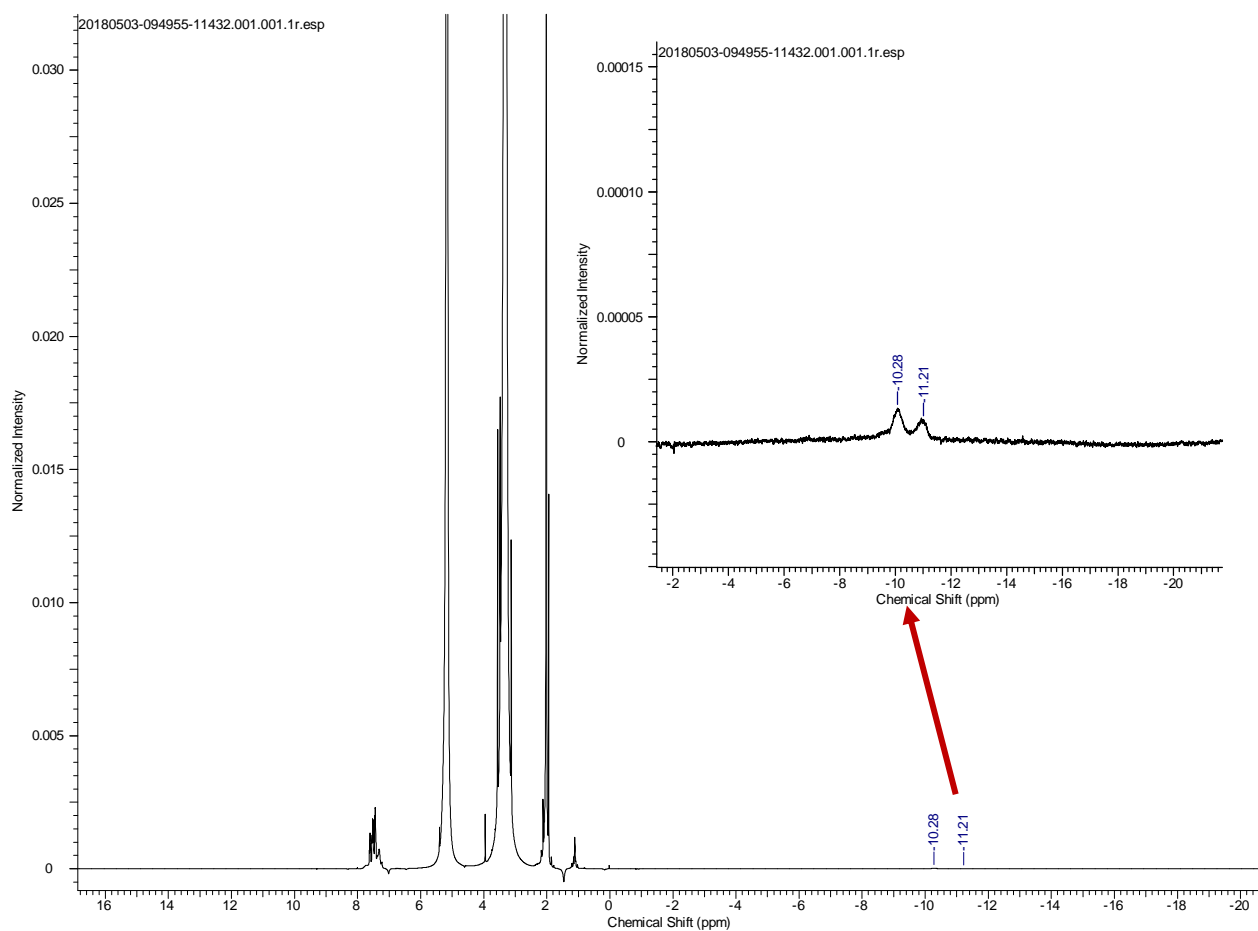


Figure 5.6: ^1H NMR spectrum of a reaction mixture of DIOP and 1 immediately after addition of acetic acid at room temperature displaying the dihydride peak (expanded view in sets)

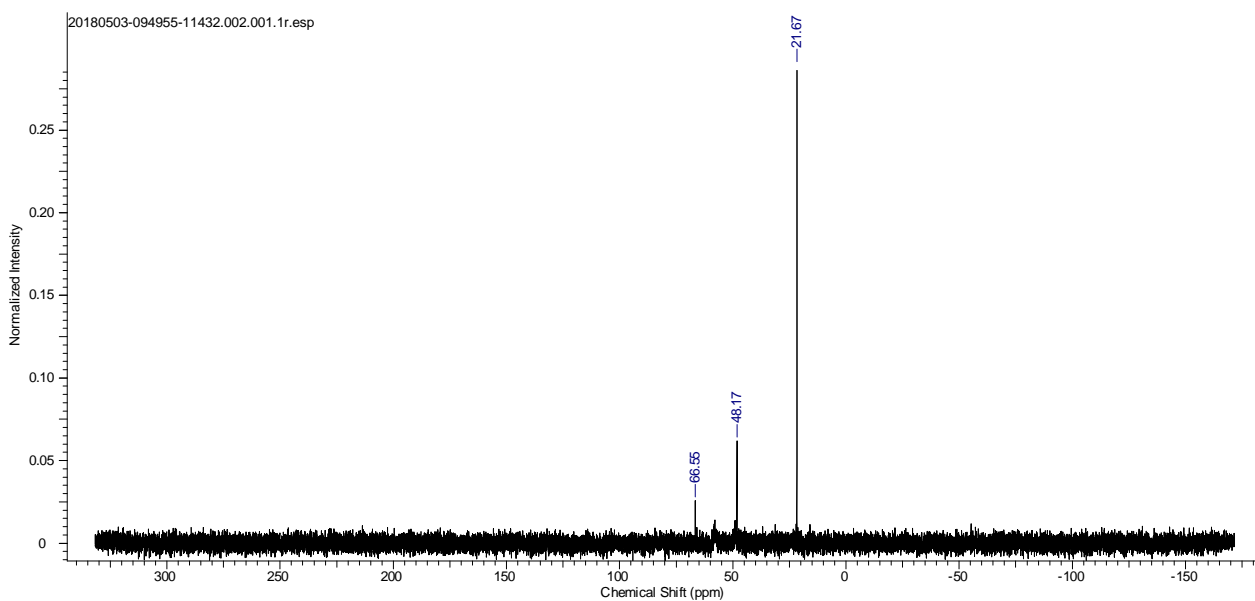


Figure 5.7: $^{31}\text{P}\{^1\text{H}\}$ NMR spectrum of a reaction mixture of DIOP and 1 immediately after addition of acetic acid at room temperature

Although proton decoupled phosphorus NMR showed absence of free ligand, the complete structure could not be elucidated due to fluxional behavior of such complexes. Fluxionality is very common in similar transition metal hydride complexes¹⁵⁰ and extensive variable temperature multinuclear NMR experiments are required to get complete structural information.

5.3.3.2: Reaction of (*S*)-tButyl-Josiphos with Fe Precursor (1)

In a NMR tube, 0.010 g (0.0000138 moles) of 1 and tButyl-Josiphos (0.0075 g, 0.0000138 moles) were dissolved in 0.4 ml of dry methanol to get a clear solution. D₂O capillary was added to it as an internal lock. Now the NMR of the reaction mixture was recorded at room temperature. Next, acetic acid (50 μ L) was added to the above NMR tube and NMR was immediately recorded at room temperature. Proton NMR spectrum revealed a singlet at -9.17 ppm (**figure 5.8**) which could possibly be assigned to Fe-dihydride complex. The corresponding phosphorus NMR displayed two doublets centered at 50.4 ppm and 29.2 ppm which can be assigned to free josiphos ligand (**figure 5.9**). It means josiphos ligand doesn't coordinate to Fe metal center at room temperature.

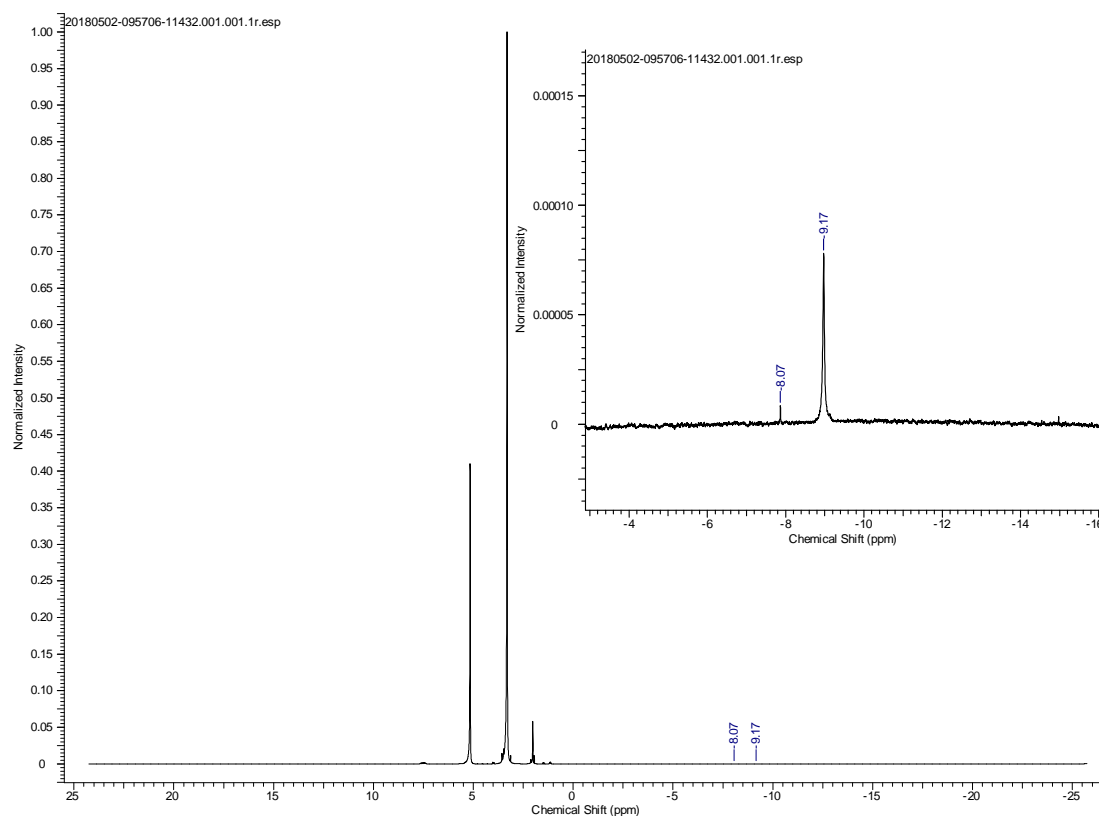


Figure 5.8: ¹H NMR spectrum of a reaction mixture of josiphos and 1 immediately after addition of acetic acid at room temperature displaying the dihydride peak (expanded view in sets)

NMR was recorded from same tube after 16 hours at room temperature and corresponding phosphorus NMR showed single peak at 83.9 ppm which can be tentatively assigned to coordinated josiphos ligand (**figure 5.10**).¹¹² since Fe-josiphos complexes are not known in literature. The slow rate of coordination of ligand is possibly responsible for longer reaction time during catalysis to get the reasonable conversion.

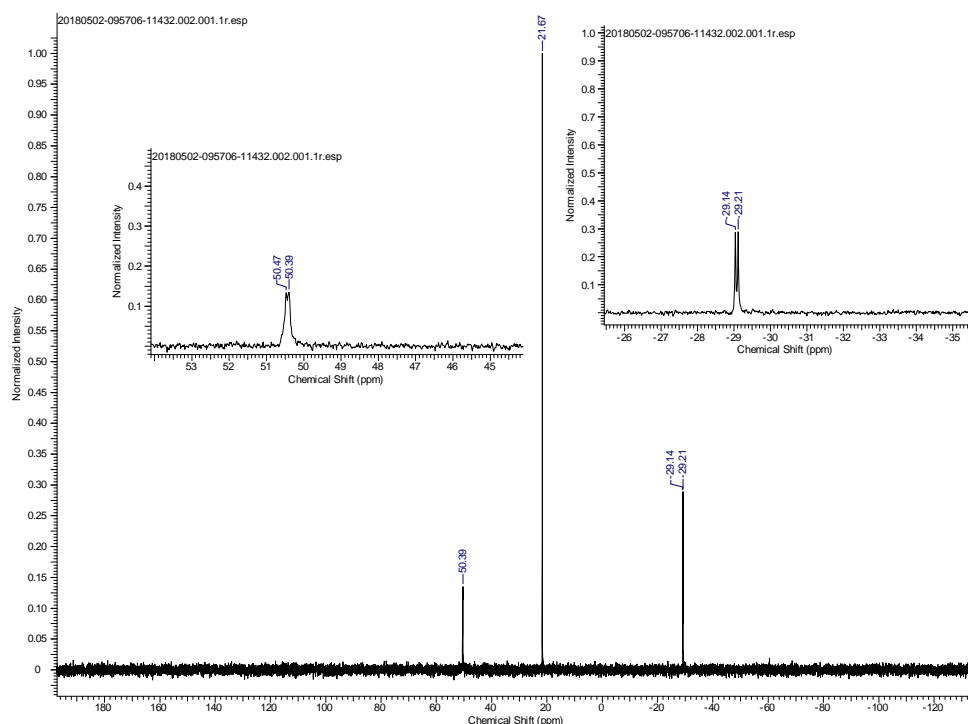


Figure 5.9: $^{31}\text{P}\{^1\text{H}\}$ NMR spectrum of a reaction mixture of josiphos and 1 immediately after addition of acetic acid at room temperature

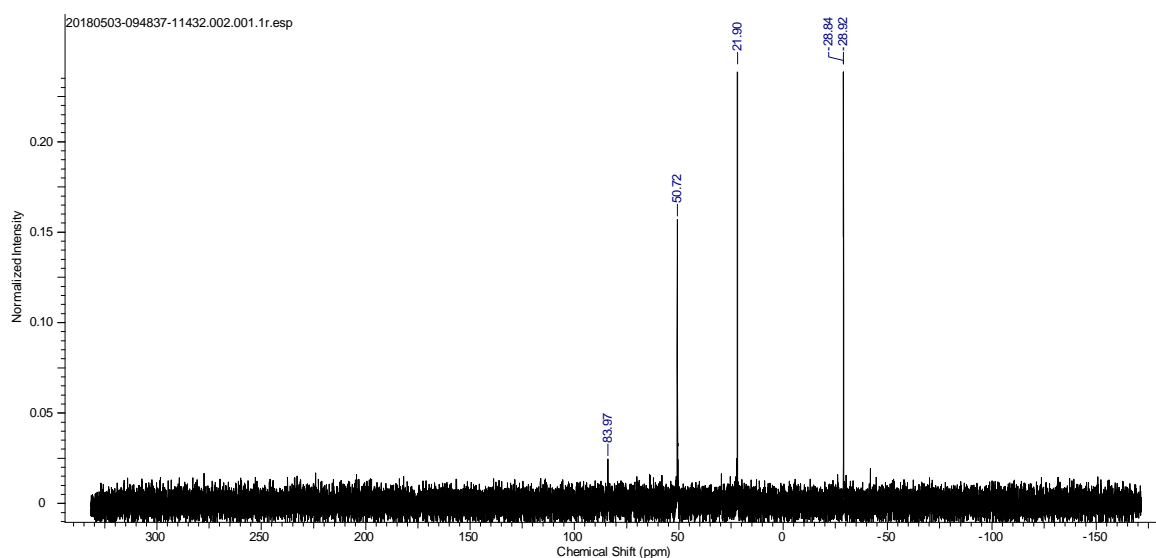


Figure 5.10: $^{31}\text{P}\{^1\text{H}\}$ NMR spectrum of a reaction mixture of Josiphos and 1 recorded after 16 hours at room temperature

NMR experiments revealed that tBu josiphos reacts slowly with the Fe precursor (1) at room temperature and very little coordination was observed even after 16 hours. This is quite obvious from catalytic experiments as well as a long reaction time upto 96 hours is needed to get reasonable conversion. Compared to tBu josiphos, coordination of (*R,R*)-DIOP is bit faster. However it is catalytically not as active as tBu josiphos.

5.4: Experimental Section

Unless noted otherwise, all manipulations were carried out under an inert atmosphere of argon using standard Schlenk line techniques or M-Braun glove box. Methanol was dried on magnesium cake. Chiral bidentate ligands (*R,R*)-DIOP, (*R,R*)-chiraphos and (*S*)-tBu Josiphos were purchased from Sigma-Aldrich and used without further purification. Heterocyclic olefins 2,3-DHF and 2,5-DHF were purchased from Sigma-Aldrich and purified by distillation. Acetic acid (glacial) was purchased from Qualigens Fine Chemicals and was dried by adding acetic anhydride (7:3). The syngas and hydrogen gas were supplied by Ms. Vadilal Chemicals Ltd, Pune, India. The hydroformylation of heterocyclic olefins was run in an Amar Equipment Pvt. Ltd. high pressure reactor equipped with pressure regulators and safety rupture valve. NMR spectra were recorded on Bruker 200, 400, and 500 MHz instruments. Chemical shifts are referenced to external reference TMS (^1H and ^{13}C) or 85% H_3PO_4 ($\Xi = 40.480747$ MHz, ^{31}P). Coupling constants are given as absolute values. Multiplicities are given as follows s: singlet, d: doublet, t: triplet, m: multiplet. *In-situ* high pressure NMR was recorded in Wilmad quick pressure valve NMR tube. GC analysis for 2,3-dihydrofuran and 2,5-dihydrofuran was carried out on an Agilent 7890B GC system using Supelco β -dex 225 (30 m* 0.25 mm * 0.25 μm) column following a known literature method.⁷⁶

5.4.1: General Procedure for Hydroformylation

In a typical hydroformylation experiment a stainless steel autoclave (450 mL) equipped with 50 ml high pressure liquid charging chamber, pressure regulator and a safety valve was used. Individual vials were charged with metal precursor $[\text{HFe}(\text{CO})_4]^-[\text{PPN}]^+$ (1) (5.5 mg, 0.0077 mmol), ligand (as in **table 5.1**), solvent (1 ml), substrate (100 equiv.) and stirring bars in a glove box. The vials were transferred to autoclave and the autoclave was purged three times with syngas ($\text{CO} : \text{H}_2 = 1:1$) before pressurizing it to the desired pressure. Suitable temperature and pressure was maintained during the reaction. After completion of the reaction, the autoclave was cooled to 0 °C, and excess gas was vented off in a well-ventilated fume-hood. The conversion and regioselectivity were determined by using gas chromatography (GC).

5.4.2: Fe Catalyzed A-HF of 2,3-DHF

Fe catalyzed A-HF of 2,3-dihydrofuran was performed following the general procedure reported earlier and GC analysis was carried out (**figure 5.12**) by following a known method.⁷⁶

GC retention time for 2,3-dihydrofuran = 3.77 min.; 2-carbaldehyde = 4.86 min. and 5.11 min.; 3-carbaldehydes = 5.31 minutes and 5.53 minutes.

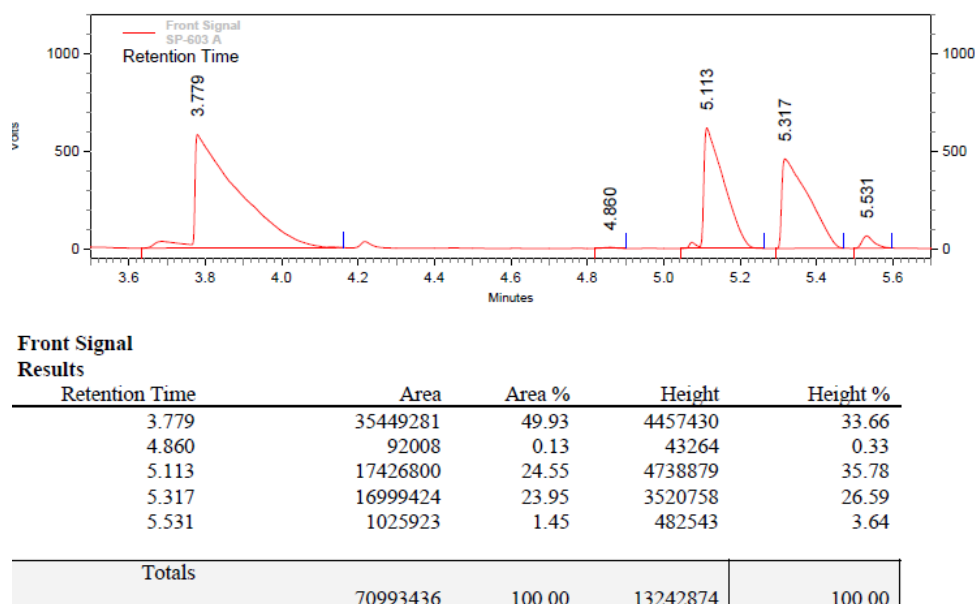


Figure 5.11: GC chromatogram of hydroformylated 2,3-dihydrofuran showing 99% ee (table 5.2, run 7)

5.4.2: Fe Catalyzed A-HF of 2,5-DHF

Fe catalyzed A-HF of 2,5-dihydrofuran was performed following the general procedure reported earlier and GC analysis was carried out (**figure 5.13**) by following a known procedure.⁷⁶

GC retention time for 2,3-dihydrofuran = 4.26 min.; 2-carbaldehyde = 4.86 min. and 5.22 min.; 3-carbaldehydes = 5.43 minutes and 5.52 minutes.

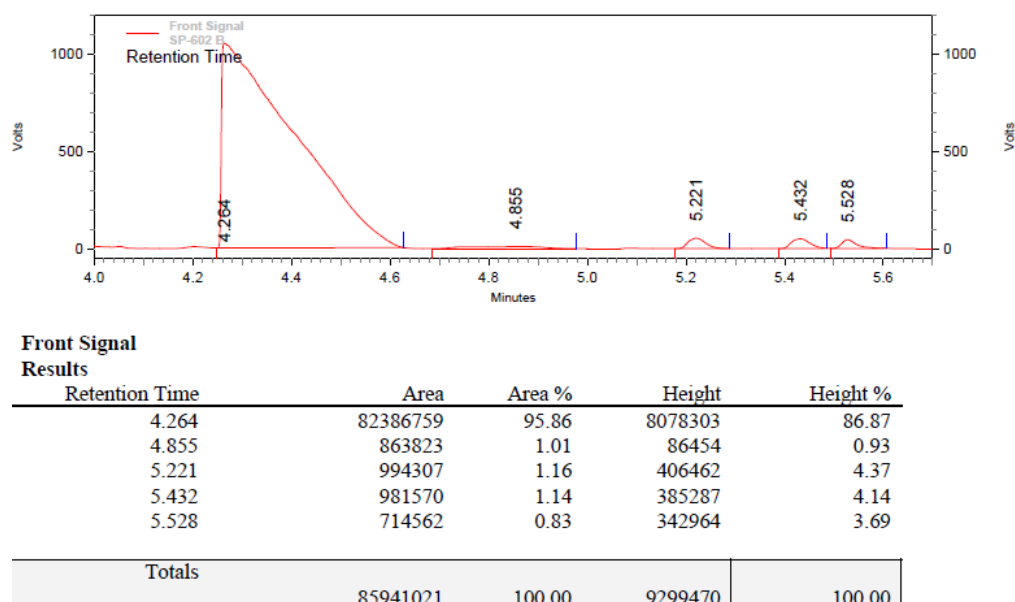


Figure 5.12: GC chromatogram of hydroformylated 2,5-dihydrofuran showing 16% ee (table 5.1, run 4)

5.5: Conclusion

In summary, the current work deals with the first iron catalyst for asymmetric hydroformylation of heterocyclic olefins under mild conditions. An iron hydride precursor 1, in combination with readily available bidentate phosphorus ligand and syngas generates the catalytically active species and delivers hydroformylation of extremely challenging substrates 2,3-dihydrofuran and 2,5-dihydrofuran with an unprecedented enantiomeric excess of 99% in case of 2,3-DHF. *In-situ* NMR experiments revealed that tBu josiphos reacts slowly with the Fe precursor (1) at room temperature and very little coordination was observed even after 16 hours. This is quite obvious from catalytic experiments as well as a long reaction time upto 96 hours is needed to get reasonable conversion. Compared to tBu josiphos, coordination of (*R,R*)-DIOP is bit faster. However it is catalytically not as active as tBu josiphos.

5.6: References

124. (a) Godard, C.; Ruiz, A.; Die´guez, M.; Pa`mies, O.; Claver, C. *Catalytic Asymmetric Synthesis*, 3rd ed.; Ojima, I., Ed.; John Wiley & Sons: Weinheim: Germany, 2010; Chapter 10. (b) Breit, B. *Acc. Chem. Res.* **2003**, *36*, 264-275. (c) Nozaki, K. *Comprehensive Asymmetric Catalysis*; Jacobsen, E. N., Pfaltz, A., Yamamoto, H., Eds.; Springer, Heidelberg, Germany, 1999; pp 381–416. (d) Claver, C.; Dieguez, M.; Pamies, O.; Castillon, S. *Top. Organomet. Chem.* **2006**, *18*, 35–64.
125. Agbossou, F.; Carpentier, J.-F.; Mortreux, A. *Chem. Rev.* **1995**, *95*, 2485-2506.
126. (a) Botteghi, C.; Paganelli, S.; Schionato, A.; Marchetti, M. *Chirality*, **1991**, *3*, 355-369. (b) For a recent review on pharmaceutical building blocks via asymmetric hydroformylation, see: Chaudhari, R. V. *Curr. Opin. Drug Discovery Dev.* **2008**, *11*, 820-828 and references therein.
127. (a) Breeden, S.; Cole-Hamilton, D. J.; Foster, D. F.; Schwarz, G. J.; Wills, M. *Angew. Chem., Int. Ed.* **2000**, *39*, 4106-4108. (b) Nettekoven, U.; Kamer, P. C. J.; Widhalm, M.; van Leeuwen, P. W. N. M. *Organometallics* **2000**, *19*, 4596-4607. (c) Ansell, J.; Wills, M. *Chem. Soc. Rev.* **2002**, *31*, 259–268. (d) van der Vlugt, J. I.; Bonet, J. M.; Mills, A. M.; Spek, A. L.; Vogt, D. *Tetrahedron Lett.* **2003**, *44*, 4389-4392. (e) van der Vlugt, J. I.; Grutters, M. M. P.; Mills, A. M.; Kooijman, H.; Spek, A. L.; Vogt, D. *Eur. J. Inorg. Chem.* **2003**, 4361-4369. (f) Barbaro, P.; Bianchini, C.; Giambastiani, G.; Parisel, S. L. *Coord. Chem. Rev.* **2004**, *248*, 2131-2150. (g) Clarkson, G. J.; Ansell, J. R.; Cole-Hamilton, D. J.; Pogorzelec, P. J.; Whittell, J.; Wills, M. *Tetrahedron: Asymmetry* **2004**, *15*, 1787-1792. (h) Breit, B.; Breuninger, D. *J. Am. Chem. Soc.* **2004**, *126*, 10244-10245. (i) Zijp, E. J.; van der Vlugt, J. I.; Tooke, D. M.; Spek, A. L.; Vogt, D. *Dalton Trans.* **2005**, 512-517. (j) Dahlenburg, L. *Coord. Chem. Rev.* **2005**, *249*, 2962-2992. (k) Han, D.; Li, X.; Zhang, H.; Liu, Z.; Hu, G.; Li, C. *J. Mol. Catal. A: Chem.* **2008**, *283*, 15-22.
128. Ewalds, R.; Eggeling, E. B.; Hewat, A. C.; Kamer, P. C. J.; van Leeuwen, P. W. N. M.; Vogt, D. *Chem.-Eur. J.* **2000**, *6*, 1496–1504.
129. Botteghi, C.; Consiglio, G.; Pino, P. *Chimia* **1972**, *26*, 141.
130. van Driessche, E. T. A.; Garton, R. D.; Caers, R. F. (to ExxonMobil Chemical Patents Inc.), U.S. Patent 2011/0184211, 2011; *Chem. Abstr.* **2010**, *152*, 314358.
131. Salomon, C.; Consielio, G.; Botteghi, C.; Pino, P. *Chimia* **1973**, *27*, 215.
132. Wink, J. D.; Kwok, T. J.; Yee, A. *Inorg. Chem.* **1990**, *29*, 5006-5008.
133. Sakai, N.; Nozaki, K.; Mashima, K.; Takaya, H. *Tetrahedron. Asymmetry*, **1992**, *3*, 583-586.
134. Babin, J. E.; Whiteker, G. T. *PCT Int. Appl.* **1993**, WO 9303839 (to UCC). *Chem. Abstr.* **1993**, *119*, 559872.

135. Buisman G. J. H., Vos, E. J.; Kamer, P. C. J.; van Leeuwen, P. W. N. M. *J. Chem. Soc. Dalton Trans.* **1995**, 409-417.
136. Buisman, G. J. H.; Kamer, P. C. J.; van Leeuwen, P. W. N. M.; *Tetrahedron Asymmetry*, **1993**, *4*, 1625-1634.
137. (a) Dieguez, M.; Pamies, O.; Ruiz, A.; Castillon, S.; Claver, C. *Chem. Commun.* **2000**, 1607-1608. (b) Dieguez, M.; Ruiz, A.; Claver, C. *J. Chem. Soc., Dalton Trans.* **2003**, 2957-2960. (c) Pamies, O.; Net, G.; Ruiz, A.; Claver, C. *Tetrahedron: Asymmetry* **2000**, *11*, 1097-1108.
138. (a) Sakai, N.; Mano, S.; Nozaki, K.; Takaya, H. *J. Am. Chem. Soc.* **1993**, *115*, 7033-7034. (b) Sakai, N.; Nozaki, K.; Takaya, H. *Chem. Commun.* **1994**, 395-396.
139. Aguado-Ullate, S.; Saureu, S.; Guasch, L.; Carbo, J. J. *Chem.-Eur. J.* **2012**, *18*, 995-1005.
140. Gleich, D.; Schmid, R.; Herrmann, W. A. *Organometallics* **1998**, *17*, 2141-2143.
141. (a) Axtell, A. T.; Copley, C. J.; Klosin, J.; Whiteker, G. T.; Zanotti-Gerosa, A.; Abboud, K. A. *Angew. Chem., Int. Ed.* **2005**, *44*, 5834-5838. (b) Klosin, J.; Landis, C. R. *Acc. Chem. Res.* **2007**, *40*, 1251-1259.
142. Clark, T. P.; Landis, C. R.; Freed, S. L.; Klosin, J.; Abboud, K. A. *J. Am. Chem. Soc.* **2005**, *127*, 5040-5042.
143. Hsu, C. Y. Ph. D. Dissertation, University of Cincinnati, **1974**; *Chem. Abstr.* **1975**, *82*, 154899.
144. (a) Consiglio, G.; Pino, P. *Isr. J. Chem.* **1976**, *15*, 221-222. (b) Consiglio, G.; Pino, P. *Helv. Chim. Acta* **1976**, *59*, 642-645. (c) Kawabata, Y.; Suzuki, T. M.; Ogata, I. *Chem. Lett.* **1978**, *7*, 361-362.
145. Kollar, L.; Consiglio, G.; Pino, P. *J. Organomet. Chem.* **1987**, *330*, 305-314.
146. (a) Pittman, C. U.; Kawabata, Y.; Flowers, L. I. *J. Chem. Soc., Chem Commun.* **1982**, 473-474. (b) Haelg, P.; Consiglio, G.; Pino, P. *J. Organomet. Chem.* **1985**, *296*, 281-290. (c) Consiglio, G.; Morandini, F.; Scalone, M.; Pino, P. *J. Organomet. Chem.* **1985**, *279*, 193-202. (d) Paeanelli, S.; Matteoli, U.; Scrivanti, A. *J. Organomet. Chem.* **1990**, *397*, 119-125. (e) Doyle, M. M.; Jackson, W. R.; Perlmutter, P. *Tetrahedron Lett.* **1989**, *30*, 5357-5360. (f) Consiglio, G.; Pino, P.; Flowers, L. I.; Pittman, C. U. *J. Chem Soc., Chem. Commun.* **1983**, 612-613.
147. Parrinello, G.; Deschenaux, R.; Stille, J. K. *J. Org. Chem.* **1986**, *51*, 4189-4195.
148. Pandey, S.; Vipinraj, K.; Shinde, D. R.; Vanka, K.; Kashyap, V.; Kurungot, S.; Vinod, C. P.; Chikkali, S. H. *J. Am. Chem. Soc.* **2018**, *140*, 4430-4439.
149. Koschker, P.; Kähny, M.; Breit, B. *J. Am. Chem. Soc.* **2015**, *137*, 3131-3137.
150. Gusev, D. G.; Berke, H. *Chem. Ber.* **1996**, *129*, 1143-1155.

Chapter 6

Summary and Outlook

6.1: Summary

As our day to day life is highly dependent on fossils fuel resources, these resources are extensively utilized. Since there is limited reserve of fossils fuel, its depletion has become a major concern to the scientific community. Various strategies are being devised to address this challenge. Use of renewable resources is certainly one of the strategies which will reduce our dependence on fossils reserves. Among the renewable resources biomass, sugar and plant oils provide direct entry to chemical modifications.

Thus sustainability can be achieved either by encouraging use of biomass derived substrates in important synthetic transformations or by replacing noble and toxic transition metals with earth abundant and economically viable first row transition metals. In this context the present thesis entitled as **“Regioselective Rh Catalyzed Isomerizing Hydroformylation and Fe Catalyzed Hydroformylation of Alkenes and Plant Oils”** describes the development of new synthetic methodologies for isomerizing hydroformylation of plant oils and also a highly efficient methodology for hydroformylation using earth abundant Fe.

In an effort to develop an efficient methodology for isomerizing hydroformylation of plant oils, the rational designing of ligands was extremely important. Three new bisphosphite ligands were proposed (**figure 6.1**) owing to their strong potential in such type of transformations indicated by literature precedents.

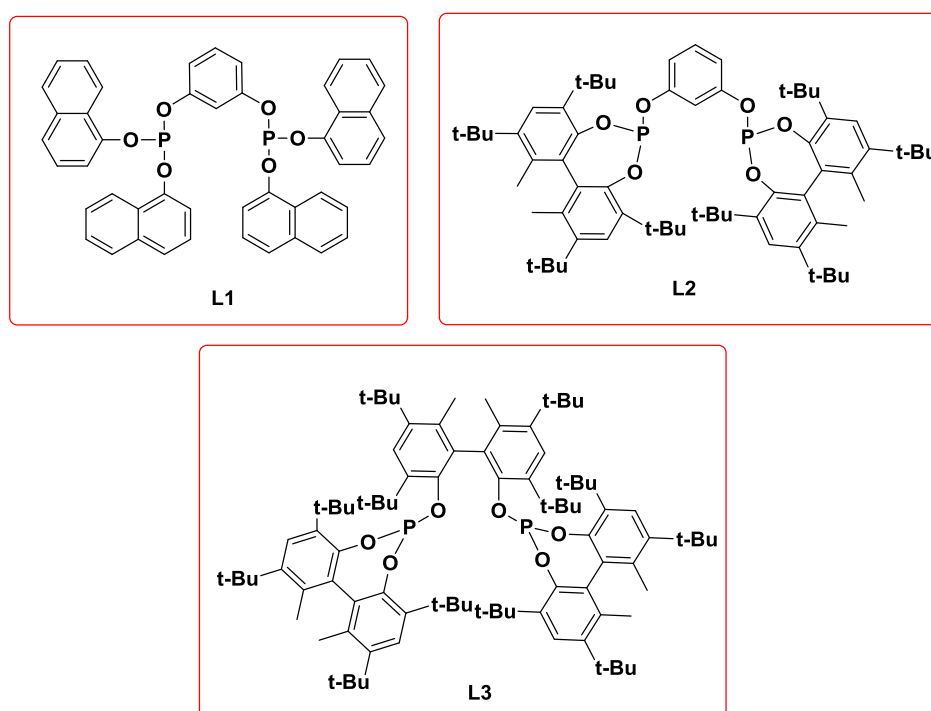
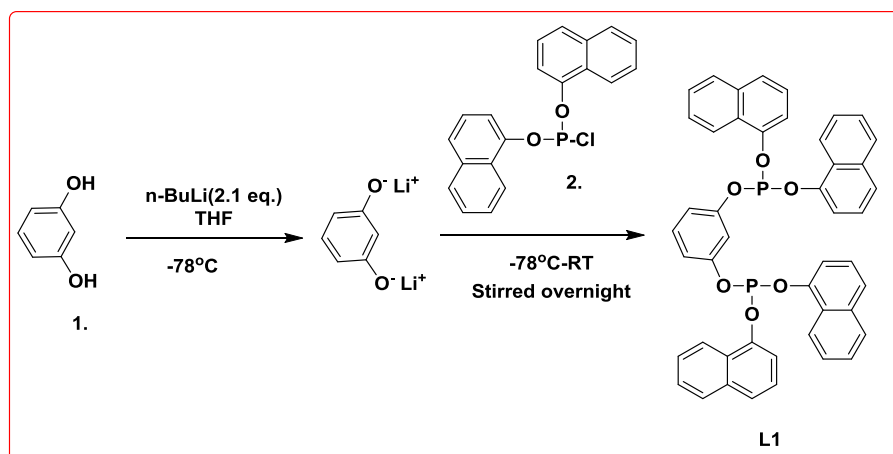


Figure 6.1: Proposed Bisphosphite ligands

Out of these three ligands L2 and L3 were found to be highly unstable and L1 was investigated in isomerizing hydroformylation of plant oils such as methyl oleate.

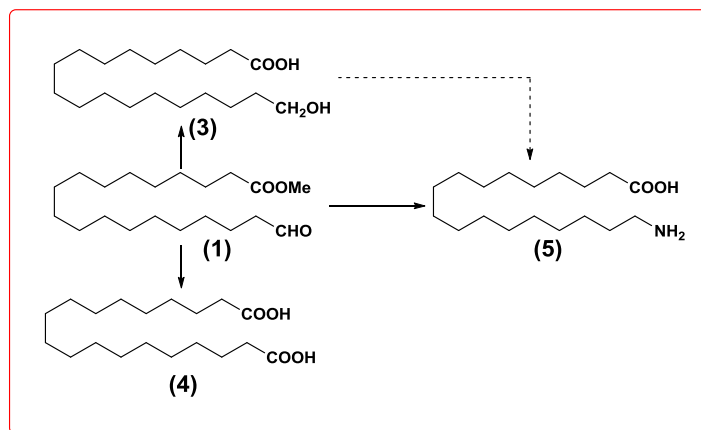
The synthesis of L1 was achieved in single step starting with resorcinol. Deprotonation of resorcinol by *n*-BuLi, followed by addition of di(naphthalen-1-yl) phosphorochloridite 2 yielded the anticipated bis-phosphite ligand L1 (**scheme 6.1**).



Scheme 6.1: Synthesis of L1

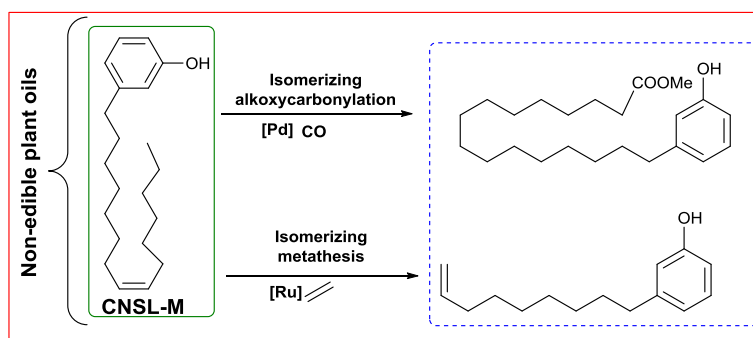
The desired Rh complex was synthesized after reacting ligand L1 with $[\text{Rh}(\text{acac})(\text{CO})_2]$ *in-situ* under syngas pressure. *In-situ* high pressure NMR spectroscopy revealed that the two phosphorus nuclei predominantly occupy bis-equatorial position in a trigonal bipyramidal rhodium complex. However, interestingly, the two phosphorus nuclei were found to be in-equivalent and displayed a $^1J_{\text{Rh-P}}$ coupling of 240-243 Hz. The performance of the bis-phosphite ligand L1 was evaluated in isomerizing hydroformylation of long-chain olefins. Severe optimization experiments were performed to get the best suited conditions. Thus, at 120 °C and ambient (1 bar) syngas pressure linear selective isomerizing hydroformylation of short chain olefins such as 1-Octene and *cis*-2-Octene was observed. Performing the isomerizing hydroformylation of extremely challenging plant oil based substrate methyl-oleate under similar conditions led to an unprecedented regioselectivity of 75% for the linear aldehyde. Above observations also revealed the trend that isomerization is favoured at higher temperature and terminal formylation is favoured at lower syngas pressure. These experimental findings might guide the future developments in the field of isomerizing-hydroformylation of long-chain internal olefins to linear selective products.

In addition to this, the synthetic utility of isomerizing-hydroformylation in organic synthesis was demonstrated by transforming the linear aldehyde (1) to 19-hydroxynonadecanoic acid (3) (**scheme 6.2**), which is a potential AB type monomer for polyester production.



Scheme 6.2: Plant oil derived α , ω -functionalized monomers/platform chemicals

Further, methyl oleate falls in the category of edible oil and its utilization can result in direct competition with the food chain. In this context, cashew nut shell liquid (CNSL) stands out as a non-edible plant sourced oil that is readily available (CNSL-450,000 metric tons per annum) on a large scale from agricultural resources. The CNSL is equipped with a functional group at one end of the molecule and a double bond deep into the long aliphatic chain. This internal double bond provides an excellent opportunity to further functionalize the plant sourced oil to useful chemicals and building blocks. Hence an unprecedented methodology (**scheme 6.3**) is developed for isomerizing hydroformylation of non-edible plant oils such as cashew nut shell liquid as only isomerizing metathesis and isomerizing alkoxy carbonylation is known in case of CNSL.



Scheme 6.3: Isomerizing functionalization of CNSL

A small library of bisphosphorus ligands (**figure 6.2**) was evaluated in the rhodium-catalyzed isomerizing hydroformylation (I-HF) of cashew nut shell liquid (CNSL). Rhodium complex of 1,2-bis((di-tertbutylphosphanyl)methyl)benzene (BDTBPMB) (L4) outperformed the other bisphosphite and bis-phosphine ligands and unveiled a moderate selectivity of 28% and 50% in the I-HF of CNSL-monoene and methoxy protected monoene respectively. The resultant aldehyde 16-(3-methoxyphenyl)hexadecanal P1' was isolated and its identity was fully established.

Application of bis-phosphine ligand L4 in the I-HF of highly challenging CNSL-cardanol (S3) and methoxy protected CNSL-cardanol yielded a linear selectivity of 74%, although with reduced conversion.

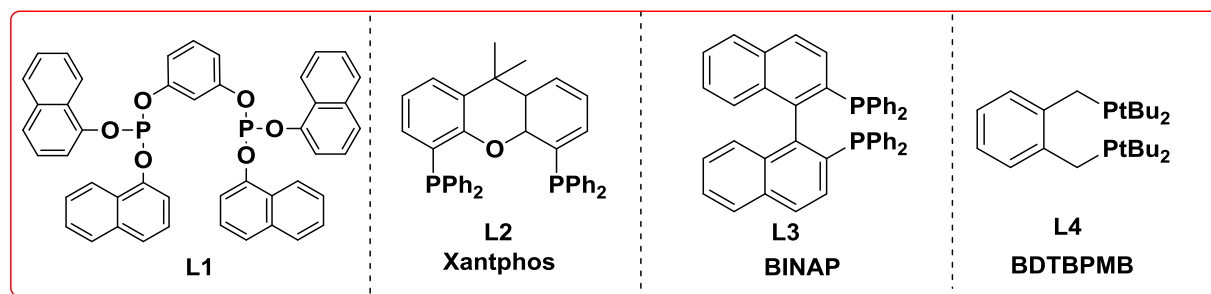


Figure 6.2: Ligands used for I-HF of cashew nut shell liquid

The higher reactivity of L4 was justified as CNSL derived substrates might adopt a folded conformation (**figure 6.3**). In the folded conformation the phenyl ring in substrates might hinder the coordination of the relatively bulky L1-catalyst to terminal-olefin and thus hamper the terminal selectivity. Whereas, relatively electron rich and less bulky L4-catalyst might still be able to coordinate to the terminal olefin, leading to better linear selectivity.

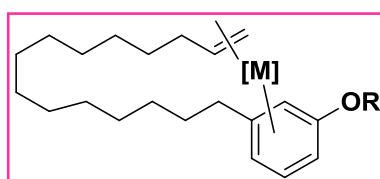


Figure 6.3: Proposed structure of folded CNSL-monoene in the presence of metal catalyst

To demonstrate the synthetic utility of our strategy, the obtained aldehyde (derived from CNSL-cardanol) was subjected to hydrogenation and the resultant 3-(16-hydroxyhexadecyl) phenol was isolated in 89% isolated yield. High-pressure NMR investigation revealed selective formation of bisequatorial BDTBPMB-rhodium complex which might be responsible for the excellent linear selectivity.

Apart from utilizing various renewable resources as substrates in important synthetic transformations, the replacement of noble metals with abundant and cheaply available first row transition metals in catalysis would be another good option to promote renewable science.

In this context, an efficient methodology for hydroformylation of olefins using earth abundant Fe metal has been developed. The iron precursor $[\text{HFe}(\text{CO})_4][\text{Ph}_3\text{PNPPh}_3]$ (1) in the presence of triphenyl phosphine operates at 10-30 bars syngas pressure below 100 °C which falls under the purview of LPO (low pressure oxo). This process utilizes readily available ligands and applies to an array of olefins. The generality of the approach has been demonstrated by subjecting various

olefins (**figure 6.4**), such as 1-octene, 1-hexene, 1-decene, 1-dodecene, 1-octadecene, trimethoxy(vinyl)silane, trimethyl(vinyl)silane, cardanol, 2,3-dihydrofuran, allyl malonic acid, styrene, 4-methyl styrene, 4-*t*Bu-styrene, 4-*t*Bu-styrene, 4-methoxy styrene, 4-acetoxy styrene, 4-bromo styrene, 4-chloro styrene, 4-vinylbenzotrile, 4-vinylbenzoic acid, and allyl benzene to iron catalyzed hydroformylation resulting in good to excellent yields for desired aldehydes. Initial optimization studies with 1-octene indicated an optimal ligand to metal ratio of 2.5, methanol as the most suitable solvent, and a temperature of 100 °C. Short chain 1-hexene could be hydroformylated at 10 bars syngas pressure and 80 °C. The developed methodology was found to tolerate various electron donating and electron withdrawing substrates successfully. Remarkably, the addition of 1 mol% acetic acid promotes the reaction to completion within 16-24 hours.

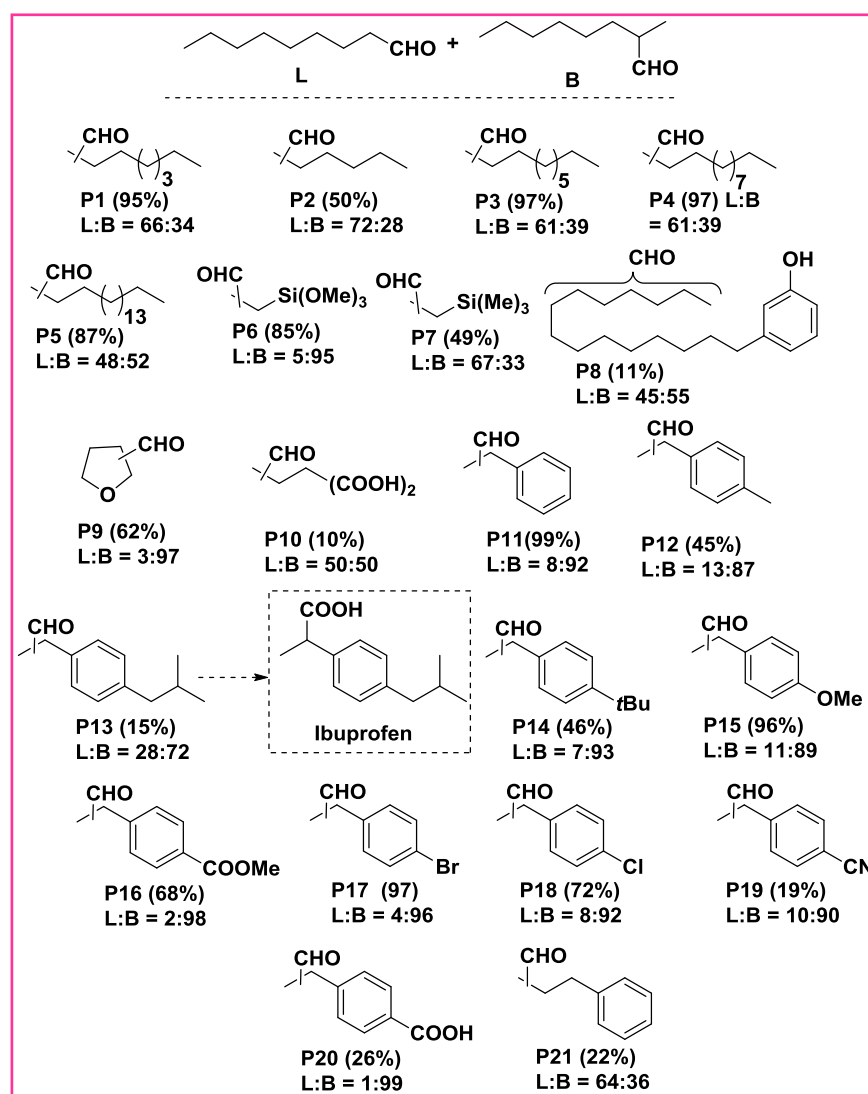


Figure 6.4: Fe catalyzed hydroformylation of various olefins

Apart from methodology, this study discussed about the first mechanistic investigations in Fe catalyzed hydroformylation (**figure 6.5**). Unfolding the elementary steps in the iron catalyzed hydroformylation will be of great significance for understanding the reactivity of the iron catalyst and might unlock the synthetic potential of this earth abundant metal in hydroformylation.

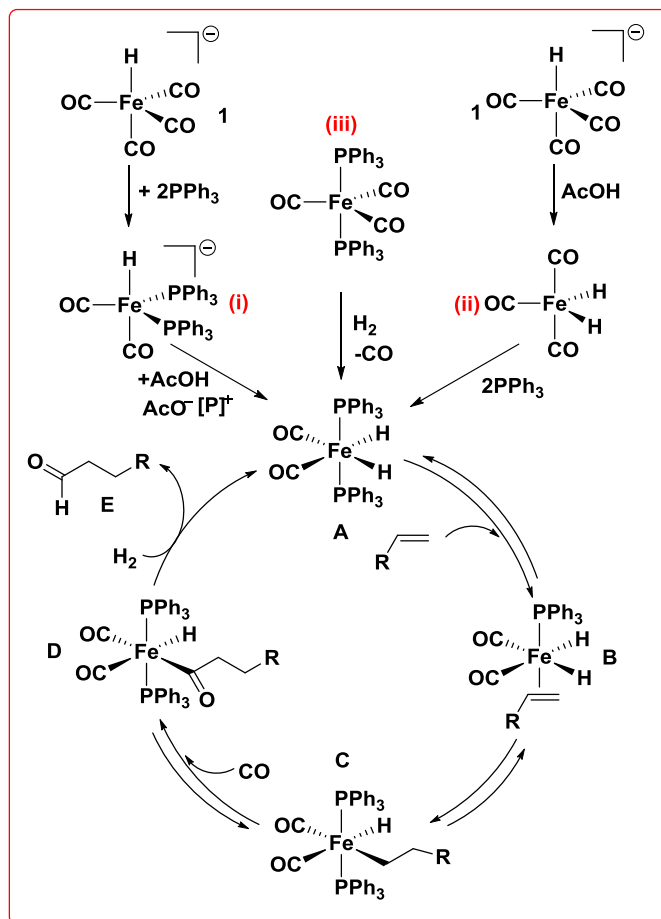
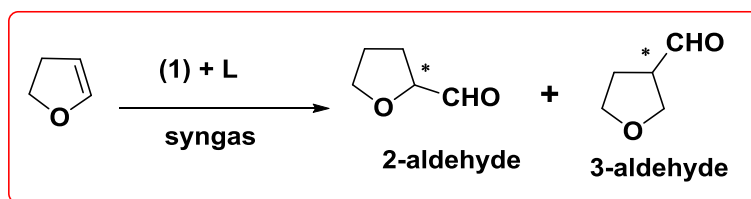


Figure 6.5: Proposed catalytic cycle for iron catalyzed hydroformylation

Combined experimental and computational investigations indicate that the di-hydride species A is the actual active catalytic species. The identity of species A was established by multiple NMR experiments, which indicated coordination of ligand L1 and formation of the iron-dihydride complex. Cyclic voltammetry results suggested a Fe(0) to Fe(II) interconversion, explaining the accelerating effect of acetic acid. Control experiments with externally added radical scavengers ruled out the possibility of a radical or an Fe (I) to Fe (III) mechanism. The experimental findings were further corroborated by DFT calculations. Among the six possible stereoisomers of iron-dihydride complex, species A was found to be the most favorable. Transition state calculations for 1-hexene insertion revealed that 1,2-insertion was favored by 1.3 kcal/mol, whereas styrene preferred 2,1-insertion by 1.7 kcal/mol. Thus, experimental and computational investigations

establish that the iron catalyzed hydroformylation follows a Fe(II) catalytic cycle, as depicted in **figure 6.5**. The role of rhodium impurities in catalyzing the hydroformylation of alkenes was investigated. These studies established that the reported hydroformylation is catalyzed by iron and it is highly unlikely that the rhodium impurities are responsible for the observed hydroformylation.

Significant advancements have been made in the field of Rh catalyzed asymmetric hydroformylation using rationally designed catalytic systems. Apart from Rh, other transition metals such as Ru, Pd, Pt have also been used to catalyze this industrially relevant transformation. However it would be worth substituting these precious and rare transition metals with earth abundant first row transition metals such as Fe. Reported here is an unprecedented methodology for Fe catalyzed asymmetric hydroformylation of olefins under mild conditions. The iron precursor $[\text{HFe}(\text{CO})_4][\text{Ph}_3\text{PNPh}_3]$ (1) in presence of chiral bidentate ligands such as (*R,R*)-DIOP and (*S*)-*t*Bu-Josiphos catalyzes the asymmetric hydroformylation of heterocyclic olefin such as 2,3-dihydrofuran (**scheme 6.4**) with reasonable conversion and results in 99% ee under optimized reaction conditions.

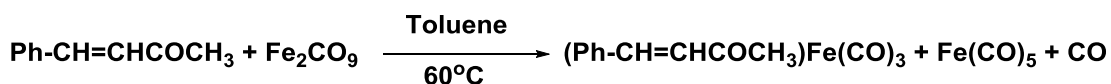


Scheme 6.4: Fe catalyzed A-HF of 2,3-dihydrofuran

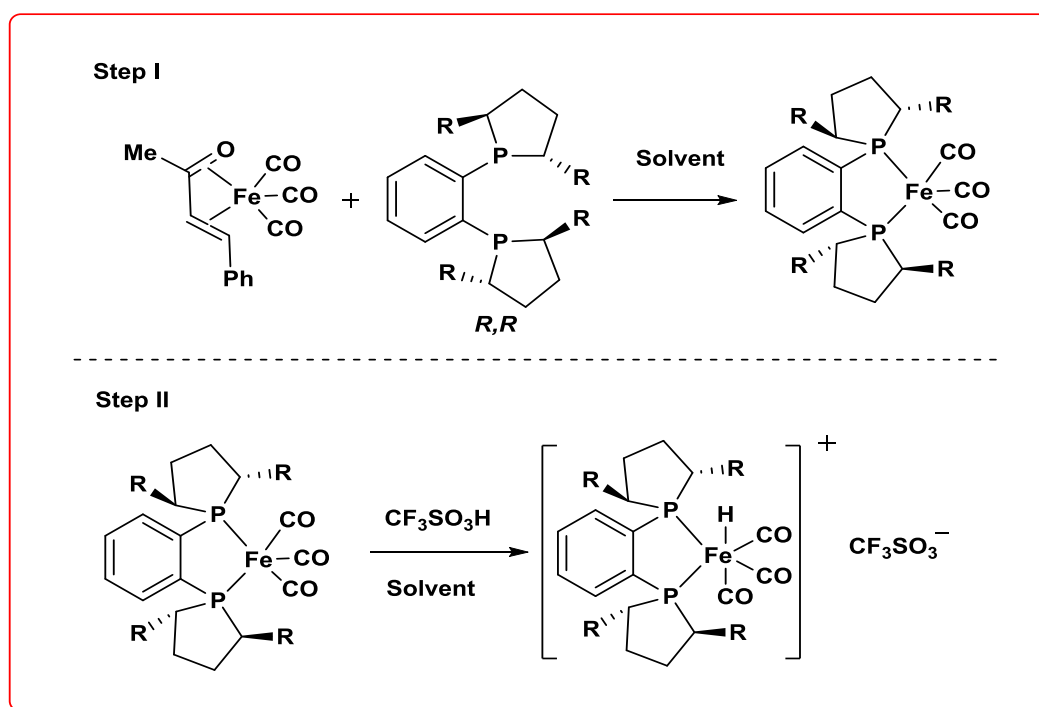
6.2: Outlook

Although the Fe catalyzed hydroformylation has significant potential to catalyze HF of various olefins having different functional groups, some improvements are still needed to make this process universal. The synthesized Fe precursor (1) reacts readily with monodentate ligands to form active metal complex. However, it fails to react with most of the bidentate ligands. As most of the chiral phosphorus ligands are bidentate, hence to extend this methodology successfully towards asymmetric hydroformylation and various other asymmetric reactions a different Fe metal precursor is highly desirable.

An attractive Fe metal precursor having strong affinity towards bidentate ligands is $[\text{Fe}(\text{CO})_3(\text{bda})]$ where bda = benzylidene acetone as evident from literature precedents. $[\text{Fe}(\text{CO})_3(\text{bda})]$ can be easily synthesized starting with Fe_2CO_9 and benzylidene acetone (**scheme 6.5**) by following a literature procedure.¹²⁰

Scheme 6.5: Synthesis of $[\text{Fe}(\text{CO})_3(\text{bda})]$

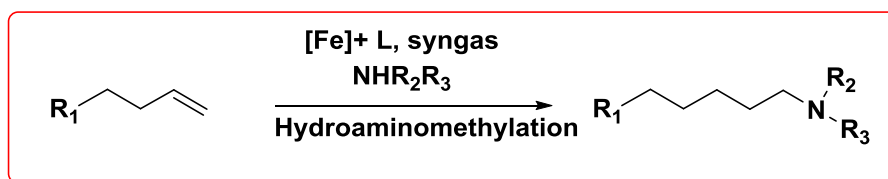
Synthesis of chiral iron complexes can be achieved in two steps from the metal precursor $\text{Fe}(\text{CO})_3(\text{bda})$ and commercially available chiral bisphosphine ligands and then after protonation of that $[\text{FeH}(\text{CO})_3(\text{DuPHOS})]^+\text{CF}_3\text{SO}_3^-$ complex will be obtained (scheme 6.6).

Scheme 6.6: Synthesis of chiral Fe Complex using (R,R) -DuPHOS

The coordination of bisphosphine ligand to iron can be confirmed by ^{31}P -NMR spectroscopy and various other spectroscopic methods. Iron hydride species can be identified by ^1H -NMR spectroscopy. Similar kinds of complexes are known in literature but only with achiral bisphosphines.

Thus synthesized complex will find application in several asymmetric catalytic reactions such as asymmetric hydroformylation, asymmetric hydrogenation, asymmetric phosphination etc. Since the synthesized initial Fe complex is in Fe (0) state, it is also expected to follow an Fe (0) to Fe (II) pathway during the catalytic cycle same as that of precursor (1).

Hydroaminomethylation reaction is another option where potential of these types of catalyst can be tested. Hydroaminomethylation reaction refers to addition of a hydrogen and an amine group across a carbon carbon double bond to give linear amines (**scheme 6.7**).



Scheme 6.7: Fe catalyzed hydroaminomethylation

Linear aliphatic amines are used for the production of solvents, fine chemicals, agrochemicals, vulcanization accelerators and pharmaceutical intermediates. Amines derived from fatty acids, also known as fatty amines, are used as fabric softener, corrosion inhibitors and as emulsifying agent. Hydroaminomethylation is mainly catalyzed by late transition metals such as Ru and Rh and field of Fe catalyzed hydroaminomethylation is still unexplored. As hydroformylation is the first step in hydroaminomethylation reactions, an Fe based catalyst capable of performing well in hydroformylation is also anticipated to deliver similar performance in this reaction as well.

Apart from this, carbonylation of alkynes is another important area where a suitable Fe based catalyst is highly desirable for monocarbonylation. Currently, Fe carbonyls such as Fe_3CO_{12} has been employed to get dicarbonylation of alkynes to succinimides. However, a well defined Fe precursor in combination of suitable ligand can give monocarbonylation successfully.

Curriculum Vitae

Swechchha Pandey

Address for correspondence:

Polyolefin Lab, CSIR-National Chemical Laboratory

Dr. Homi Bhabha road, Pune- 411008

Email: sg.pandey@ncl.res.in
swechchhabhu@gmail.com



Present status

Working with Dr. Samir Chikkali at CSIR- National Chemical Laboratory. I will be completing my doctoral work by May 2018.

Educational Qualification:

PhD in Organometallic Catalysis (Expected to be complete by May-2018)

UGC-Senior Research Fellow, registered with AcSIR-New Delhi at CSIR-National Chemical Laboratory, Pune, India.

M.Sc. (Organic Chemistry)

Banaras Hindu University, Varanasi, India with **First Class, (CGPA= 8.52/10)** in June 2012.

B.Sc. (Chemistry)

Banaras Hindu University, Varanasi, India with **First Class, (70.7%)** in June 2010.

Research Experience:

1) M.Sc. Research Project entitled “Pyrano fused quinolines” at Banaras Hindu University, Varanasi with **Prof. R. M. Singh**.

Duration: 4 Months (during 2011-2012)

2) UGC-Junior Research Fellow for PhD from 7th January 2013 on the topic “Refining of plant oils to give renewable polyethylene mimics” with **Dr. Samir H. Chikkali** at CSIR-National Chemical Laboratory, Pune.

3) UGC-Senior Research Fellow for PhD from 7th January 2015 on the topic “Regioselective Rh catalyzed isomerizing hydroformylation and Fe catalyzed hydroformylation of alkenes and plant oils” with **Dr. Samir H. Chikkali** at CSIR-National Chemical Laboratory, Pune.

Pre-Synopsis done on 22nd December 2017, PhD is expected to be complete in May 2018.

Duration: 7th January 2013 to till date.

Ph.D. Thesis : Swechchha Pandey

Curriculum Vitae

Publications:

1. **Pandey, S.;** Chikkali*, S. H. Highly regioselective isomerizing hydroformylation of long-chain internal olefins catalyzed by rhodium bis-phosphite complex, *ChemCatChem.*, **2015**, 7, 3468 - 3471.
2. **Pandey, S.;** Shinde D.R.; Chikkali*, S. H. Isomerizing Hydroformylation of Cashew Nut Shell Liquid, *ChemCatChem.*, **2017**, 9, 3997-4004.
3. Deshmukh, S.; Gaikwad, S.; **Pandey, S.;** Mali, P.; Chikkali*, S. H. Synthesis of meta-substituted monodentate phosphinite ligands and implication in hydroformylation, *J. Chem. Sci. (India)*. **2017**, 129, 1143 – 1152.
4. Rajasekar, P.; **Pandey, S.;** Paithankar, H.; Chugh*, J.; Boomishankar*, R. Imido-P(V) Trianion Supported Enantiopure Neutral Tetrahedral Pd(II) Cages *Chem. Commun.*, **2018**, 54, 1873-1876
5. **Pandey, S.;** Vipin Raj, K.; Shinde, D. R.; Vanka, K.; Kashyap, V.; Kurungot, S.; Chikkali*, S. H. Iron Catalyzed Hydroformylation of Alkenes under Mild Conditions: Evidence of an Fe(II) Catalyzed Process; *J. Am. Chem. Soc.* **2018**, 140, 4430-4439.

Patents:

1. Samir H Chikkali and **Swechchha Pandey**, Novel compounds and process for preparation of the same from plant oil, IPA: IN201611034415 (**2016**).
2. Samir H. Chikkali and Swechchha Pandey, Process for the preparation of novel compounds from Cashew Nut Shell Liquid. WO 2018066005 A1 (2017).
3. Samir H Chikkali and **Swechchha Pandey**, Fe catalyzed hydroformylation of olefins under mild conditions, IPA No. IN201711015470 (**2017**).
4. Samir H Chikkali, **Swechchha Pandey** and Anirban Sen A phosphine-phosphite ligand , process for preparation and application thereof, Provosional application filed (**2018**).

Papers/posters presented at international/national conferences

- ❖ Presented a poster Science day celebrations @ NCL.
- ❖ Oral presentation in MACRO 2017 @ Thiruvananthapuram, Kerala, India.
- ❖ Presented a poster in MTIC 2017 @ CSIR-NCL, Pune
- ❖ Invited oral presentation in IFC-2018 @ IISER-Pune

Curriculum Vitae

Academic References:

Dr. Samir H. Chikkali

Senior Scientist
Polymer Science & Engineering division
CSIR-National Chemical Laboratory, Pune
Email: s.chikkali @ncl.res.in
Phone: Office- 020 2590 3145
Fax: 020-2590 2629

Dr. E. Balaraman

Senior Scientist
Division of Organic Chemistry
CSIR-National Chemical Laboratory, Pune
Email: eb.raman@ncl.res.in
Phone (O): 020 2590 2144

Dr. Amitava Das

Director, CSIR-Central Salt and Marine Chemicals Research Institute
Gijubhai Badheka Marg, Bhavnagar-364002,
Gujarat (INDIA)
Ph. No. 2569496, Ext. 6000, 6010
Email: a.das@csmcri.res.in

Erratum
